EPFL

Thèse n° 9672

Mechanism of KRAS-driven T cell infiltration in colorectal cancer

Présentée le 17 novembre 2023

Faculté des sciences de la vie
Unité du Prof. Radtke
Programme doctoral en approches moléculaires du vivant

pour l'obtention du grade de Docteur ès Sciences

par

Amber Dawn BOWLER

Acceptée sur proposition du jury

Prof. M. De Palma, président du jury
Prof. F. Radtke, directeur de thèse
Prof. T. Petrova, rapporteuse
Prof. E. Meylan, rapporteur
Prof. J. Huelsken, rapporteur

École polytechnique fédérale de Lausanne

2023

"I made a bet. I lost. But it still paid off."

— Ryan Reynolds, 2022

Colonoscopies save lives.

To my deeply loving parents and best friends, Curtis and Anita Bowler. . .

Acknowledgements

First and foremost, I would like to express my deepest gratitude to my thesis advisor, Freddy. His unwavering support, insightful feedback, and invaluable mentorship have played an instrumental role in my journey through this research. His patience and dedication in guiding me through the complexities and challenges of our work have not only shaped this thesis but have also significantly contributed to my growth as a scientist. Thank you for your constantly pushing me to my limits to succeed and for fostering an environment of intellectual curiosity and rigour. These are values I will carry forward with me, thanks to your mentorship. Thank you.

My sincere appreciation extends to my thesis committee as well. Drs. DePalma, Huelsken, Petrova and Meylan, your invaluable insights, constructive criticisms, and thought-provoking questions have driven me to refine and expand my research perspective. Each meeting with you was an opportunity for growth, and I am thankful for the time and intellectual energy you've invested in reviewing my work. Your guidance has been integral in shaping this thesis and has certainly influenced my scientific thinking and approach. I am truly grateful for your guidance on this academic endeavor.

To Ute Koch, who was my first contact point in the lab and who has given me invaluable input and friendship over the years: what a pleasure it has been to know such a caring and passionate being. Your worth is beyond what you may realise, your strength inspiring and your science is simply impeccable.

To my lab colleagues, past and present, thank you for making our lab not just a place for research, but also a community to grow within. To Pasqualina, my first desk mate, I have loved knowing your kindness and optimism; thank you for all of the support you gave me these last months in the lab, it was beyond appreciated. Jelena, you are so witty, so kind and so caring, what a blessing it has been to spend time with you each day. Thank you to Marianne, who helped me with many an experiment and to find many a brunch location. Nadine thank you for teaching me and inspiring me to learn bioinformatics during the Covid lockdown, and for the invaluable wine conseils. To Christelle for being an absolute sun-beam of a human and always reminding me (and everyone) "it is time for coffee!"– oh! and for introducing me to la moutarde de Bénichon. To Michele, Charlotte and Raj – I was so happy to have worked with you.

To AB– I am so so so so soooooooo happy that you joined the lab, it has been such a blast to AB around with you. To Mariia, your seemingly infinite kindness is amazing, and I look forward to many more game nights. To Mario and Erhan, it has been a pleasure to work together. Delphine, Linlin, Fabia, Fred, and Helena it was a delight to work together. To the latest addition to the lab: Maxime, I look forward to see you thrive in the lab and to after work drinks. To the latest iteration of Bay 3: it has been so much fun, and I will miss you three. Joaquim, it has been so nice to get to know you, and I hope we can also do board game nights in the future. Elia, it has been an amazing experience working alongside you. Thank you for graciously sharing a bench and desk with me for the last year– I cannot wait to see what you do with them. To Morgane, what fun we have had together in bay 3 since (at least?) four years– I hope we can caddie together one day.

To Rachel and Ana, it has been inspiring and joyful to work with the both of you, and I look forward to staying in touch. To Ana: I am so excited for this new change coming in your life! Vincent Roh, thank you so much for helping me when I desperately needed it. Daniele, you are not only a great friend, but also an great bioinformatician – thanks again!

Thank you to the facilities for their constant support that was so efficient that at times it was "invisible". The HCF - Jessica, Gianni, Nathalie and Agatha. The CPG - Pierre, Laeticia, Margaux, Marina, Ibra, Léticia, Valerie, Sandrine, Arthur, Phoukham, Emilie, Isabelle, Xavier,

and Julie (and all of the others behind the scene) merci beaucoup! The GECF: Bastien, Elisa, Lionel. The BIOP, the BSF, and the FCCF - thank you so so much!

To my floor colleagues: Estelle, Maxime, Angela, Mathieu, Wouter, Mae, Alan, Nahal, Tim, Bruno, Amaia, Ali, Natalya, Albert, Justine, Marina, Kate, Céline, Aspasia, Vamsi, Carlos, Roberta, Asli, Elena, Konstantina, Divyanshu, Ruxandra, Kanu, Hazel, Tao, Alexandre, Célie, Pierre, Luqing, and all of the others, past and present, thank you for being so miuch fun to know.

To my dear friends, thank you so much for being there. I value our friendship more than my cell phone avoidance may allow you to know. Greg and Tina, my first friends in Lausanne and besties 5 ever–no back-sies. Rob, the bestest co-patriot there ever was. Fleur, Lolo, Aga, Simge – may the game nights continue. To Fréderica and Mateusz – you were, and continue to be, the best lock-down buddy choices ever; also: satellite bay forever. Dear Aaron, you are one of the kindest people I have ever known, and I look forward to spending more time together for brunches or cultural activities. Yahya, Olga, Céline, and Fabio for not only being the best colleagues but also amazing friends. Larise, Alexey, Yolanda, Stefan, Sam, Chris, Daniele, Francesco (and others mentioned previously and after this)– can we rent a chalet together when we are 40? Lila, for being one of the sweetest people I have known, I look forward to continued friendship. Miss Luisa, the other half of the blondie revolution, I will always treasure our friendship. AK, Angelique and Margherita, Team North America soul sisters from day one, I love you all so much (PS AK is an honorary member of the team).

To my friends and family back home: Grandma and Grandpa Bowler, Grandma DeAnna – I love you so. Aunts and Uncles that I love so much: Ted, JoAnn, Jodi, Paul, Mary, Bert, Paul, Julie, Mark, Annette, Gary and Sue. This PhD was also supported by treasured non-genetic Aunts and Uncles: Melinda, Jay, Doug, Toni, Hugh, and Marilyn. Genetic and non-genetic cousins: Robyn, Alec, Rose, and Evan; Tristan, Ryan, Jessie, Jennifer, Natalie, Jammie, Michelle, Sid, Nicole, Kiera, Payton, Taleah, and Lily. I love you all very much.

To my loving, infinitely kind, sweet and funny boyfriend Alex: I am so happy to have met you, and I cannot wait for the years to come with you. Ti amo. To Alex's parents, Marco and Marisa, thank you so much for raising an amazing man, and for being so wonderful to me. To

my big brother Kyle and sister-in-law Mia, I love you both so so much, and am so excited to see where life is taking you. To my dear parents, I cannot say enough, so I will say only this: I love you so very much, thank you for raising me and loving me.

Gaioli in Chianti, 5 October 2023 A. B.

Abstract

Colorectal cancer is the second-leading cause of cancer death worldwide. Early-stage disease can be detected with preventative medical screening and is treatable with surgical resection. Sixty-percent of patients, however, are diagnosed with advanced-stage disease[1]. With the current treatment options including mainly chemotherapeutic regimens and targeted therapy where applicable, five year survival for these patients is a mere 14%. Immunotherapeutic strategies that bolster the anti-tumor capabilities of the immune system have offered hope to patients, clinicians and researchers alike by rendering complete and/or durable responses in some cancer patients[2,3]. High T cell infiltration is associated with favorable treatment outcomes (immunotherapy and chemotherapy inclusive) in human CRC[4–6]. Because cytotoxic T cells rely on direct contact with their targets, treatments that potentiate or drive T cell recruitment into tumors represent an opportunity to improve treatment outcomes[7].

In this work, we investigate the tumor microenvironment (TME) of three genetic mouse models of colorectal cancer with accumulating mutations that reflect the oncogenic driver mutation of colorectal cancer, namely, APC, KRAS and p53[8]. We therefore compared the TME of $Apc^{lox/lox}$ $CDX2CreERT2^{Tg/+}$ (A-mice), $Apc^{lox/lox}$ $LSL\text{-}Kras^{G12D/+}$ $CDX2CreERT2^{Tg/+}$ (AK-mice), and $Apc^{lox/lox}$ $LSL\text{-}Kras^{G12D/+}$ $Trp53^{lox/lox}$ $CDX2CreERT2^{Tg/+}$ (AKP-mice) by flow cytometry and single-cell RNA sequencing (scRNAseq). We found that constitutively-active KRAS tumors were associated with increased T cell presence within the tumors compared to tumors without the mutation. scRNAseq enabled the precise definition of tumor cell clusters

and thus the direct comparison of the transcriptome of tumors with (AK- and AKP-mice) and without the KRAS activation (A-mice), enabling us to unravel the link between KRAS activation and T cells in the TME.

We found that Annexin A1 (Anxa1) was differentially expressed by *Kras*$^{G12D/+}$ bearing tumors compared to tumors without. Furthermore, we show that *ANXA1* expression is significantly associated with high immune cell infiltration in colorectal cancer patients. Deeper analysis into the function of Anxa1 and its role in T cell recruitment in the TME of CRC is required. Ultimately, a therapy that recruits T cells (perhaps inspired by Anxa1) could be combined with an immunotherapeutic regimen to increase its efficacy. Moreover, we validated that these mouse models respond modestly to αCTLA4 or αCD40 monoclonal antibody treatment, and thus could be advantageously combined with a T cell recruitment therapy.

Additionally, we defined how the TME of mouse models with differential tumor-driving mutations (A-, AK- and AKP-mice) changed over time. With a longitudinal study, were able to observe that T cell abundance is dynamic over time within all three models and that the moment of maximal T cell infiltration for each model was dependent on the oncogenic-driver mutations borne by the mouse model. Single-cell TCR-sequencing of AKP-tumors showed robust TCR expansion in response to tumor formation, suggesting that APC, KRAS and p53 mutations within the same model is sufficient to induce an adaptive immune cell response.

Key words: colorectal cancer, tumor microenvironment, immunotherapy, genetically engineered mouse models, Annexin A1

Résumé

Le cancer colorectal est la deuxième cause de décès par cancer dans le monde. La maladie à un stade précoce peut être détectée grâce à un dépistage médical préventif et peut être traitée par résection chirurgicale. Soixante pour cent des patients sont cependant diagnostiqués à un stade avancé de la maladie. Avec les options thérapeutiques actuelles, qui comprennent principalement des régimes chimiothérapeutiques et des thérapies ciblées le cas échéant, la survie à cinq ans de ces patients n'est que de 14%. Les stratégies immunothérapeutiques qui renforcent les capacités anti-tumorales du système immunitaire ont donné de l'espoir aux patients, aux cliniciens et aux chercheurs en apportant des réponses complètes et/ou durables chez certains patients atteints de cancer. Une infiltration élevée de cellules T est associée à des résultats thérapeutiques favorables (immunothérapie et chimiothérapie confondues) dans le cancer colorectal humain[4-6]. Étant donné que les cellules T cytotoxiques dépendent du contact direct avec leurs cibles, les traitements qui potentialisent ou stimulent le recrutement des cellules T dans les tumeurs représentent une opportunité d'améliorer les résultats du traitement[7].

Dans ce travail, nous étudions le microenvironnement tumoral (MET) de trois modèles de souris génétiques de cancer colorectal avec des mutations accumulées qui reflètent la mutation pilote oncogénique du cancer colorectal, à savoir, APC, KRAS et p53[8]. Nous avons donc comparé la MET de *Apc$^{lox/lox}$ CDX2CreERT2$^{Tg/+}$* (souris-A), *Apc$^{lox/lox}$ LSL-Kras$^{G12D/+}$ CDX2CreERT2$^{Tg/+}$* (souris-AK), et *Apc$^{lox/lox}$ LSL-Kras$^{G12D/+}$ Trp53$^{lox/lox}$*

CDX2CreERT2$^{Tg/+}$ (souris-AKP) par cytométrie en flux et séquençage de l'ARN d'une seule cellule (scRNAseq). Nous avons constaté que les tumeurs qui portent KRAS constitutivement actives étaient associées à une présence accrue de cellules T dans les tumeurs par rapport aux tumeurs sans mutation. scRNAseq a permis de définir précisément les groupes de cellules tumorales et donc comparer directement le transcriptome des tumeurs avec (souris -AK et -AKP) et sans activation KRAS (souris-A), ce qui nous a permis d'élucider le lien entre l'activation KRAS et les cellules T dans le MET.

Nous avons constaté que le proteine Annexin A1 (Anxa1) était exprimée de manière différentielle dans les tumeurs avec *KRAS*$^{G12D/+}$ par rapport aux tumeurs sans qui le manque. En outre, nous montrons que l'expression de *ANXA1* est significativement associée à une forte infiltration de cellules immunitaires chez les patients atteints de cancer colorectal. Une analyse plus approfondie de la fonction d'Anxa1 et de son rôle dans le recrutement des cellules T dans le MET du cancer colorectal est nécessaire. En fin de compte, une thérapie qui recrute les cellules T (peut-être inspirée par Anxa1) pourrait être combinée à un régime immunothérapeutique pour augmenter son efficacité. Par ailleurs, nous avons validé le fait que ces modèles de souris répondent modestement au traitement par anticorps monoclonal αCTLA4 ou αCD40, et qu'ils pourraient donc être avantageusement combinés à une thérapie de recrutement des cellules T.

En plus, nous avons défini comment l'EMT des modèles de souris présentant des mutations tumorales différentielles (souris A-, AK- et AKP) évoluait au fil du temps. Grâce à une étude longitudinale, nous avons pu observer que l'abondance des cellules T est dynamique dans le temps au sein des trois modèles et que le moment de l'infiltration maximale des cellules T pour chaque modèle dépend des mutations oncogéniques porteuses du modèle de souris. Le séquençage TCR unicellulaire des tumeurs AKP a montré une expansion robuste du TCR en réponse à la formation de la tumeur, ce qui suggère que les mutations APC, KRAS et p53 dans le même modèle sont suffisantes pour induire des néoantigènes tumoraux contre lesquels les hôtes peuvent monter une réponse.

Mots clefs : cancer colorectal, microenvironnement tumoral, immunothérapie, souris

génétiquement modifiée, Annexin A1

Contents

List of Figures

List of Tables

1 Introduction

1.1 The healthy colon

The gastrointestinal tract represents an internal contact point between our bodies and the outside world. The food we eat passes through the esophagus to the stomach to the small intestine where millions of villi and crypts absorb nutrients. After passing through the hedge maze of the small intestine, waste is then passed into the large intestine, or colon. The main objective here is to absorb any excess liquid and electrolyte from the feces and prepare the waste to exit the body. In order to achieve this function and, as opposed to the small intestine, the colon has only crypts and no villi. Colonic crypts contain intestinal stem cells that continuously give rise to differentiated daughter cells, orchestrating a constant trafficking of specialised gut epithelial cells through the colonic crypt epithelium upward to the lumen of the colon. The intestinal stem cell division is so rapid that mammalian colons completely renew every 4-5 days[9]. Stem cells give rise to a semi-differentiated cell type called transit amplifying cells that quickly divide and give rise to specialsed colonic epithelial cells. Among these cells, three main differentiated cell types make up the crypt: enterocytes, enteroendocrine cells, and goblet cells.

Enterocytes are the most abundant cell type in the colonic crypt. Their primary function is the absorption of water and electrolytes from the indigestible remains of food, called chyme.

This function is critical for maintaining fluid balance in the body and chyme solidification. Enterocytes posses surface structures called microvilli that enables their function due to their absorptive function by increasing their membrane surface area. Enteroendocrine cells, although the least abundant cell type in the colon, play a vital role in the regulation of digestive processes. They produce various hormones that help regulate fluid balance, release bile and pancreatic enzymes, as well as regulate intestinal motility. Mucus-secreting goblet cells are abundant within healthy colonic crypts. Goblet cell-derived mucus serves as a protective barrier for the colonic epithelium against mechanical stress and potential pathogens while also providing a hospitable environment for beneficial gut microbiota[10].

Epithelial cells are not, however, the only major cell type that resides in the colonic crypt: intraepithelial lymphocytes incorporate themselves amongst the epithelial cells in the lining of the colon. These cells play a crucial role in immune surveillance, defending against pathogenic bacteria or virally-infected cells while tolerating the presence of beneficial gut microbiota. Furthermore, just beneath the epithelial layer is a thriving microenvironment called the lamina propria (LP) of the colon that is composed of numerous cell types including, but not limited to fibroblasts, immune cells (T cells, B cells, neutrophils, mast cells, macrophages, dendritic cells and plasma cells), as well as vascular and lymphatic endothelial cells[10]. Fibroblasts are the most abundant cell type in the LP and are responsible for the production and maintenance of the extracellular matrix which provides the structural scaffolding around which the epithelial and other cells organise. Vascular vessels run throughout the LP providing oxygen and fresh immune cells to the environment and carrying away the water, electrolytes and vitamins absorbed from the chyme. Lymphatic vessels similarly carry away excess fluid from the tissue while also provide means of transport for immune cells to and from proximal lymph nodes. Immune cells patrol the colon for pathogens and infected cells[10].

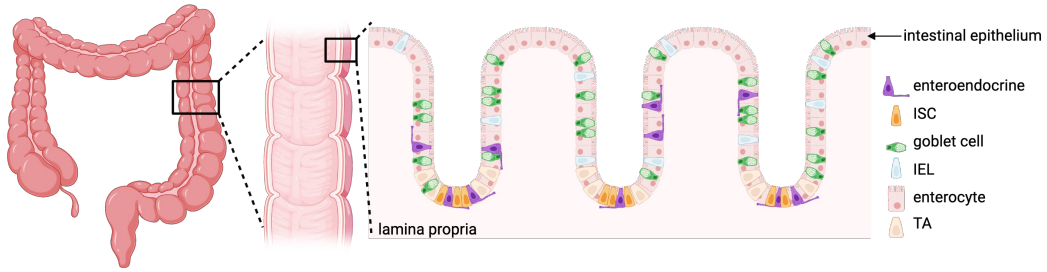

Figure 1.1 Gross and crypt-level morphology of the human colon. Left: the human large intestine (comprised of the cecum, ascending, transverse and descending colon, Center: cross section of the colon, Right: diagram showing the spatial organisation of intestinal epithelial cells in the colonic crypt. ISC: intestinal stem cell. IEL: intraepithelial lymphocyte. TA: transit-amplifying cell. Created with BioRender.com

1.2 Colorectal Cancer

Worldwide, colorectal cancer (CRC) is the second-leading cause of cancer death after lung adenocarcinoma (LUAD), responsible for about 800,000 deaths each year[1,11]. Over 50% of cases can be partially attributed to lifestyle factors like smoking, poor diet or excess alcohol consumption[1]. Unfortunately, colorectal cancer is asymptomatic until late-stage disease, highlighting the importance of regular colonoscopies where indicated. Early-stage disease can be easily treated with surgical resection with or without chemotherapy, but about 60% of patients have advanced disease upon diagnosis[1]. Regular screening by colonoscopy for patients over 45 years of age has reduced incidence and mortality of the disease overall[11]. Recent studies, however, show that the disease may be becoming more frequent in younger patients and that tumors are more advanced upon diagnosis[1,12]. The reasons for these shifts is currently unknown, but are suspected to be associated with evolving environmental and lifestyle influences which could lead to the accumulation of oncogenic mutations.

Colorectal cancer is known to develop through a progressive accumulation of mutations in colonic epithelial cells over time beginning with loss of function mutations in the adenomatous polyposis coli (APC) gene[13,14]. Without functional APC, cells form small, benign adenomas that grow and divide faster than adjacent healthy cells. As time goes on this rapid rate of proliferation potentiates further mutations which can be silent or in oncogenes and tumor

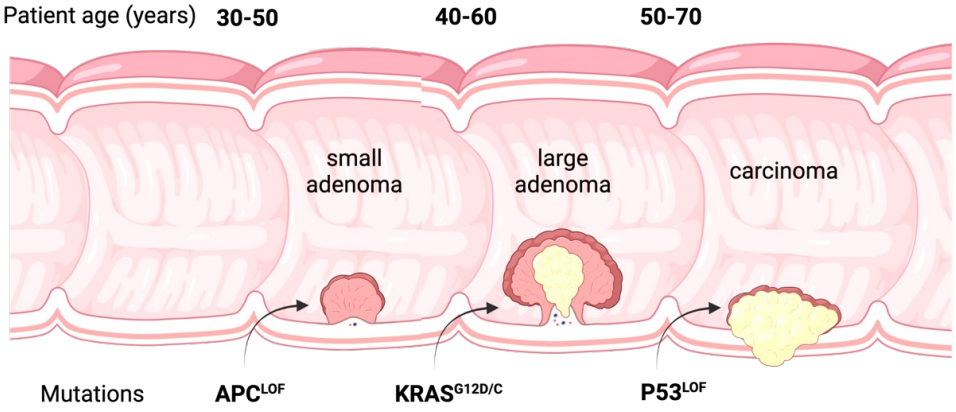

Figure 1.2 Adenoma to carcinoma progression model proposed by Vogelstein. Tumor initiation in CRC begins with loss of function of APC usually in patients 30-50 years of age, over time activating KRAS mutations accumulate increasing the severity of the disease. The addition of TP53 mutations is associated with progression from adenoma to carcinoma. Adapted from Vogelstein *et al.* [14]. Created with BioRender.com

suppressors like kirsten rat sarcoma (KRAS) and tumor protein p53 (TP53)[14]. These additional mutations in KRAS drive tumor progression from adenoma to a more rapidly dividing adenoma, while P53 loss of function mutations are associated with the progression from adenoma to carcinoma and eventually metastasis[8,14], Figure 1.2. The molecular pathways affected by these cumulating mutations have been well-defined.

1.2.1 WNT signaling

WNT is a portmanteau for Wingless and Int-1-related family of proteins[15]. The WNT pathway is essential in embryonic development and the maintenance of various adult tissue including hair follicles, liver, the hematopoietic system and the intestine[16,17]. The APC protein is part of a multi-protein destruction complex (made up of AXIN, GSK-3β and CKIα) in the WNT signaling pathway that plays a pivotal role in regulating tissue homeostasis by tagging β-catenin for destruction. In the presence of Wnt ligands, the APC-containing multiprotein complex is inhibited by Dishevlled downstream of the WNT receptor Frizzled, Figure 1.3a. Consequently, β-catenin is stabilised and liberated to translocate to the nucleus and associates with T cell factor (TCF) transcription factors to induce growth and proliferation related gene expression[17,18], Figure 1.3a. In the absence of WNT ligands, however, the multi-protein

complex phosphorylates the N-terminus of β-catenin. The phosphorylation of β-catenin leads to its eventual ubiquitination and subsequent proteasomal degradation, Figure 1.3b. In the intestine, the transcription factor complex partner of β-catenin is TCF4 and together they induce the expression of genes that enable self-renewal of the intestine[18]. As a consequence of APC loss-of-function mutations in gut epithelial cells, the destruction complex can no longer assemble to tag β-catenin for degradation and it can associate with TCF4 to induce transcription of growth and proliferation genes, Figure 1.3c. The transformed cells thus cycle more often than their neighboring cells, leading to the formation of small adenomas, the first step in oncogenic transformation of CRC.

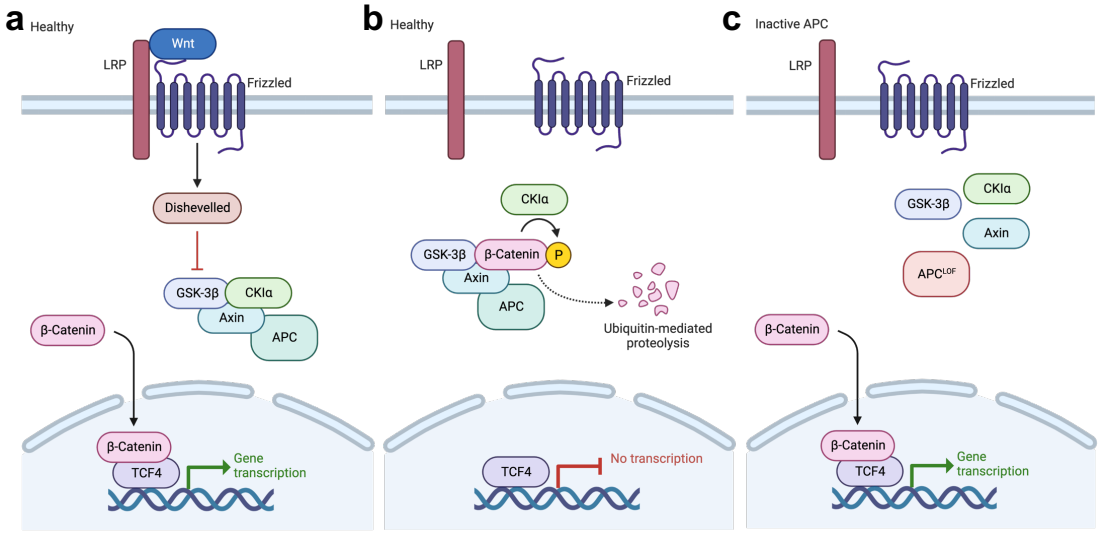

Figure 1.3 WNT signaling in healthy and mutant APC contexts in intestinal epithelial cells. **a.** In the presence of WNT ligands, the destruction complex composed of proteins APC, AXIN, GSK-3β and CKIα are inhibited by Disheveled. β-catenin can enter the nucleus and initiate transcription in coordination with TCF4. **b.** In the absence of WNT-ligands the destruction complex phosphorylates β-catenin, enabling it's ubiquitination and eventual proteolysis. **c.** In the context of a loss-of-function APC mutation the destruction complex can no-longer effectively phosphporylate β-catenin, enabling it to act within the nucleus. Adapted from Radtke & Clevers [18]. Created with BioRender.com.

1.2.2 MAPK signaling

KRAS signals through a large protein family made up of many serine and threonine kinases collectively referred to as the mitogen-activated kinase (MAPK) family. The MAPK signaling cascade is present in all eukaryotic cell types where its effect is highly context-dependent[19].

These proteins that mainly propagate signals relayed to them by G-proteins phosphorylated by receptor tyrosine kinases (such as epidermal growth factor receptor (EGFR)) in response to extracellular stimuli (epidermal growth factor (EGF)-ligand)[19]. KRAS itself is a hydrolase enzyme that binds to guanosine triphosphate (GTP) created by the tyrosine kinase receptor, phosphorylates MAPK family members, then releases guanosine diphosphate (GDP)[19]. The phosphorylation signal then propagates from rapidly accelerated fibrosarcoma (RAF) to mitogen activated protein kinase (MEK) to extracellular-related protein kinase (ERK), which can pass into the nucleus to activate transcription factor targets for DNA binding, Figure 1.4a. In the absences of an extracellular signal, this cascade does not occur, Figure 1.4b. Thus, in the healthy context, MAPK signaling is tightly controlled by extracellular stimuli and their receptors. For example, MAPK signaling controls the differentiation of goblet and paneth cells in the intestine, but the signaling is tightly controlled by Shp2[20].

MAPK signaling can, however, unravel into an incorrigible signaling cascade with a single point mutation. KRAS is frequently mutated at the 12^{th} or 13^{th} residue where the glycine is mutated into an aspartic acid or cysteine (notated as $KRAS^{G12D/C}$ or $KRAS^{G13C/D}$). These mutations result in the formation of a constitutively active KRAS protein capable of constant phosphorylation of RAF proteins[21], Figure 1.4c. The constant flux of active ERK to the nucleus results in active transcription of pro-growth and proliferation genes, again conferring more rapid division to cells bearing the $KRAS^{G12D}$ mutation. Tumors bearing APC and KRAS mutations, however, are rarely observed to be invasive[14]. Further alterations are required for the disease to become invasive.

1.2.3 P53 signaling

TP53 is the gene that produces the p53 protein, a transcription factor long known as the "guardian of the genome" due to its vital role in the control of cell division and induction of apoptosis in cells that have been subject to DNA damage[22]. In response to DNA damage or oncogene-mediated replication stress ATM and ATR kinases trigger the p53 pathway[23]. At homeostasis, p53 is maintained at a low level by constant degradation induced by MDM2,

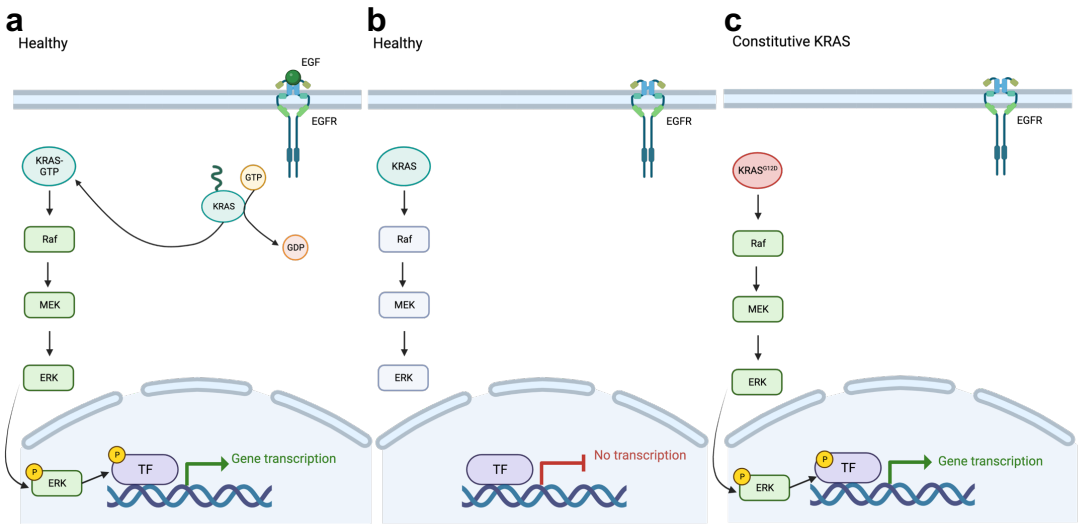

Figure 1.4 MAPK signaling cascade in the healthy and mutant-KRAS contexts. In the healthy context, **a.** upon EGF binding to EGFR, KRAS proteins carry a phosphorylation signal to RAS which propagate through MEK to ERK, which translocates to the nucleus to induce transcription of growth and proliferation genes **b.** in the absence of EGF, the cascade is not active. **c.** In the case of KRAS-activating mutations such as KRAS^{G12D}, the cascade is constantly active– even in the absence of EGF–resulting in uncontrolled growth of the mutant cell. Created with BioRender.com.

an E3 ubiquitin ligase[23]. Upon ATM and ATR activation of p53, p53 is not longer tagged for degradation by MDM2, leading to an increased concentration of p53 in the cell. P53 plays an important part in cell cycle arrest, DNA repair, induction of apoptosis and senescence[24], Figure 1.5. P53 is capable of inducing cell cycle arrest through activation of transcription for P21/WAF1/CIP1[23]. Cell cycle arrest gives time to the DNA repair machinery to repair damage before the cell can replicate, but could also be permanent and result in senescence[25,26]. Senescence is an efficient defense against cancer, resulting in the accumulation of non-cycling live cells as opposed to infinitely proliferative cancer cells[27,28]. On the other hand, should the DNA damage be too severe or irreparable, p53 induces the expression of a family of proteins known as "BH3-only" including PUMA and NOXA which inhibit anti-apoptotic proteins BCL-XL, BCL-2 and MCL-1[29]. The inhibition of anti-apoptotic proteins thus allows pro-apoptotic proteins BAX and BAK to initiate apoptosis of the cell[29]. Whether a cell undergoes cell cycle arrest or apoptosis is thought to be a function of post-translational modification of p53 and the proteins it interacts with[23].

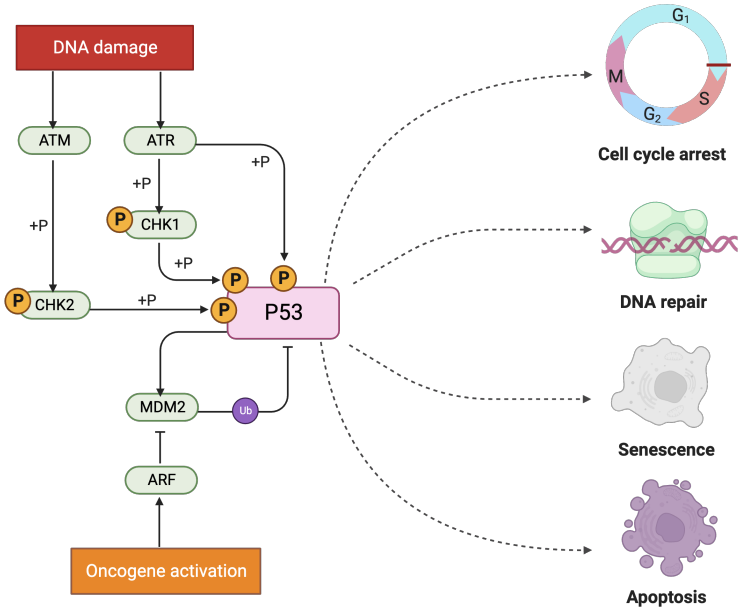

Figure 1.5 Function and regulation of P53 in the context of DNA damage and oncogenic activation. DNA damage induces the activation of ATM and ATR in the healthy context, subsequently activating P53 to induce cell cycle arrest, DNA repair, senescence or apoptosis. P53 also promotes the transcription of MDM2, an E3 ubiquitin ligase, that targets P53 for destruction, thus establishing a "self-regulated" feedback loop. When malignant transformation begins in a cell, ARF associates with MDM2 and prevents the degradation of P53, allowing it to fight against oncogenic transformation. Adapted from Bieging *et al.* [28] and created with BioRender.com.

Somatic p53 mutations are thus among the most frequent in colorectal cancer as they allow the highly proliferative cells to escape the threat of oncogene-induced senescence or apoptosis mediated by p53[14,28]. p53 mutations are correlated with an increasingly invasive histological phenotype, presumably because the growth and proliferation induced by other mutations are no longer kept in check.

1.3 Treatment options for colorectal cancer

How a patient with colorectal cancer is treated is determined jointly by the oncologist and patient, largely informed by the stage of the disease at diagnosis and the patient's overall health. If during a routine screening a polyp is identified it is removed along with some adjacent healthy tissue. Stage I and II colorectal cancer are also treated with surgical

resection, but the tumor-draining lymph nodes are additionally removed. Stage II colorectal cancer may also be treated with adjuvant chemotherapy following surgery including drugs such as 5-fluorouracil (5FU) or oxaliplatin. 5FU is a thymidylate synthase inhibitor effectively depriving dividing cells of an essential nucleotide required for DNA replication[30]. Oxaliplatin is a platin-based drug that causes inter- as well as intra-strand DNA crosslinks which prevent proper DNA replication and transcription, which results in cell death[31]. Stage III, in which it has been found that the disease has invaded the local lymph nodes, colorectal cancer is treated with surgical resection followed by chemotherapy. Patients diagnosed with stage IV disease at diagnosis are treated with modalities appropriate to their tumor including, but not limited to: surgical resection of the primary tumor and metastases, chemotherapy, targeted therapy and immunotherapy[32].

Chemotherapy for advanced-stage colorectal cancer do not only consist of 5FU or oxaliplatin, but also combinations of these drugs with other multiple chemotherapy modalities. The FOLFIRI regimens, for example incorporate folinic acid (FOL, a vitamin B derivative that synergizes with 5FU[30]), 5FU (F), and irinotecan (IRI, a topoisomerase inhibitor) for more effective treatment. Other chemotherapy combinations include FOLFOX (folinic acid, 5FU and oxaliplatin) and XELIRI (Xeloda [a drug very similar to, but less toxic than 5FU] and irinotecan). These chemotherapy regimens may be used in combination with targeted therapies.

Targeted therapies aim to clip the Achilles heel of each cancer by targeting the tumor-driving mutations and proteins such as BRAF, EGFR, or vascular endothelial growth factor (VEGF)[32]. For example, cetuximab is a commonly used monoclonal antibody (mAb)-based EGFR inhibitor to abrogate MAPK signaling. Aflibercept and bevacizumab are VEGF inhibitors for treatment of metastatic colorectal cancer frequently used in combination with chemotherapy regimens[33]. All targeted treatments, however, require the patient to bear the mutation that is being targeted, and unfortunately colorectal tumors bear numerous somatic mutations[34]. Patients treated with targeted therapy thus often experience relapse because tumor cells without the targeted mutation survive the treatment[35].

Immunotherapy represents a more recent beacon of hope for oncologists, patients and researchers, as some patients have achieved complete and durable remission[2,3,36]. There are now a variety of immunotherapeutic modalities under investigation[36], but the general aim of immunotherapy is to assist the immune system in its fight against neoplastic cells. The pioneering and clinically successful immunotherapies for the treatment of cancers were ipilimumab (αCTLA4 mAb), nivolumab (αPD1 mAb) and atezolizumab (αPD-L1 mAb)[37,38].

Physiologically, T cells are activated on the condition of major histocompatibility complex (MHC) antigen presentation by an APC to the T cell receptor (TCR) of a T cell. The duration of this interaction *in vivo*, however, is often not long enough to achieve a biologically effective T cell activation[39]. CD28 is a TCR co-receptor that acts as a co-stimulatory molecule which, when engaged by CD80 or CD86 (expressed on the surface of dendritic cells) strengthens the activation signal within the T cell despite the transient TCR stimulation, Figure 1.6a. Though this T cell activation is productive in the context of infection or neoplasia, cells self-regulate their activation very tightly and activation leads to the production of cytotoxic T lymphocyte antigen 4 (CTLA4) (a paralog of CD28) that when engaged by CD80 or CD86 has a signal dampening effect[39]. In the context of cancer immunotherapy, antagonistic CTLA4 antibodies have thus been used to help support or maintain stimulated T cells in their active state[36], Figure 1.6a.

On the other hand, the programmed cell death protein 1 (PD1) is a checkpoint molecule expressed by activated T cells that prevents them from attacking other cells derived from the host. When engaged by it's ligand, programmed cell death ligand 1 (PDL1), the T cell experiences negative signaling enable by SHP2 that inhibits the MAPK signaling cascade within the T cell, negating the effects of TCR and CD28 stimulation[36]. PD-L1 is not only expressed by benign self cells like macrophages and dendritic cells, but also by tumor cells, preventing their destruction by educated T cells[36]. For this reason, targeting this interaction with antagonist monoclonal antibodies eliminates this clever immune evasion mechanism of the malignant cells.

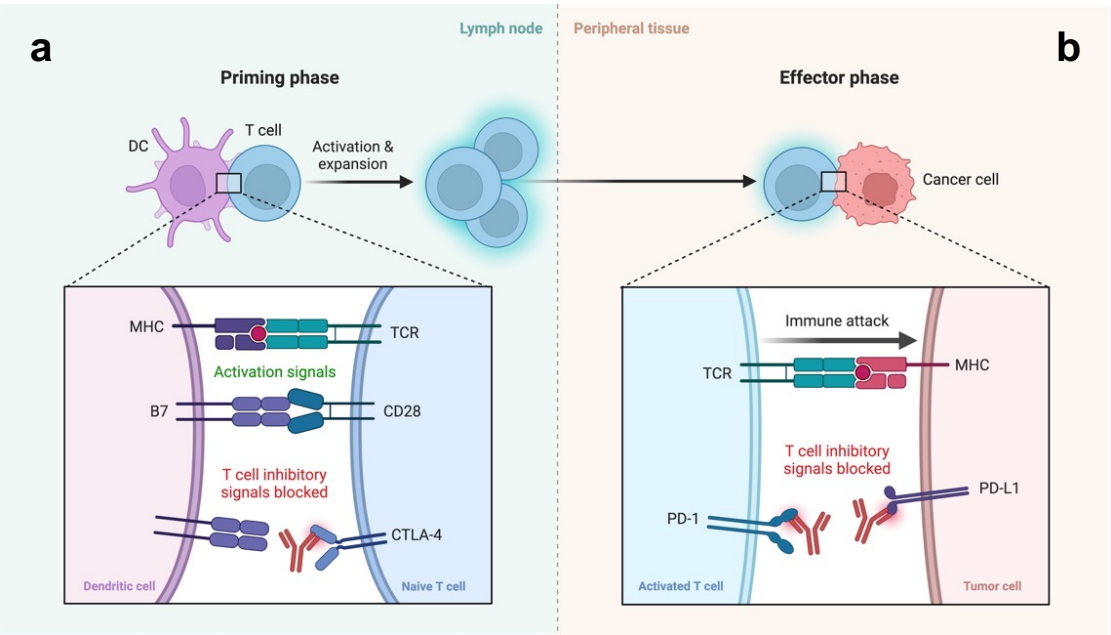

Figure 1.6 Role of CTLA4 and PD1 checkpoint blockade molecules and consequences of targeting them with monoclonal antibodies. In the healthy context, **a.** upon EGF binding to EGFR, KRAS proteins carry a phosphorylation signal to RAS which propagate through MEK to ERK, which translocates to the nucleus to induce transcription of growth and proliferation genes **b.** in the absence of EGF, the cascade is not active. **c.** In the case of KRAS-activating mutations such as $KRAS^{G12D}$, the cascade is constantly active– even in the absence of EGF–resulting in uncontrolled growth of the mutant cell. Adapted from Ribas [40], retrieved from BioRender.com.

Not every patient qualifies for immunotherapy, in fact the target group for immunotherapies is fewer than 15% of the population[41]. This is because immunotherapeutics like pembrolizumab and ipilimumab rely heavily on tumor antigen presentation by dendritic cells which requires the tumor cells themselves to present neoantigens on MHCI molecules[42]. As mentioned above, because cancer cells are derived from the host's own cells, they are often able to evade tumor immunity because they appear to be "self" to professional antigen presenting cell (pAPC)s. Fifteen percent of the human population, however, have mismatch repair deficient (MMRd) machinery in their cells, which in turn increases the tumor mutational burden as mutations accumulate over the many cellular divisions over time and especially in the context of oncogene-driven proliferation[41]. The molecular bases of MMR-deficiency in patients are typically germline mutations in MMR genes like *MSH2, MSH6, PMS2* or *MLH1*, or epigenetic silencing of the latter[43]. Patients with these mutations carry a microsatellite instable (MSI) signature phenotype which is identified using PCR amplification at known

microsatellite loci throughout the genome and comparing the length of the PCR products to that of normal cells[43,44]. Across all cancers, MSI tumors tend to respond very well to immunotherapy[45]. This could be due to differential T cell infiltration of tumors or tumor neoantigen expression by MSI tumors. It has been shown that MSI tumors have higher T cell infiltration compared to microsatellite stable (MSS) patients[6]. Although difficult to directly measure, MSI patients are predicted to have higher neoantigen burden than MSS patients based on RNA sequencing[46]. In the context of immunotherapies, MMRd is highly advantageous as dendritic cells perhaps begin to recognize the neoplastic cells as "non-self" and target them for destruction by educating T cells which can be supported by therapies like ipilimumab[36,41,42].

More recent developments involve the use of agonistic antibodies for molecules that can induce increased activation of immune cells. For example, CD40 is a molecule expressed on the surface of macrophages and dendritic cells that, when bound by CD40L (usually expressed transiently on the surface of $CD4^+$ T cells upon antigen recognition[47]) increases the activation of dendritic cells and macrophages[48,49]. The pAPCs are then mobilised toward greater antigen presentation[50]. Immunotherapy is currently a white-hot area of research and several teams are working on engineering novel, more specific, less toxic, and more powerful versions of these molecules[51,52]. Areas of particular progress to-date include bi- and tri-specific antibodies as well as cell-based therapies like chimeric antigen receptor (CAR) T cells and engineered dendritic cell vaccines[51,53]. The tumor microenvironment largely determines which immunotherapies will be effective base on which cells are present, and which molecules they express.

1.4 The tumor microenvironment

Within the tumor microenvironment (TME), there are not only tumor cells but also many other cell types and factors that contribute to cancer progression and response to treatment[54,55]. Tissue context, local immunity and systemic immunity are all contributing factors in cancer

initiation, progression and response to therapy[56]. Within epithelial tissues, the structure is provided by extracellular components such as laminin, collagen and fibronectins, produced mainly by fibroblasts. In a healthy context, fibroblasts produce these extracellular components upon activation that contribute to tissue rigidity and structure, but oncogenic transformation can lead to perpetual fibroblast activation that actively contributes to tumor progression[57].

The structure established by the extracellular matrix may or may not be vascularised depending on the soluble factors secreted by tumor cells or fibroblasts. As an effect their rapid division, tumors establish an hypoxic environment, thereby inducing a family of transcription factors called hypoxia-inducible factors (HIF)[58]. These factors activate transcription of genes that produce cytokines and soluble factors that help to support the tumor's establishment and growth[58]. In particular, VEGF has been robustly shown to drive angiogenesis in the TME, allowing the tumor to siphon nutrients from the host to support its rapid growth[59]. Anti-angiogenic therapy has been an area of particular interest in colorectal cancer, with the development of several promising therapies including anti-VEGF inhibitors, aflibercept and bevacizumab that have shown success in the clinics. With vascularisation comes the possibility of extravasation of immune cells into the local environment[56].

For each type of immune cell–from B cell to T cell to myeloid cells–it is possible to find the cells in the TME of many tumors[55]. Whether and which immune cells enter the TME is known to be driven by soluble factors produced by tumor cells or alternatively activated neighboring cells that induce the extravasation and migration of the cells to the TME[60]. The presence of each immune type and the factors that they produce and secrete can heavily influence tumor progression[56]. For example, in our lab we showed that neutrophils within colorectal cancer tumors produce matrix metalopeptidase 9 (MMP9) that liberates latent TGFβ[61]. The consequence is of high TGFβ is a rather immune-suppressive microenvironment characterised by T cell exclusion and or exhaustion[62] that further supports tumor progression.

High T cell infiltration is associated with favorable treatment outcomes in human CRC[4–6]. Moreover, high infiltration of cytotoxic T cells in the invasive margin of CRC hepatic metas-

tases predicts a better response to chemotherapy and prolonged survival[63]. These findings suggest that the repertoire of immune cells within tumors determines development and/or progression of these intestinal lesions and is predictive for patient survival. The identification of new ways to influence the tumor immune repertoire could therefore have a dramatic impact for CRC therapy, for example by overcoming resistance to immune checkpoint blockade inhibitors[7].

1.5 Mouse models of CRC

In order to study the TME, and importantly the effects of immunotherapy, of CRC in the pre-clinical setting, genetically engineered mouse models (GEMM)s are utilised due to their indispensable recapitulation of tumorigenesis in an immune-competent setting[64,65]. Tumor-driving mutations *Apc*, *Kras*^{G12D}, and *Trp53* have been engineered into mouse models for conditional expression in the intestine using the Cre-lox system driven by the *Villin*, *Lgr5* or *Cdx2* promoters[66]. The *Villin*-Cre model results in conditional allele recombination in the small intestine, while the *Lgr5*-Cre exhibits recombination in the stem cells of the small intestine and colon, and the *Cdx2*-Cre demonstrates recombination restricted to the colon[66]. All of these mouse models enable the study of intestinal tumors, but the *Cdx2*-Cre model is arguably the most analogous to human disease due to the recombination restricted to the colon[66].

A major limitation of these GEMMs, however, is the fact that mice frequently reach humane endpoint criteria before the disease is able to begin the invasive process, let alone formation of metastases[66]. This is largely due to the fact that tumor formation in the mouse intestine can quickly block the transit of waste through the digestive system. Among genetic models, several different combinations of conditional alleles have been tested for their propensity to manifest metastatic disease in mice, and all to date demonstrate low penetrance and prohibitory latency[66]. The study of metastatic and advanced-stage colorectal cancer pre-clinically has thus been restricted to orthotopic transplant models of colorectal

cancer into immunodeficient mouse lines[67–69]. Though the metastatic penetrance in these mouse models is high, and thus enables the study of tumor cell-intrinsic mechanism of progression or response to therapy, the study of the interaction of the tumor with immune cells and response to immunotherapy is excluded[64,66,67].

1.6 Introduction to ANXA1

In this work, we conduct single-cell RNA sequencing as a hypothesis-generating approach to discover secreted factors that influence the immune cell repertoire of colorectal cancer mouse models. This section is a short introduction to the candidate that was most interesting: Annexin A1.

The initial discovery of Annexin A1 (ANXA1) closely followed the introduction of glucocorticoids for the treatment of inflammation in the clinics. *Rubor*, *calor*, *tumor* and *dolor* make up the four calling cards of inflammation – a term used to describe a rather heterogeneous disease-state context that can be acute or chronic initially defined by the "redness", "heat", "swelling" and "pain" that manifested as a result of increased immune presence in the tissue. The role of the immune system is to overcome infection or to aid in tissue repair after injury, but such responses must be measured (not too much, not too little) and tightly orchestrated temporally otherwise chronic inflammation or autoimmunity can settle in the affected tissue, either of which can cause tissue damage and pain in the area. Glucocorticoids were identified first by Hench, Kendall and Reichstein between 1930 and 1945 for which they received the Nobel prize in 1950[70]. Patients with a variety of inflammatory diseases like rheumatoid arthritis now had relief from their debilitating symptoms, but the question remained as to what these compounds were and how they worked. By 1975 we knew that glucocorticoids affected their anti-inflammatory function by inhibiting the synthesis of pro-inflammatory eicosanoids[71] and by 1980 we knew this function was driven by second-messenger proteins induced by the glucocorticoids that acted upstream of COX1 and 2 in the eicosanoid synthesis cascade[72]. Finally, in 1986 Pepinsky and team isolated a 37 kDa protein from the peritoneum of rats

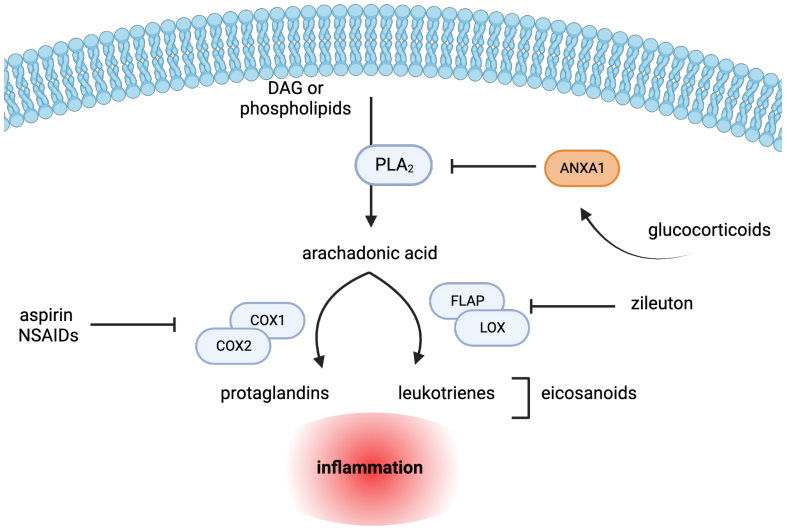

Figure 1.7 The eicosanoid synthesis pathway and its inhibitors. Phospholipase A2 (PLA2) synthesizes arachidonic acid from membrane phospholipids and diacylglycerol (DAG). arachidonic acid is turned into prostaglandins by cyclooxygenase 1 or 2 (COX1, COX2) or leukotienes by 5-lipoxygenase (LOX) and 5-LOX-activating protein (FLAP). Leukotrienes and protoglandins recruit immune cells and result in inflammation. Aspirin and non-steroidal anti-inflammatory drugs (NSAIDs) are COX1/2 inhibitors that prevent prostaglandin synthesis, relieving mild inflammation and associated pain. Zileuton is a LOX inhibitor effective at reducing leukotriene synthesis and relieving asthmatic symptoms. Glucocorticoids induce ANXA1 expression, and ANXA1 functions as a PLA2 inhibitor by sequestering its substrates, efficiently reducing the production of arachidonic acid and thus prostaglandins and leukotrienes. Adapted from Hwa *et al.* [75]. Created with BioRender.com.

that demonstrated clear inhibitory function on phospholipase A2 (PLA2) which liberates arachidonic acid by de-esterification of membrane-derived phospholipids[73], Figure 1.7. In a subsequent study the same team was able to sequence and clone this protein[74]. The PLA_2 inhibitory protein was given the name Lipocortin at the time, but is now known as Annexin A1 (ANXA1).

Annexin A1 is now known to be a member of the annexin protein family, so-named due to their propensity to annex or closely associate to the inner membrane of cells that express the protein. It was shown that ANXA1 inhibits PLA_2 by sequestering its substrates (phospholipids and diacylglycerol (DAG)) to the membrane in a calcium-dependent manner[76,77]. ANXA1 is one of three annexin family members that is known to be secreted. The main receptor of ANXA1 is formyl peptide receptor 2 (FPR2), which is often constitutively expressed on neutrophils and lowly expressed by some macrophages. FPR2 is a G protein coupled receptor

(GPCR); Upon ANXA1 binding, a canonical GPCR cascade begins with the phosphorylation of the G protein which in turn associates with PIP_2 and PLC to produce DAG and IP_3. Inositol triphosphate associates with calcium channels along the endoplasmic reticulum resulting in the release of calcium into the cytoplasm. The calcium release allows any intracellular ANXA1 to associate with the membrane where it can be secreted through ATP-binding cassette A1 (ABCA1)). ANXA1 can thus act in an autocrine, juxtacine and paracrine manner.

2 Aims

Treatment outcomes in patients with CRC correlate with the degree of immune cell (especially cytotoxic lymphocyte) infiltration within the tumor[6,7]. The degree of tumor immune infiltration has been correlated with the various mutations within the malignant cells[78], but *how* the mutations drive the tumor immune microenvironment changes remains to be shown. In this thesis, we utilize mouse models with accumulating tumor-driving mutations to study their effects on the tumor microenvironment.

2.1 Aim 1: Determine whether the tumor immune microenvironment of murine colorectal tumors changes in response to accumulating tumor driving mutations.

The first aim of this thesis is to determine whether the tumor microenvironment of murine colorectal tumors change in response to the accumulation of tumor-driving mutations. To address this aim, we utilise three GEMMs with cumulating driver mutations known to drive the progression of colorectal cancer[8]. We assess the immune cell repertoire by flow-cytometric analysis and by single-cell RNA sequencing for phenotypic and function hints of how the observed differences between the tumor microenvironments of the model can be used to select and potentiate immunotherapy response. We further searched for potential

mechanisms driven by the tumor-driving mutations that could influence the immune cell infiltration in the tumors.

2.2 Aim 2: Assess the temporal impact on the TME of accumulating tumor-driver mutations in CRC mouse models

In order to address the second aim of the thesis, to monitor how the tumor microenvironment changes over time in murine colorectal tumors with different tumor-driving mutations, we used the same models as in the first aim, but extended the latency of the disease by lowering the dose of tumor-inducing compound. We were thereby able to assess the immune cell infiltrates by flow cytometry and single-cell RNA sequencing at four different time points. Furthermore, with this model, we aimed to determine whether fewer tumor-driving allele recombination events could allow the development of more invasive tumors in the mouse model, enabling the study of tumors that represent an area of great clinical need.

2.3 Aim 3: Contribute to the development of a light-inducible colon-on-a-chip tumorigenesis model for colorectal cancer.

In collaboration with the Lutolf group, we aim to utilize their innovative 3D hydrogel scaffold organoid models to study spatially and temporally controlled tumorigenesis. By modifying A-, AK- and AKP-derived healthy colon organoids to express light-sensitive Cre, we hope to trigger gene recombination in precise regions, enabling the observation of tumor development and progression over time. We intend to validate these tumor-like structures as genuine cancerous growths, potentially contributing valuable insights to the field of cancer biology.

3 Materials and methods

3.1 Mouse work

3.1.1 Ethics, husbandry and housing

The mouse studies presented in this work were performed in accordance with regulations imposed by the canton of Vaud, Switzerland which protect the welfare of all animals, as specified in licenses VD3035.1 and VD3823. Mice were housed in the conventional breeding facility at EPFL under standard conditions (12 hour light/dark cycle at 23℃). Breeding cages were established with one male and two females of 6-9 weeks of age, and maintained until the females reached 26 weeks of age. When breeding heterozygous transgenic animals, the transgene was present in the male, and not the females. After weaning from the mother, mice were kept preferentially with at least one cage mate with a maximum of five mice per cage. Food and water were provided *ad libitum*. Housing and nesting materials with supplemental enrichment were provided when implicated. Toe biopsies for genotyping of GEMM's were collected between day 7 and 12.

3.1.2 Genetically engineered mouse models

The *Apc*$^{lox/lox}$ *Cdx2-CreERT2*$^{Tg/+}$ (A-mice) mice were a kind gift from Professor Tatiana Petrova (UNIL). Conditional alleles have been generated by placing two *LoxP* sites around exon 14 of the *Apc* gene as well as a neomycin resistance cassette 3' of E14 and 5' of the distal *LoxP* site[79]. Recombination is mediated by the CreERT2 recombinase under control of the *Cdx2* promoter[80]. Since the *Cdx2* promoter is mainly active in the cecum and proximal colon of mice, Cre-mediated recombination is restricted to the colon. Cre-only control mice (*Cdx2-CreERT2*$^{Tg/+}$) were generated by back-crossing A-mice with C57BL6/J mice.

A-mice were then crossed with mice bearing a heterozygous constitutive active mutant form of *LSL-Kras*^{G12D} (preceded by a *Lox-stop-lox* cassette)[81] and homozygous conditional *Trp53* alleles[82]. This cross resulted in the generation of *Apc*$^{lox/lox}$ *LSL-Kras*$^{G12D/+}$ *Trp53*$^{lox/lox}$ *Cdx2-CreERT2*$^{Tg/+}$ (AKP-mice) mice. AKP-mice were back-crossed with C57BL6/J mice for 5 generations. These back-crosses also allowed the isolation of *Apc*$^{lox/lox}$ *LSL-Kras*$^{G12D/+}$ *Cdx2-CreERT2*$^{Tg/+}$ mice (AK-mice).

Immunocompromised NSG (NOD.*Cd-Prkdz*^{scid} *IL2rg*^{tm1Wjl}/Szj (Jackson laboratories, SN005557)) mice were used to validate that organoids engineered to express a photo-activatable cre, which had under gone recombination of *Apc, Kras* and *Trp53* alleles were indeed tumor cells[83] .

3.1.3 Genotyping

Mice bred on-site (A-, AK-, AKP-, and CDX2-Cre mice) were genotyped before weaning, which occurs between 21 and 28 days of age. Toe biopsies or tissue samples were digested in PCR buffer with non-ionic detergents (PBND) Buffer (50 mM KCl, 10 mM Tris-HCl pH 8.3, 2.5 mM $MgCl_2 \cdot 6H_2O$, 0.1 mg/mL gelatin, 0.45% v/v NP40, and 0.45% v/v Tween 20) + Proteinase K (1.5 mg/mL) for 4–48 hours shaking (600 rpm) at 56℃. Proteinase K was then inactivated for 20 minutes at 99℃. Genotyping polymerase chain reaction (PCR)s were

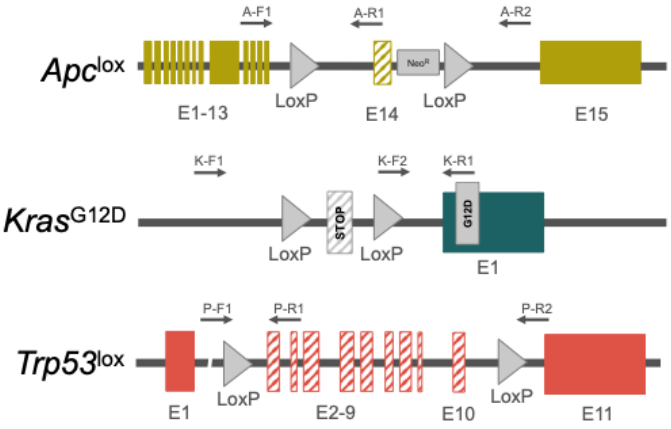

Figure 3.1 Conditional alleles and primer annealing site schematics. Scheme of engineered Apc, Kras, and Trp53 conditional alleles and genotyping primer annealing sites. E - exon, F - forward, R - reverse. Striped exons are removed after recombination, solid exons remain after recombination.

		FR primer	Sequence
Apc	A-F1	300	5'-GTT CTG TAT CAT GGA AAG ATA GGT GGT C-3'
	A-R1	301	5'-CAC TCA AAA CGC TTT TGA GGG TTG ATT C-3'
	A-R2	302	5'-GAG TAC GGG GTC TCT GTC TCA GTG AA-3'
Kras	K-F1	333	5'-AGC TAG CCA CCA TGG CTT GAG TAA GTC TGC A-3'
	K-F2	331	5'-GTC TTT CCC CAG CAC AGT GC-3'
	K-R1	332	5'-CTC TTG CCT ACG CCA CCA GCT C-3'
Trp53	P-F1	261	5'-CAC AAA AAC AGG TTA AAC CCA G-3'
	P-R2	261.5	5'-GAA GAC AGA AAA GGG GAG GG-3'
	P-R1	262	5'-AGC ACA TAG GAG GCA GAG AC-3'
CDX2-CreERT2	C-F1	197	5'-GAA CGT GCA AAA CAG GCT CTA G-3'
	C-R1	198	5'-AAG GCC AGG CTG TTC TTC TTA G-3'

Table 3.1 Table of genotyping primers

conducted using the primers listed in Table 3.1, also refer to Figure 3.1 for a schematic of primer binding sites on each allele.

3.1.4 Tumor induction and endpoint analyses of A-, AK- and AKP-mice

Mice of both sexes, received a single i.p. injection of tamoxifen in sunflower oil. For age of induction, dose and concentration of tamoxifen solution, see Table 3.2. Mice were then monitored two times per week until experimental endpoint, and the animals were euthanised and analysed. Cecae were retrieved from the peritoneal cavity and placed in phosphate-

	age	genotype	tamoxifen dose	tamoxifen solution
"Standard dose"	8-12 weeks	Ctrl-mice	18 mg/kg	5 mg/mL
	8-12 weeks	A-mice	18 mg/kg	5 mg/mL
	8-12 weeks	AK-mice	9 mg/kg	2.5 mg/mL
	8-12 weeks	AKP-mice	9 mg/kg	2.5 mg/mL
"Low-dose"	8-14 weeks	Ctrl-mice	12 mg/kg	1 mg/mL
	8-14 weeks	A-mice	12 mg/kg	1 mg/mL
	8-14 weeks	AK-mice	6 mg/kg	1 mg/mL
	8-14 weeks	AKP-mice	6 mg/kg	1 mg/mL
"Very low dose"	8-12 weeks	Ctrl-mice	4 mg/kg	0.5 mg/mL
	8-12 weeks	A-mice	4 mg/kg	0.5 mg/mL
	8-12 weeks	AK-mice	2 mg/kg	0.5 mg/mL
	8-12 weeks	AKP-mice	2 mg/kg	0.5 mg/mL

Table 3.2 Tamoxifen injection conditions for experiments in this work including age at injection, genotype, dose (mg/kg) and concentration of tamoxifen solution (mg/mL).

buffered saline (PBS) on ice. The cecae were then opened vertically, rinsed thoroughly with PBS, blotted gently with a paper towel to remove excess liquid, and weighted on a scale. Tumor number and size (in mm) were recorded by visual inspection. A 4-6 mm strip of each cecum was cut, swiss rolled and placed in a cassette in a 4% formaldehyde PBS solution in a beaker and kept rocking at 4℃ overnight. The cassettes were then transferred into a 70% ethanol solution until drying in the histokinette. Smaller strips were cut and embedded in optimal cutting temperature (OCT)-compound (Sakura, 4583) for immuno-fluorescence histology. Briefly, moulds were placed on top of dry ice submerged in ethanol, OCT was added to the mould with care taken to avoid bubble formation, and the biopsy was pressed to the bottom of the form until the block was frozen. Frozen OCT blocks could then be transferred to small plastic bags for storage with labels, and kept at -80℃. If the tissue was tumor-bearing, tumors were excised with curved forceps for digestion into single cells, and care was taken to avoid the retrieval of healthy adjacent tissue. For healthy colons, connective tissue was removed and the entire tissue was subjected to tissue dissociation. For some experiments, tail biopsies, tumor biospies, mesenteric lymph nodes, inguinal lymph nodes, lung, dissociated tumor single-cell pellets, liver and spleen were also collected.

3.2 Single cell preparations from tumor and healthy tissue

To prepare a single-cell suspension of cells from cecal tissue, the tissue was subjected to digestion using the GentleMACS Octo Tissue Dissociator with heaters (Miltenyi, 130-096-427). Tissue was added to C-tubes (Miltenyi, 130-093-237) and covered with 5 mL of digestion media (RPMI, FBS 5%, Dispase II 0.5 mg/mL (Roche, 42916300), Collagenase IV 1mg/mL (Gibco, 17104-019), and DNAse I 10 μg/mL). The C-tubes were then placed on the machine with heaters and the program "37C_m_TDK_1" was run for 42 minutes. The samples were then filtered through a 70 μm nylon strainers (Falcon, 352350) into a 50 mL falcon tube, centrifugated for 5 minutes at 300xg and then transferred into 15 mL lo-bind tubes (Eppendorf, 0030 122.208) for downstream analysis like 10X genomics single-cell RNA sequencing, organoid generation, flow cytometry, and *ex vivo* stimulation.

3.3 Organoid generation and culture

3.3.1 Organoid generation

Following digestion of tumor or tissue to a single-cell suspension, the cells were washed two times in PBS then suspended at a density of 2-3,000 cells per 40 uL matrigel (Corning, 356231) dome in a 24 well plate. 600 μL of media were added to the culture, supplemented with Rho-kinase inhibitor Y-27632 (1 μM) and Normocin (100 μg/mL), a broad-spectrum antimicrobial reagent. Normocin was maintained in the culture medium for two passages, then removed.

3.3.2 Organoid culture

In this study, a mouse intestinal organoid culture was maintained using a variety of media depending on the specific requirements of the experiment. The base medium, referred to as "BM", was prepared by combining 50mL of Advanced DMEM/F-12 medium (ThermoFisher, 12634-034), Gentimycin (1%), 500 μL of Glutamax (1X), and 500 μL of HEPES (10 mM). To

Organoid growth and selection media supplements		
	growth requirements	**selection requirements**
colon organoids	hEGF, mNoggin, Wnt3a, R-spondin	N/A
A tumoroids	hEGF, mNoggin	(remove Wnt3a, R-spondin)
AK tumoroids	mNoggin	(remove Wnt3a, R-spondin) mNoggin + gefitinib
AKP tumoroids	mNoggin	(remove Wnt3a, R-spondin) mNoggin + gefitinib + Nutlin3a
AKPT tumoroids	no extra components	(remove Wnt3a, R-spondin, and mNoggin) + gefitinib + Nutlin3a

Table 3.3 Table of organoid media supplements for growth or selection

prepare the pre-ENR medium for tumoroids, the BM medium (47.5 mL) was supplemented with B27 (1X), N2 (1X), and N-acetylcysteine (NAC, 1.25 mM). For healthy small-intestinal organoids, ENR medium was prepared from pre-ENR medium supplemented with hEGF (50 ng/mL), mNoggin (10 ng/mL), and R-spondin (1 μg/mL). For colon organoids, WENRN medium was used, which was ENR medium supplemented with Wnt3A (10 ng/mL) and Nicotinamide (NAM, 10 mM). Upon thawing of any type of organoid or tumoroid, the medium appropriate for the specific organoid type was supplemented with Y-27632 2HCl (10 μM). Different growth requirements and selection requirements were used for different types of tumoroids. For example, A-tumoroids required hEGF and mNoggin for growth. It was noted by Drost *et al.* [84] that AKP organoids grown *in vivo* were "well-differentiated", leading to the hypothesis that paneth cells may be present in AKP organoid cultures and thus endogenously provide EGF. To select for only clones bearing the KRAS active mutation, gefitinib, an EGFR inhibitor, gefitinib, must be included in the culture. Nutlin3a (5-10 μM, Cayman Chemical) was added to culture to induce cell death inside cells with full length/functional P53, as it induces P21, which leads to death. Noggin was required in the absence of SMAD4 deletions.

3.4 Flow cytometry

Following digestion to single-cells, red blood cell lysis, or *ex vivo* stimulation, cells were plated into 96 well-plate v bottom plates. Cell were centrifuged at 500xg for 3 minutes, the supernatant was removed by flicking into a sink, then washed once more with 150 μL staining media supplemented with EDTA and NBCS (SM++) (HBSS without calcium and magnesium (Corning, MED21-022-CV), 2.5 mM ethylenediaminetetraacetic acid (EDTA), 2% newborn calf serum (NBCS)). The cells were then suspended in 50 μL surface stain

solution (prepared in SM++) for the required cocktail and incubated at 4℃ for 30 minutes in the dark. 100 μL SM++ was then added and the cells were centrifuged, then washed once more with 150 μL SM++. After supernatant removal, the cells were thoroughly re-suspended in 50 μL SM++, then 50 μL of IC fixation buffer (Invitrogen, 00-8222) was added to each well using a multichannel pipette while the plate is placed gently on a vortexer. The cells were incubated at RT for 30 minutes in the dark, then 50 μL of SM++ was added and the cells were centrifuged. If the cells require intracellular staining, after supernatant removal the cells were washed twice with 1X permeabilization buffer (Invitrogen, 00-8333-56), then suspended in 50 μL of the intracellular antibody cocktail (which is prepared in 1X permeablization buffer) and incubated overnight at 4℃. In the morning, 100 μL of SM++ were added and the cells were washed once more. The samples were then re-suspended in 100 μL SM++ for flow cytometric analysis.

antigen	conjugate	clone	identifier
CD8a	AF647	YTS169.4	made at EPFL
F4/80	AF647	BM8	123122
TCF1	AF647	C63D9	6709
CD45	APC	30F11	17-0451-1632
GzmB	AF647	GB11	560212
CD45.1/2	APCeF780	A20; 104	47-0454-82
TCRb	APCeF780	H57-597	47-5961-82
CD11b	BV711	M1/70	101242
CD4	FITC	GK1.5	made at EPFL
CD62L	FITC	MEL-14	11-0621-85
CD8a	FITC	YTS169.4	made at EPFL
IL17a	FITC	18H10.1*	53-7172-80
CD25	Pac Blue	PC61.5	made at EPFL
Ly6C	Pac Blue	HK1.4	128013
CD8a	PE	53-6.7	12-0081-82
FoxP3	PE	FJK-16s	88-8111
MHCII IA/IE	PE	M5/114.15.2	15-5321-83
CD4	PE-Cy7	GK1.5	25-0041-82
TCRb	PE-Cy7	H57-597	109222
CD4	PerCP.EF710	GK1.5	46-0041-82
CD11b	PerCpCy5.5	M1/70	45-0112-80
CD44	PerCpCy5.5	IM7	45-0441-82
CD45.1/2	PerCpCy5.5	A20; 104	45-0453-82
Ly6G	PerCpCy5.5	1A8	127616
IFNg	VF450	XMG1.2	75-73611-U025

Table 3.4 FACS antibodies used in this work.

"My" cocktail			
fluorophore	**antigen**	**clone**	**antigen location**
UV	dead	ZombieUV	surface
Pac Blue	Ly6C	HK1.4	surface
BV711	CD11b	M1/70	surface
FITC	CD8	YTS169.4	surface
PerCP.EF710	CD4	GK1.5	surface
PE	MHCII	M5/114.15.2	surface
PE-Cy7	TCRb	H57-597	surface
AF647	F4/80	BM8	surface
APCeF780	CD45.1/2	A20; 104	surface

Table 3.5 Myeloid ("My") flow cytometry cocktail antibodies and their sub-cellular location.

"MyR" cocktail			
fluorophore	**antigen**	**clone**	**antigen location**
UV	dead	ZombieUV	surface
Pac Blue	Ly6C	HK1.4	surface
BV711	CD11b	M1/70	surface
FITC	CD4	GK1.5	surface
PerCpCy5.5	Ly6G	1A8	surface
PE	MHCII	M5/114.15.2	surface
PE-Cy7	TCRb	H57-597	surface
AF647	CD8	YTS169.4	surface
APCeF780	CD45.1/2	A20; 104	surface

Table 3.6 Myeloid revisited ("MyR") flow cytometry cocktail antibodies and their sub-cellular location.

"Fox" cocktail			
fluorophore	**antigen**	**clone**	**antigen location**
UV	dead	ZombieUV	surface
FITC	CD8	YTS169.4	surface
PerCpCy5.5	CD11b	M1/70	surface
PE	FoxP3	FJK-16s	intracellular
PE-Cy7	CD4	GK1.5	surface
APC	CD45	30F11	surface
APCeF780	TCRb	H57-597	surface

Table 3.7 Foxp3 ("Fox") flow cytometry cocktail antibodies and their sub-cellular location.

"Mem" cocktail			
fluorophore	**antigen**	**clone**	**antigen location**
UV	live/dead	ZombieUV	surface
Pac Blue	CD25	PC61.5	surface
BV711	CD11b	M1/70	surface
FITC	CD62L	MEL-14	surface
PerCpCy5.5	CD44	IM7	surface
PE	CD8	53-6.7	surface
PE-Cy7	CD4	GK1.5	surface
AF647	CD45	30F11	surface
APCeF780	TCRb	H57-597	surface

Table 3.8 Memory ("Mem") flow cytometry cocktail antibodies and their sub-cellular location.

"Th" cocktail			
fluorophore	**antigen**	**clone**	**antigen location**
UV	live/dead	ZombieUV	surface
VF450	IFNg	XMG1.2	intracellular
BV711	CD11b	M1/70	surface
FITC	IL17a	18H10.1	intracellular
PerCpCy5.5	CD45.1/2	A20; 104	surface
PE	CD8	53-6.7	surface
PE-Cy7	CD4	GK1.5	surface
AF647	GzmB	GB11	intracellular
APCeF780	TCRb	H57-597	surface

Table 3.9 T helper ("Th") flow cytometry cocktail antibodies and their sub-cellular location.

3.4.1 *ex vivo* tumor-infiltrating lymphocyte stimulation

Freshly isolated single-cell suspensions of tissues were suspended in a 5 mL FACS tube with a cap in 250 μL RPMI 5% FBS, 1% gentamycin supplemented with 1X Cell Stimulation Cocktail (Invitrogen, 00-4975) which contains phorbol myristate acetate (PMA) and ionomycin. The samples were placed in a cell culture incubator (37℃, 5% CO2) for 3.5 hours, then washed in SM++ and subjected to staining for flow cytometry.

3.4.2 Data acquisition

Flow-cytometric data were acquired on a BD FACS SORP LSR II (Becton Dickinson) and flow-cytometric data were analyzed using FlowJo (Tree Star V10). Analysis strategies are outlined in the respective results sections. Cell viability was assessed using Zombie-UV fixable viability dye (BioLegend, 423107). All primary and secondary antibody conjugates are listed in adjacent tables.

3.5 Histology

3.5.1 Sectioning and staining

Parraffin-embedded tissue was sectioned into 4 μm thick sections from and mounted on Superfrost plus slides (Epredia, J1800AMNZ). Slides were allowed to dry for two days at

Antigen	Clone	Anigen Retrieval	Species	Dilution	Supplier	Catalog
β-catenin	14/Beta-catenin	pH 6.0	mouse	1/200	BD	610153
pERK	D13.14.4E	pH 6.0	rabbit	1/100	CST	CST-4370
p53	Polyclonal CM5	pH 6.0	rabbit	1/400	Novocastra	NCL-L-p53-CM5p
CD3e	SP7	pH 6.0	rabbit	1/200	Thermo Fisher	MA1-90582
PD-1	EPR20665	pH 9.0	rabbit	1/400	Abcam	AB214421
CTLA-4	F-8	pH 9.0	mouse	1/200	Santa-Cruz	SC-376016
FoxP3	FJK-16s	pH 9.0	rat	1/500	Thermo Fisher	14-5773-82
CD8a	4SM15	pH 9.0	rat	1/100	Thermo Fisher	14-0808-82
Anxa1	Polyclonal	pH 6.0	rabbit	1/1000	Sigma Alrich	HPA011271-25UL

Table 3.10 Antibodies used for immunohistochemistry in this work.

room temperature. Sections were stained with Hematoxylin and Eosin (H&E) to assess the morphology of the tumor. Immunohistochemistry staining was performed to assess the spatial distribution of proteins of interest, Table 3.10. Briefly, sections were subjected to dewaxing and re-hydration, washed in PBS then heated to 95℃ for 20 minutes in antigen retrieval buffer. Sections were blocked with 1X PBS supplemented with 1% BSA for one hour then washed and primary antibody was applied and incubated overnight at 4℃ under agitation, Table 3.10. The sections were washed with PBS, quenched (3% H2O2 in 1X PBS), washed and incubated with secondary antibody (ImmPRESS HRP antibodies or simple HRP-conjugated antibodies) for one hour at RT under agitation. The slides were then washed and exposed to a 0.67 mg/mL solution of 3, 3'-diaminonezidine (DAB) (Sigma-Aldrich, D5905) in a 50 mM Tris-HCl (pH 6) solution supplemented with 0.2% H2O2 for up to 10 minutes. The slides were then washed once more, counter-stained with hematoxylin and mounted with a coverslip.

3.5.2 Analysis and quantification

Stained slides were scanned using the Olympus Slide Scanner at 40X magnification. Resulting images were analysed using QuPath, an open-source image processing software[85]. Positive cell detection was conducted on the immunohistochemical staining using three distinct methods (simple positive-cell detection, nuclear or cytoplasmic positive cell detection, or laminae propia or epithelial positive cells), depending on the needs of the experiment. If the staining was simple, with uniform staining pattern (i.e. all cells have strong cytoplasmic

staining, or clear nuclear staining), then the "positive cell detection" plugin was used to quantify positive cells based on the mean optical density of an annotated region.

For stains that exhibited multiple staining patterns (i.e. some cells have nuclear staining, some have membrane staining, etc.), the integrated machine learning functions were employed to automate the quantification of these cells. For example, this method was employed for β-catenin staining to discern membranous staining and saturated nuclear staining. Training regions were carefully annotated to include all possible phenotypes of staining. For example, nuclear stains could be assigned a class of either "nuclear positive" or "nuclear negative", see Figure 3.2. A random tree classifier was then trained using these annotations. This process was performed for each staining phenotype. β-catenin staining analysis involved the specification of not only nuclear staining (Figure 3.2) but also membranous and cytoplasmic staining. Each classifier was applied to all annotations within a given data set.

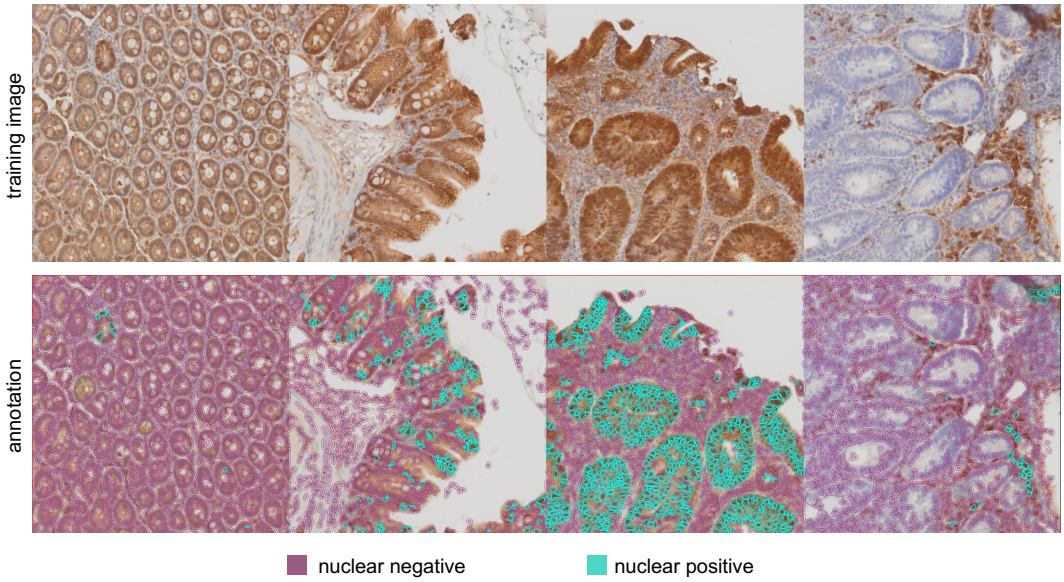

Figure 3.2 Example of training a machine learning classifier to quantify positive nuclear stains in cells using QuPath **TOP.** Raw brightfield images of colon from an A-mouse stained for β-catenin. **BOTTOM.** Annotation that was used to train the positive nuclear staining classifier. Blue outline shows positive cells, and purple outline shows negative cells.

3.6 Single-cell RNA sequencing

Following tumor dissociation to single cells, the samples were suspended in 40 mL PBS 0.04% BSA (PBS+) and centrifuged (300xg, 7 min, 4°C). All but 5 mL of the supernatant was aspirated and the cell pellet was re-suspended in the 5 mL of media. A small aliquot was taken for cell-counting, and the sample was then transferred to a 15 mL low-bind tube (Eppendorf, 0030 122.208), and 10 additional mL of PBS+ were added before centrifugation. Up to 1e7 cells were taken for input to the Miltenyi Dead Cell Removal Kit workflow using LS-MACS magnetic columns. A small aliquot of the flow-through from the columns was taken for cell counting and viability assessment. The flow-through was centrifuged. The samples were then suspended at a density of 1e6 cells/mL and passed through a 40 μm FlowMi cell strainer (Bel-Art, BAH136800040). Two-hundred μL of cell-suspension with ≤25% dead cells were required for submission to the 10X workflow. Cell viability, quality (absence of aggregates and debris), and concentration were confirmed just before cell submission to the 10X workflow by trypan blue dye exclusion visualised with a hemacytometer.

3.6.1 TME of A, AK and AKP mice sequencing

The Chromium Single Cell 3' Reagents Kit v3.1 chemistry (10X Genomics, PN-1000128) was used for this experiment. Four thousand cells per sample were targeted for collection. The libraries were prepared according to 10X Genomics' instructions. Each library was sequenced on their own HiSeq4000 flow cell (300 million reads), which achieved an approximate depth of 75,000 reads/cell.

3.6.2 Longitudinal study of AKP tumors

Four TotalSeq-C hashing antibodies (each conjugated to a unique DNA tag; Biolegend, Table 3.11) were used to pool 4 samples into a single 10X well. The samples were distributed into each well and stained with the antibodies in such a way that each group and each antibody was represented in each well, see Table 3.12. The target number of cells to collect was

Name	Anitgen	Clone	Supplier	Dilution	Catalog	Conjugate
TotalSeq_C0301	CD45; H2 (MHCI)	30/F11; M1/42	BioLegend	1/200	155861	DNA barcode: ACCCACCAGTAAGAC
TotalSeq_C0302	CD45; H2 (MHCI)	30/F11; M1/42	BioLegend	1/200	155863	DNA barcode: GGTCGAGAGCATTCA
TotalSeq_C0303	CD45; H2 (MHCI)	30/F11; M1/42	BioLegend	1/200	155865	DNA barcode: CTTGCCGCATGTCAT
TotalSeq_C0304	CD45; H2 (MHCI)	30/F11; M1/42	BioLegend	1/200	155867	DNA barcode: AAAGCATTCTTCACG

Table 3.11 Hashing antibodies used in this study.

20,000 per well (5'000 cells/sample). Four total 10X wells were used to generate libraries with the Chromium Single Cell 5' Reagents Kit and Mouse TCR Amplification Kit (10X Genomics, PN-1000265 and PN-1000254). The libraries were sequenced on the NovaSeq6000 at a depth of 2,200 million reads per 10X well, approximately 550 million reads per sample which achieved an approximate depth of 110,000 reads per cell.

mouse id	group	weeks	hashing ab	10X well
RAD-106286	control	24	301	4
RAD-104432	tumor1	24	301	1
RAD-104627	tumor2	24	301	2
RAD-104628	tumor3	24	301	3
RAD-108571	control	18	302	1
RAD-107603	tumor1	18	302	2
RAD-107608	tumor2	18	302	3
RAD-107864	tumor3	18	302	4
RAD-109681	control	12	303	2
RAD-109053	tumor1	12	303	3
RAD-109273	tumor2	12	303	4
RAD-110198	tumor3	12	303	1
RAD-110866	control	6	304	3
RAD-110865	tumor1	6	304	4
RAD-111602	tumor2	6	304	1
RAD-111859	tumor3	6	304	2

Table 3.12 Assignment of colon samples (RAD-XXXXXX numbers are unique identifiers for mice used in our laboratory) to hashing antibodies and 10X wells.

3.7 Bioinformatics and statistics

3.7.1 Bioinformatic analysis for TME of A, AK and AKP mice single-cell RNA sequencing

Reads obtained from fastq files were mapped and counted with 10x Genomics Cell Ranger version 5.0.1 using the mouse mm10 reference genome. Using R version 4.2.0, raw gene

expression matrices were obtained using Seurat (4.2.0). Genes detected in fewer than ten cells and cells with less than 200 detected features were filtered out and excluded from analysis, resulting in 30,025 cells and 19,339 genes retained in the experiment. The cells were filtered to remove cells expressing > 20% mitochondria genes (presumably dead cells). Only cells expressing less than 9000 features were kept, eliminating potential doublets. Erythrocytes were also removed as they were dominating the principal component analysis (PCA), by removing cells with more than 10% HBB read counts. After filtering 21,816 cells remained and were utilized for downstream analysis consisting of log-normalisation and data integration between two batches (batch1: A1, A2, AK1, AK2, AKP1, AKP2 and batch 2: AKP3, colon1 and colon2). Next, the Seurat protocol with VST was used to find the top 4,000 variable genes and the first 30 dimensions for data integration in CCA space. After scaling the data only 25 PCs were retained for UMAP projection and a resolution of 0.2 was used to annotate the major clusters. Subannotation was then performed in each of those clusters.

Scuttle (v 1.6.0) was used to sum the expression of a gene in each cell type and sample. The function filterByExpr() from edgeR (v 3.38.0) was used to filter genes with default parameters. Significant genes were assessed using edgeR glmQL fits and also compared to voom significant genes using the limma package (v 3.52.0) using as a covariate the batch information. Volcano plots were generated using ggplot2 (v 3.3.6). Gene ontology for biological processes (BP) and molecular function (MF) were conducted using clusterProfiler (v 3.0.4) function enrichGO with pvalue cutoff of 0.05.

NichenetR (v. 1.0.0) ligand and receptor network was used to understand the differentially expressed Ligands or receptors in each of the cell types by overlapping the lists of differentially expressed genes previously obtained with the ligand receptor network (downloaded from https://zenodo.org/record/3260758/files/lr_network.rds) to obtain interesting ligands and or potentially interesting receptors. The nichenet procedure was used to then obtain the pearson correlation coefficient between the potential targets (obtained using the weighted network: https://zenodo.org/record/3260758/files/weighted_networks.rds) of differentially expressed ligands and the list of differentially expressed genes in receiver cells.

3.7.2 Bioinformatic analysis of longitudinal study of AKP tumors

Raw sequencing data were generated from two independent runs with the aim to increase sequencing depth. Cell Ranger version 6.0.1 was used to map and count reads obtained from fastq files with 10x Genomics using a demultiplexing strategy (https://kb.10xgenomics.com/hc/en-us/articles/4402869925133) for 5' VDJ data using the mouse mm10 reference genome and the mouse VDJ reference refdata-cellranger-vdj-GRCm38-alts-ensembl-5.0.0 downloaded from the 10X Genomics webpage. In brief, there are two de-multiplexing steps that can not be done at the same time. In the first step, the RNAseq reads from different samples are demultiplexed and using the *bamtofastq* function, with which fastq files for each sample was obtained. The fastq files are then remapped to the mouse reference genome (mm10) and VDJ reads such that the barcodes of each cell could be traced to their parent sample.

Using R version 4.1.2, raw gene expression matrices were obtained using Seurat package (v 4.1.0). Ambient RNA contamination was estimated from empty droplets using SoupX package (v 1.6.1) and subsequently removed. Genes detected in fewer than three cells and cells with less than 200 detected features were filtered out and excluded from analysis, isolating 29,522 cells and 22,441 genes for downstream analysis. Cells expressing > 30% mitochondria genes were removed to excluded dead and dying cells. Only cells expressing between 200 and 5,000 features with a minimum of 500 UMIs were kept. Finally, 26,295 cells remained and were utilized for downstream analysis consisting of log-normalisation and dimension reduction by PCA using the 4,000 most variable genes selected by the VST method. After scaling the data, 35 PCs were retained for UMAP projection and a resolution of 0.1 was used to annotate the major clusters, and subannotation was performed in each of those clusters. Scuttle package (v 1.4.0) was used to sum the expression of a gene in each cell type and sample. The function filterByExpr() from the package edgeR (v 3.36.0) was used to filter genes with default parameters. Significant genes were assessed using edgeR glmQL fits. Volcano plots were generated using ggplot2 (v 3.3.5).

Immunarch (v. 0.6.7) was used to compute the overlap of TCR repertoires, the composi-

tion of the repertoires and to perform analysis of the V and J usage. Other TCR analyses were performed using R version 4.2.0 and ggplot2 (v 3.3.6). The clonal information and the single-cell RNAseq data were merged using the barcode information from the cells.

4 Results

4.1 Aim 1: Determine whether the tumor immune microenvironment of murine colorectal tumors changes in response to accumulating tumor-driving mutations

4.1.1 CDX2-driven CreERT2 expression drives recombination of canonical tumor-driving mutations to form colon adenocarcinomas in mouse models.

Mutations in a few key genes are known to drive tumorigenesis in human colorectal cancer[14]. We therefore used three genetically engineered mouse models (GEMMs) with conditional alleles that reflect this knowledge. Accordingly, the models included alleles with APC deletions *Apc*$^{lox/lox}$*Cdx2-CreERT2*$^{Tg/+}$ -mice (A-mice), additional activating KRAS mutations *Apc*$^{lox/lox}$ *LSL-Kras*$^{G12D/+}$ *Cdx2-CreERT2*$^{Tg/+}$-mice (AK-mice) and, further, truncated P53 alleles *Apc*$^{lox/lox}$ *LSL-Kras*$^{G12D/+}$ *Trp53*$^{lox/lox}$ *Cdx2-CreERT2*$^{Tg/+}$-mice (AKP-mice), Figure 4.1a. Temporal and tissue-specific control of conditional gene recombination was achieved using the tamoxifen-inducible CreERT2 recombinase under the control of the CDX2 promoter which is primarily active in the cecum and proximal colon of the transgene-carrying mice[80]. Mice without or with only the CDX2-CreERT2 transgene were used as healthy controls, Figure

4.1a. To induce tumor formation, mice received a single i.p. injection of tamoxifen and tumors were allowed to develop for 6 weeks before analysis, Figure 4.1b. A-mice received double the dose (18 mg/kg) of tamoxifen compared to AK- and AKP-mice (9 mg/kg) in order to achieve a similar tumor burden across genotypes in terms of tumor number and size, Figure 4.1c and d.

In order to validate that the expected genetic alterations did occur we extracted genomic DNA from total tumor and performed PCR to detect DNA with and without LoxP sites as well as recombined DNA, Figure 4.1e. Control animals that were used to examine the healthy colon were confirmed to not carry the *Cre* transgene while tumor-bearing animals did, Figure 4.1f. Because tumors are composed of a heterogenous amalgamation of cells, including targeted and non-targeted epithelial cells, endothelial cells, fibroblasts and immune cells, tumor-bearing mice were anticipated to carry DNA of engineered and recombinant alleles. Accordingly, A-, AK- and AKP-tumors bore both LoxP alleles as well as the recombinant band for the *Apc* allele, Figure 4.1f. AK- and AKP-tumors contained wildtype (WT), LoxP and recombinant alleles for *Kras*, while A-tumors contained only WT DNA molecules, Figure 4.1f. Finally, while A- and AK-tumors contained only WT *Trp53*, AKP-tumors contained the conditional alleles as well as recombinant alleles, as expected, Figure 4.1f. PCR, however, is not quantitative and cannot provide information on the proportion of tumor cells bearing the mutant alleles.

Thus, we inspected the sequencing reads of the epithelial compartment of single-cell RNA sequencing (scRNAseq) data from the mouse models in order to determine approximate proportions of recombinant alleles. The conditional allele for *Apc* contains LoxP sites that flank exon 14 (E14), which is removed upon Cre-mediated recombination, Figure 4.2a. In order to positively identify mutant and transcripts it is necessary to identify reads which map to Exons 13 and 15 and recombinant reads would not contain E14, Figure 4.2b. Reads that did not map to E13 and E15 were determined to be non-conclusive for this analysis. The barcodes of the reads were then used to assess the proportion of cells with each variation of the *Apc* allele, Figure 4.2c. The majority of cells did not contain reads which corresponded to

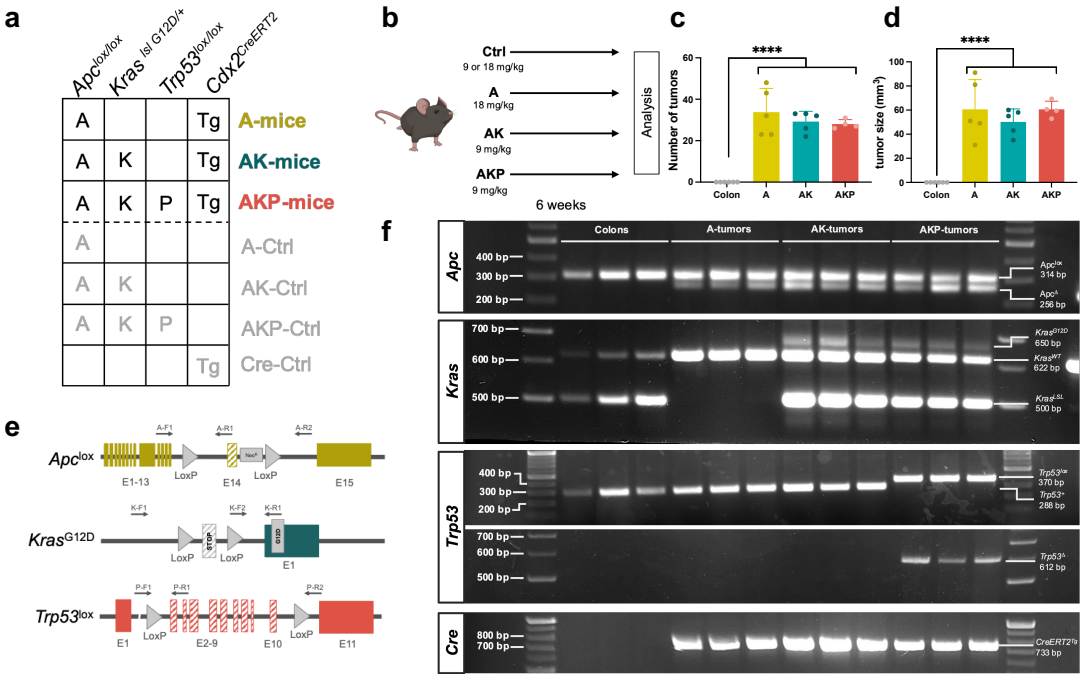

Figure 4.1 CDX2-driven CreERT2 expression enables recombination of canonical tumor-driving mutations resulting in colon tumor formation. **a.** Scheme of different mouse models with corresponding conditional alleles used in the study. **b.** Experimental overview: Ctrl, A-, AK- and AKP-mice received a single i.p. dose of tamoxifen and were euthanised and analysed 6 weeks post-tamoxifen administration. **c.** Bar plots of tumor burden 6-weeks post-tamoxifen as measured by number of tumors and **d.** tumor size. **e.** Schematic of conditional alleles and the binding site and direction of primers used for genotyping. **f.** Agarose-gel electrophoresis of PCR products of genotyping PCR performed on genomic DNA derived from total tissue or tumor of A-, AK- and AKP-mice. Brackets and stars are indicative of the adjusted p value result of a one-way analysis of variance (ANOVA) with Tukey's multiple corrections to account for multiple comparisons. key: $p \leq 0.05$ = *, $p \leq 0.01$ = **, $p \leq 0.001$ = ***, $p \leq 0.0001$ = ****, and non-significant (n.s.) comparisons are not shown. A-mice– *Apc*$^{lox/lox}$ *CDX2CreERT2*$^{Tg/+}$, AK-mice– *Apc*$^{lox/lox}$ *LSL-Kras*$^{G12D/+}$ *CDX2CreERT2*$^{Tg/+}$, and AKP-mice– *Apc*$^{lox/lox}$ *LSL-Kras*$^{G12D/+}$ *Trp53*$^{lox/lox}$ *CDX2CreERT2*$^{Tg/+}$.

conclusive reads, Figure 4.2c. When non-conclusive cells were excluded from the analysis, we could determine a relative frequency of recombination of the *Apc* allele to be 0%, 18%, 14% and 9% in colon, A-, AK- and AKP-tumors, respectively, Figure 4.2d. Colon epithelial cells do not contain mutant alleles, as expected, Figure 4.2d. On the other hand, tumors contain about 10-20% of cells bearing the truncated *Apc* allele, Figure 4.2. Furthermore, the approximate recombination frequency of *Apc* decreases as the number of conditional alleles in the mouse increases. It is important to note, however, that a maximum of 11 cells per group contained conclusive reads which represents a minute fraction of approximately 1,500-2,000 epithelial cells per tumor group.

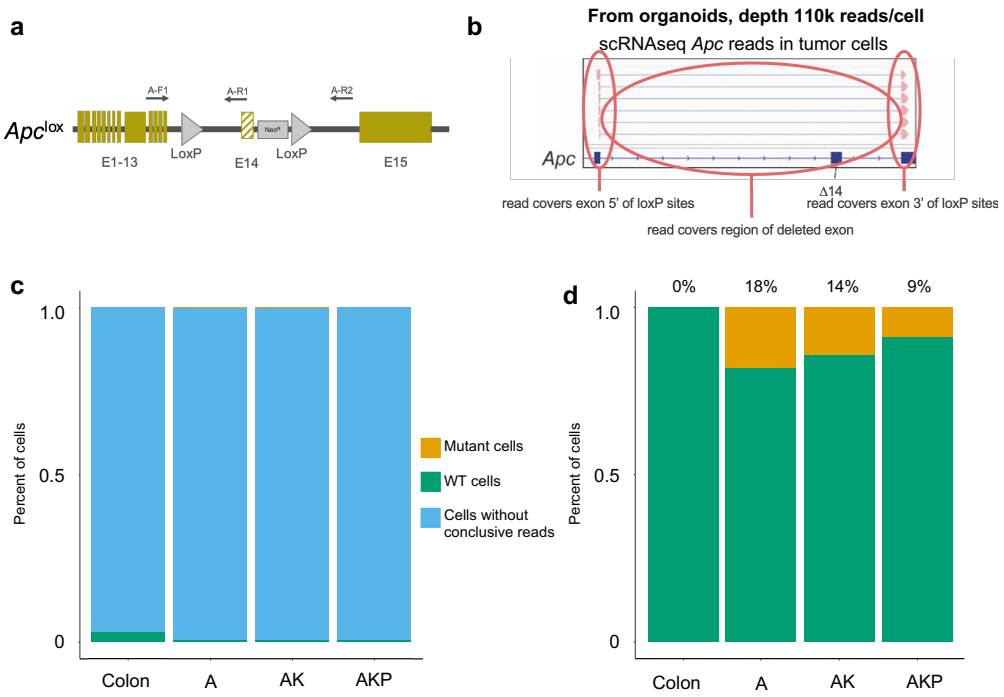

Figure 4.2 Determination of *Apc* mutant allele frequency among epithelial cells in colon, A-, AK- and AKP-mice. **a.** Schematic of *Apc* conditional allele, LoxP sequences flank exon 14 (E14, striped). Stripes represent exons removed following recombination. **b.** Example of scRNAseq reads that allow affirmative identification of *Apc* recombinant and WT alleles. Data provided by L. Francisco-Lorenzo Martin from AKP-tumor-derived organoids, sequenced at a depth of 110k reads/cell. **c.** Stacked bar plot showing proportion of epithelial cells that contain reads that correspond to mutant or WT *Apc* or cells that did not have a conclusive read. **d.** Approximate proportion of mutant and WT-bearing cells in Colon, A-, AK- and AKP-epithelial cells, with non-conclusive cells removed. Data includes 11, 11, 7 and 11 cells, respectively.

We next attempted to determine what proportion of epithelial cells bore the *Kras* mutant

allele. The *Kras* conditional allele contains two LoxP sequences that flank a DNA segment that contains a quadruple repeat of the SV40 PolyA sequence which we leveraged to attempt to determine the recombination frequency of the allele, Figure 4.3a. We therefore created a new reference genome for the experiment by appending the SV40 PolyA sequence to the mm10 genome, Figure 4.3b. The raw sequencing files were then mapped to the new reference genome to determine the expression of the SV40 PolyA sequence by each cell, Figure 4.3b. Explicitly, cells bearing the non-recombined conditional allele will have reads of the SV40 PolyA sequence, while recombinant *as well as* cells without reads in that area will appear to have no SV40 polyA expression, Figure 4.3b. Therefore, this method will be biased by the presence of many false positives. Ultimately, what we observed is that Colon (composed of two AK-Ctrl mice), AK- and AKP-tumors contained reads that correspond to the conditional allele, Figure 4.3c. These cells, however, were greatly outnumbered by recombinant or cells without reads in this region, Figure 4.3c. Therefore, when we attempt to determine a proportion of cells bearing the *Kras* mutant allele, we can see that the proportion of cells with the conditional allele decreases from about 25% in the healthy colon to 5-10% in AK- and AKP-tumors, Figure 4.3d. This would represent approximately 20-15% of cells bearing recombinant alleles, but due to the presence of false positives, this conclusion is made with great uncertainty.

Finally, because the conditional allele of *Trp53* has similar construction to the *Apc* allele (LoxP sequences that flank exons 2-10) we employed a similar analysis, Figure 4.4a. Similarly to the analysis in *Apc*, reads that map to exons 1 and 11 were required to make a definitive annotation of cells containing the recombinant allele, Figure 4.4b. Despite many reads in the region, there were no reads in the AKP-tumor samples that corresponded to the recombinant *Trp53* allele, Figure 4.4c. This indicates that the recombination of the *Trp53 in vivo* is likely to be a rare event.

Having confirmed that the expected genetic alterations did indeed occur by PCR, and having determined an approximate recombination frequency with scRNAseq, we next employed immunohistochemistry (IHC) to assess whether and which cells demonstrated perturbations

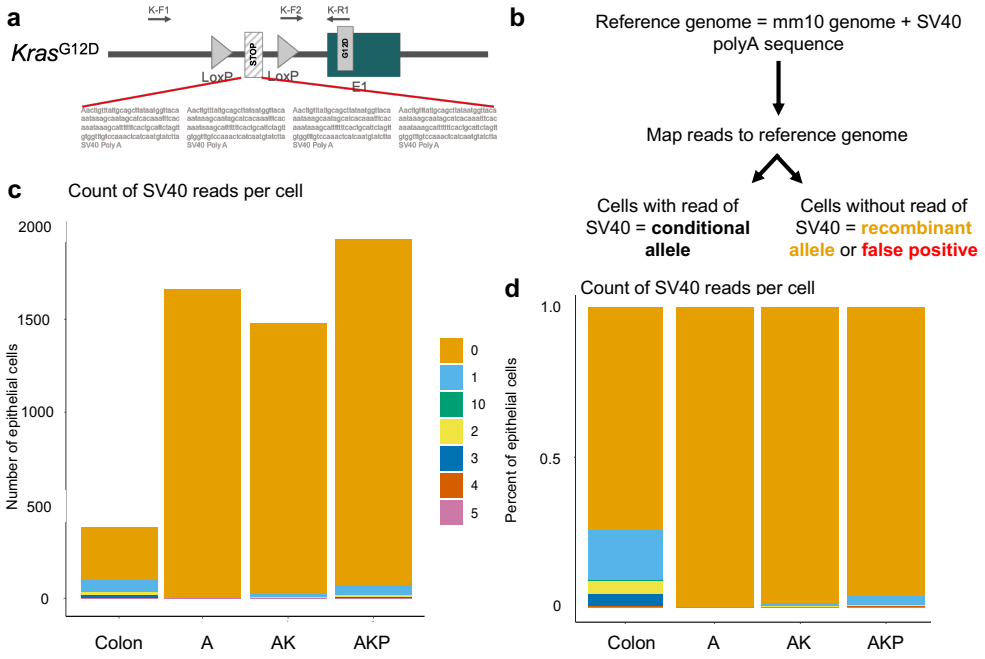

Figure 4.3 Determination of *Kras* WT allele frequency among epithelial cells in colon, A-, AK- and AKP-mice. **a.** Schematic of *Kras* conditional allele, LoxP sequences flank a STOP sequence which includes a quadruple repeat of the SV40 polyA sequence. Stripes represent elements removed following recombination. **b.** Overview of analysis strategy. **c.** Stacked bar plot showing count of SV40 PolyA reads per cell which corresponds to the non-recombinant conditional *Kras* allele, by number of cells. **d.** Approximate proportion of cells containing (not orange) and not containing reads of the SV40 PolyA sequence.

in the signaling pathways in which the targeted alleles are implicated. We therefore performed immunohistochemistry to confirm that the Wnt, Mapk, and p53 signaling pathways were indeed altered as expected in each tumor among malignant cells. The protein APC is part of a multi-protein destruction complex in the Wnt signaling pathway. In the absence of Wnt ligands, the multi-protein complex phosphorylates the N-terminus of β-catenin, leading to its ubiquitination and subsequent proteasomal degradation. In the presence of Wnt ligands, the APC-containing multi-protein complex can no longer tag β-catenin for degradation. Consequently, β-catenin is stabilised and liberated to translocate to the nucleus and associates with TCF4 to induce growth and proliferation related gene expression[18]. Immunohistochemical staining on A- AK- and AKP-tumor sections revealed increased nuclear β-catenin staining in all three tumor types, as a consequence of CDX2-CreERT2 mediated *Apc* gene truncation

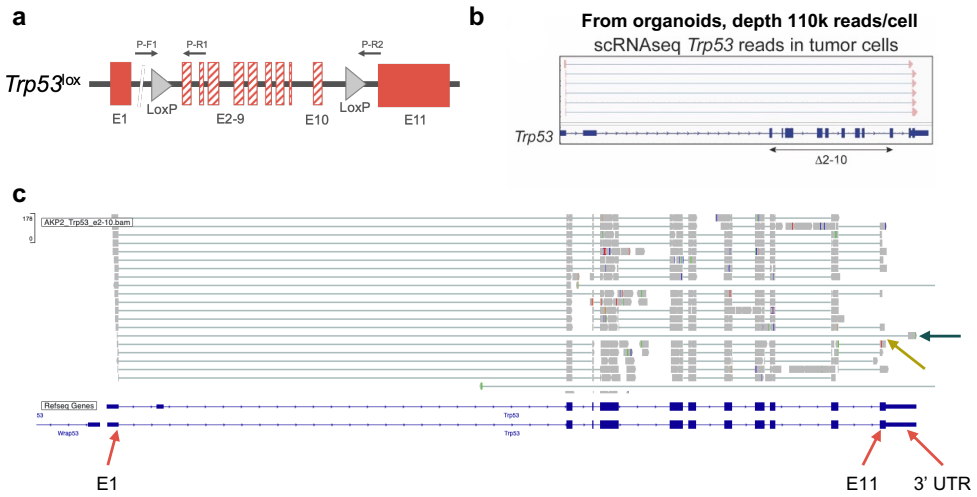

Figure 4.4 Determination of *Trp53* mutant allele frequency among epithelial cells in colon, A-, AK- and AKP-mice. **a.** Schematic of *Trp53* conditional allele, LoxP sequences flank exons 2 through 10. Stripes represent elements removed following recombination. **b.** Example of scRNAseq reads that allow affirmative identification of *Trp53* recombinant and WT alleles. Data provided by L. Francisco-Lorenzo Martin from AKP-tumor-derived organoids, sequenced at a depth of 110k reads/cell. **c.** Reads in the *Trp53* locus of an AKP-tumor sample. Blue arrow indicates a potentially conclusive read, but the read does not map to exon 11 itself (yellow arrow), but rather the 3' untranslated region.

comapred to the healthy colon, Figure 4.5a and b. Interestingly, active Wnt-signaling cells represented about 25-30% of cells. We observed a variety of phenotypes ranging from crypts with a healthy appearance (membranous and light cytoplasmic staining) to those exhibiting an oncogenic nuclear-saturated phenotype, indicating heterogeneous recombination among the epithelial cells of the colon, Figure 4.5a, black (healthy) and red (malignant) boxes. Furthermore, within healthy crypts, β-catenin can be seen localised to the membrane of epithelial cells, Figure 4.5a. This association is emblematic of β-catenin's role in the formation of adherens junctions where it forms a complex with E-cadherin, and thus promotes cell adhesion[86].

The MAP-kinase signaling cascade is stimulated by EGF binding to the EGFR. EGF stimulation leads to the GTP-based activation of KRAS, and the signal proceeds through RAF to MEK to ERK, which when phosphorylated, translocates to the nucleus and induces expression of growth and proliferation genes by phosphorylating target transcription factors[87]. To validate the successful recombination of the oncogenic $Kras^{G12D/+}$ allele and subsequent

induction of constitutive KRAS activity in AK and AKP compared to A mice, we stained for phosphorylated ERK1/2. Subsequent quantification of the images was conducted among epithelial cells (as opposed to stromal cells) and reported as percent of positive cells per normalised area. Relatively high-level expression of pERK was detected in healthy colons where pERK contributes to the differentiation of goblet cells[20]. Among tumors, elevated levels of pERK of approximately 20% of epithelial cells were observed in AK- and AKP-tumors in comparison to tumors lacking the *Kras* alteration (A-mice, with about 5% $pERK^+$ area) Figure 4.5c and d, thereby confirming the anticipated increases in MAPK signaling.

P53 is a positive regulator of stress and DNA damage-induced cell cycle arrest and apoptosis and evasion of apoptosis is a common trait of cancer cells[88,89]. Sections of colon, A-, AK- and AKP-tumors were subjected to IHC staining for p53. P53 was detectable among all tumor conditions, possibly induced by replication stress induced by the rapid proliferation afforded by the other mutations[90], Figure 4.5e. The healthy colon, however, was had very little staining, as can be expected for cells at equilibrium, Figure 4.5e. Among AKP-tumors, but not A- and AK-tumors, it was possible to observe malignant crypts with a paucity of p53 positive cells, but these crypts were rare, Figure 4.5e. Finally, quantification of the $p53^+$ epithelial cell area shows that approximately 30% of AKP-tumor epithelial cells were $p53^-$, Figure 4.5f. It is important to note, however, that the negative cells could be composed of adjacent healthy epithelial cells as well as recombinant tumor cells.

We therefore found that tumors of GEMMs used in this study do indeed contain the expected recombinant alleles, and approximated the frequency of their presence. The frequency of the *Apc* mutant allele was approximately 10-20% in epithelial cells, across the models while IHC showed that about 25-30% of tumor demonstrated constitutive Wnt signaling. The mutant *Kras* allele may have been active in 15-20% of epithelial cells in AK- and AKP-tumors, while not present in A-tumors. On the signaling level, about 20% of AK- and AKP-epithelial cell area was $pERK^+$ compared to about 5% in A-tumors. On the other hand, though detectable by PCR, *Trp53* mutant allele induction appears to be a rare event in AKP-tumors when approximation of mutant allele frequency is attempted using scRNAseq

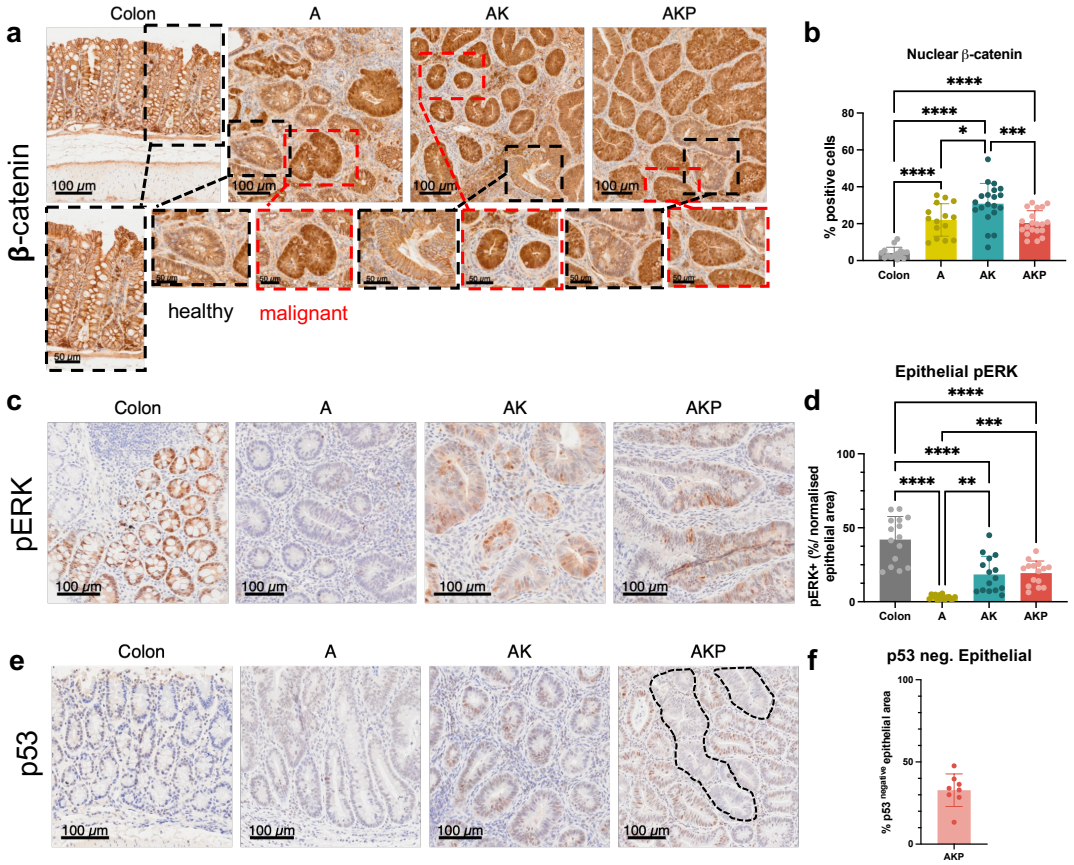

Figure 4.5 Validation of genetically engineered mouse models: immunohistochemical evidence of dysregulated β-catenin, phospho-ERK, and P53 at the protein level. Brightfield images of IHC performed for **a.** β-catenin (crypts with a healthy phenotype are boxed and magnified in black; malignant crypts are boxed and magnified in red) **c.** p-ERK and **e.** P53 in healthy colon, A- AK- and AKP-tumors. Quantifications conducted using QuPath positive cell detection of 3 arbitrarily-selected regions within each sample for nuclear β-catenin, phospho-ERK and p53 (negative epithelial fraction = 100% – positive cell area%) are shown in panels **b**, **d** and **f** respectively. Brackets and stars are indicative of the adjusted p value result of a one-way ANOVA with Tukey's multiple corrections to account for multiple comparisons. key: $p \leq 0.05$ = *, $p \leq 0.01$ = **, $p \leq 0.001$ = ***, $p \leq 0.0001$ = ****, and non-significant (n.s.) comparisons are not shown. These stainings and quantifications were conducted by Elia Escoffier for a Master's project under my supervision.

and IHC. WE then sought to determine how the mutant allele frequency in our mouse models compared to human tumors.

In order to determine the fraction of cells bearing tumor-driving mutations, we analysed the the cancer genome atlas (TCGA) colon adenocarcinoma (COAD) whole exome sequencing (WES) dataset, Figure 4.6a. Because WES contains all cell types, not only tumor cells, we used the consensus purity estimates from Aran *et al.* [91]. The cancer cell fraction (CCF) bearing mutant alleles was then calculated for each sample for mutation of interest (*APC, KRAS,* and *TP53*) as described in Tarabichi *et al.* [92] which is simply the variant allele frequency (VAF) corrected for the sample purity and local copy number. The majority of patient samples demonstrated a clonal presence of tumor-driving mutations (i.e. a CCF close to 1), Figure 4.6b. *KRAS* hotspot mutations are the most clonal among patients with only a few patients with less than 50% frequency, Figure 4.6b. About 50% of patients bearing *APC* mutations were not purely clonal, but were reresented in >50% of the CCF. Finally, *TP53* mutations were largely clonal, with the majority of tumors bearing the mutation in >50% of cells, but there was also a small fraction of patients in which the CCF was about 30%, Figure 4.6. Therefore, the GEMMs used in this study produce tumors with driving mutations represented at a lower frequency than in patient tumors.

Histological staining of colon, A-, AK- and AKP-tumors with H&E revealed that the tumors were predominantly adenomas (Figure 4.7a), without invasion through the muscularis mucosae. The colon adenomas are characterised by a lack of differentiated colonic cells such as goblet cells and an accumulation of undifferentiated cells, Figure 4.7a. Notably, at higher magnifications, many immune cells can be observed in the lamina propria of tumors from every model, Figure 4.7b. The identity, however, of the immune cells cannot be conclusively determined from the H&E images, so we moved to investigate the immune contexture of A-, AK-, and AKP-mice.

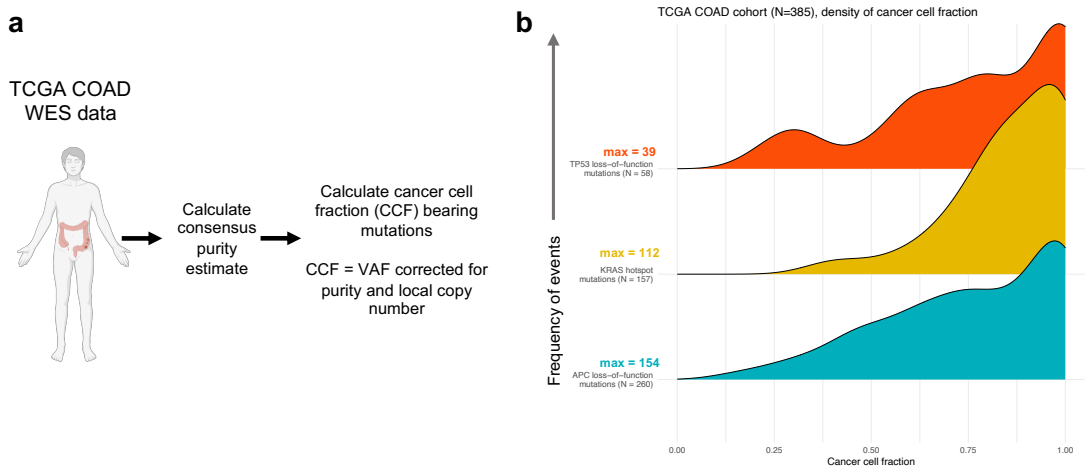

Figure 4.6 Cancer cell fractions bearing mutant alleles in human colorectal cancer. **a.** Overview of experiment. TCGA: The cancer genome atlas, COAD: colorectal adenocarcinoma, WES: whole exome sequencing. **b.** Cancer cell fraction containing *APC* loss-of-function, *KRAS* hot-spot (amino acids 12, 13, 61 and 146) or *TP53* loss-of function mutations. Analysis performed by Daniele Tavernari, PhD, Oricchio Lab, EPFL

4.1.2 The colon tumor immune microenvironment changes significantly as mouse models of CRC gain oncogenic-driver mutations

In order to define the repertoire of the tumor-infiltrating immune cells in A-, AK- and AKP-mice, we induced tumor-driving allele recombination with a single i.p. injection of tamoxifen as described above, Figure 4.1b. Tumors were allowed to develop for 6 weeks then the animals were euthanised and tumors were analysed by flow cytometric analysis. The gating strategy employed for this analysis is detailed in Figure4.8.

Overall, the normal colon as well as the TME of the A-, AK- and AKP-tumors were highly infiltrated with $CD45^+$ hematopoietic cells, which represented about 70% of live cells analysed, Figure 4.9a. AKP-tumors demonstrated a greater variation in proportion of $CD45^+$ cells in the TME than the other models, but there was no statistical difference between the means. While the levels of immune infiltration between healthy colon and tumors were similar, their make-up was not. Healthy colons had fewer $CD11b^+$ myeloid cells infiltrating in the tissue than A-, AK- and AKP-tumors, Figure 4.9b. Interestingly, AK- and AKP- tumors had similar levels of neutrophils ($TCR\beta^-CD11b^+MHCII^-SSC^{hi}Ly6C^{lo}$) and professional APCs

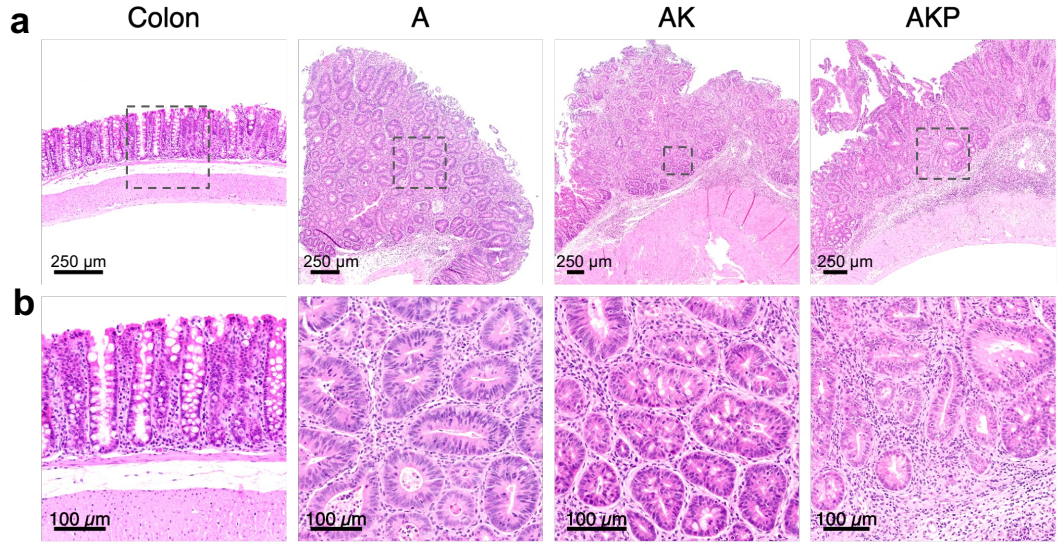

Figure 4.7 CDX2-driven CreERT2 expression drives recombination of canonical tumor-driving mutations to form colon adenocarcinomas. **a, b** Brightfield images of healthy colon (Ctrl mice), A-, AK- and AKP-tumors. Dotted line boxes in **a** are shown at greater magnification in **b**; scale bars are shown in the panels.

($TCR\beta^{-}CD11b^{+}MHCII^{+}$) to the healthy colon, Figure 4.9d and e, but significantly more monocytes ($TCR\beta^{-}CD11b^{+}MHCII^{-}$) and macrophages ($TCR\beta^{-}CD11b^{+}MHCII^{+}F4/80^{+}$), Figure 4.9c-f. A-tumors, however, had significantly more tumor-infiltrating myeloid cells than the healthy colon, as well as AK- and AKP-tumors, including monocytes, neutrophils, APCs and macrophages, Figure 4.9b-f. AK- and AKP-tumors had similar proportions of all myeloid cells, monocytes, neutrophils, APCs and macrophages, Figure 4.9c-f, having a smaller proportion of each cell type compared to A-tumors. In addition to myeloid populations, this flow cytometry cocktails also included markers for common T cell subsets.

With regard to $TCR\beta^{+}$ T cells, A-tumors had significantly fewer T cells compared to healthy colon4.10. In contrast, AK- and AKP-tumors had significantly increased $TCR\beta^{+}$ T cell infiltration compared to A-tumors and somewhat increased T cells infiltration compared to normal colon. Taken together this data suggests that tumors bearing mutations in *APC* seem to suppress T cell infiltration, possibly mediated by neutrophils as we previously reported[61]. We further found that the acquisition of an oncogenic *Kras* mutation on top of an *Apc* mutation is sufficient to revert the T cell exclusion from the TME of the CRC mouse models, indicating

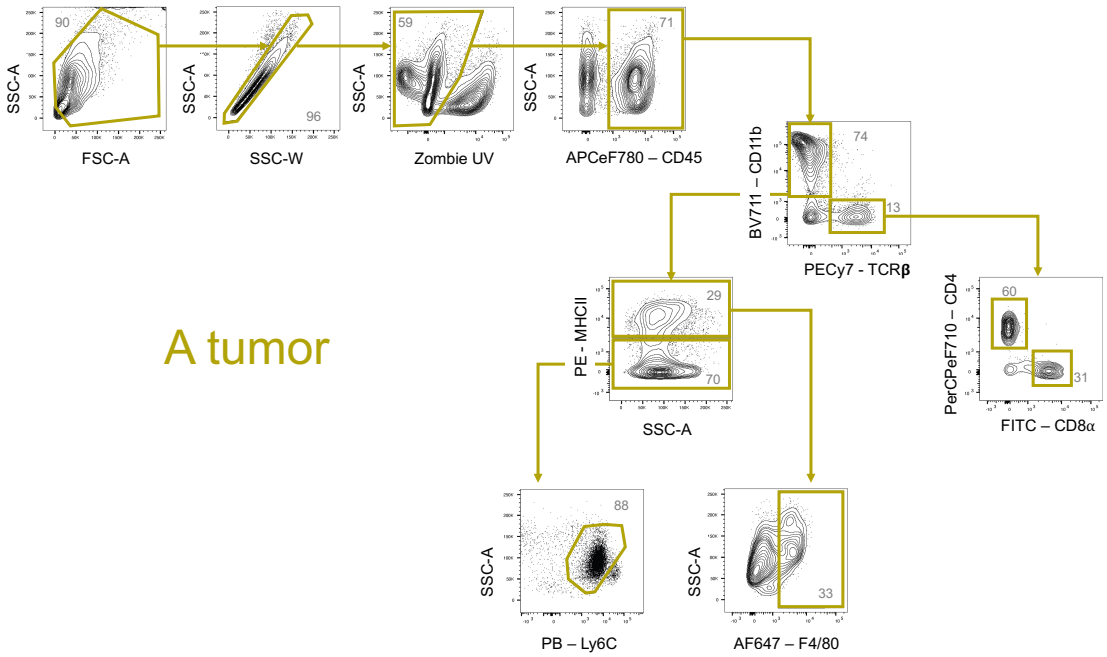

Figure 4.8 Representative gating strategy of "My" flow cytometry cocktail in an A-mouse tumor. Debris was excluded, followed by doublets. Live cells were identified as cells negative for Zombie-UV fixable dye. Immune cells were discerned by their expression of CD45, then myeloid and T lymphocyte lineages were differentiated by their expression of CD11b or TCRβ, respectively. T cells were divided by type: CD4 helper T cells or CD8 cytotoxic T cells. In the myeloid lineage, MHCII expression was used to discern those with and without professional antigen presentation capabilities. Among amateur ($MHCII^{-}$) myeloid cells, neutrophils were identified by their high side scatter, given by their segmented nuclei and granulation, and low Ly6C expression ($SSC^{hi}Ly6C^{lo}$). Within the professional myeloid population F4/80 was used to identify macrophages.

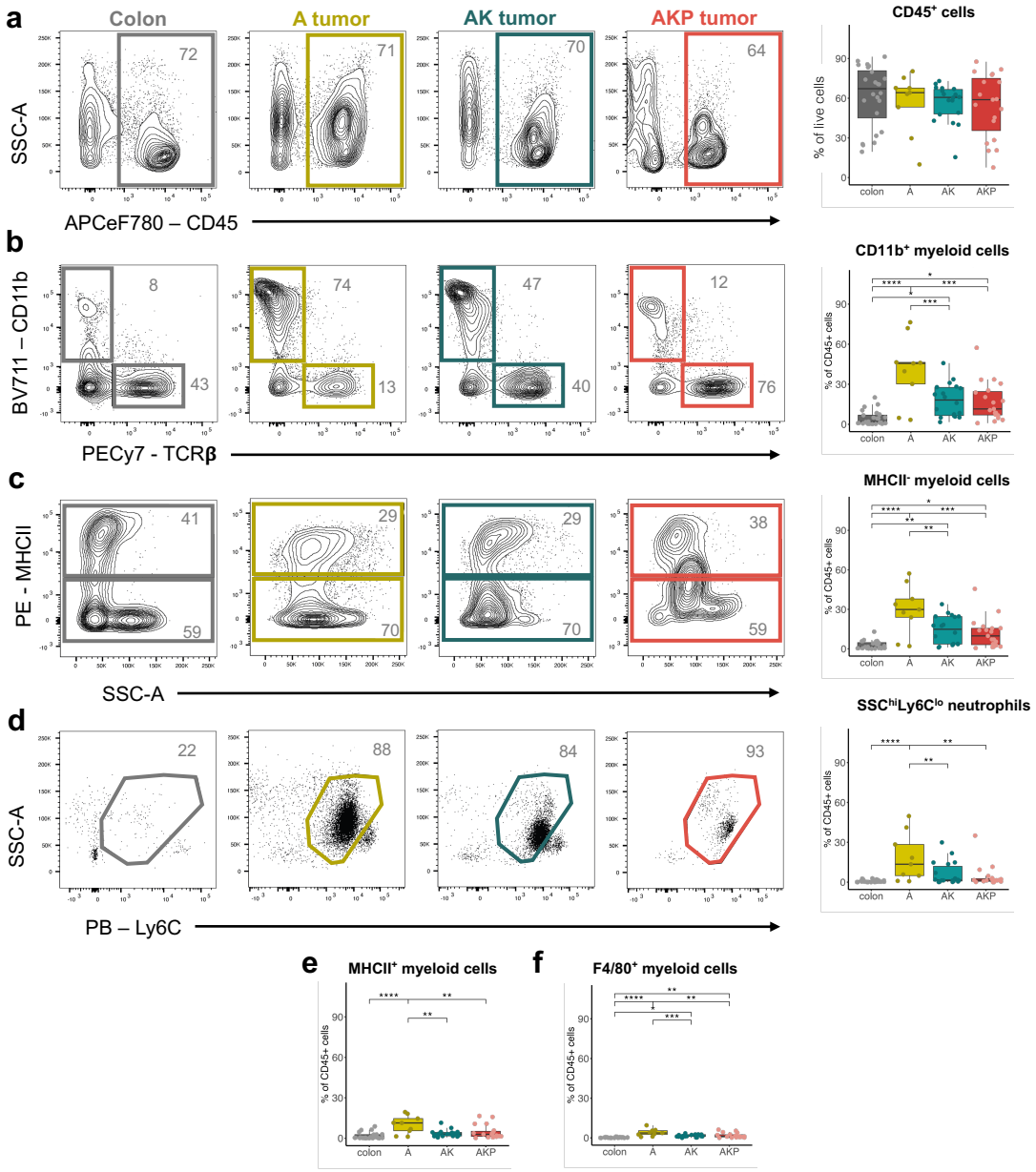

Figure 4.9 Flow cytometry shows that A-tumors have high myeloid cell infiltration while KRAS-mutant tumors have fewer. **a.** Mean percent of live tissue-infiltrating $CD45^+$ cells. Mean proportion of tumor-infiltrating **b.** $CD11b^+$ Myeloid cells **c.** $CD11b^+MHCII^-$ monocytes, **d.** $CD11b^+MHCII^-SSC^{hi}Ly6C^{lo}$ neutrophils, **e.** $CD11b^+MHCII^+$ professional APCs, and **f.** $CD11b^+MHCII^+F4/80^+$ macrophages, as percent of $CD45^+$ cells. Data shown is from 9 independent experiments; n= 24, 9, 18, and 19 animals for colon, A, AK, and AKP groups, respectively. Brackets and stars are indicative of the adjusted p value result of a one-way analysis of variance (ANOVA) with Tukey's multiple corrections to account for multiple comparisons. key: $p \leq 0.05$ = *, $p \leq 0.01$ = **, $p \leq 0.001$ = ***, $p \leq 0.0001$ = ****, and non-significant (n.s.) comparisons are not shown.

that KRAS-mediated signaling is directly or indirectly involved in T cell inclusion in the TME. Next, we more specifically analyzed different T cell subsets within the TME of our CRC mutant mouse models.

Consistent with the TCRβ^+ T cells, CD4$^+$ helper T cells were significantly more present in AK- and AKP-tumors compared to A-tumors and healthy colon, Figure 4.10. Cytotoxic, CD8$^+$ T cells, followed the same trend as their CD4$^+$ counterparts, but the trend was not significant as tumors had variable CD8$^+$ infiltration, Figure 4.10b. Across all tumors, there were more CD4$^+$ T helper cells than CD8$^+$ cytotoxic T cells in the tumor microenvironment, Figure 4.10b and c. Though the CD4/CD8 phenotype is informative of a general role for T cells within the TME, CD4 cells for example can play many roles including pro- and anti-tumor roles and CD8 T cells may or may not be activated.

In order to more precisely assess additional subsets of tumor-infiltrating lymphocytes (TILs) in A-, AK- and AKP-mice, we conducted flow cytometry intracellular (IC) staining for FoxP3, Figure 4.11. FoxP3 is a transcription factor expressed by regulatory T cells (Tregs), which play an immune-suppressive role in tissue thereby ensuring self-tolerance but often prevent anti-tumor immunity in the cancer context[93,94]. In our mouse models, we found that the healthy colon of mice is indeed patrolled by Tregs (presumably abrogating autoimmunity within the gut) and that A-, AK- and AKP-tumors tended to have relatively few Tregs in the TME compared to colon. For AK-tumors this trend was indeed significant, Figure 4.12a and b. The relatively low representation of Tregs within the TME of our tumor-bearing mic suggest that effector T cells are unlikely to be suppressed by Tregs and thus could become activated and effect their function.

To approximate the level of T cell activation, single-cell suspensions of the tissues were stimulated with PMA and ionomycin *ex vivo* and the intracellular proteins of interest such as granzyme b (GZMb), interleukin 17a (Il17a) and IFNγ were assessed by flow cytometry within the same panel. In order to set gates, fluorescence minus intracellular staining (FMIC) controls were established and recorded by dividing the single-cell samples

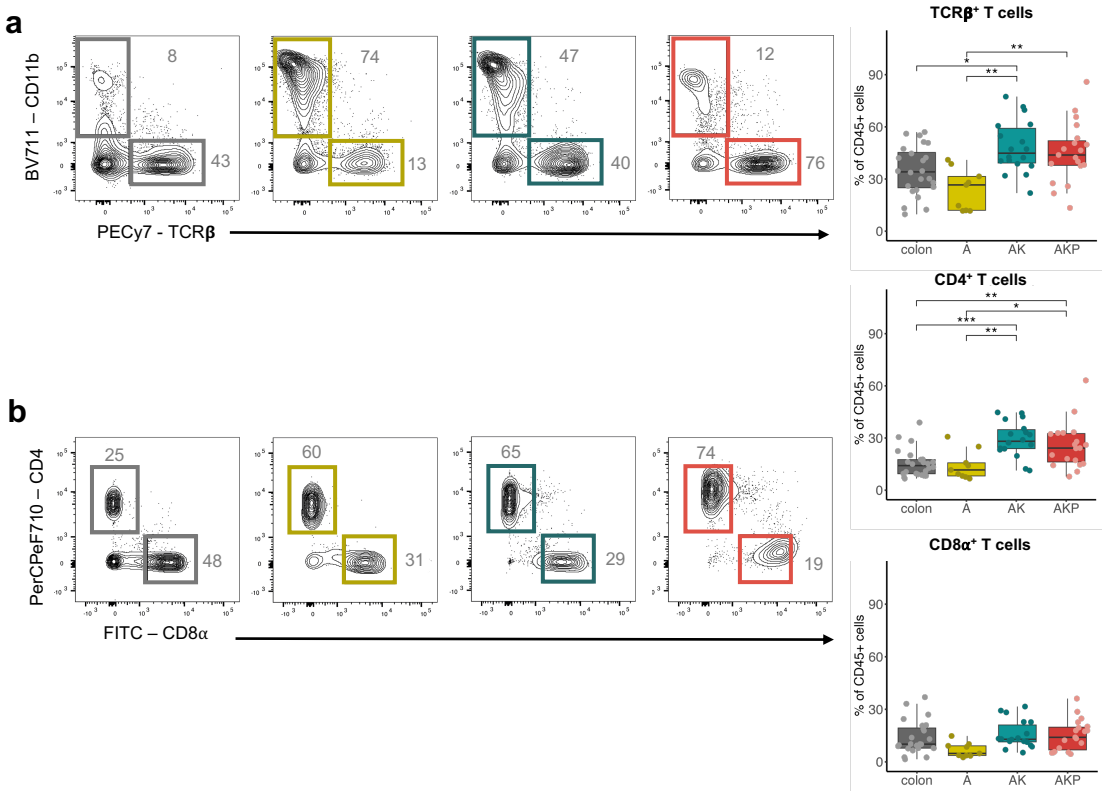

Figure 4.10 KRAS-mutant tumors are significantly more infiltrated with T cells than those without KRAS activation. Data shown is from 9 independent experiments; n= 24, 9, 18, and 19 animals for colon, A, AK, and AKP groups, respectively. Brackets and stars are indicative of the adjusted p value result of a one-way ANOVA with Tukey's multiple corrections to account for multiple comparisons. key: $p \leq 0.05$ = *, $p \leq 0.01$ = **, $p \leq 0.001$ = ***, $p \leq 0.0001$ = ****, and non-significant (n.s.) comparisons are not shown.

in half after surface staining, and only applying intracellular antibodies to one group, Figure 4.13. Granzyme B, a serine protease, serves as a key effector molecule in the tumor microenvironment promoting apoptosis of target tumor cells via proteolytic cleavage of several caspase enzymes[95–98]. Th17 cells are a subset of CD4 helper T cells characterised by their expression of Il17a, a cytokine with multiple, opposed roles within the TME. Il17a has been shown in multiple contexts to recruit neutrophils and promote angiogenesis, but evidence has been accumulating that implies that it may also promote tumorigenesis and promote immune evasion by cancer cells[99–101]. Finally, the cytokine IFNγ has long been known to be an anti-tumor effector molecule which is secreted mainly by type 1 helper T cells (Th1) and cytotoxic ($CD8^+$) T cells. IFNγ has been shown to contribute to anti-tumor immunity through induction of apoptosis or cell cycle arrest in tumor cells, enhancing antigen

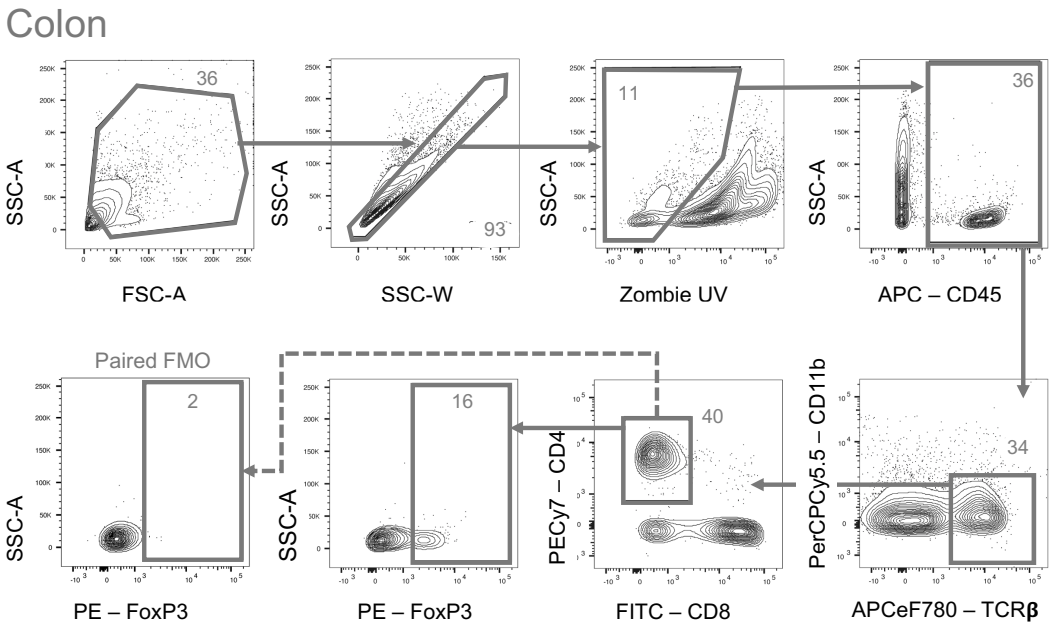

Figure 4.11 Representative gating strategy of "Fox" flow cytometry cocktail in an Ctrl-mouse healthy colon. Debris was excluded, followed by doublets. Live cells were identified as cells negative for Zombie-UV fixable dye. Immune cells were discerned by their expression of CD45. T cells were positively identified by their expression of TCRβ then helper T cell lineage was identified by their expression of CD4 (CD8 was used to definitively exclude cytotoxic T lymphocytes). Intracellular staining coupled with pair-wise FMO controls for FOXP3 transcription factor was used to positively identify regulatory T cells.

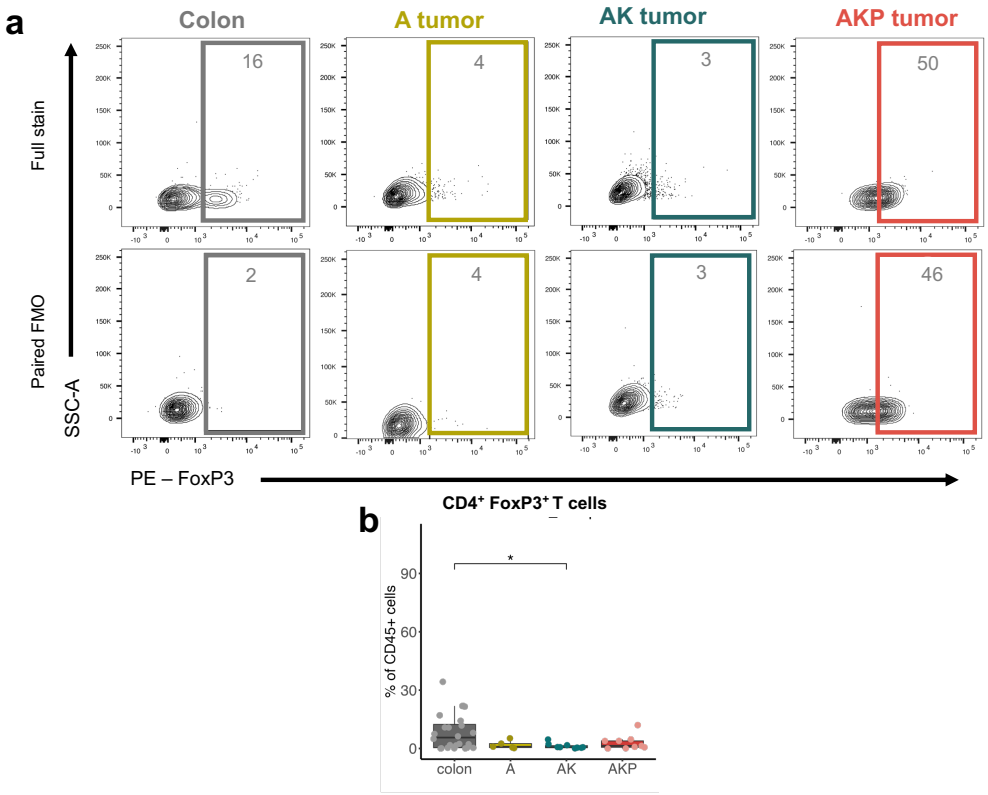

Figure 4.12 Regulatory T cells are less abundant in tumors than in healthy colon. **a.** representative scatter plot of SSC-A vs. PE-FoxP3 for colon, A-, AK- and AKP-tumors. Top panel shows full stain, bottom panel shows paired FMOs. **b.** Quantification of $CD4^+FoxP3^+$ regulatory T cells in colon, A-, AK- and AKP-tumors. Data shown is from 5 independent experiments; n= 24, 5, 10, and 9 animals for colon, A, AK, and AKP groups, respectively. Brackets and stars are indicative of the adjusted p value result of a one-way ANOVA with Tukey's multiple corrections to account for multiple comparisons. key: $p \leq 0.05$ = *, $p \leq 0.01$ = **, $p \leq 0.001$ = ***, $p \leq 0.0001$ = ****, and non-significant (n.s.) comparisons are not shown.

presentation by both professional APCs and tumor cells, and through the recruitment and activation of immune cells to the tumor site[102–106]. It has also been observed, however, that IFNγ can also contribute to cancer cell stemness and thus promote metastasis[107–110].

In the tumors of our mouse models of colorectal cancer we found that among TCRβ^+ T cells, AK-tumors had greater IFNγ production compared to A-tumors, Figure 4.14a. AKP-tumor infiltrating T cells also had significantly more IFNγ production compared to the healthy colon, but the trend was non-significant in comparison to A- and AK-tumors Figure 4.14a. Among all T cells, GZMb and IL17a expression did not significantly differ between models, but AK-tumors had more GZMb-expressing T cells when compared to the colon, Figure 4.14b

and c. We then examined specifically the $CD4^+$ helper T cell expression of IFNγ and IL17a. AK-tumors had more $IL17a^+CD4^+$ Th17 cells than the healthy colon, Figure 4.14. There was also a non-significant trend of Th17 presence in A- and AKP-tumors compared to the healthy colon, a recapitulation of a phenotype observed in human colorectal cancer[111,112]. No significant differences were observed when the tumors were compared to each other, but AK- and AKP-tumors tended to have more Th17 cells compared to A-tumors, Figure 4.14d and e.

We next measured the expression of the cytokines GZMb and IFNγ in cytotoxic CD8+ T cells. AK-tumor-infiltrating $CD8^+$ T cells produced significantly more IFNγ and GZMb compared to the healthy colon, Figure 4.14f and g. All tumor types had more IFNγ and GZMb production than the healthy colon, but the trend was not significant for A- and AKP-tumors and, furthermore, there were no significant differences between the tumors, Figure 4.14f and g. Cytotoxic T cells in AK-tumors, however, produce more IFNγ than A-tumors, and AKP-tumor-infiltrating cells exhibited variable IFNγ expression, Figure4.14f. Finally, all tumors tend to have slightly higher GZMb expression among the CD8+ cytotoxic T cells compared to those in healthy tissue (Figure 4.14g), but only AK tumors had significantly higher GZMb expression among this population.

Taken together, this data shows that there is greater T cell activation within tumors compared to the healthy colon, and when the tumors gain constitutive KRAS signaling the T cells may become more activated. Coupled with the observation that AKP-tumors demonstrated non-significantly elevated levels of the cytokines of interest and that the expression of the cytokines was more variable than in the other tumors, the data suggests that inactivation of p53 in tumor cells may slightly abrogate the T cell activation conferred by the KRAS mutation. Despite the general level of T cell activation, the T cells were clearly unable to overcome the tumor. We therefore asked whether this inability to confer efficient anti-tumor immunity was due to spatial exclusion from the malignant epithelial cells, a common phenotype observed in human adenocarcinomas[60].

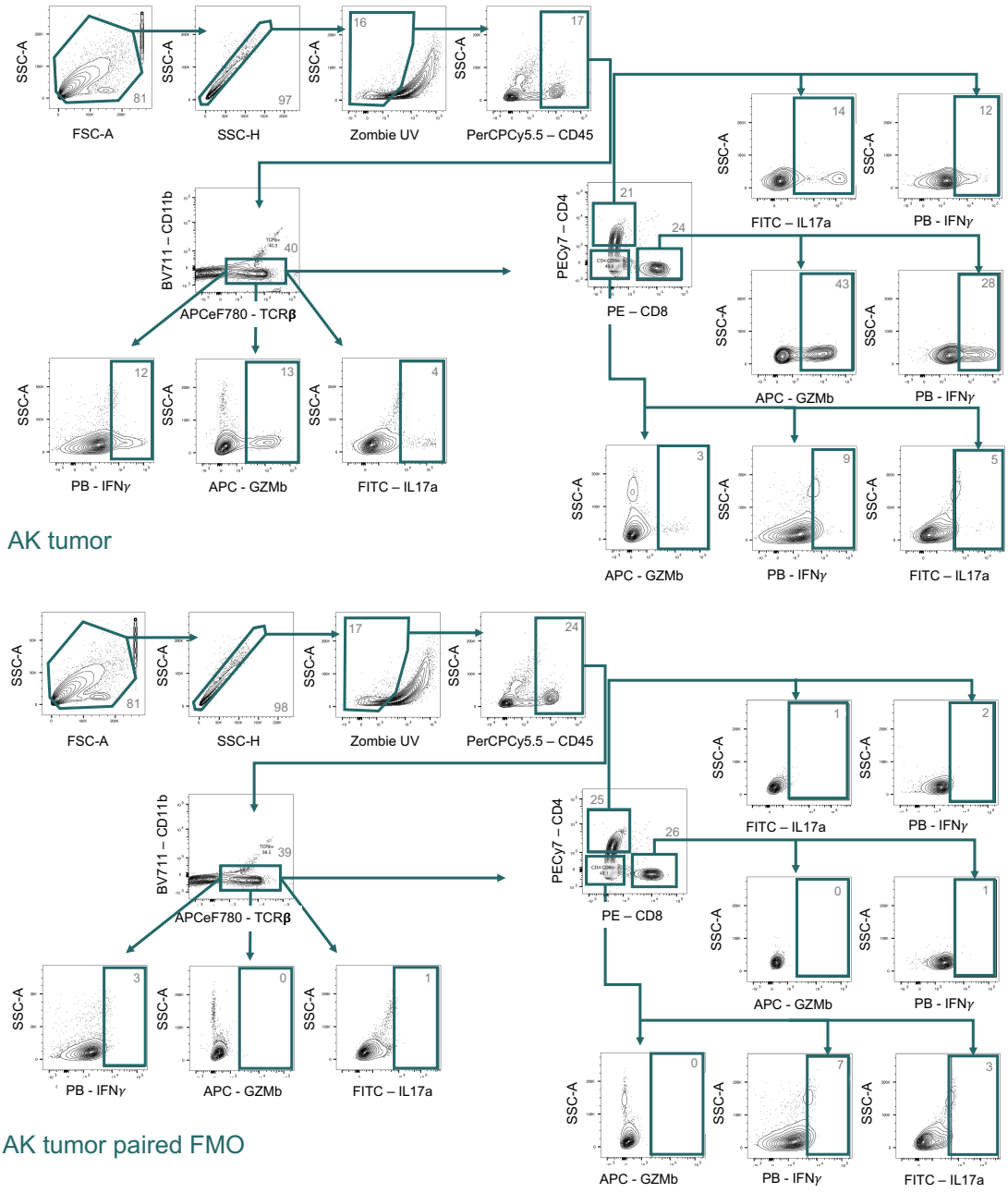

Figure 4.13 Representative gating strategy of "Th" cocktail in an AK-tumor. Debris was excluded, followed by doublets. Live cells were identified as cells negative for Zombie-UV fixable dye. Immune cells were discerned by their expression of CD45. T cells were identified by TCRβ expression, then separated by their expression of CD4 and CD8. Their IC expression of GZMb, IFNγ and IL17a were then assessed. TOP: full stain including IC targets in an AKP-tumor, BOTTOM: paired FMIC.

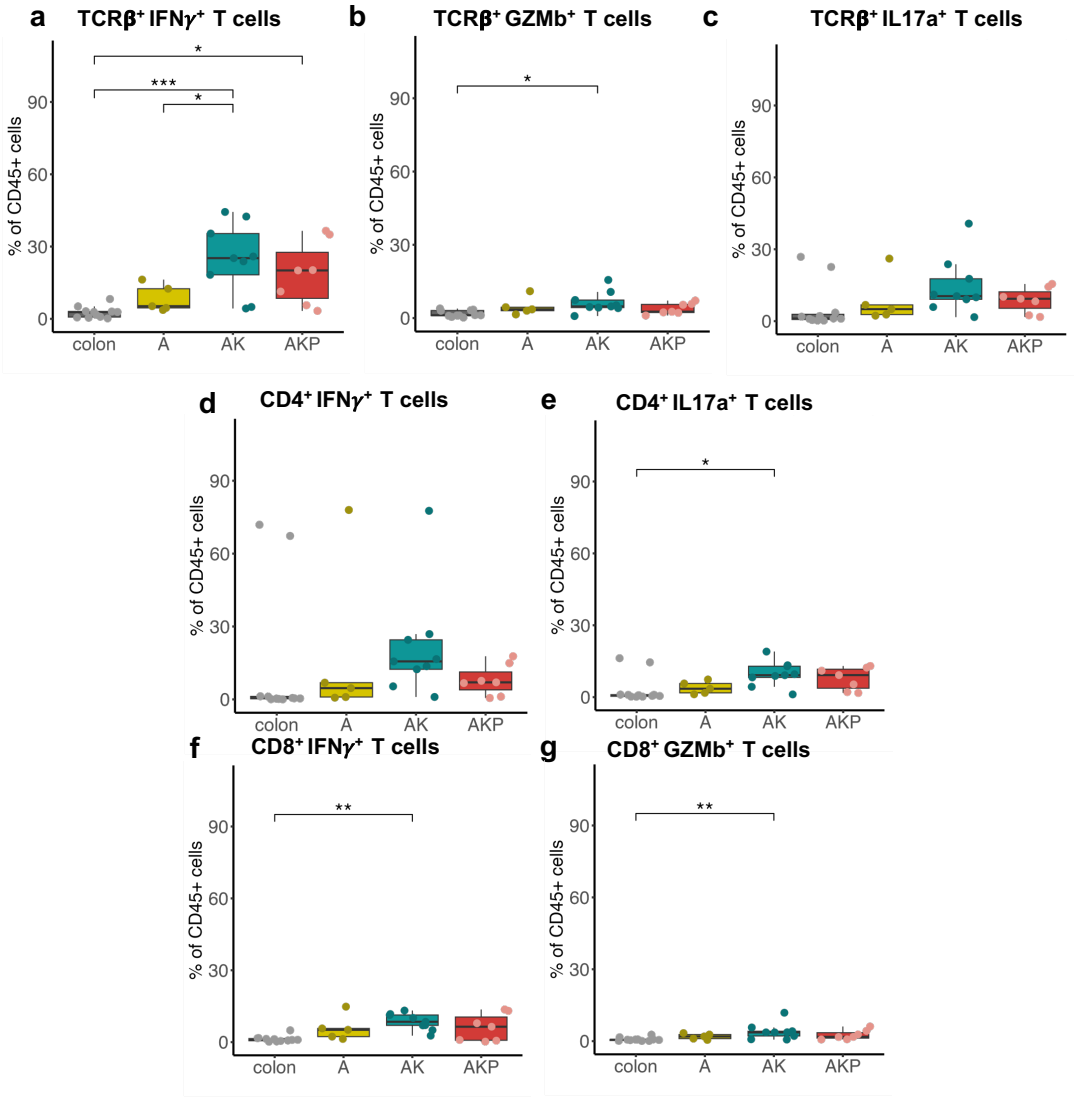

Figure 4.14 Flow cytometry and immunohistochemistry reveal trends toward increase T cell activation in KRAS mutant tumors. Cells were stimulated *ex vivo* with PMA and ionomycin for 3.5 hours, and their intracellular IFNγ^+, GZMb, and IL17a was measured by flow cytometry. Mean percent of tissue-infiltrating **a.** TCRβ^+IFNγ^+ T cells, **b.** TCRβ^+GZMb$^+$ T cells **c.** TCRβ^+IL17a$^+$ T cells, **d.** CD4$^+$IFNγ^+ helper T cells, **e.** CD4$^+$IL17a$^+$ Th17 cells, **f.** CD8$^+$IFNγ^+ cytotoxic T cells, and **g.** CD8$^+$GZMb$^+$ cytotoxic T cells as percent of CD45$^+$ cells. Data shown is from two independent experiments; n= 11, 5, 9, and 7 animals for colon, A, AK, and AKP groups, respectively. Brackets and stars are indicative of the adjusted p value result of a one-way analysis of variance (ANOVA) with Tukey's multiple corrections to account for multiple comparisons. key: $p \leq 0.05$ = *, $p \leq 0.01$ = **, $p \leq 0.001$ = ***, $p \leq 0.0001$ = ****, and non-significant (n.s.) comparisons are not shown.

We performed IHC staining on paraformaldehyde-fixed paraffin-embedded samples of healthy colon, A-, AK- and AK-tumors for CD3 (a TCR co-receptor expressed on all mature T cells), CD8 and FoxP3 to determine the localisation of these cells within the tissue. We found that $CD3^+$ T cells were within the lamina propria of A, AK, and AKP-mice, Figure 4.15a. Remarkably, many $CD3^+$ cells appear to make direct contact with malignant crypts in AK- and AKP-tumors, and is particularly pronounced in AKP-tumors, Figure 4.15. Quantification of the staining showed that the same trend observed by flow cytometry could also be observed by IHC: AK- and AKP-tumors have significantly more tumor-infiltrating $CD3^+$ T cells compared to A-tumors and healthy colon, Figure 4.15b. Staining for CD8 revealed similar findings to those from the CD3 staining. Cytotoxic T cells were observed to be in close proximity to malignant crypts of A-, AK-, and AKP-tumors, but was particularly notable in AK- and AKP-tumors, Figure 4.15c. In line with the previously shown trends observed in the flow cytometry data, quantification revealed that AK- and AKP-tumors had significantly more $CD8^+$ T cells than A-tumors by IHC, Figure 4.15d. Irrespective of the intimate contact between cytotoxic cells and the tumors, the tumors remained, indicating that another component of the TME such as Tregs could be blocking anti-tumor immunity.

We therefore conducted IHC staining for FOXP3 on colon, A-, AK- and AKP-tumors and obtained results that deviate slightly from those acquired by flow cytometry. By IHC, healthy colons contained Tregs at a lower frequency than tumors (Figure 4.15e and f), while flow cytometry assessment of FOXP3 showed the healthy colon to have more Tregs than the tumors, Figure 4.12b. Furthermore, IHC quantification of the FOXP3 staining showed significant differences in the proportions of tumor-infiltrating Tregs between A-, AK- and AKP-tumors, Figure 4.12f. A-tumors had the greatest proportion of Tregs (by IHC) followed by AK-tumors then AKP-tumors and the healthy colon, Figure 4.12f. The overall proportion of Tregs (as measured by IHC), however, is quite low at 0-2% of all detected cells. Whether the statistically significant differences between A-tumors with 2% of Tregs and AKP-tumor with 1% of Tregs has *biologically* significant impact on anti-tumor immunity or tumor progression remains to be shown.

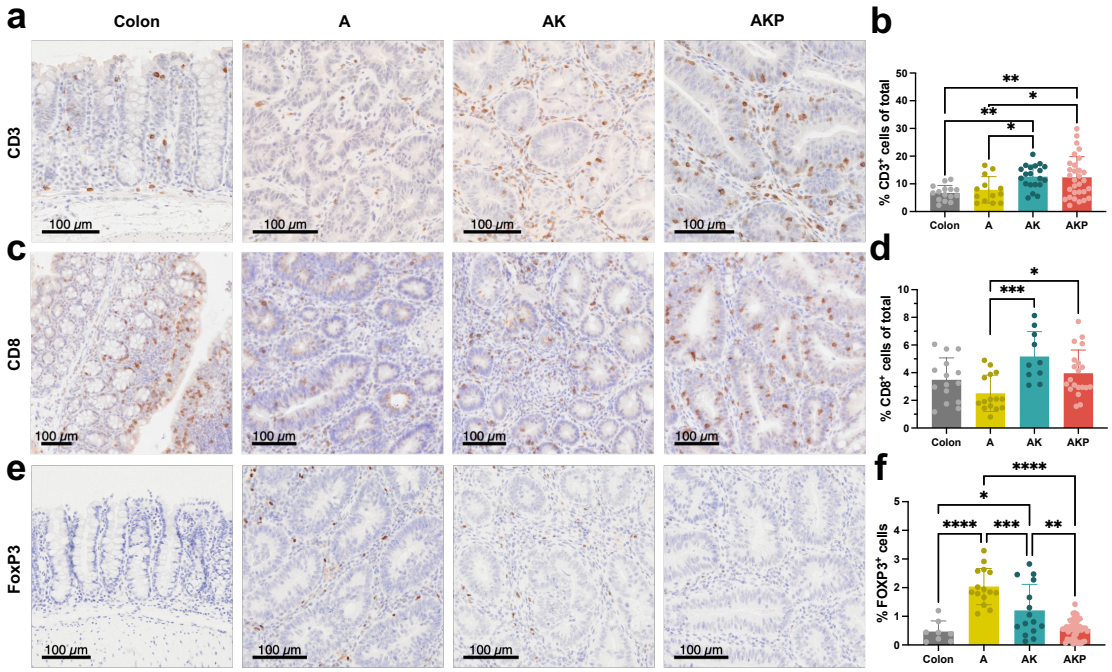

Figure 4.15 Immunohistochemistry reveals distinct proportion and localisation of tumor-infiltrating T lymphocytes in CRC tumors with different driver mutations. Mean percent of tissue-infiltrating **a.** Representative images of CD3 IHC in each group **b.** quantification of CD3 IHC. **c.** Representative images of CD8 IHC in each group **d.** quantification of CD8 IHC. **e.** Representative images of FOXP3 IHC in each group,**f.** quantification of FOXP3 IHC. Brackets and stars are indicative of the adjusted p value result of a one-way ANOVA with Tukey's multiple corrections to account for multiple comparisons. key: $p \leq 0.05$ = *, $p \leq 0.01$ = **, $p \leq 0.001$ = ***, $p \leq 0.0001$ = ****, and non-significant (n.s.) comparisons are not shown. The CD8 and FoxP3 stainings and quantification were conducted by Elia Escoffier for a Master's project under my supervision, the CD3 staining was conducted by the HCF facility at EPFL, and I performed the quantification.

Taking into consideration the cumulative data between flow cytometry and IHC, AK- and AKP-tumors were infiltrated at a higher frequency with T cells than A-tumors. We therefore postulated that T cell infiltration is associated with constitutive MAPK signaling in the GEMMs of CRC. Thus, we sought to answer the question of how constitutive MAPK signaling could lead to increased T cell infiltration in tumors. In order to answer this question, we performed scRNAseq to determine differentially expressed transcripts between relatively "cold" A-tumors and "hot" AK- and AKP-tumors.

4.1.3 scRNAseq allows definition and identification of small cell clusters present in A-, AK- and AKP-tumors and healthy colon.

In order to answer the question of how T cells are preferentially included in KRAS-mutant tumors, as well as to acquire further information on the TME of the GEMMs, we performed scRNAseq paired with IHC and flow cytometric analysis, Figure 4.16a. We aimed to collect 4,000 cells per sample for scRNAseq and sequenced at a depth of 75,000 reads/cell. The reads were mapped to the mm10 reference genome. Several components of the raw gene expression matrices were then used to filter low-read genes, doublets, dead cells, and so-called "empty" cells out of the data. After data cleaning, between 1,700 and 3,000 cells from each sample remained in the analysis for a total of 21,816 cells, Figure 4.16b. Following cell filtering, the gene expression matrix was $\log_2$ normalised, integrated and scaled. Twenty-five principal components were retained for uniform manifold approximation and projection (UMAP)-based dimensional reduction. Unsupervised clustering with a resolution of 0.2 was used to define 10 clusters in the data, Figure 4.16c. The clusters were then annotated based on their expression of *bona fide* transcripts, Figure 4.16d. Explicitly, T cells were identified by their expression of *Cd3e, Cd4, Cd8a* and *Gzma*[113]. Strong *Igha* expression distinguished plasma cells. Neutrophils constitutively expressed the calcium-dependent transcript *S100a9*, and mast cells were spotted for their *Kit* expression[114,115]. Macrophages were initially difficult to distinguish from their dendritic cell cousins, but *Cd68, C1qc, Flt3* and *Fscn1* expression patterns revealed the divergence between these clusters[114,115]. *Dcn* and *Postn*, transcripts

for proteins involved in collagen fibril assembly and fibrosis, were clear indicators of fibroblasts. Epithelial cells, including both healthy and malignant cells, were delineated with *Epcam* and *Krt19*. Endothelial cells were discriminated by their *Pecam1* expression. Lastly, B cells were profiled by their *Cd79a* expression. Following cluster annotation, differential abundance analysis could be conducted to validate our flow cytometry and IHC findings.

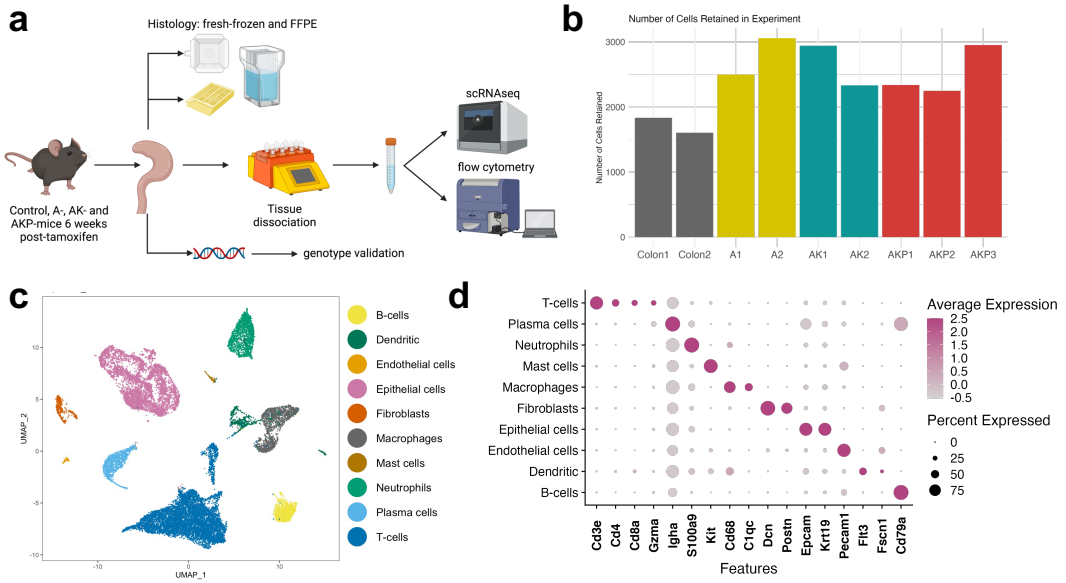

Figure 4.16 scRNAseq sequencing allows definition of many cell types in mouse models of CRC. **a.** Experimental scheme. Mice received a single i.p. injection of tamoxifen to allow for tumor formation. Mice were euthanised and analysed 6 weeks post-tamoxifen. Samples were taken for histology, DNA extraction (for genotype validation) and subjected to tissue dissociation. Dissociated samples were submitted, pairwise, to scRNAseq and flow cytometry analysis. **b.** Number of cells remaining in single-cell experiment after quality control and filtering, **c.** UMAP projection of cells and their clusters (after unsupervised clustering) captured in the experiment, **d.** Dot Plot showing average expression and percent of cells expressing transcripts within annotated unsupervised clusters of key transcripts used to annotate each cluster in the experiment.

scRNAseq allowed for the identification of more subtypes of immune cells within the TME compared to flow cytometry. For example, B cells could be observed as a large component of the healthy colon that was nearly excluded from all tumors, Figure 4.17a. Epithelial cells underwent evident expansion in tumors compared to the healthy colon, Figure 4.17a. Dendritic cells, macrophages and plasma cells became more abundant in tumors than in the healthy colon, Figure 4.17a. Fibroblasts became less abundant in tumor groups compared to the healthy condition, Figure 4.17a. Neutrophils, which were nearly undetectable in the

healthy colon became prominent in A-tumors, decreased in AK-tumors and became nearly absent again in AKP-tumors, highlighting the inverse correlation of neutrophils and T cells in the TME we previously described[61].

T cells, which made up about 50% of cells in the healthy colon and submucosae, were much less abundant in A-tumors, and increased in abundance in AK- and AKP-tumors, Figure 4.17a. This data confirms our flow cytometric findings, and a linear regression found a significant positive 92% correlation with an R^2 value of 0.85 (correlation^2 = R^2; correlation = $\sqrt{R^2}$= $\sqrt{0.85}$ = 0.92) between annotated T cells in the scRNAseq experiment and the paired flow cytometry data from the same mouse, Figure 4.17b. Additionally, R^2 value from the regression between annotated myeloid cells in the scRNAseq experiment (the sum of dendritic cells, neutrophils, and macrophages) was 0.87 (93% correlation), further increasing our confidence in both modalities we employed for the analysis of the TME in our mouse models, Figure 4.17c. Driven by curiosity, we also correlated T cells measured by CD3 IHC with the T cell abundance data from scRNAseq and flow cytometry, Figure 4.17d. A multiple linear regression determined the R^2 value between the three methods to be 0.77, and significantly positively correlated, Figure 4.17d. Encouraged by these confirmations of the quality of the data, we next moved to more precisely define what types of cells were present within the TME of A-, AK- and AKP-tumors.

In order to discover what sub-types of cells were present within the A-, AK- and AKP-tumors, we performed subclustering on the main clusters identified in the data, namely the myeloid, T, and epithelial cell clusters. Subclustering involves removing all other cells from the experiment except those in the cluster of interest. Beginning from count matrices, top variable genes, integration and scaling was performed on the data which was then submitted to principle component analysis (PCA) and unsupervised clustering. This allows the clustering to reflect the differences between the cells that remain in the experiment, as opposed to those in the entire tumor. Top genes that differentiate each cluster from the others can then be found to inform their annotation.

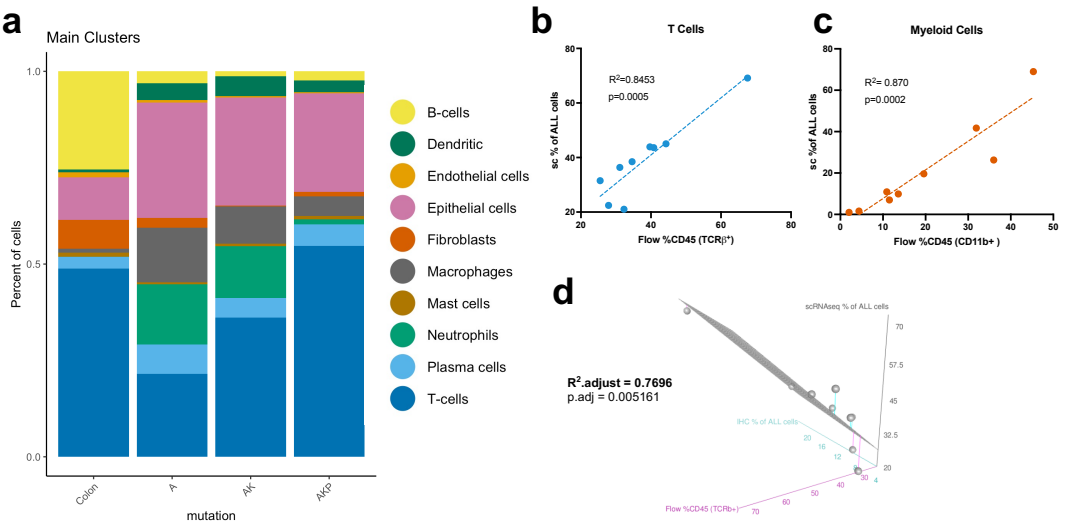

Figure 4.17 scRNAseq confirms findings in flow cytometry and immunohistochemistry. **a.** Stacked barplot with frequency of each cell cluster within each group (colon, A-, AK- and AKP-tumor), **b.** paired linear regression of T cells quantified by scRNAseq and flow cytometry, **c.** paired-sample linear regression of myeloid cells detected by scRNAseq and flow cytometry, and **d.** 3D scatter plot and multiple linear regression of T cells detected by scRNAseq, flow cytometry (TCRβ^+) and IHC ($CD3^+$).

Fourteen myeloid clusters were identified by unsupervised clustering, Figure 4.18a. Because of their shared ancestry, annotating myeloid cells is very complex. Several of our annotations were informed by cell types identified in a pan-cancer human dataset for tumor-infiltrating myeloid cells[116]. Neutrophils, however, formed a distinct cluster in the UMAP projection away from the dendritic cells and macrophages, Figure 4.18a. There were five neutrophil clusters within the data which were distinguished by their *S100a9* expression. The clusters were annotated with the top genes that differentiated them from all of the other myeloid clusters, *Hmox1, Anxa1, Irf1* and *Retnlg*[117]. Pathways enriched in each cluster were assessed using String Pathways[118]. The *Anxa1*$^+$ neutrophil subset had clear enrichment of activation pathways, the *Retnlg*$^+$ demonstrated enriched migratory pathways, and the *Irf1*$^+$ had high interferon-related pathways, and the remaining cluster did not have any clear pathway enrichment and was simply annotated by the top gene that distinguished it from the others, *Hmox1*, Figure 4.18b. Having identified the subsets of neutrophils which represent the "amateur" component within the microenvironment, we next examined the professional antigen presenting compartment, namely dendritic cells and macrophages.

Four dendritic clusters were present in the experiment. We identified two clear populations and two populations that were less straightforward to annotate. We were able to identify DC3 dendritic cells within the dataset, characterised by *Ccr7* expression, which have been reported among human and murine tumors, and may be ideal targets for agonistic CD40 immunotherapy[114,116,119]. Furthermore, *Ccr9* expression indicated the presence of plasmacytoid dendritic cells (pDC)s, a dendritic cell subtype associated with poor prognoses in cancer[120]. Macrophages were distinguished from dendritic cells by their higher relative expression of *Apoe*[121,122], Figure 4.18b. A third dendritic cell population was characterised by *Kit* expression, a receptor tyrosine kinase not necessarily exclusively affiliated with dendritic cells. We then examined the other major pAPC population: macrophages. Recently, the complement protein C1QC was identified to be a marker for an anti-tumor macrophage population in colorectal cancer due to its enrichment of complement activation, antigen processing and presentation[115,116,123]. We found two *C1qc*$^+$ positive populations, one which was distinguished from the others by *Ptgs1*(COX1), *Vcam* and *Mmp14* expression, indicative of an alternatively activated M2 phenotype characterised by promotion of angiogenesis and inflammation clearing[124,125], Figure 4.18b. The other population, Macro_C1qc was mainly characterised by its expression of C1Q proteins, indicating a rather pro-inflammatory phenotype. *Ccr2* expression distinguished the remaining two macrophage clusters, a receptor associated with monocyte recruitment in the gut[126]. The top transcripts differentiating these populations from the other clusters were *Inhba* and *Vcan*. Interestingly, both express *Ass1*, an important component in the urea cycle that is vital for the innate activity of macrophages[127].

In terms of relative abundance of tissue infiltrating myeloid cells, several trends can be noted, but valid statistical tests cannot be performed due to the fact that only two samples of Colon, A- and AKP-tumors were sequenced for the experiment. First, the healthy colon has very few myeloid lineage cells as compared to malignant conditions, Figure 4.18c. A-tumors had a pronounced expansion of neutrophils (Figure 4.18d), mainly made up of *Irf1* and *Retnlg*$^+$ migratory neutrophils. A small number of *Hmox1*$^+$ neutrophils were also present in the A-tumors, Figure 4.18c. Among AK-tumors, the number of neutrophils were slightly

fewer than in A-tumors (Figure 4.18d), which can perhaps be accounted for by a decrease in the number of migratory-like neutrophils, Figure 4.18c. Interestingly, *Anxa1*$^+$ neutrophils appeared (though in small numbers) in the AK-tumors and the *Hmox1*$^+$ population became less abundant, Figure 4.18c. A dramatic loss of neutrophils was observed within AKP-tumors, Figure 4.18d. In fact, the *Hmox1*$^+$ and *Anxa1*$^+$ clusters were not present in AKP-tumors at all and the few neutrophils that remained were migratory and *Irf1*+ neutrophils, Figure 4.18c.

Macrophages were the next most prominent myeloid cell type in the tumors, but were also present in the healthy colon, Figure 4.18d. A-tumors had the greatest number of macrophages, and the *Inhba*$^+$ population was the most abundant, followed in number by the *Vcan*$^+$, *C1qc*$^+$ and M2 populations. When tumors gained KRAS mutations–as in AK- and AKP-tumors–there appears to be an expansion of M2 macrophages (Figure 4.18c), a previously observed phenotype[128]. In turn, and particularly in AKP-tumors, there were fewer *Inhba*$^+$ and *Vcan*$^+$ macrophages, Figure 4.18c. Finally, dendritic cells were the least numerous and dynamic myeloid cells in the experiment, Figure 4.18d. A-tumors appeared to have the largest population of *Kit*$^+$ dendritic cells. Dendritic_DC3s, Dendritic_pDCs and the generic Dendritic clusters were represented in every tumor type in small numbers, Figure 4.18c.

Overall, we observed a variety of tumor-infiltrating myeloid cells using scRNAseq including several clusters previously identified in other studies of human and murine cancers[115,116,123], and the difference in abundance of myeloid cells observed between the mouse models of colorectal cancer by flow cytometry were also identifiable by this modality. In brief, the myeloid cell abundance dropped as the mouse models of CRC gained tumor-driving mutations. Our next goal was to discover which types of T cells resided within the tumors.

Unsupervised clustering of the healthy colon T cells and tumor-infiltrating lymphocyte (TIL)s defined 11 populations, Figure 4.19a and b. We first inspected the cells for expression of canonical TCRs, TCR co-receptors and their chains to isolate each cell type. $\gamma\delta$-T cells were identifiable by their expression of *Tcrg-C1* and *Trdc* and appeared to be mature (*Cd44*$^+$)

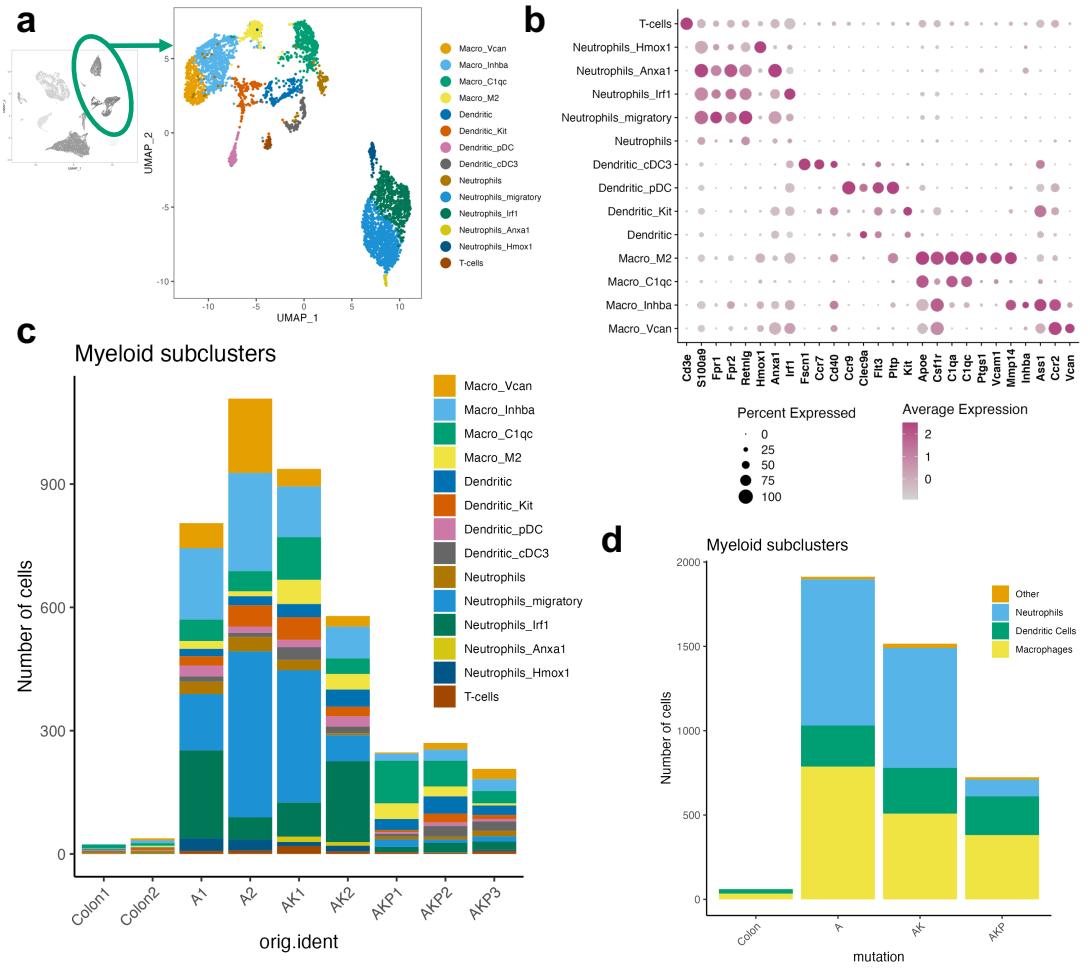

Figure 4.18 Myeloid cell abundance drops as CRC GEMMs gain driver mutations. **a.** UMAP projection of sub-clustering analysis of myeloid cells after unsupervised clustering **b.** dotplot demonstrating expression of key transcripts which informed cluster annotation **c.** stacked bar plot of number of cells per sample within each myeloid subcluster.

with *Il17a* production[129,130], Figure4.19c. Two varieties of intra-epithelial lymphocyte (IEL)s were apparent in the data set, most notably by their expression of CD8$\alpha\alpha$ co-receptor (*Cd8a*$^{+}$ *Cd8b*$^{-}$) and their expression of an approximately even distribution of $\alpha\beta$- and $\gamma\delta$-TCRs[98,131]. Cytotoxicity segregated these two clusters, indicated by *Gzmb* expression in the Cytotoxic cluster that was abrogated in the IEL cluster, Figure 4.19c. Innate T lymphocytes such as natural killer cells (NK) cells and type 2 innate lymphoid cell (ILC2)s could be identified by their respective expression of *Prf1* and *Gata3*, Figure 4.19c. Tregs were identified by their clear *Foxp3* expression and *Il10* production; *Il17a*, the namesake interleukin distinguished T

helper 17 cell (Th17) cells. An evident proliferative cluster of T cells emerged with a mixture of T cell subtype markers expressed, suggesting that proliferative cells have more in common with each other than their own subset (i.e. Th1, Th17, or CD8$^+$). Classical CD8$\alpha\beta$ and CD4$^+$ T cells were also present in the experiment, and clearly expressing *Cd44* and *Ifn*γ, Figure 4.19. Finally, naive cells could be distinguished by *Sell* (CD62L), *Ccr7*, and *Lef1* transcripts.

We know that the healthy colon is heavily patrolled by T lymphocytes because it represents the barrier between the "inside" of the body and the outside world[132]. Indeed, within the mouse healthy colon, we captured almost 1,000 T cells from each healthy sample–one quarter of our target number of cells for 10X sequencing, Figure 4.19d. IELs were the largest population in the healthy colon, and the cytotoxic IEL population was most abundant in the healthy condition, Figure 4.19e. Naive *Sell*$^+$ cells made up a substantial proportion of T cells in healthy tissue, a sign that the adaptive immune system is poised for prompt response in case of foreign antigen presentation in the colon (most probably within tertiary lymphoid structure (TLS)s), Figure 4.19e. In terms of the TILs, the number and frequency of naive T cells was much lower in A-, AK- and AKP-tumors compared to the healthy colon, suggesting that the majority of T cells within the tumors had been educated, Figure 4.19d and e. Overall, the number of TILs in A-tumors were fewer than in the healthy colon, AK- and AKP-tumors, Figure 4.19d and e. The composition of the T cell compartment had very similar proportions of many of the cell types compared to AK- and AKP-tumors, which had clear expansions of CD4 and CD8 T cells, Figure 4.19d and e. Similar to the other tumor types, however, A-tumors also had fewer IELs and perhaps more Th17 T cells, Figure 4.19d. Overall, within the T cell compartment of the TME, we observe a general expansion of T cells within tumors compared to the healthy colon including Th17 cells.

In accordance with the flow cytometric analysis, the absolute number of T cells was greater in KRAS-mutant tumors of the AK- and AKP-mice, Figure 4.19d. Presumably due to natural variation, we captured a large number of T cells from the AKP3 tumor sample, but the proportion of each cell cluster was comparable to the other two replicates, Figure 4.19d. AK- and AKP-tumors alike had a collective expansion of CD4 and CD8 T cells compared

to the healthy colon and A-tumors, Figure 4.19d. Th17 cells were notably more numerous in the KRAS-mutant tumors compared to A-tumors (and also healthy colon) in contrast to Tregs which appeared most numerous in A-tumors and became less abundant in AK- and AKP-tumors, Figure 4.19d and e. The flow cytometry data on Tregs (FOXP3$^+$, Figure 4.12) is thus at odds with the scRNAseq and histology (Figure 4.15e and f) data on the same parameter, indicating that more than likely, there are a small number of Tregs in the healthy colon, A-tumors bear a greater number of the cells, and AK- and AKP-tumors have fewer Tregs than A-tumors, as indicated by the histology and scRNAseq, Figures 4.15e and4.19e. Given that there are more T cells in AK- and AKP-tumors compared to A-tumors, we then investigated what might be blocking them from effecting their anti-tumor function.

There are many factors that can contribute to cancer evasion of anti-tumor immunity. For example, because cancer cells originate from the host's own cells, T cells may be unable to recognise the malignant cells as anything other than self. On the other hand, educated T cells can become "exhausted", a state characterised by hypofunctionality and the expression of one or many checkpoint blockade molecules that attenuate their activation[133]. Interested to discover which phenotype of TILs were present in the CRC mouse models, we inspected the T cell subcluster of the scRNAseq data for the expression of various exhaustion molecules including *Ctla4*, *Lag3, Havcr2* (TIM3) and *Pdcd1* (PD1), Figure 4.20a. It was clear that *Ctla4* was the dominant checkpoint molecule expressed among the T cells (Figure 4.20a), and not *Pdcd1*, as is common among CRC patients[134]. We validated that CTLA4 was also highly expressed on the protein level using IHC, and found more CTLA4$^+$ cells within AK-tumors compared to the healthy colon, A- and AKP-tumors, Figure 4.20b and c. Interestingly, when we inspected the *Ctla4* transcript expression among colon, A-, AK- and AKP-tumors, we found that the RNA levels were not directly reflected on the protein level, Figure 4.20f. Namely, the scRNAseq data seems to show that T cells in all tumor types have the same relative level of CTLA4 expression, but the quantification of the IHC showed that AK tumors had significantly higher expression of the checkpoint molecule than A- and AKP-tumors, Figure 4.20. Furthermore, we validated that PD1 expression was low

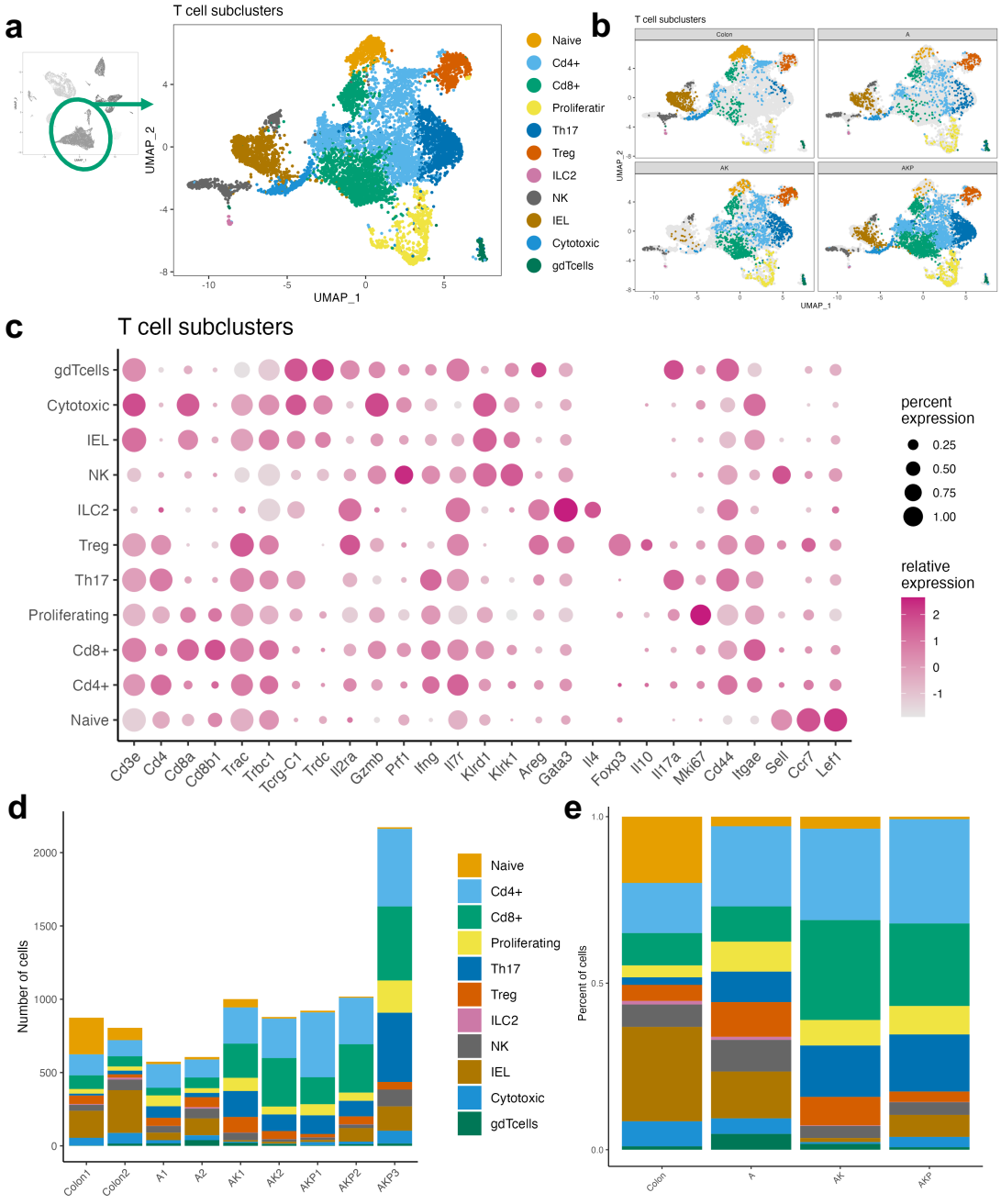

Figure 4.19 T lymphocytes expand as CRC GEMMs gain tumor-driver mutations.**a.** UMAP projection of sub-clustering analysis of T cells after unsupervised clustering **b.** UMAP projection split by group: colon, A-, AK- and AKP-tumors **c.** dotplot demonstrating expression of key transcripts which informed cluster annotation **d.** stacked bar plot of count of cells per sample within each T cell subcluster, **e.** stacked bar plot of proportion of cells per group within each T cell subcluster.

or absent in all tumors, Figure 4.20d and e. Taken together, this data shows that many of the tumor-infiltrating T cells in AK- and AKP-tumors were in an exhausted state that may be able to be overcome using immunotherapy. We therefore tested the efficacy of CTLA4 and CD40-based immunotherapeutic antibodies in A-, AK- and AKP-mice.

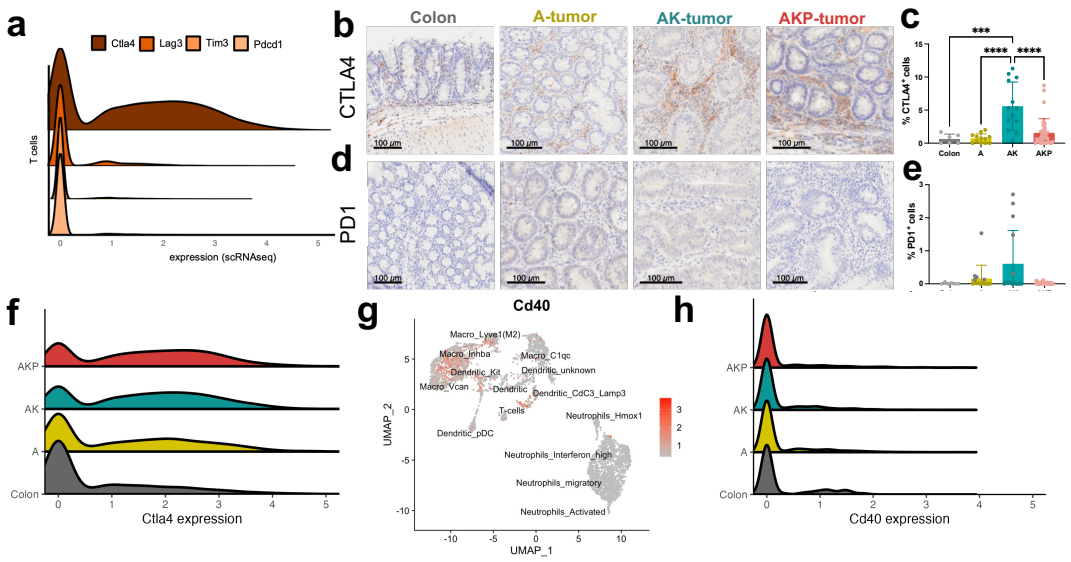

Figure 4.20 The predominant exhaustion molecule in tumor-infiltrating T cells in CTLA4 and not PD1 in CRC mouse models. **a.** Ridgeplots of expression of select checkpoint molecules among all T cells in the scRNAseq experiment. **b.** IHC for CTLA4 in colon tissue and **c.** quantification. **d.** IHC for PD1 in mouse models and **e.** quantification. **f.** Ridgeplot of Ctla4 expression in T cells split by groups. **g.** Feature plot of Cd40 transcripts among myeloid cells and **h.** ridgeplot of Cd40 expression among myeloid cells in the scRNAseq experiment.

4.1.4 Immunotherapy is partially effective in mismatch repair proficient mouse models of CRC

Because we did not explicitly expect the mouse models of CRC to respond to the immunotherapy due to their mismatch repair proficient (MMRp) status, we sought a potential combination therapy to combine with CTLA4 monoclonal antibody treatment. We previously observed that macrophage populations within the myeloid cluster of tumors expressed *Cd40* transcripts, Figures 4.18b and 4.20g. CD40 is expressed on the surface of many antigen presenting cells that—when stimulated by CD40L—can induce activation in the antigen presenting cell and promote antigen presentation ultimately facilitating Th1 and $CD8^+$ memory T cell

expansion[42,115,119,135]. Though the expression levels of *Cd40* were relatively low (Figure 4.20h), we decided to test whether scRNAseq-guided immunotherapy regimens were effective in MMRp mouse models of CRC.

Tumor formation was induced in A-, AK- and AKP-mice with tamoxifen. Three weeks were allowed for tumor growth before treatment started on day 21 and continued for 3 weeks, Figure 4.21a. Mice were treated twice per week with αCTLA4 antagonistic mAb at 5 mg/kg and once per week with αCD40 agonistic mAb at 5 mg/kg; IgG in PBS served as a control and was administered twice per week at 5mg/kg, Figure 4.21a. Mice were euthanised 6 weeks post-tamoxifen and analysed for their tumor burden and their TME was scrutinised by flow cytometry. A-mice did not show any reduction in tumor number, volume nor average size as a result of αCTLA4, αCD40 or combination therapy of the two when compared to control, Figure 4.21b–d. Given the more abundant CTLA4 expression in AK-tumors (Figure 4.20), if one of the three CRC mouse models could respond to αCTLA4 therapy it would be AK-mice. Indeed, AK-mice had significantly fewer and smaller tumors as well as reduced total tumor volume in response to αCTLA4 therapy when compared to control 4.21b–d. CD40 agonism was successful in reducing the overall tumor volume and number in AK-mice, but not the average tumor size, Figure 4.21b–d. Though αCTLA4 and αCD40 were effective as monotherapies in AK-mice, their use in combination was only effective in slightly reducing the total tumor volume in the mice, Figure 4.21c. In AKP-mice αCTLA4 and αCD40 monotherapies had no significant effect on tumor burden, though a trend toward anti-tumor efficacy can be observed especially when comparing these parameters in AKP-tumors to A-tumors, Figure 4.21b–d. The average tumor size of AKP-mice, however, was slightly reduced with the combination of αCTLA4 and αCD40 therapies, Figure 4.21d. Encouraged by the modest efficacy of the immunotherapies, in particular CTLA4 blockade in AK-tumors, we next investigated what changes occurred within the TME of each mouse model that could explain these results.

We found that among monotherapy treatment with αCTLA4 significantly reduced the proportion of myeloid cells in the healthy colon, and αCD40 therapy demonstrated the same

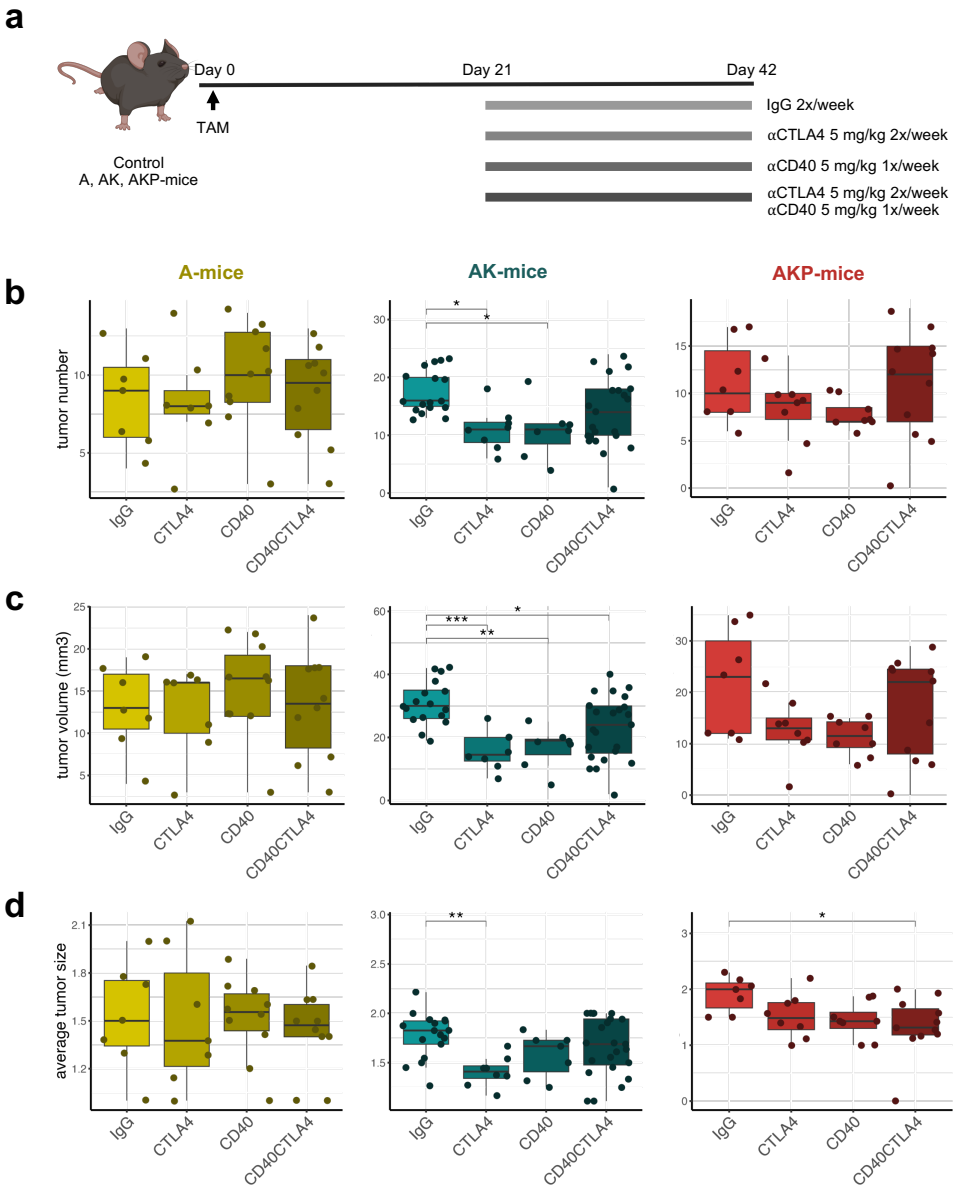

Figure 4.21 Immunotherapy is mildly effective in AK- and AKP-mice, but not A-mice. **a.** Schematic of the experiment. Tumor formation was initiated with tamoxifen, tumors were allowed to develop for 3 weeks, then treatment with IgG (5mg/kg, 2x/week), CTLA4 (5mg/kg, 2x/week), CD40 (5mg/kg, 1x/week), or a combination of CD40 and CTLA4 monoclonal antibodies for three weeks. The mice were then euthanised and their tumor burden assessed. **b.** Number of tumors, **c.** tumor volume and **d.** average tumor size after treatment in A-, AK- and AKP-mice. Data is from 8 independent experiments; The experiments included at least three groups from the experiment with care taken to include bridging samples between batches. Data shown includes the following number of mice in each respective group: colon (n=20, 10, 4 and 21), A-mice (n=7, 7, 10 and 10), AK-mice (n=17, 8, 8 and 7), and AKP-mice (n=7, 8, 8, and 11) for treatments IgG, CTLA4, CD40 and CD40CTLA4, respectively. Brackets and stars are indicative of the adjusted p value result of a one-way ANOVA with Tukey's multiple corrections to account for multiple comparisons. key: $p \leq 0.05$ = *, $p \leq 0.01$ = **, $p \leq 0.001$ = ***, $p \leq 0.0001$ = ****, and non-significant (n.s.) comparisons are not shown.

trend, Figure 4.22a. Reduced myeloid cell abundance was less apparent but could be seen in AK-tumors, but not A- and AKP-tumors. Across all groups, there was no significant change in the proportion of monocytes upon treatment, Figure 4.22b. Professional antigen presenting cell abundance, however, underwent major changes in response to therapy. αCTLA4 treatment conferred a significant loss of APCs in the TME of AK- and AKP-tumors as well as the healthy colon when compared to control, Figure 4.22c. CD40 agonism induced the same response (fewer MHCII$^+$ cells) in AK- and AKP-tumors, but the effect in the healthy colon was not statistically significant, Figure 4.22c. A-tumors, however, showed no significant change in the proportion of APCs in the tumor, which notably had fewer APCs than AK- and AKP-tumors to begin with, Figure 4.22c. We also examined the proportion of macrophages (by F4/80 expression) and found no significant changes in the healthy colon, A-tumors and AK-tumors, but did observe a reduction in the proportion of macrophages in AKP tumors upon single-agent therapy, Figure 4.22d.

Notably, the combination of the two monoclonal antibodies was not statistically different from the control conditions across all models, a potential counter-indication of the use of these antibodies in combination in colorectal cancer. This combination of therapies has been shown to be effective in a mouse model of melanoma, but was combined with IL2 stimulation in addition to the monoclonal antibodies[136]. Further experiments would need to be conducted to determine why the combination treatment is not effective in this context. Regarding the TME, the most profound change in response to the immunotherapies was in pAPCs, Figure 4.22. Given the efficacy of the treatments in AK- and AKP-mice and the significant loss of MHCII$^+$ cells in response to monotherapy, this data taken together could be indicative of an efflux of dendritic cells from the TME to the lymph node or a nearby TLS to educate T cells when immunotherapy is administered[l]. We therefore examined the T cell compartment of the tumors for signs of activation and their abundance within the tumors.

Overall, TCRβ^+ T cells within the TME and healthy tissue did not change significantly

[l]The tumor-draining lymph nodes as well as distal lymph nodes were collected from these mice, but they have not yet been analysed by IHC to verify this hypothesis.

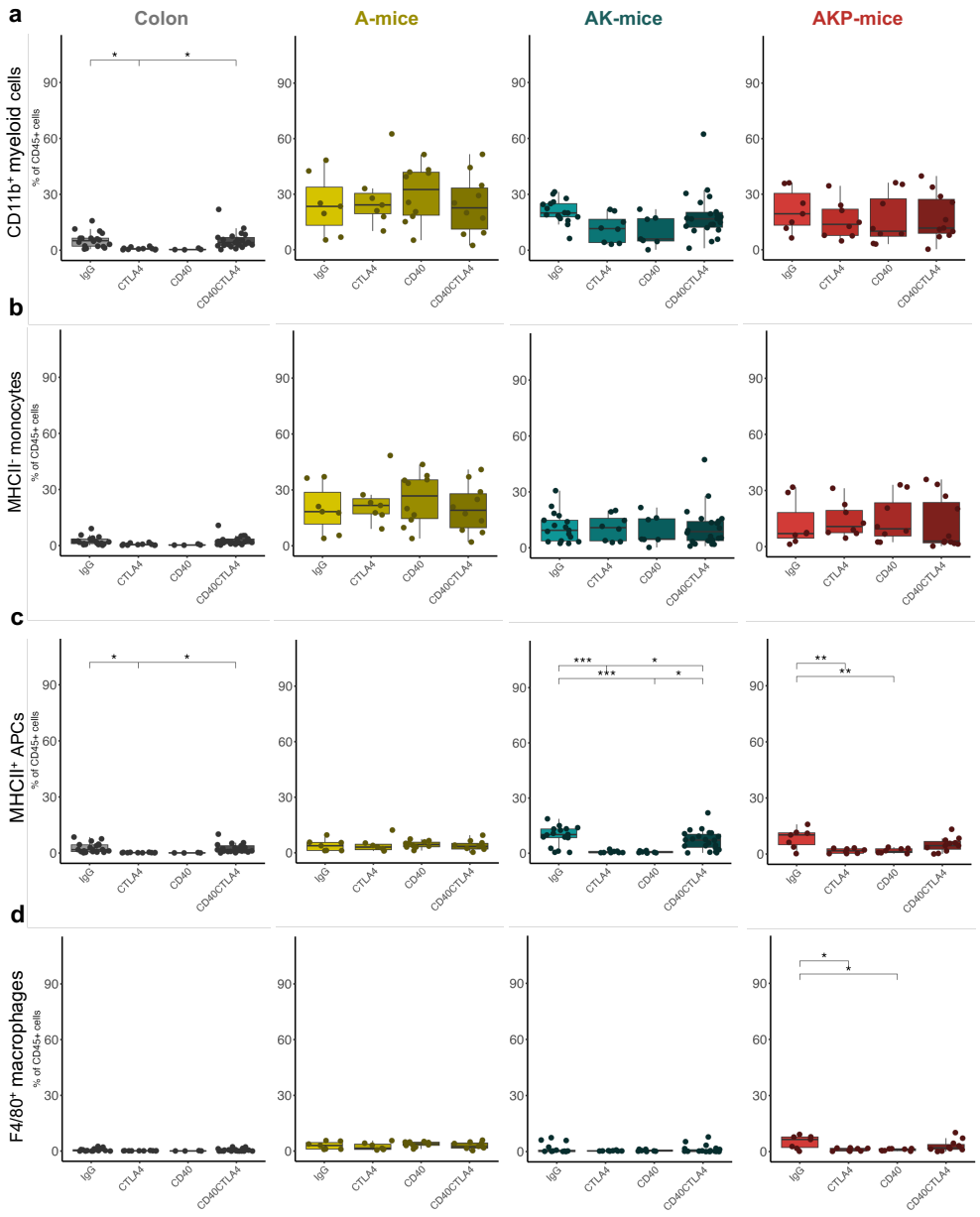

Figure 4.22 anti-CTLA4 and anti-CD40 monotherapy causes pAPC efflux from the TME of AK- and AKP-tumor. Cell populations as measured by flowcytometric analysis of **a.** $CD11b^{+}$ myeloid cells, **b.** $MHCII^{-}$ monocytes, **c.** $MHCII^{+}$ professional antigen presenting cells, and **d.** $F4/80^{+}$ macrophages. Data is from 8 independent experiments; The experiments included at least three groups from the experiment with care taken to include bridging samples between batches. Data shown includes the following number of mice in each respective group: colon (n=20, 10, 4 and 21), A-mice (n=7, 7, 10 and 10), AK-mice (n=17, 8, 8 and 7), and AKP-mice (n=7, 8, 8, and 11) for treatments IgG, CTLA4, CD40 and CD40CTLA4, respectively. Brackets and stars are indicative of the adjusted p value result of a one-way ANOVA with Tukey's multiple corrections to account for multiple comparisons. key: $p \leq 0.05$ = *, $p \leq 0.01$ = **, $p \leq 0.001$ = ***, $p \leq 0.0001$ = ****, and non-significant (n.s.) comparisons are not shown.

with monotherapy nor combination treatments, Figure 4.23a. Interestingly, the combination treatment in AK-tumors had significantly more T cells than either of the monotherapies, but did not have significantly more T cells than control, Figure 4.23a. The proportion of helper T cells in healthy colon, A-tumors and AKP-tumors did not change in response to αCTLA4, αCD40 and combination therapy, Figure4.23b. AK-tumors, however, had a significant loss of $CD4^+$ T cells from the TME upon administration of immunotherapy when compared to the healthy colon and combination treatment, perhaps an indication that they have migrated to a nearby TLS or lymph node for licensing, Figure 4.23b. There was no significant difference between control and monotherapy treatments across all groups in terms of $CD8^+$ cytototoxic T cells, but AK-tumors treated with the combination had more $CD8^+$ T cells than the monotherapy treatments, Figure 4.23c. Finally, there were no significant differences in proportion of Tregs upon treatment in any of the models, Figure 4.23. We next explored the activation status and cytokine production by the TILs.

GZMb-expressing T cells did not change significantly upon treatment in any of the models, Figure 4.24a. AK-tumors and healthy colon, however, showed a trend toward increased CD8 GzmB production upon monotherapy treatment, Figure 4.24. Th17 cells were significantly more prominent in AK-tumors treated with monotherapy compared to control and combination treatment while the other models demonstrated no such changes, Figure 4.24b. Next, we assessed the IFNγexpression in CD4 and CD8 T cells. Unexpectedly, healthy colon CD4 and CD8 T cells produced significantly more IFNγupon combination treatment when compared to control and monotherapy treatments, Figure 4.24c. Among tumors there were no significant changes in IFNγ^+ CD4 or CD8 T cells, but a notable trend toward fewer IFNγ^+ T cells upon monotherapy treatment was present, Figure 4.24d.

Collectively, the treatment of A-, AK-, and AKP-mice with CTLA4 antagonist and CD40 agonist mAbs showed no significant difference in any parameters measured in A-mice. AK-mice, however, had reduced tumor burden as the result of monotherapy treatment, but not combination treatment with αCTLA4 and αCD40. AKP-mice also seemed to respond positively to the immunotherapeutics as single-agents, but this trend was not significant, while

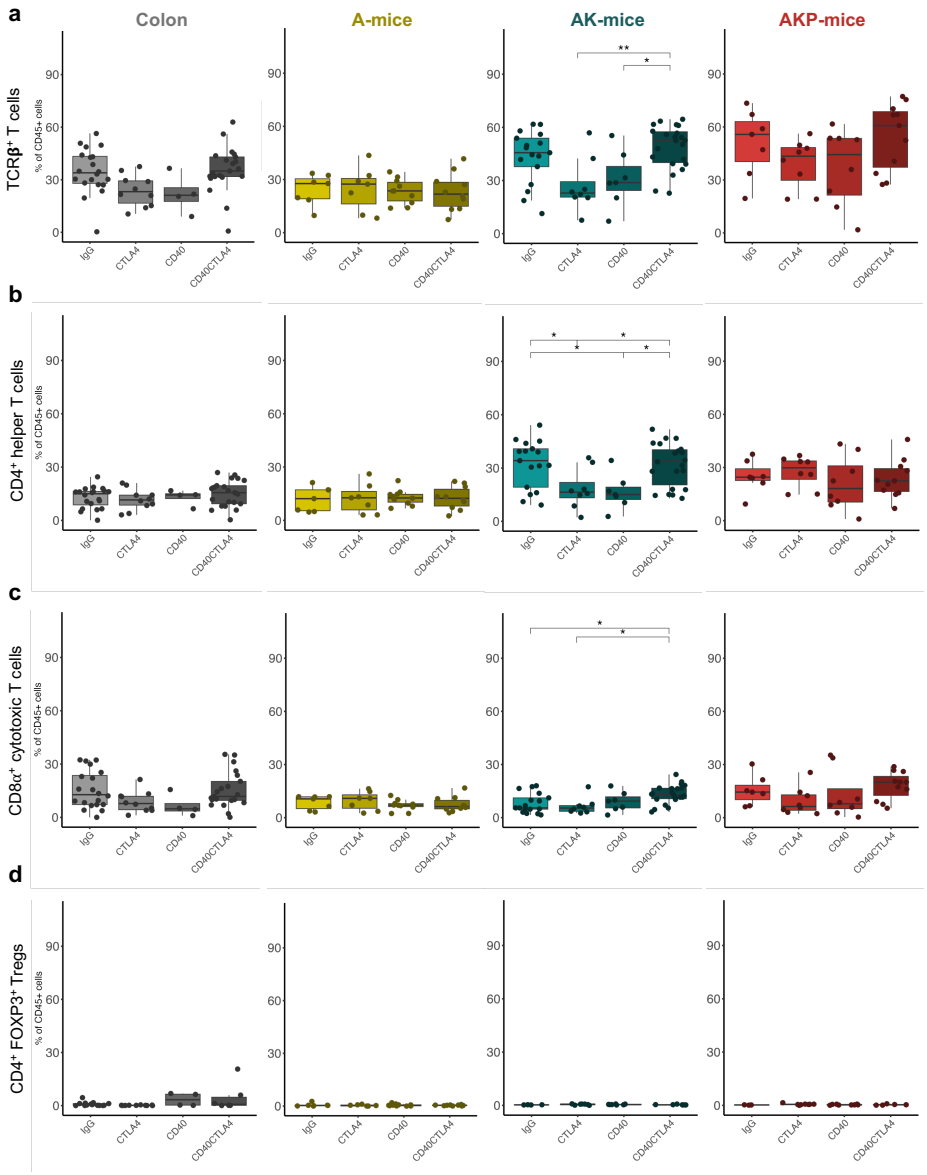

Figure 4.23 CD4$^+$ T cells exit the TME upon treatment with αCTLA4 or αCD40 immunotherapy. Flow cytometric analysis quantification of **a.** TCRβ $^+$ T cells, **b.** CD4$^+$ T cells, **c.** CD8$^+$ T cells, and **d.** FOXP3$^+$ Tregs. Data in **a, b, and c** is from 8 independent experiments; The experiments included at least three groups from the experiment with care taken to include bridging samples between batches. Data shown includes the following number of mice in each respective group: colon (n=20, 10, 4 and 21), A-mice (n=7, 7, 10 and 10), AK-mice (n=17, 8, 8 and 7), and AKP-mice (n=7, 8, 8, and 11) for treatments IgG, CTLA4, CD40 and CD40CTLA4, respectively. Data in **d** is from 7 independent experiments; colon (n=16, 10, 4 and 5), A-mice (n=7, 7, 10 and 10), AK-mice (n=4, 7, 7 and 8), and AKP-mice (n=3, 8, 8, and 5) for treatments IgG, CTLA4, CD40 and CD40CTLA4, respectively. Brackets and stars are indicative of the adjusted p value result of a one-way ANOVA with Tukey's multiple corrections to account for multiple comparisons. key: $p \leq 0.05$ = *, $p \leq 0.01$ = **, $p \leq 0.001$ = ***, $p \leq 0.0001$ = ****, and non-significant (n.s.) comparisons are not shown.

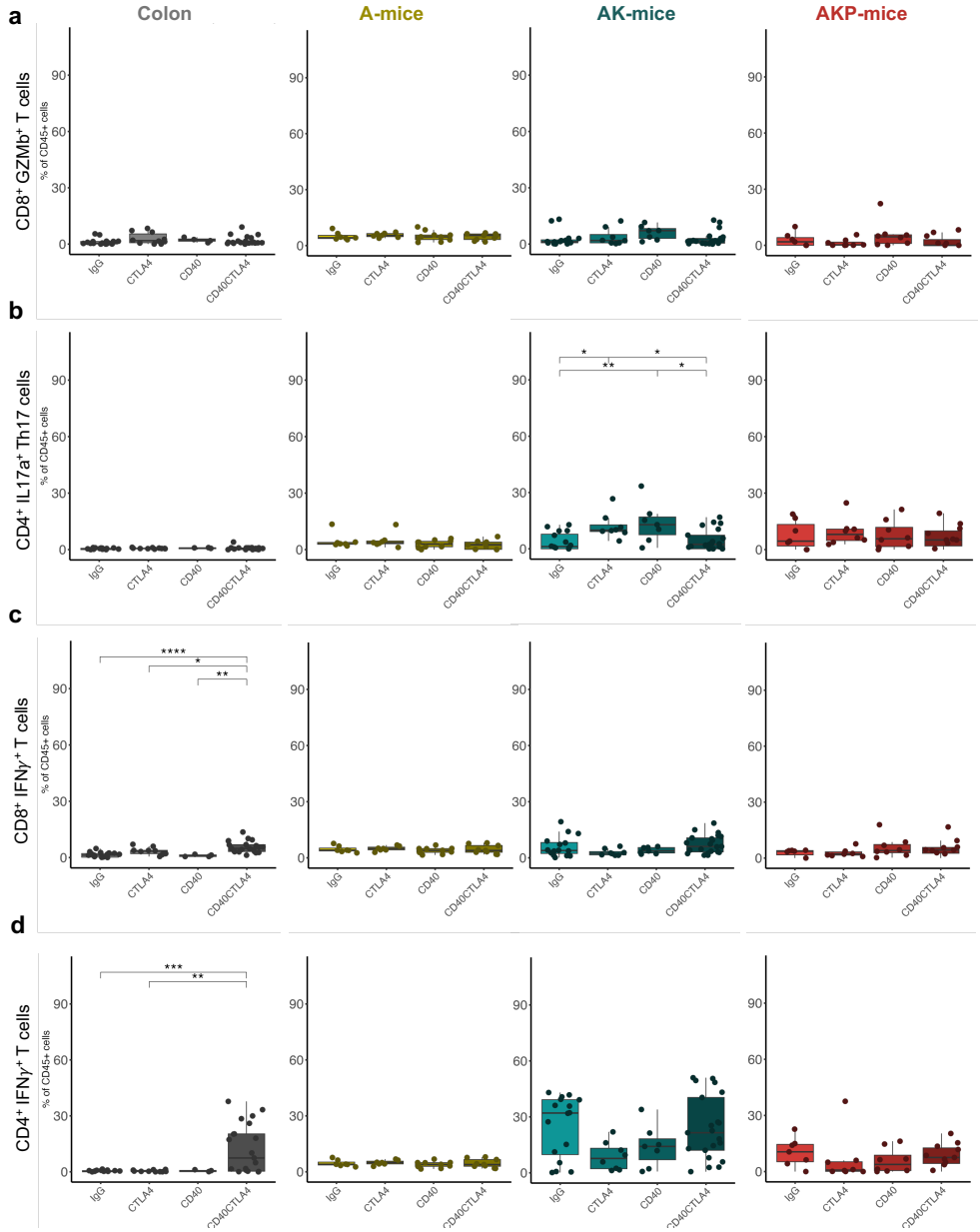

Figure 4.24 Th17 cells accumulate as a result of αCTLA4 or αCD40 treatment in AK-tumors. Flow cytometric analysis quantification of **a.** $CD8^+GZMb^+$ T cells, **b.** $CD4^+IL17a^+$ T cells, **c.** $CD8^+IFN\gamma^+$ T cells, and **d.** $CD4^+IFN\gamma^+$ T cells. Data is from 8 independent experiments; the experiments included at least three groups from the experiment with care taken to include bridging samples between batches. Data shown includes the following number of mice in each respective group: colon (n=19, 10, 4 and 21), A-mice (n=7, 7, 10 and 9), AK-mice (n=17, 8, 7 and 22), and AKP-mice (n=7, 8, 8, and 11) for treatments IgG, CTLA4, CD40 and CD40CTLA4, respectively.

the average tumor size of AKP-tumors was slightly decreased with combination treatment. The effect of immunotherapy was similar in AK- and AKP-tumors. Professional APCs left the TME along with helper T cells, presumably trafficking to the tumor draining lymph node or a nearby TLS for T cell education and licensing[II]. AK-tumors which responded best to the therapies had (non-significantly) more $GZMb^{+}$ cytotoxic T cells and significantly more Th17 cells in the TME which may have contributed to a stronger anti-tumor microenvironment in these conditions. This experiment showed that in tumors with greater T cell infiltration (AK- and AKP-tumors) immunotherapy can indeed be leveraged to afford at least a minor anti-tumor effect. Thus, we return to the question of what gene expression changes are conferred by constitutive $KRAS^{G12D}$ that could drive T cell infiltration in our mouse models of colorectal cancer. We expect these genetic alterations to occur in the epithelial compartment, and that cells bearing the conditional alleles would have a tumor phenotype. We thus annotated and scrutinized the epithelial subcluster of the scRNAseq experiment for tumor and healthy colon epithelial markers.

Twelve epithelial clusters were identified by unsupervised clustering, Figure 4.25a. Three tumor clusters were identified and annotated according to expression of transcripts that differentiated each cluster from the other epithelial clusters, Figure 4.25b. Tumor_Anxa was characterised by *Anxa1* and *Anxa8* transcripts, Tumor_Onecut2 had high *Onecut2* and *Axin2* expression, and the Tumor_Wnt cluster expressed many gut Wnt-associated receptors and ligands as well as *Ifitm3*, Figure 4.25b.

Ifitm3 was also expressed by a large epithelial cluster, Epithelial_Ifitm3, Figure 4.25b. Next, glutathione peroxidase 2 (*Gpx2* was expressed on a second rather general enterocyte population we annotated as Epithelial_Gpx2. Transit amplifying cells were identified by the top genes that distinguished it from the other epithelial clusters including *Mki67* and stem-like genes, Figure 4.25b. The Endocrine, Enterocyte, Mature Enterocyte, Tuft and Goblet clusters were identified by their respective expression of *Chga, Dmbt1, Krt20, Trpm5* and *Muc2* transcripts, Figure 4.25b.

[II] Again, this remains to be shown

Differentiating malignant cells from the relatively proliferative tissue from which they emerge is a challenging task that is beginning to be addressed, as evidenced by the recent creation of the R package inferCNV of the Trinity CTAT Project. Within our data, we struggled to differentiate the rapidly dividing epithelial cells of the colon (annotated as Epithelial_TA, Epithelial_Gpx2 and Epithelial_Ifitm3) from the actual malignant cells (annotated as Tumor_Anxa, Tumor_Onecut2, and Tumor_Wnt). In order distinguish actual cancer clusters we combined a list of genes known to be involved in the cell cycle and proliferation (*Mki67, Mcm2, Mcm4, Mcm7* and *Pcna*) with a list of genes known to be upregulated in cancer metabolism[137] (*Hk2, Slc2a1, Slc38a5, Prps2, Gls, Cad, Slc7a5* and *Slc1a5*) to assess the level of growth, proliferation and metabolism in each cluster. For each gene in the growth, proliferation and metabolism gene set, a mean expression z-score was calculated and a violin plot was generated for the mean z-scores in each cluster, Figure 4.25c. The tumor clusters had a clear positive mean score above the other epithelial and especially over the epithelial clusters that were difficult to separate from the tumor cells, Figure 4.25c. We assessed the same gene set on pooled tumor and epithelial clusters and the difference became even more pronounced, Figure 4.25d. Furthermore, when the tumor clusters were assessed based on genotype the gene set confirmed the correct annotation of the three tumor clusters in this experiment, Figure 4.25e. We thereby established a reliable method to discern pathological colonic tissue from tumor cells, which enabled us to assess the role of KRAS-mutant tumor cells specifically, where the mutant protein was actually active.

Among A-, AK- and AKP-tumors, tumor cells made up 25-30% of cells and the remaining 70% belonged to the non-tumor epithelial clusters, Figure 4.26a and b. Healthy colon was composed mainly of Enterocytes, followed in number by the Goblet cluster, Epithelial_TA, Epithelial_Gpx2 and Epithelial_Ifitm3 clusters, Figure 4.26c. All of the cell types that were present in the healthy colon were expanded in number in all tumor types, Figure 4.26c. The major tumor populations in A-mice were the Tumor_Wnt cluster and the Tumor_Onecut2 cluster while the Tumor_Anxa cluster was less abundant, Figure 4.26c. The Tumor_Anxa and Tumor_Onecut2 clusters were more numerous in AK-mice, Figure 4.26a. Interestingly,

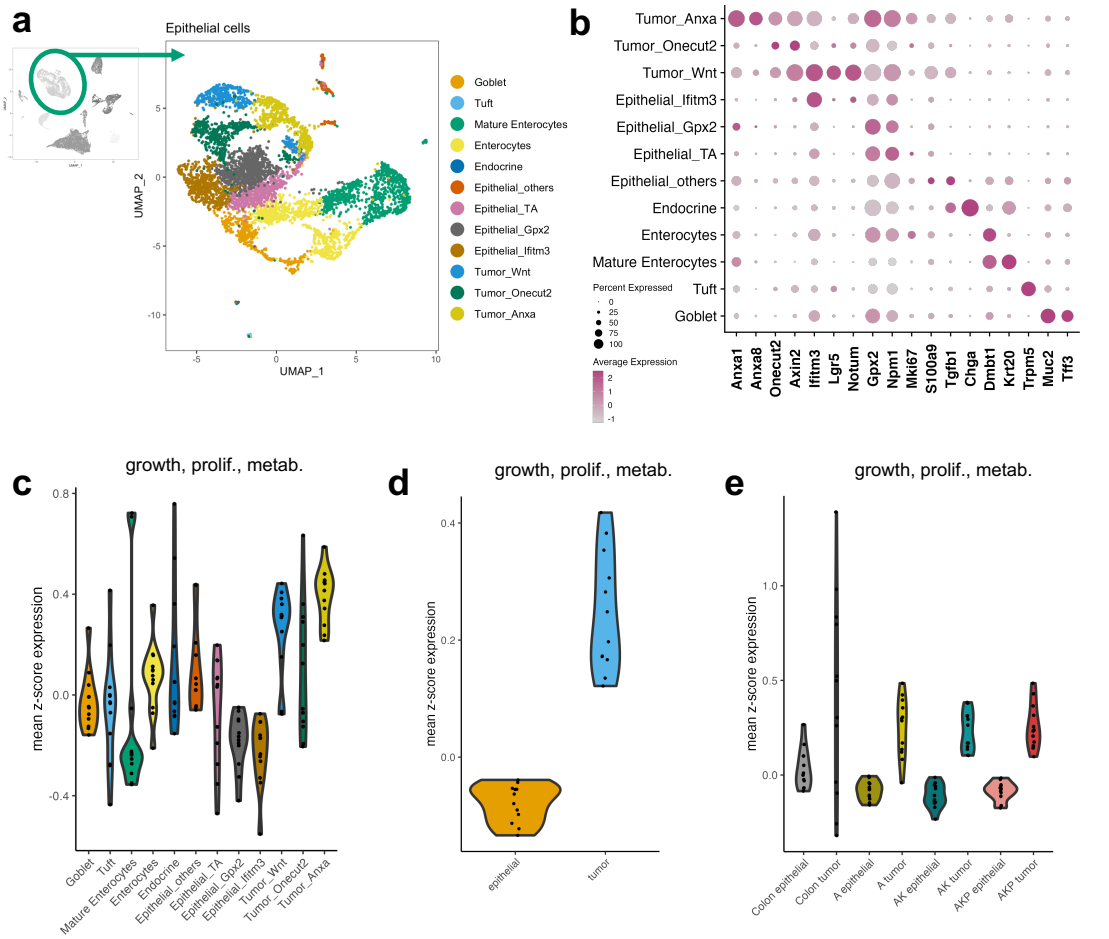

Figure 4.25 Growth, proliferation and cancer metabolism gene set facilitates the annotation of malignant clusters. **a.** UMAP projection of epithelial cells after unsupervised clustering **b.** dotplot demonstrating expression of key transcripts that informed cluster annotation **c.** violin plots of mean z-score from each sample in the data set for growth, proliferation and cancer metabolism gene list, split by cluster **d.** violin plots of mean z-score from each sample in the data set for growth, proliferation and cancer metabolism gene list split by epithelial and tumor annotation, **e.** violin plot of mean z-score from each sample in the data set for growth, proliferation and cancer metabolism gene list (partially composed of cancer metabolism genes from Pavlova & Thompson [137] split by epithelial and tumor clusters annotations and genotype.

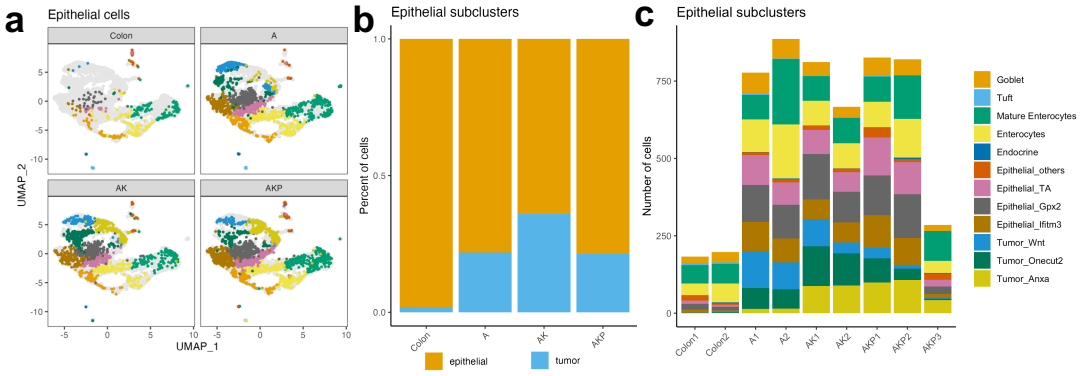

Figure 4.26 Mouse models of CRC with accumulating driver mutations have three distinct tumor clusters. **a.** UMAP projection of cells from each group (colon, A-, AK- and AKP-tumor) within epithelial cell sub-cluster, **b.** stacked barplot showing frequency of epithelial and tumor clusters within each model and **c.** stacked barplots showing the count of cells within each cluster by sample.

while the Tumor_Anxa cluster remained prominent in the AKP-mice, the Tumor_Onecut2 and Tumor_Wnt clusters shrunk compared to their abundance in AK-tumors, Figure 4.26a.

We next assessed the epithelial compartment for the expected altered signaling pathways. Specifically, we performed gene set enrichment analysis (GSEA) for the HALLMARK_KRAS_signaling_UP gene set using the differentially expressed genes within the epithelial cluster between A-mice and AK-mice to validate that KRAS signaling had indeed increased in AK tumors, Figure 4.27a. In the differential gene expression (DGE) between A- and AK-mice the normalised enrichment score (NES) was -1.442, indicating that KRAS signaling gene set was indeed more enriched in the epithelial compartment of AK-mice compared to that of A-mice, Figure 4.27a. Next, we asked whether AK-mouse epithelial compartment had a more enriched P53 signature compared to the AKP-mouse epithelial cells where the P53 pathway is expected to be hindered by P53 truncation, Figure 4.27b. GSEA was performed for the HALLMARK_P53_PATHWAY gene set in the DGE between AK- and AKP-epithelial compartments and resulted in a significant NES of 1.398, indicating that the P53 pathway was more enriched in AK-tumors compared to AKP-tumors, as anticipated, Figure 4.27b. Having confirmed that the oncogenic signaling pathways were perturbed as expected we next analysed differentially expressed genes in the epithelial compartment that could explain the increased T cells in mutant KRAS tumors.

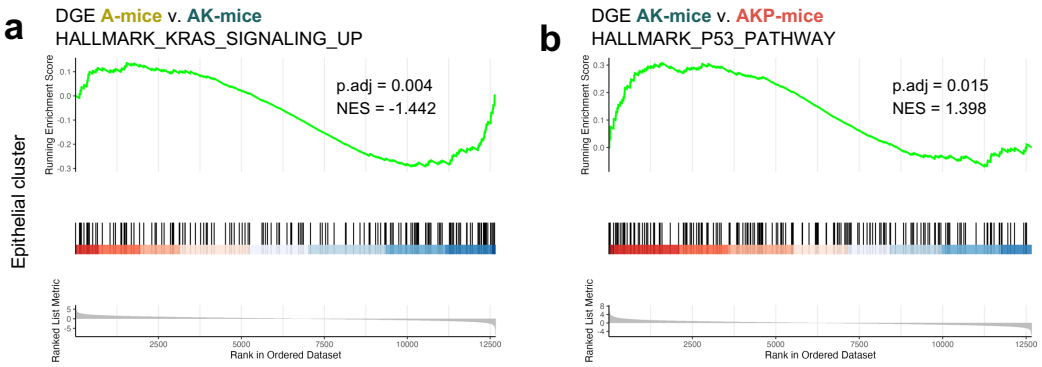

Figure 4.27 Gene set enrichment analysis confirms greater KRAS activity in KRAS mutant tumors and reduced P53 activity in P53 deleted tumors. **a.** GSEA for HALLMARK_KRAS_signaling_UP in DGE of the epithelial cluster of A-mice compared to AK-mice,**b.** GSEA for HALLMARK_P53_PATHWAY in DGE of the epithelial cluster of A-mice compared to AK-mice. DGE: differential gene expression, GSEA: gene set enrichment analysis, p.adj: adjusted p-value, NES: normalised enrichment score.

4.1.5 ANXA1 is associated with T cell infiltration in mouse models of CRC and immune infiltration in human CRC

In order to unravel the link between KRAS signaling and T cell infiltration, we conducted pseudobulk-based DGE with each tumor cluster to find the genes that were differentially expressed between AK- and AKP-tumors compared to A-tumors[III]. We then extracted genes which were differentially expressed (by pseudobulk) from all tumor clusters and kept for inspection only the genes which are bona fide ligands according to an R package for receptor-ligand communication potential between cells in scRNAseq data called NicheNetR[139]. Finally, we compared the resulting gene lists from AK- and AKP-tumor clusters to A-tumor clusters, and found five common up-regulated transcripts, Figure 4.28a. These five transcripts thus represent the common differentially expressed ligands with high fold change ($\log_2$FC≥1) between two tumor types with high T cell infiltration and KRAS activation (AK- and AKP-tumors) compared to tumors with fewer T cells and no constitutive KRAS activity, and were to

[III]This method was the final strategy adopted after several different strategies were tried that aimed to answer the question. Briefly, the previous methods involved 1) wilcoxn-based DGE of epithelial cells that (we discovered) gave artificial power to genes highly expressed by multiple cells[138] 2) pseudo-bulk DGE of the epithelial cluster, in which the signal from the tumor cells was over-powered by pathological epithelial cells, and 3) pseudobulk-based DGE without ligand filtering which produced several growth/proliferation related transcripts unrelated to immune cell recruitment.

be assessed for their feasible role in T cell recruitment.

Significant DGE with high fold change does not mean that the transcripts are expressed at a biologically meaningful level. For example, inspection of expression of *Il1rn, Cxcl1* and *Gdf15* transcripts by each cell in either healthy colon clusters or tumor clusters shows that though the transcripts were significantly increased in AK- and AKP-tumor compared to A-tumors, there was not a dramatic change in the expression of these transcripts between the tumors, Figure 4.25c. *Anxa1* and *Plxnb2* transcripts, however, demonstrated a robust expansion in KRAS mutant tumors, Figure 4.25c. Though *Plxnb2* was included in the list of ligands from NicheNetR[139], the protein produced by this transcript is a transmembrane receptor, so it was eliminated as a candidate for T cell recruitment. Furthermore, we performed NicheNet receptor-ligand analysis on the data, with the full list of differentially expressed ligands as the signal senders and all clusters in the experiment as potential recipient cells. The output of the NicheNet analysis is a pearson correlation coefficient (PCC) for each ligand and receiver cell pair which represents the likelihood that the ligand in question is affecting the gene expression changes observed in the receiver cells. PCCs $\geq$0.1 indicate a significant likelihood of communication between the ligand and recipient cell. Among the five candidates, *Anxa1* was the only ligand that had a significant potential with any cluster, and it was likely to communicate with the Epithelial_Gpx2, Plasma cell, and T cell clusters, Figure 4.28b. Finally, we validated that ANXA1 was also differentially expressed on the protein level. We therefore performed IHC for ANXA1 and found indeed that ANXA1 was highly expressed in AK- and AKP-tumors compared to A-tumors, Figure 4.28d. ANXA1 was clearly expressed by malignant crypts in AK- and AKP-tumors while A-tumor malignant crypts lacked ANXA1 staining, Figure 4.28d and e. Furthermore, ANXA1 was highly expressed by immune cells in all tumors, Figure 4.28d and e. Taken together, this data shows that *Anxa1* is a ligand commonly differentially expressed by AK- and AKP-tumors compared to A-tumors that may recruit T cells to the tumor microenvironment.

ANXA1 was first discovered for its role in the suppression of arachidonic acid production upon glucocorticoid administration[73]. Though reduced production of pro-inflammatory

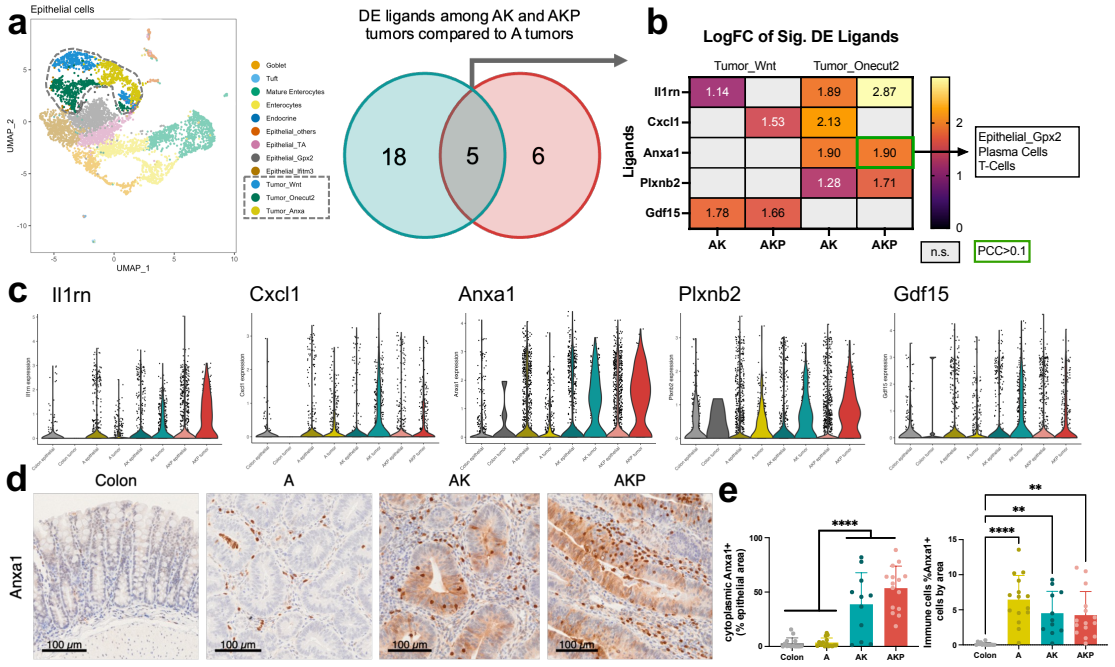

Figure 4.28 Annexin A1 expression is significantly higher in KRAS mutant tumor cells. **a.** Venn diagram of number of differentially expressed bona fide ligands among AK (blue) and AKP (red) tumor clusters compared to A-tumors. **b.** heatmap of differential expression (log_2 fold-change) in the Tumor_Wnt and Tumor_Onecut2 clusters, green box = ligand which has Pearson Correlation Coefficient ≥0.1 from NicheNet ligand-receptor analysis, within Epithelial_Gpx2, Plasma Cells and T-cells. Non-significantly upregulated transcripts are indicated with grey fill. **c.** Violin plots of ligands identified in **a** split by genotype and tumor or epithelial-type cluster. **d.** IHC for ANXA1 in the tumor models and healthy colon **e.** quantification of epithelial (left) and laminae propria (right) ANXA1 IHC. IHC staining and quantification performed by Elia Escoffier. DE: differentially expressed, LogFC: logarithmic fold change, PCC: pearson correlation coefficient.

eicosanoids is a key mechanism by which glucocorticoids relieve inflammation, the induction of ANXA1 not only sequesters the substrates of PLA2[76,77], but is also secreted and directly impacts immune cells. ANXA1 is a ligand for FPR2, a formyl peptide receptor highly expressed by neutrophils[140]. Upon ANXA1 binding to FPR2 (a GPCR) the MAPK pathway is activated[141,142]. The consequence of MAPK pathway activation is vastly different between neutrophils, monocytes and T lymphocytes. Explicitly, ANXA1 has been robustly shown to induce apoptosis in neutrophils through the dephosphorylation of the pro-apoptotic protein BAD[143,144]. Meanwhile, ANXA1 binding to FPR2 on immature monocytes induces differentiation into macrophages[145]. Whereas in T cells, ANXA1 has been shown to induce proliferation, Th1 and Th17 differentiation as well as IFNγproduction in T cells[145,146].

Considering the previous results from our lab wherein neutrophils were shown to prevent T cells from entering the TME[61], and additionally considering ANXA1's ability to induce neutrophil apoptosis[143], it is probable that the increased ANXA1 expressed by AK- and AKP-tumors prevents neutrophils from entering the TME by inducing their apoptosis. This is in agreement with the observed reduction of neutrophils in AK- and AKP-tumors compared to A-tumors, Figure 4.9d. In our models, ANXA1 could also cause the T cells which can now enter the TME to differentiate into Th17 or Th1 cells and induce their proliferation. Indeed we found more T cells overall, and more Th17 and IFNγ^+ T cells in AK- and AKP-tumors compared to A-tumors, Figures 4.10 and 4.14.

On the other hand, upon EGF stimulation or constitutive KRAS activity a phosphorylation cascade ensues through RAF, MEK and finally to ERK, which translocates to the nucleus to phosphorylate and activate transcription factors that orchestrate the transcription of various genes. Recent efforts have compiled the many lists of ERK's phosphorylation targets[147]. We queried this list for known transcription factors[148,149] then queried the encyclopedia of DNA elements (ENCODE) database[150] to determine whether these transcription factors are known to bind the ANXA1 promoter, Table 4.1. ESR1, MYC, FOS, and NR3C1 (glucocorticoid receptor (GCR)) are all direct targets (and STAT3 is an indirect target) of ERK with binding sites in the ANXA1 promoter, making them plausible drivers of ANXA1 expression in KRAS-

mutant tumors, Table 4.1. On the transcript level in our mouse models, *Esr1* was lowly expressed among epithelial cells, while *Fos* was expressed at a high level in healthy and malignant cells, Figure 4.29a and b. *Nr3c1*, *Stat3* and *Myc*, however, demonstrated enriched expression within tumor clusters, Figure 4.29c–e. Whether and through which transcription factor ERK drives ANXA1 expression in AK- and AKP-tumors remains to be shown.

Uniprot ID	Gene Name	AA	Site	class	organism	BS ANXA1
P19419	ELK1	S	324	direct	human, mouse	no
P19419	ELK1	T	336	direct	human, mouse	no
P03372	**ESR1**	**S**	**104**	**direct**	**human**	**yes**
P03372	**ESR1**	**S**	**106**	**direct**	**human**	**yes**
P03372	**ESR1**	**S**	**118**	**direct**	**human**	**yes**
P14921	ETS1	T	38	direct	human, mouse	no
P42224	STAT1	S	727	direct	human, mouse	no
P40763	**STAT3**	**S**	**727**	**indirect**	**human**	**yes**
P01106	**MYC**	**T**	**58**	**direct**	**human**	**yes**
P01106	**MYC**	**S**	**62**	**direct**	**human**	**yes**
P01100	**FOS**	**T**	**232**	**direct**	**human**	**yes**
P01100	**FOS**	**T**	**325**	**direct**	**human, rat**	**yes**
P01100	**FOS**	**T**	**331**	**direct**	**human, rat**	**yes**
P01100	**FOS**	**S**	**374**	**direct**	**human, rat**	**yes**
P17480	UBTF	T	201	direct	rat	no
P28324	ELK4	S	381	direct	human	no
P28324	ELK4	S	387	direct	human	no
P04150	**NR3C1**	**S**	**226**	**direct**	**human, rat**	**yes**

Table 4.1 Table of transcription factors and their amino acid sites that are phosphorylation targets of ERK. Transcription factors that are direct targets of ERK with a binding site in the ANXA1 promoter are indicated in dark green. Transcription factors that are indirect targets of ERK with a binding site in the ANXA1 promoter are indicated in light green. Data shown are results of queries from Ünal *et al.* [147] and ENCODE Project Consortium [150]. BS: binding site. AA: amino acid.

To determine whether ANXA1 expression is relevant in the human disease context, we assessed expression data from the TCGA COAD dataset. *ANXA1* expression greater than the mean was specified as "high" and expression less than the mean was specified as "low", Figure 4.30. Microenvironment Cell Populations-counter (MCP-counter)[151] was used to determine extent of 8 immune cell and 2 stromal cell populations, and revealed that greater *ANXA1* expression was correlated with immune cell infiltration, Figure 4.30a. Clustering of the patient transcriptomic data led to the definition of 8 clusters. We noted that clusters 1, 4, 6, 7 and 8 were affiliated with high *ANXA1* expression, Figure 4.30a. Using a 2x2 contingency table, we showed that high *ANXA1* expression is significantly associated with

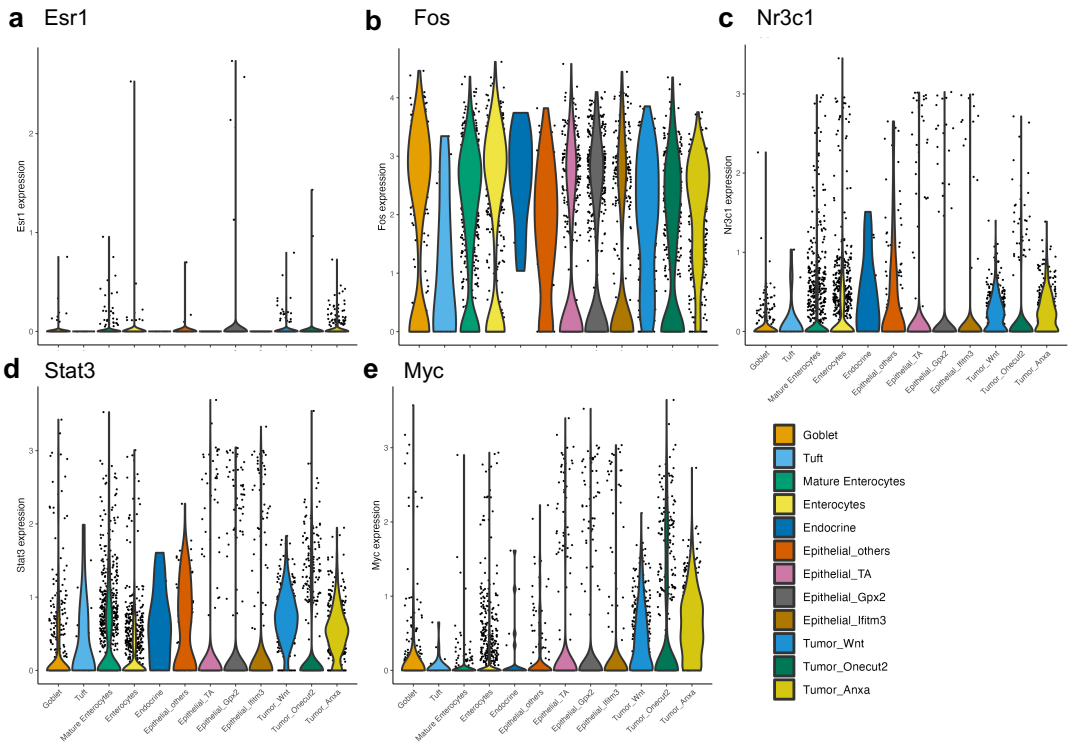

Figure 4.29 Expression of ERK-target transcription factors within epithelial cells of colon, A-, AK- and AKP-tumors. Violin plots showing expression of transcription factors **a.** *Esr1*, **b.** *Fos*, **c.** *Nr3c1*, **d.** *Stat3* and **e.** *Myc* among all clusters within the epithelial subcluster of the scRNAseq experiment.

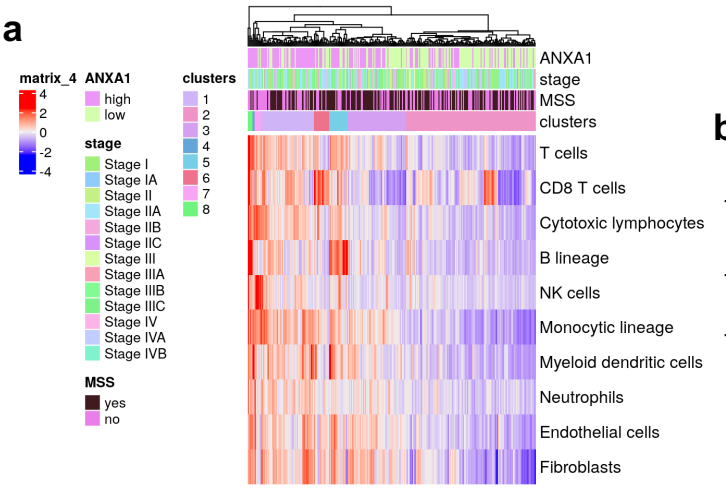

b

	ANXA1 high	ANXA1 low
Clusters (1, 4, 6, 7, & 8)	58	22
Clusters (2, 3 & 5)	83	119

Fisher's exact test
p-value = 2.86e-6
(OR: 3.72, 95% CI: [2.08, 6.99])

Figure 4.30 *ANXA1* expression is associated with immune cell infiltration in human colorectal cancer. **a.** heatmap and unsupervised clustering of expression of immune cell-related transcripts. **b.** 2x2 contingency table for *ANXA1* high and *ANXA1* low expression in immune enriched patient clusters(1,4,6,7, and 8 from panel a) and immune deficient patients clusters (2, 3 and 5 from panel a). OR: odds ratio, CI: confidence interval.

the present of the immune high clusters, indicating a relationship between *ANXA1* expression and immune cell infiltration in colorectal cancer, Figure 4.30b. Fisher's exact test revealed an odds ratio (OR) of 3.72 with a 95% confidence interval (CI) of 2.08 to 6.99, indicating that *ANXA1* expression in the immune-enriched clusters was 3.72 times more likely to be high, Figure 4.30b.

Altogether, we have shown that A-, AK- and AKP-murine models of CRC have significantly different immune cells within their respective TMEs. In particular, AK- and AKP-tumors have significantly more T cells than A-tumors, and T cell-infiltrated tumors respond mildly to monotherapy with αCTLA4 or αCD40 immunotherapy. To determine how the tumor immune microenvironment is influenced by oncogenic driver mutations, we conducted scRNAseq and found that *Anxa1* is significantly more expressed in KRAS-mutant tumors (AK- and AKP-tumors) compared to tumors without the KRAS mutation (A-tumors). We further showed that human CRC tumors with high *ANXA1* expression are significantly more likely to be highly immune infiltrated, indicating a potential role for ANXA1 in attraction of immune cells to the TME. Further experimentation *in vivo* and *in vitro*, however, are necessary to determine the

whether of ANXA1 is able to influence immune cell migration and whether KRAS does indeed drive ANXA1 expression.

4.2 Aim 2: assess the temporal impact on the TME of accumulating tumor-driver mutations in CRC mouse models

One of the key limitations of the study in the previous aim is that our mouse models for colorectal cancer represent a model for adenocarcinomas, not advanced-stage disease like invasive carcinomas or metastasis. In human disease early-stage adenomas can be easily removed surgically and the disease can be monitored for recurrence with regular colonoscopies. Though surgery is neither minor nor trivial, it is highly efficient at removing the disease. Patients with this stage of disease do not therefore currently present a major clinical need for novel or experimental treatments like immunotherapeutics. Patients that develop or are diagnosed with advanced-stage disease, however, do represent a major area of clinical need.

Our mouse models demonstrate the formation of a tumor "carpet" in the cecum as multiple CreERT2 molecules become active in $CDX2^{+}$ cells when tamoxifen is administered. As a consequence of the efficient induction of tumor formation in the cecum of the mice, a significant disturbance in the passage of waste through the cecum can manifest. In this case the mice could eventually experience mortality due to impaction upstream of the cecum rather than effects of the cancer and metastases on vital organs as would be the case in human disease. Furthermore, the timeline of the mouse model transforming from healthy colon to a colon confluent with adenomas occurs within 6 short weeks and invasive phenotypes were extremely rare in A-, AK- and AKP-tumors alike. These characteristics are dissimilar to the manifestation of human disease wherein single cells undergo the loss of active APC which leads to increased cell division and the formation of small, discreet polyps[8]. Over time, and in part due to the increased rate of replication, transformed cells can acquire further mutations that potentiate malignant transformation and invasion. These processes, however, take *time*.

Having made these observations and in order to more closely replicate the human disease condition with our genetic models we tested the induction of tumor recombination with lower doses of tamoxifen. We hypothesized that lower doses of tamoxifen would result

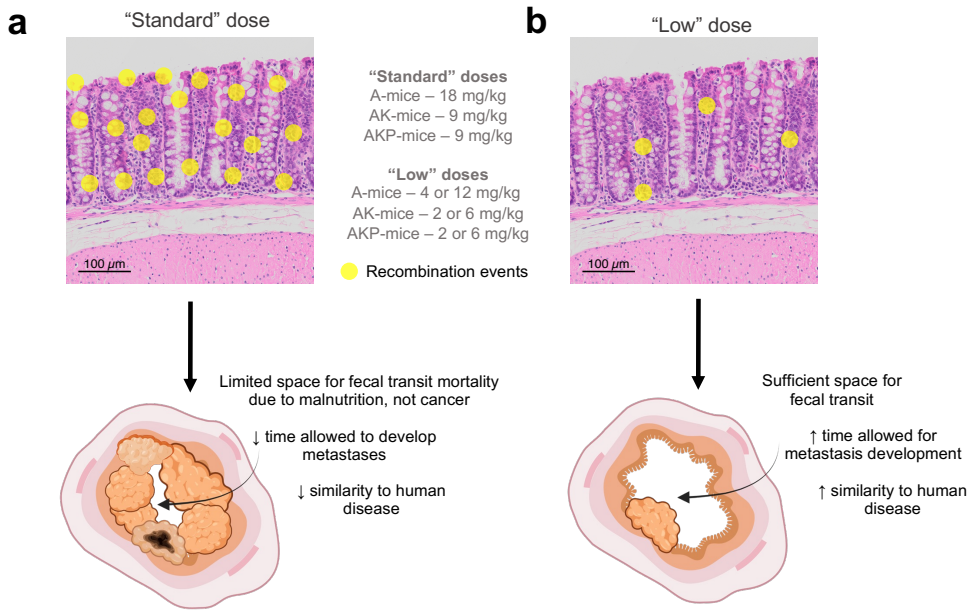

Figure 4.31 Rationale for a low-dose tamoxifen model to study murine colorectal cancer progression in genetic mouse models. **a.** top, a "standard" dose (18 and 9 mg/kg) used in the previously described results in a large tumor "carpet" forming among the targeted cells (bottom). **b.** We hypothesized that a low dose of tamoxifen could lead to fewer recombination events in targeted cells, resulting in fewer and perhaps more discreet tumors (bottom) thus allowing the animals to survive long enough for the tumor to invade and metastasize. Created with BioRender.com.

in fewer CreERT2 recombinase enzymes' translocation to the nucleus, and thus fewer recombinant loci in the colon, Figure 4.31a and b. With fewer recombinant events, we anticipated that the tumor development from adenoma to carcinoma to metastasis may be observable because the animals could survive *longer* due to the lack of impairment of transit of waste through the cecum, Figure 4.31b.

We therefore administered tamoxifen at 12 mg/kg for control and A-mice, and 6 mg/kg in AK- and AKP-mice[IV], Figure 4.32a. We additionally aimed to conduct a "longitudinal" study with this experiment to monitor the changes of the tumor microenvironment within and between the different genotypes. Classical longitudinal studies monitor the same subject at regular intervals over time. In this experiment, because it is impossible to retrieve biopsies from the murine tumors without major life-threatening damage to the mice, we created four

[IV] Prior to this experiment, we previously attempted a similar experiment with tamoxifen administered at 2 mg/kg (A-mice, n=8) and 4 mg/kg (AK- and AKP-mice, n=9 and 8, respectively). After 6 months, there were no signs of disease in any of the mice.

cohorts of mice that would represent four time points in tumor development, namely, 6-, 12- 18- and 24-weeks post-tamoxifen, Figure 4.32a. The mice were monitored closely for the duration of the experiment for signs of disease until the predetermined endpoint. Upon euthanasia, the ceca of the mice were assessed for tumor presence and nearly all mice bearing the CDX2-CreERT2 transgene indeed developed disease, Figure 4.32b. A strip of colon from each mouse was prepared for histology and the mesenteric lymph node (MLN), spleen, lung and liver of each mouse were collected for histology. The colonic tumors were additionally assessed for their immune cell repertoire by flow cytometry, and a selection of samples from the AKP-mice were submitted to 10X Genomics 5' scRNAseq with TCR amplification.

The colons prepared for IHC were sectioned and stained with H&E. All colons were assessed for their tumor grade according to the TNM system[152], Figure 4.33a. The TNM system uses tumor in situ (Tis) and T1-3 to describe the degree of invasion at the primary tumor site (Tis = tumor *in situ*, while T1 indicates slight invasion and T3 indicates extreme invasion). In colorectal cancer, these grades are established by the layer of tissues invaded by the tumor, Figure 4.33a. Tis is classified by tumor presence in the mucosae. T1 involves invasion through the muscularis mucosae (MM), a thin layer of muscle that separates the mucosae and submucosae (SM). T2 tumors exhibit invasion beyond the SM into the muscularis propria (MP), a much thicker layer of smooth muscle that separates the submucosa and serosa. Finally, T3 tumors in CRC exhibit invasion into the serosa. Tumor draining lymph nodes (tdLN) of T1-T3 tumors should be inspected for malignant colonisation. If the tumor-draining lymph node (tdLN) is positive for invasion, common metastatic organs like the lung and liver should be inspected for metastases.

The majority of primary tumors in the 6 and 12 mg/kg experiment were classified as Tis, Figure 4.33b. Among A-tumors–though more than half of analysed tumors were classified as Tis–T1 tumors were observed at all time points, and a T2 tumor was found at 24-weeks post-tamoxifen, Figure 4.33b and Figure 4.34a. Compellingly, all AK-tumors were classified as Tis; no T1 or T2 invasive tumors were found amongst the assessed AK-colons, Figures

a

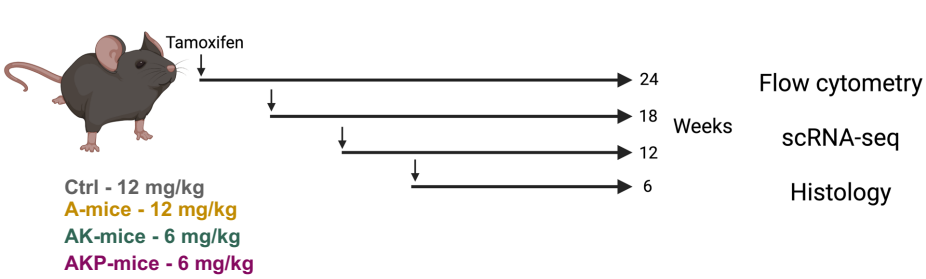

b

Mice with tumors	Ctrl	A	AK	AKP
6w	0/6	6/6	5/5	6/6
12w	0/7	8/8	3/3	7/7
18w	0/4	4/4	5/5	4/4
24w	0/11	6/6	8/9	6/6
early	0/1	8/8	7/7	10/10
total	0/29	32/32	28/29	33/33

Figure 4.32 Experimental design and tumor incidence with administration of 2 and 4 mg/kg of tamoxifen in A-, AK- and AKP-mice. **a.** Mice were administered a single i.p. injection of tamoxifen of 12 mg/kg for control and A-mice and 6 mg/kg for AK- and AKP-mice. There were four induction groups, 24, 18, 12 and 6 weeks before a predetermined endpoint. Upon euthanasia, the mice were subjected to flow cytometry and histology, and AKP-mice were subjected to scRNAseq. **b.** Table showing the number of mice with tumors at endpoint in each group. Some mice had to be euthanised prior to the predetermined endpoint, their data is shown in the "early" row. A summary row – "total"– for each genotype is shown at the bottom.

4.33b and 4.34b. Among AKP-tumors we were able to identify that again, the majority of tumors were classified as Tis (Figure 4.34c), several tumors were classified as T1 invasive tumors a, Figure 4.33b. At 24-weeks post-tamoxifen, one mouse had a T3 tumor (Figure 4.34e), one had a Tis tumor with a positive MLN (Figure 4.34d) and two mice were found to have metastases in the lung and liver, Figures 4.33b and 4.34f–g.

Collectively, this data indicates that our reasoning was correct: reducing the dose of tamoxifen administered to transgenic mice can indeed lead to the manifestation of more invasive disease. The metastatic penetrance of this dose of tamoxifen, however, is still rather uncertain. Of 6 mice in the 24-weeks post-tamoxifen AKP-mice group, two developed metastases which represents 33%. The group size for this experiment is rather small and the experiment should be repeated with a larger cohort to validate or adjust the rate of metastasis that can be expected in AKP-mice. Surprisingly, some A-mice developed invasive disease while AK-mice did not. It was previously shown that APC loss is required for CRC initiation and maintenance, and that additional KRAS mutations and P53 loss drive the tumor towards a more invasive phenotype,[153]. The implications of the previous study is that APC deletion may not be sufficient for tumor progression, but our observations in this study stand at odds with that assumption: perhaps, if given enough time, APC-deleted tumors can progress to carcinomas. Several validation steps need to be conducted to formally validate this hypothesis including whole genome sequencing of the tumor cells to validate that the APC is the only non-silent mutation. Furthermore, the fact that AK-tumors did not exhibit an invasive phenotype is curious, given that the addition of a KRAS mutation has previously been shown and observed to increase the invasion of CRC tumors[14,153].

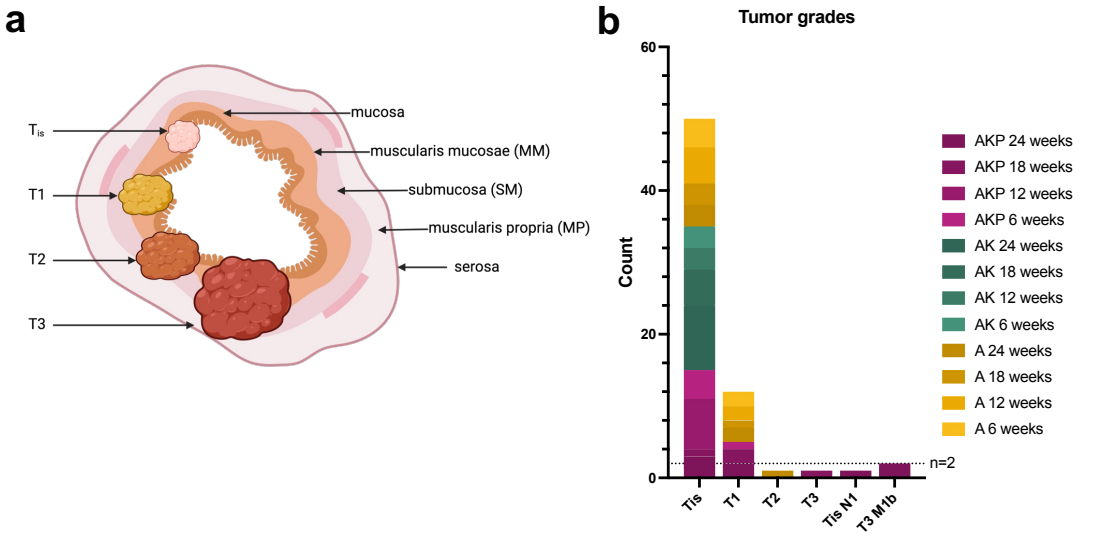

Figure 4.33 A- and AKP- but not AK-mice bear more invasive tumors with low-dose tamoxifen. **a.** TNM tumor grading system in colorectal cancer. Primary tumors of CRC are classified as Tis (Tumor *in situ*), T1 (invasion beyond MM), T2 (invasion beyond MP) and T3 (invasion into the serosa). Adapted from Tauriello *et al.* [62]. **b.** stacked bar plot showing the number of tumors classified as Tis, T1, T2 and T3 as well as the presence or absence of tdLN metastasis (N) or other organ metastases (M). Panel **a** created with BioRender.com.

4.2.1 A-, AK- and AKP-tumors induced with low-dose tamoxifen maintain distinct tumor microenvironments over time

Our second aim in the low-dose tamoxifen experiment was to monitor how the TME evolves over time in the healthy colon as well as A-, AK- and AKP-tumors. Because there are four genotypes in the experiment and four time points, the data will first be presented as a comparison between the genotypes at each time point. We will then explore the immune make-up of the tumors within each genotype over time in the following section.

Flow cytometric analysis was performed on single-cell suspensions derived from the tissue following enzymatic-assisted mechanical dissociation. The same flow cytometry panels used in the previous study were employed for this study, see Figures 4.8, 4.11, and 4.13 for gating strategies. At early timepoints (6- and 12- weeks post-tamoxifen), AKP-tumors had fewer immune cells within the TME as compared to the healthy colon and AK-tumors, Figure 4.35a. $CD45^+$ cell infiltration was not significantly different between the models at 18- and

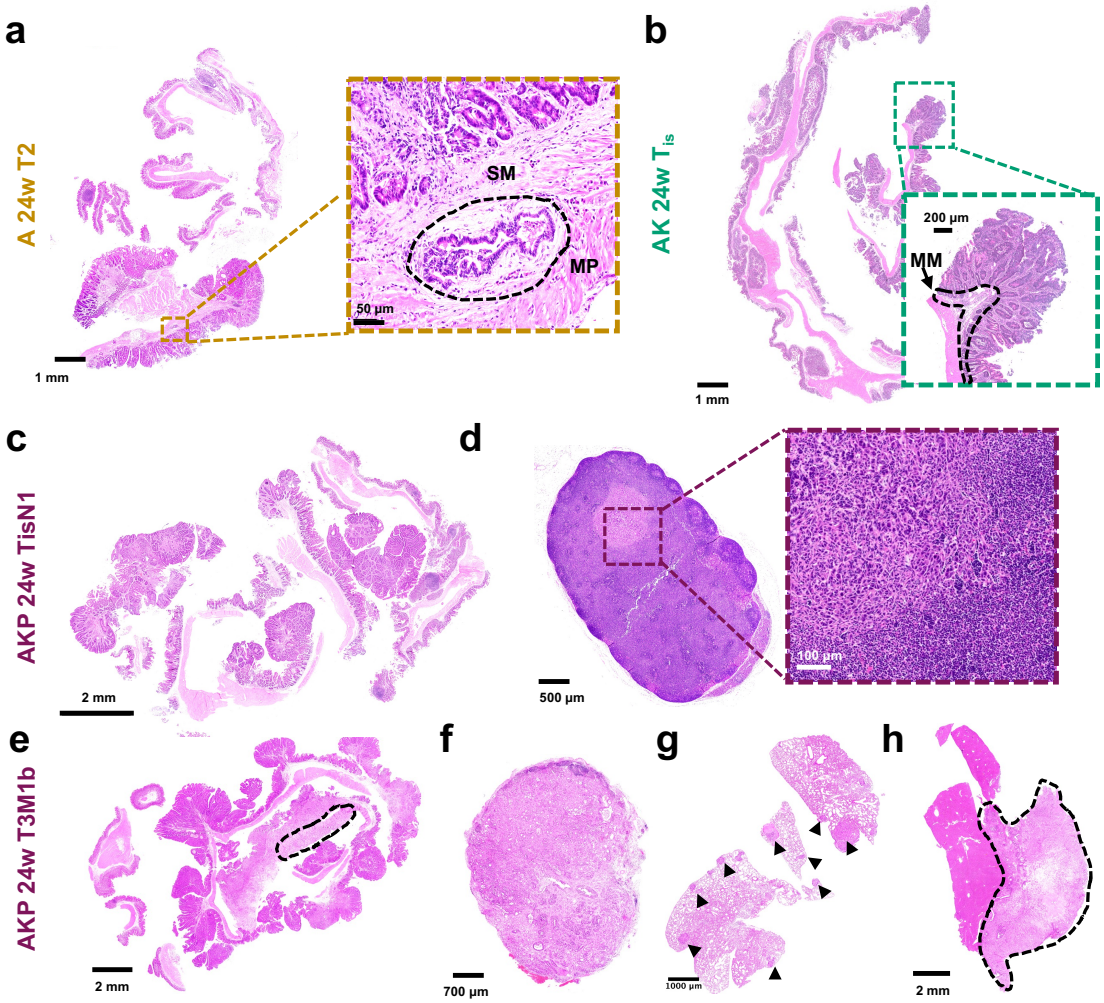

Figure 4.34 Metastatic penetrance and tumor morphology of low-dose tamoxifen A-, AK- and AKP-mice. **a.** H&E staining of an A-tumor at 24 weeks post-tamoxifen with invasion through the MP. **b.** H&E staining of an AK-tumor at 24 weeks post-tamoxifen with a tumor of grade Tis, c. H&E staining of an AKP-tumor at 24 weeks post-tamoxifen with no apparent invasion, but the same mouse had a **d.** MLN with evident adenocarcinoma metastasis. **e.** An AKP mouse in the 24 week post-tamoxifen group with T3 adenocarcinoma with evident invasion into the muscularis (dotted lines). **f-h.** H&E staining of the MLN, lung, and liver from the same mouse shown in **e**. Black arrows and black dotted lines indicate metastases.

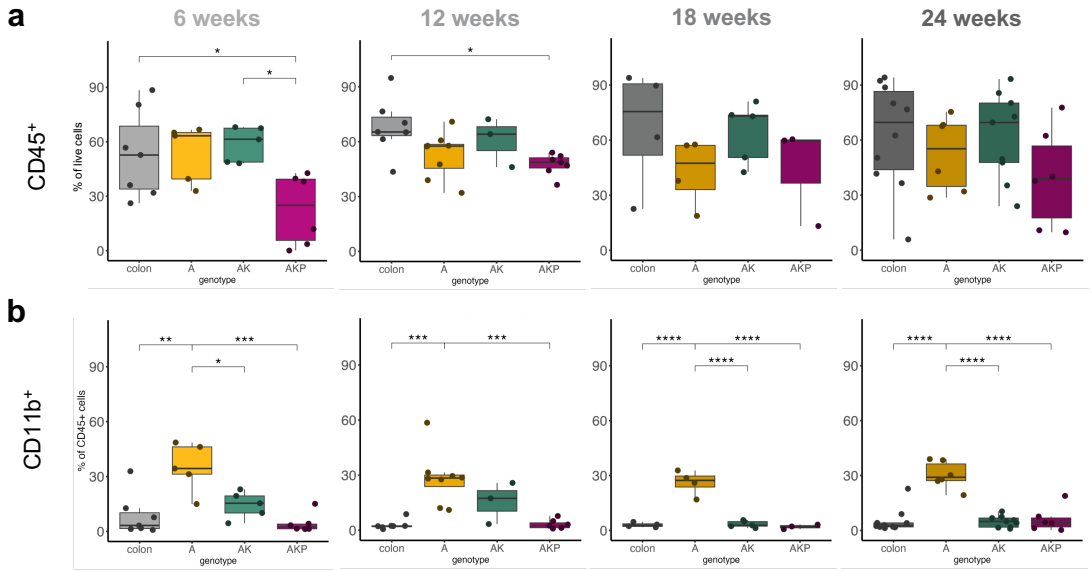

Figure 4.35 AKP-tumors have fewer immune cells than A- and AK-tumors at early time points and A-tumors contain significantly more myeloid cells than other tumors over time. Flow cytometry for **a.** $CD45^+$ and **b.** $CD11b^+$ immune cells at 6, 12, 18 and 24 weeks in colon, A-, AK- and AKP-tumors. Data shown includes the following number of mice in each respective group: colon (n=7, 7, 4 and 10), A-mice (n=5, 8, 4 and 6), AK-mice (n=5, 3, 5 and 9), and AKP-mice (n=6, 7, 3, and 6) for timepoints 6-, 12-, 18- and 24-weeks, respectively. Data in **d** is from two independent experiments; brackets and stars are indicative of the adjusted p value result of a one-way ANOVA with Tukey's multiple corrections to account for multiple comparisons. key: $p \leq 0.05$ = *, $p \leq 0.01$ = **, $p \leq 0.001$ = ***, $p \leq 0.0001$ = ****, and non-significant (n.s.) comparisons are not shown.

24-weeks post-tamoxifen, but varied between 5% to 85% of live cells, with A- and AKP-tumors tending to have fewer immune cells than the healthy colon and AK-tumors, Figure 4.35a. We then assessed the proportion of cells with myeloid lineage, and found that–as in the "standard-dose" model–A-tumors bore significantly more $CD11b^+$ cells than the healthy colon and AKP-tumors over time, Figure 4.35b. At 6- and 12-weeks post-tamoxifen, there was a trend for AK-tumors having more $CD11b^+$ cells as compared to colon and AKP-tumors, Figure 4.35b. Interestingly, the difference between A- and AK-tumors at 12-weeks was not significantly different, while at later timepoints AK-tumors had similar representation of myeloid cells in their TME as colon and AKP-tumors, Figure 4.35b.

We next sought to understand the differential abundance of $MHCII^-$ monocytes, $SSC^{hi}Ly6C^{lo}$ and $MHCII^+$ professional APCs between the models over time. Monocyte infiltration mirrored that of the $CD11b^+$ cells in general, Figure 4.36a. Namely, A-tumors had significantly more

monocytes than colon and AK-tumors over time, and more monocytes than AK-tumors at 6-, 18- and 24-weeks, Figure 4.36a. The difference in monocyte infiltration between AK-tumors and the other groups was not significant at 12-weeks, Figure 4.36a. Neutrophils were significantly higher in A-tumors compared to colon, AK- and AKP-tumors at 6- and 24-weeks post-tamoxifen, Figure 4.36b. A-tumors had significantly more neutrophils than colon and AKP-tumors at 12-weeks post-tamoxifen, and more neutrophils than AK-tumors at 18-weeks post-tamoxifen, Figure 4.36b. pAPC were significantly enriched in A-tumors compared to the healthy colon and AKP-tumor throughout time, Figure 4.36c. While AK-tumors 6-weeks post-tamoxifen had fewer pAPC than A-tumors, the $MHCII^+$ myeloid subset was comparable between A- and AK-tumors 12-weeks post-tamoxifen, Figure 4.36c. At later timepoints, however, the pAPC in AK-tumors significantly dropped and the AK-tumor thus had fewer pAPC compared to A-tumors at 18- and 24-weeks post-tamoxifen, Figure 4.36c.

We then examined the T cell compartment of the TME in the tumor models over time. Regarding total T cell infiltration, measured by $TCR\beta^+$ T cells we did not note any significant differences between the models' T cell infiltration across all timepoints, Figure 4.37a. AKP-tumors, however, seemed to display a larger variation in the amount of T cells compared to the other models at early time points, Figure 4.37a. Similarly, $CD4^+$ and $CD8^+$ T cell subsets demonstrated no significant differences in their presence between the different tumor types and healthy colon, Figure 4.37b and c. An interesting trend does exist, however, at the later time points (18- and 24-weeks post-tamoxifen) wherein A-tumors may have fewer $TCR\beta^+$, $CD4^+$ and $CD8^+$ T cells compared to AK- and AKP-tumors, Figure 4.37a–c. We next assessed whether any differences existed between the tumors with respect to Tregs, Th17 and cytotoxic effector T cells.

In order to assess the amount of Tregs present in the tumors, the single-cell suspensions derived from the tumors were stained for FOXP3. We found that there were few Tregs in all models over time, with infiltration ranging between 0 and 5% of $CD45^+$ cells, Figure 4.38a. At early time points (6- and 12-weeks post-tamoxifen) there was no significant difference in the proportion of Tregs in the tumors, but A- and AKP-tumors tended to have more Tregs

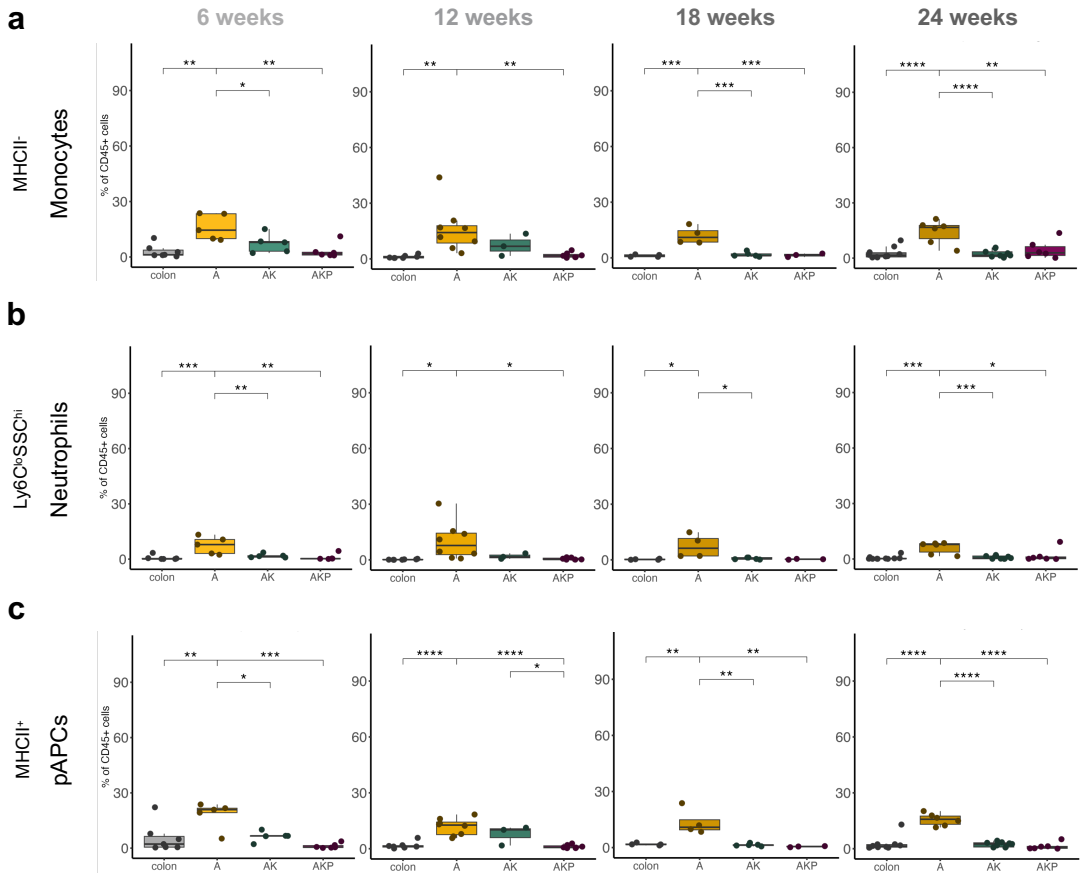

Figure 4.36 Monocytes, neutrophils and professional antigen cells are significantly more prominent in A-tumors over time compared to AK- and AKP-tumors. **a.** MHCII^{-} monocytes, **b.** neutrophils (SSC^{hi}Ly6C^{lo}) and **c.** professional APCs (CD11b^{+}MHCII^{+}) in colon, A-, AK- and AKP-tumors at 6-, 12-, 18- and 24-weeks post-tamoxifen. Data shown includes the following number of mice in each respective group: colon (n=7, 7, 4 and 10), A-mice (n=5, 8, 4 and 6), AK-mice (n=5, 3, 5 and 9), and AKP-mice (n=6, 7, 3, and 6) for timepoints 6-, 12-, 18- and 24-weeks, respectively. Data in **d** is from two independent experiments; brackets and stars are indicative of the adjusted p value result of a one-way ANOVA with Tukey's multiple corrections to account for multiple comparisons. key: $p \leq 0.05$ = *, $p \leq 0.01$ = **, $p \leq 0.001$ = ***, $p \leq 0.0001$ = ****, and non-significant (n.s.) comparisons are not shown.

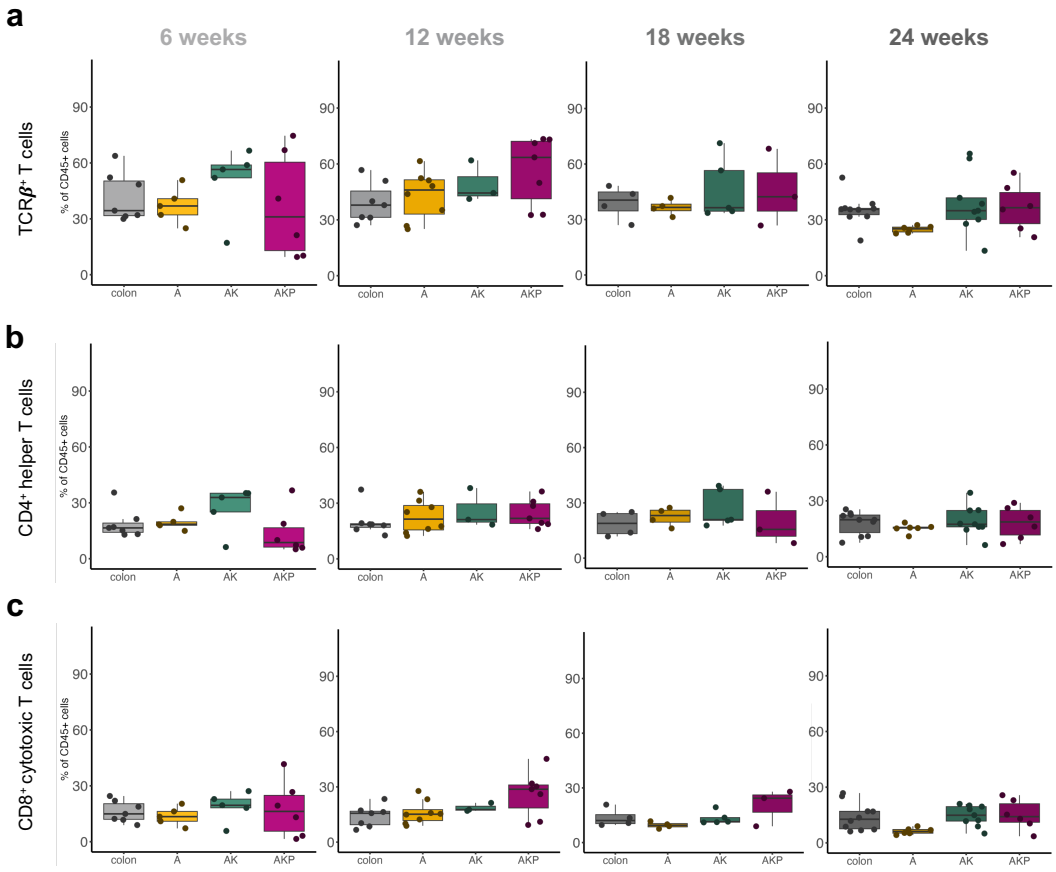

Figure 4.37 There is no significant difference in the abundance of T cells between A-, AK- and AKP-tumors at any timepoint. **a.** TCRβ^+ T cells, **b.** CD4$^+$ helper T cells and **c.** CD8$^+$ cytotoxic T cells in colon, A-, AK- and AKP-tumors at 6-, 12-, 18- and 24-weeks post-tamoxifen. Data shown includes the following number of mice in each respective group: colon (n=7, 7, 4 and 10), A-mice (n=5, 8, 4 and 6), AK-mice (n=5, 3, 5 and 9), and AKP-mice (n=6, 7, 3, and 6) for timepoints 6-, 12-, 18- and 24-weeks, respectively. Data in **d** is from two independent experiments; brackets and stars are indicative of the adjusted p value result of a one-way ANOVA with Tukey's multiple corrections to account for multiple comparisons. key: $p \leq 0.05$ = *, $p \leq 0.01$ = **, $p \leq 0.001$ = ***, $p \leq 0.0001$ = ****, and non-significant (n.s.) comparisons are not shown.

than AK-tumors, Figure 4.38a. At later timepoint the trends for AK-tumors having fewer Tregs compared to A- and AKP-tumors became significant, and at 24-weeks post-tamoxifen, they also had significantly more Tregs than the healthy colon, Figure 4.38a. IL17a$^+$ CD4$^+$ Th17 cells clearly favored AK-tumors at 12- and 18-weeks post-tamoxifen, though the comparisons were only significant at 12-weeks, Figure 4.38b. With respect to CD8$^+$ T cells expressing GZMb$^+$, there was a non-significant trend of the cytotoxic T cells accumulating within AK-tumors over A- and AKP-tumors at 12-weeks that was perhaps maintained at 18- and 24-weeks, Figure 4.38c.

We next measured the proportion of IFNγ-producing T cells in the TME of the tumors. Overall, in comparisons between the different genotypes, there was no statistical difference for IFNγ^+ TCRβ^+, CD4$^+$ nor CD8$^+$ T cells, Figure 4.39a-c. A few trends, however, can be noted: AK-tumors tended to have more TCRβ^+IFNγ^+ T cells compared to A- and AKP-tumors throughout time, Figure 4.39a. All tissues had extremely few CD4$^+$ and CD8$^+$ IFNγ^+ T cells at 6-weeks post-tamoxifen, Figure 4.39b and c. From 12-weeks post-tamoxifen onwards, AK-tumors contained the most IFNγ^+ CD4$^+$ and CD8$^+$ T cells of all tumor types, and had similar amounts of these cells compared to the healthy colon, Figure 4.39b and c.

Overall, when the TME of low-dose tamoxifen A-, AK- and AKP-tumors were compared over time, a couple of trends emerged. A-tumors bear more myeloid-lineage cells (including monocytes, neutrophils and pAPC) than the other tumors. In turn, there was a non-significant trend towards fewer T cells in A-tumors compared to AK- and AKP-tumors. Interestingly, as time in the experiment increased, the Treg population became more numerous in A- and AKP-tumors while Th17 cells accumulated in AK-tumors at 12-weeks post-tamoxifen especially. Finally, there was a non-significant trend for GZMb$^+$ cytotoxic T cells to be more present in AK- and AKP-tumors over time. We next compared each component of the TME within each genotype over time in order to observe how the TME in each tumor type evolved over time.

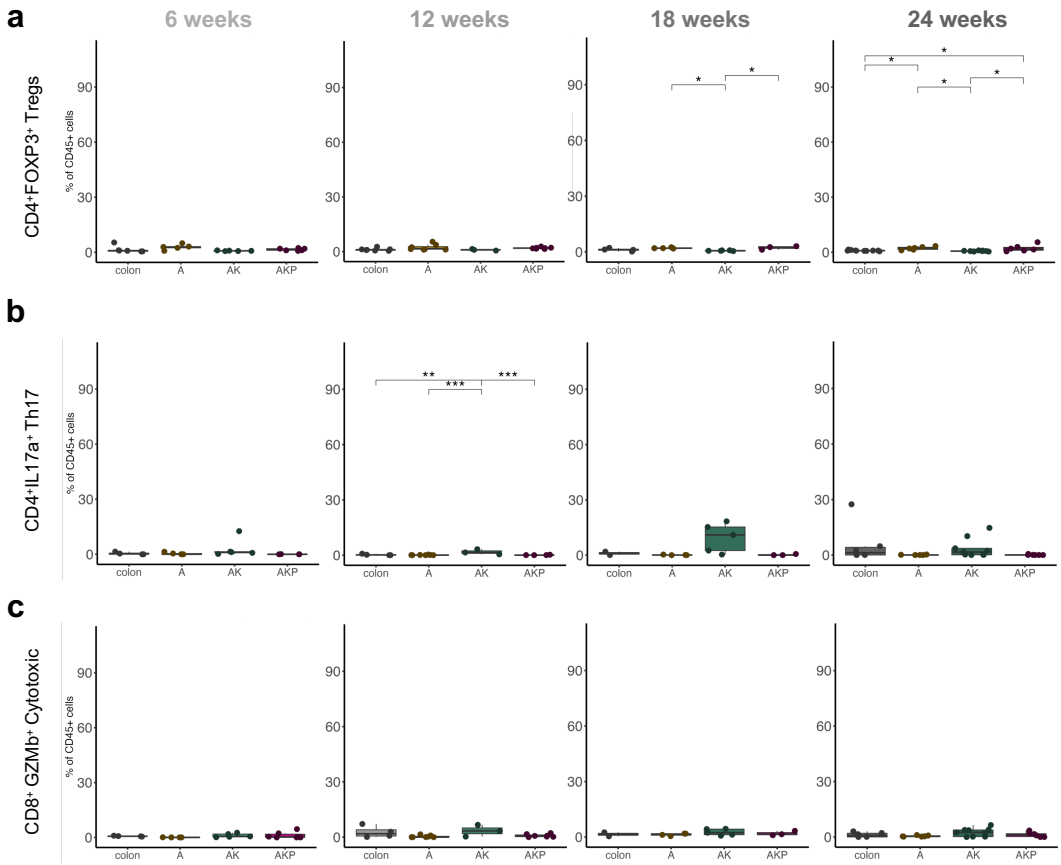

Figure 4.38 A- and AKP-tumors tend to have more Tregs than AK tumors which have more Th17 cells. **a.** $CD4^+FOXP3^+$ Tregs, **b.** $CD4^+IL17a^+$ Th17 cells and **c.** $CD8^+GZMb^+$ cytotoxic T cells in colon, A-, AK- and AKP-tumors at 6-, 12-, 18- and 24-weeks post-tamoxifen. Data for FoxP3 includes the following number of mice in each respective group: colon (n=6, 7, 4 and 10), A-mice (n=5, 8, 4 and 6), AK-mice (n=5, 3, 5 and 9), and AKP-mice (n=6, 7, 3, and 6) for timepoints 6-, 12-, 18- and 24-weeks, respectively. Data for IL17a and GZMb includes the following number of mice in each respective group: colon (n=4, 4, 2 and 6), A-mice (n=5, 8, 4 and 6), AK-mice (n=5, 3, 5 and 9), and AKP-mice (n=6, 7, 3, and 6) for timepoints 6-, 12-, 18- and 24-weeks, respectively. Data in **d** is from two independent experiments; brackets and stars are indicative of the adjusted p value result of a one-way ANOVA with Tukey's multiple corrections to account for multiple comparisons. key: $p \leq 0.05$ = *, $p \leq 0.01$ = **, $p \leq 0.001$ = ***, $p \leq 0.0001$ = ****, and non-significant (n.s.) comparisons are not shown.

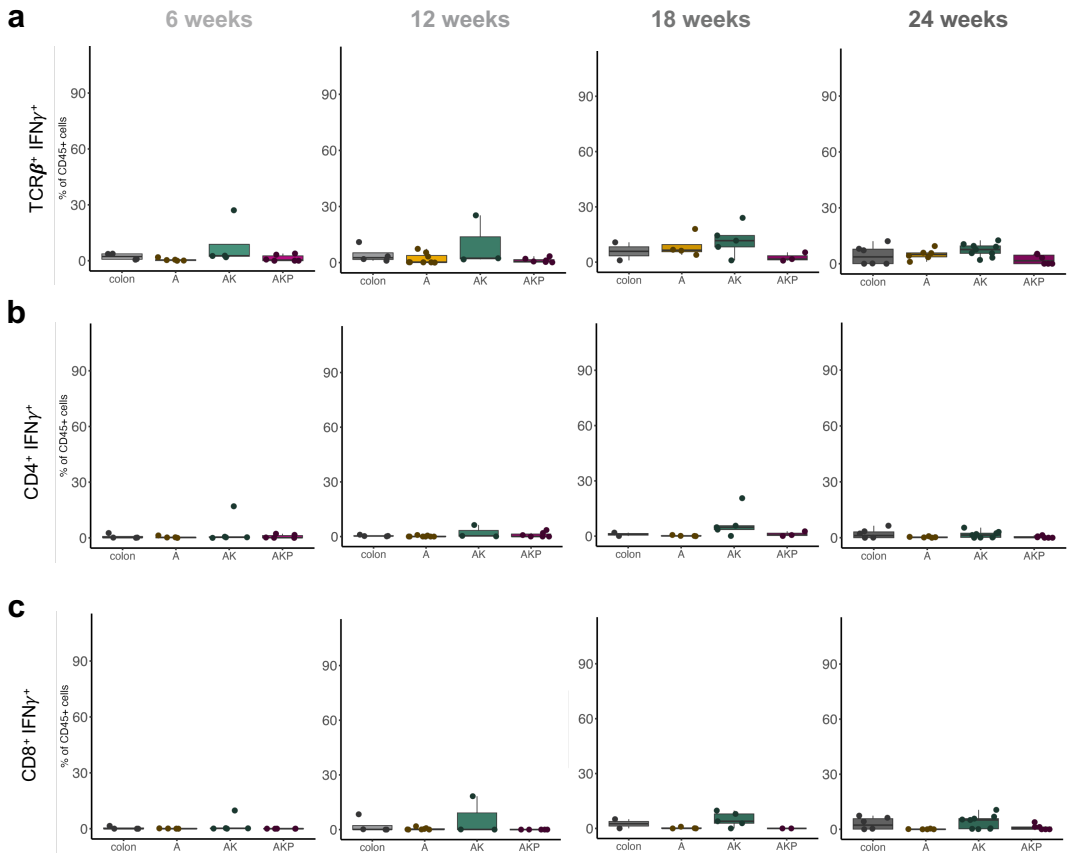

Figure 4.39 The frequency of interferon-γ-producing T cells is not statistically different between A-, AK- and AKP-tumors over time. **a.** TCRβ^+IFNγ^+ T cells, **b.** CD4$^+$IFNγ^+ T helper cells and **c.** CD8$^+$IFNγ^+ cytotoxic T cells in colon, A-, AK- and AKP-tumors at 6-, 12-, 18- and 24-weeks post-tamoxifen. Data shown includes the following number of mice in each respective group: colon (n=4, 4, 2 and 6), A-mice (n=5, 8, 4 and 6), AK-mice (n=5, 3, 5 and 9), and AKP-mice (n=6, 7, 3, and 6) for timepoints 6-, 12-, 18- and 24-weeks, respectively. Data is from two independent experiments; brackets and stars are indicative of the adjusted p value result of a one-way ANOVA with Tukey's multiple corrections to account for multiple comparisons. key: $p \leq 0.05$ = *, $p \leq 0.01$ = **, $p \leq 0.001$ = ***, $p \leq 0.0001$ = ****, and non-significant (n.s.) comparisons are not shown.

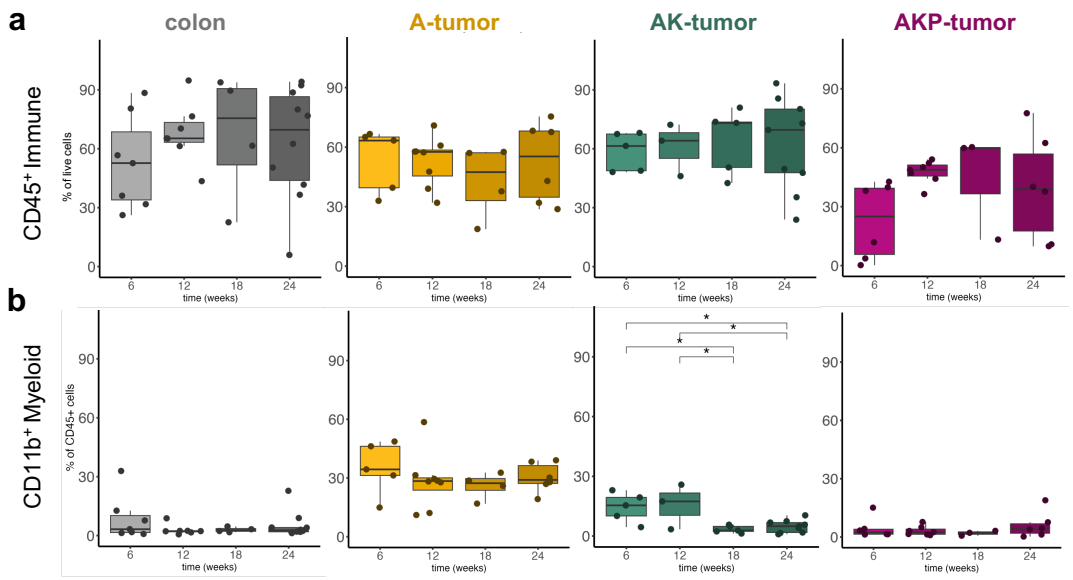

Figure 4.40 AK-tumors exclude myeloid cells at later time points. **a.** CD45$^+$ cells as % of live cells and **b.** CD11b$^+$ myeloid cells as % CD45$^+$ cells in colon, A-, AK- and AKP-tumors at 6-, 12-, 18- and 24-weeks post-tamoxifen. Data shown includes the following number of mice in each respective group: colon (n=7, 7, 4 and 10), A-mice (n=5, 8, 4 and 6), AK-mice (n=5, 3, 5 and 9), and AKP-mice (n=6, 7, 3, and 6) for timepoints 6-, 12-, 18- and 24-weeks, respectively. Data in **d** is from two independent experiments; brackets and stars are indicative of the adjusted p value result of a one-way ANOVA with Tukey's multiple corrections to account for multiple comparisons. key: $p \leq 0.05$ = *, $p \leq 0.01$ = **, $p \leq 0.001$ = ***, $p \leq 0.0001$ = ****, and non-significant (n.s.) comparisons are not shown.

4.2.2 T cell accumulation peaks and pAPC efflux are observable in A-, AK- and AKP-tumors over time

Immune cell infiltration as measured by CD45$^+$ cells did not change significantly in any model over time, Figure 4.40a. AKP-tumors at 6 weeks, however, had a great variation of tumor-infiltrating immune cells from almost 0% up to 40% of live cells, Figure 4.40a. When we inspected the representation of CD11b$^+$ myeloid cells in the TME, more of these cells were in A-tumors at 6-weeks than later timepoints (12-, 18- and 24-weeks) but this trend was not significant, Figure 4.40b. AK tumors had a dramatic loss of tumor-infiltrating myeloid cells at later timepoints (18- and 24-weeks) compared to early timepoints (6- and 12-weeks), Figure 4.40b. The relatively small CD11b$^+$ population in AKP-tumors remained small over time, Figure 4.40b. We next asked whether myeloid subsets were variable within each tumor type over time.

There were no major changes in the proportion of monocytes, neutrophils nor pAPC in the healthy colon over time, Figure 4.41a–c. Monocyte infiltration in A- and AKP-tumors did not fluctuate over time, Figure 4.41a. Though not significant, the reduction in proportion of myeloid cells in general ($CD11b^+$) was mirrored in the monocyte population of AK-tumors, Figure 4.41a. The neutrophil population was stable in A- and AKP-tumors and again showed a non-significant trend for reduction of neutrophils in late time points in AK-tumors, Figure 4.41b. Though there were no significant changes over time, 6-weeks post-tamoxifen tumors perhaps had more pAPC, which then dropped in abundance at 12-weeks then slowly augmented over time, Figure 4.41c. Significant loss of pAPC was observed in 18- and 24-week AK-tumors compared to the earlier two timepoints, Figure 4.41c. AKP-tumors once again displayed a rather stagnant pAPC population, Figure 4.41c.

Next, we assessed the level of T cell infiltration within each tumor type over time. There were no significant changes in the prevalence of $TCR\beta^+$, $CD4^+$ nor $CD8^+$ T cells in the healthy colon, though there was a trend toward fewer cytotoxic T cells over time, Figure 4.42a–c. Within A tumors, total T cells peaked at 12-weeks post-tamoxifen where there were significantly more T cells compared to 24-weeks post-tamoxifen, Figure 4.42a. Over time AK-tumors exhibited a non-significant trend toward the progressive loss of total T cells, Figure 4.42a. Total T cells in AKP-tumors, like A-tumors, peaked at 12-weeks post-tamoxifen and then declined slightly in number over time, Figure 4.42a. There were no significant changes in the abundance of $CD4^+$ T cells in any of the tumors over time, but the patterns observed in the total T cells were reflected here: A- and AKP-tumors had a peak of $CD4^+$ T cells at 12-weeks post-tamoxifen and the population progressively reclined in AK-tumors, Figure 4.42b. Cytotoxic $CD8^+$ T cells also peaked at 12-weeks post-tamoxifen in A- and AKP-tumors, Figure 4.42c. In A-tumors, there were significantly fewer cytotoxic T cells at 24-weeks compared to 12-weeks post-tamoxifen, Figure 4.42c. Once again, AK-tumors demonstrated a progressive loss of these T cells, except there was a minor, not significant, increase in the cytotoxic T cells at 24 weeks, Figure 4.42c. Our next curiosity was whether T cell subsets of interest (Tregs, Th17 and $GZMb^+$) could be observed changing within the

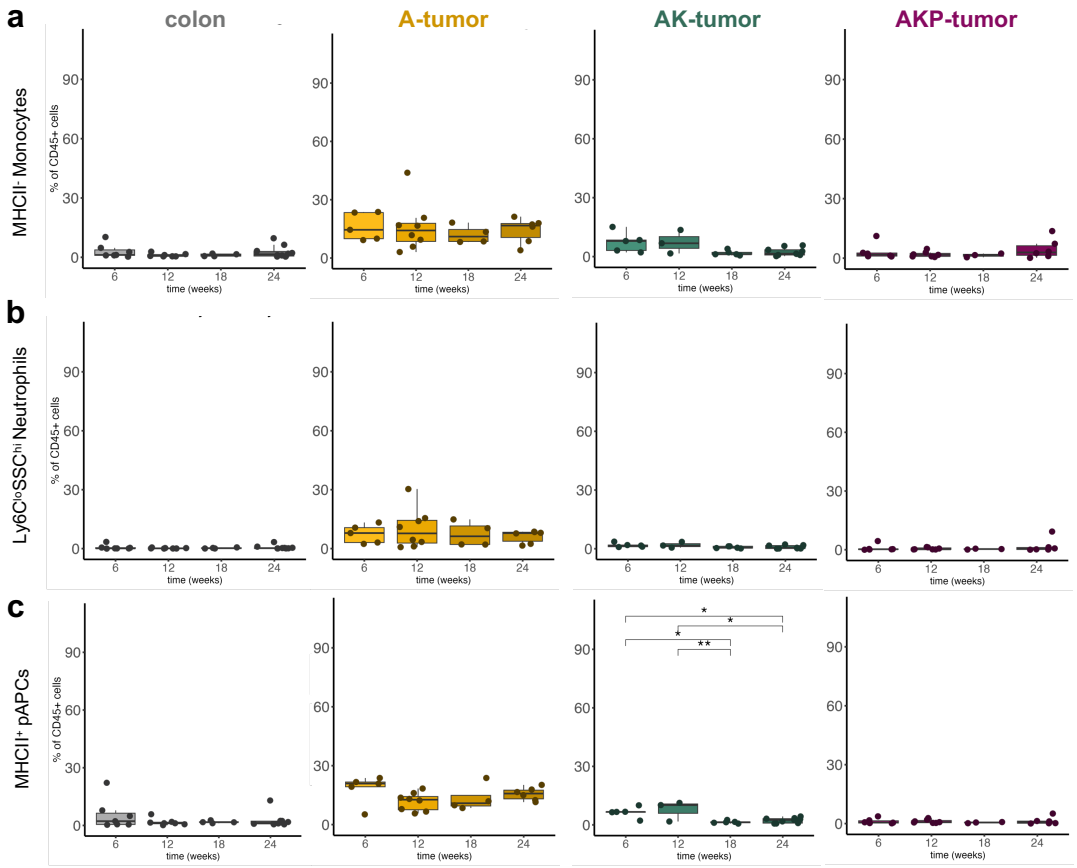

Figure 4.41 The efflux of myeloid cells from AK-tumors at later time points is in large part due to the efflux of professional APCs. **a.** MHCII^{-} monocytes, **b.** neutrophils (SSC^{hi}Ly6C^{lo}) and **c.** professional APCs (CD11b^{+}MHCII^{+}) in colon, A-, AK- and AKP-tumors at 6-, 12-, 18- and 24-weeks post-tamoxifen. Data shown includes the following number of mice in each respective group: colon (n=7, 7, 4 and 10), A-mice (n=5, 8, 4 and 6), AK-mice (n=5, 3, 5 and 9), and AKP-mice (n=6, 7, 3, and 6) for timepoints 6-, 12-, 18- and 24-weeks, respectively. Data in **d** is from two independent experiments; brackets and stars are indicative of the adjusted p value result of a one-way ANOVA with Tukey's multiple corrections to account for multiple comparisons. key: $p \leq 0.05$ = *, $p \leq 0.01$ = **, $p \leq 0.001$ = ***, $p \leq 0.0001$ = ****, and non-significant (n.s.) comparisons are not shown.

TME of the tumor models over time.

Regulatory T cells did not change significantly over time in the colon, A-, AK- nor AKP-tumors, Figure 4.43a. Th17 cells did not change significantly in any of the models over time, but there was a non-specific trend for their presence in AK-tumors 18-weeks post-tamoxifen, Figure 4.43b. The cytotoxic GZMb$^+$ T cells were significantly enriched in A-tumors at 18-weeks compared to the 6- and 12-weeks post-tamoxifen timepoints, Figure 4.43c. From 12- to 24-weeks post-tamoxifen in AK-tumors there was a non-significant trend for greater cytotoxic T cell infiltration, Figure 4.43a. We next assessed the T cells for IFNγproduction. In the healthy colon, there was a trend toward increasing IFNγproducing T cells over time, Figure 4.39a. In A-tumors there was a significant increase in the proportion of IFNγ^+ T cells at 18-weeks post-tamoxifen compared to the 6- and 12-week timepoints which remained elevated at 24-weeks but was not significant when compared to the other timepoints, Figure 4.39a. Among AK-tumors, IFNγ-producing T cells perhaps peaked at 12- and 18- weeks post-tamoxifen while AKP-tumors' IFNγ^+ T cell population moderately and non-significantly increased over time, Figure 4.39a. The IFNγ-producing CD4 and CD8 T cell subsets were not dynamic over time, Figure 4.39b and c.

Overall, we can observe that low-dose tamoxifen A-, AK- and AKP-tumors are generally infiltrated with immune cells (as in the "standard" dose models), Figure 4.45. There are more differences between models than within each model over time. A-tumors, for example are characterised by their abundant myeloid cell population including pAPC, monocytes and neutrophils while AK- and AKP tumors have fewer of these cells, Figure 4.45. Interestingly, AK-tumors have more myeloid cells (pAPC and monocytes) early-on in the experimental timeline compared to later, Figure 4.45. The fact that AK-tumors begin the experiment with many MHCII$^+$ cells and finish with fewer could be indicative of pAPC migration to nearby lymph nodes for T cell education[V]. It is worth emphasising at this point that we did not observe any invasive tumors in AK-mice within this experiment, while we did observe

[V] Once again, the lymph nodes have been collected (and in this case have been assessed for metastases) but this hypothesis remains to be proven

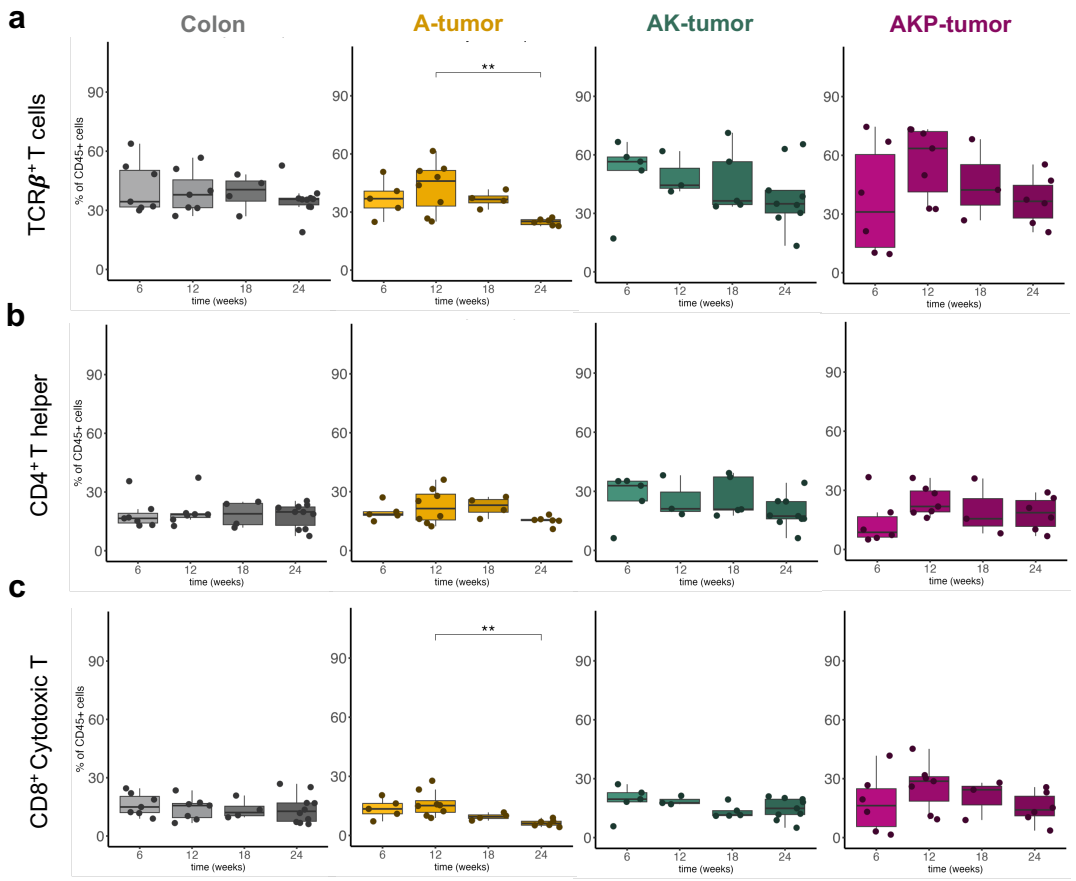

Figure 4.42 A-tumors exclude T cells over time. **a.** TCRβ^+ T cells, **b.** CD4$^+$ helper T cells and **c.** CD8$^+$ cytotoxic T cells in colon, A-, AK- and AKP-tumors at 6-, 12-, 18- and 24-weeks post-tamoxifen. Data shown includes the following number of mice in each respective group: colon (n=7, 7, 4 and 10), A-mice (n=5, 8, 4 and 6), AK-mice (n=5, 3, 5 and 9), and AKP-mice (n=6, 7, 3, and 6) for timepoints 6-, 12-, 18- and 24-weeks, respectively. Data in **d** is from two independent experiments; brackets and stars are indicative of the adjusted p value result of a one-way ANOVA with Tukey's multiple corrections to account for multiple comparisons. key: $p \leq 0.05$ = *, $p \leq 0.01$ = **, $p \leq 0.001$ = ***, $p \leq 0.0001$ = ****, and non-significant (n.s.) comparisons are not shown.

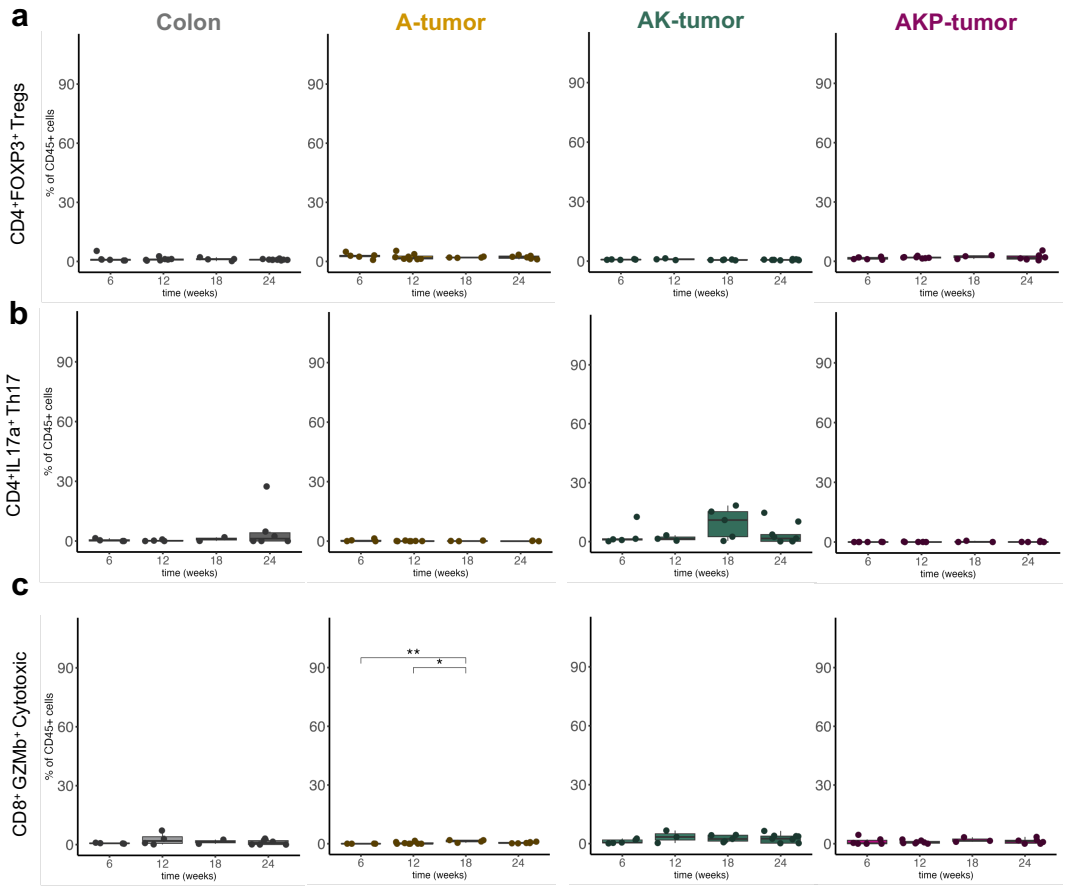

Figure 4.43 Granzyme B$^+$ CD8 T cells are significantly enriched but not numerous at later time points in A-tumors. **a.** CD4$^+$FOXP3$^+$ Tregs, **b.** CD4$^+$IL17a$^+$ Th17 cells and **c.** CD8$^+$GZMb$^+$ cytotoxic T cells in colon, A-, AK- and AKP-tumors at 6-, 12-, 18- and 24-weeks post-tamoxifen. Data for FoxP3 includes the following number of mice in each respective group: colon (n=6, 7, 4 and 10), A-mice (n=5, 8, 4 and 6), AK-mice (n=5, 3, 5 and 9), and AKP-mice (n=6, 7, 3, and 6) for timepoints 6-, 12-, 18- and 24-weeks, respectively. Data for IL17a and GZMb includes the following number of mice in each respective group: colon (n=4, 4, 2 and 6), A-mice (n=5, 8, 4 and 6), AK-mice (n=5, 3, 5 and 9), and AKP-mice (n=6, 7, 3, and 6) for timepoints 6-, 12-, 18- and 24-weeks, respectively. Data in **d** is from two independent experiments; brackets and stars are indicative of the adjusted p value result of a one-way ANOVA with Tukey's multiple corrections to account for multiple comparisons. key: $p \leq 0.05$ = *, $p \leq 0.01$ = **, $p \leq 0.001$ = ***, $p \leq 0.0001$ = ****, and non-significant (n.s.) comparisons are not shown.

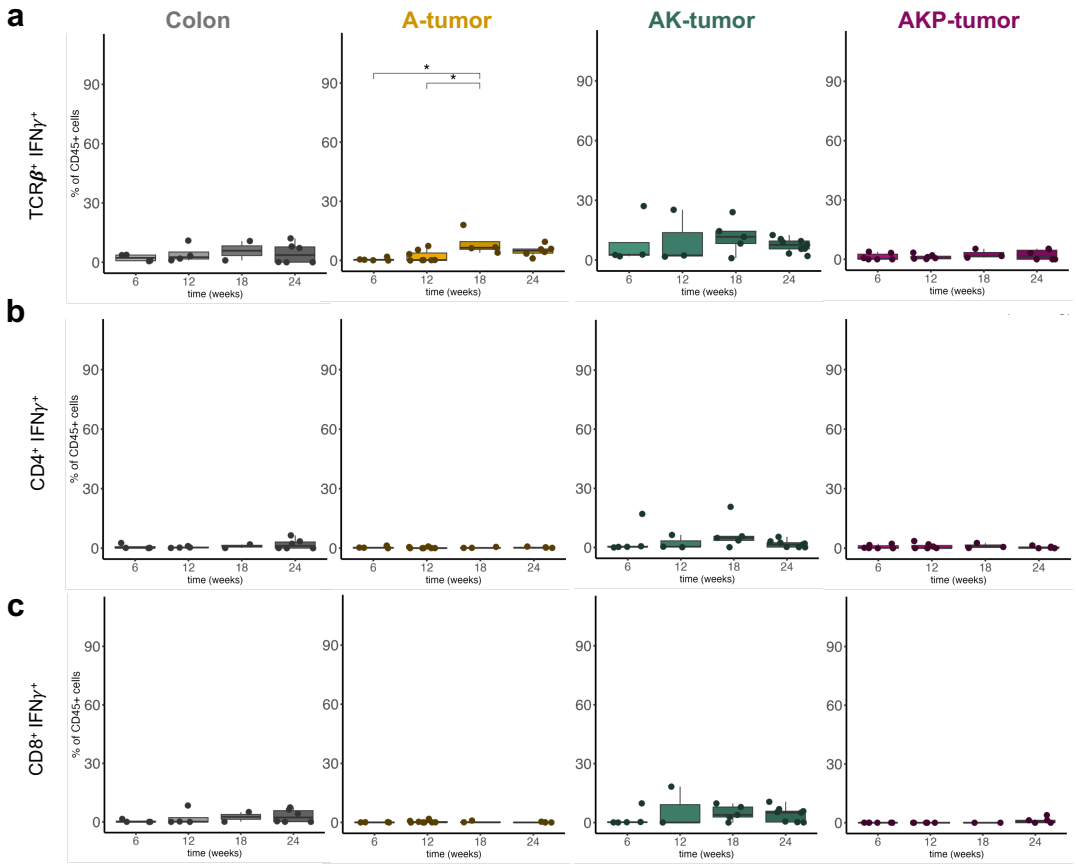

Figure 4.44 Interferon γ-producing T cells are enriched in later time points among A-tumor in small number. **a.** TCRβ^+IFNγ^+ T cells, **b.** CD4$^+$IFNγ^+ T helper cells and **c.** CD8$^+$IFNγ^+ cytotoxic T cells in colon, A-, AK- and AKP-tumors at 6-, 12-, 18- and 24-weeks post-tamoxifen. Data shown includes the following number of mice in each respective group: colon (n=4, 4, 2 and 6), A-mice (n=5, 8, 4 and 6), AK-mice (n=5, 3, 5 and 9), and AKP-mice (n=6, 7, 3, and 6) for timepoints 6-, 12-, 18- and 24-weeks, respectively. Data in **d** is from two independent experiments; brackets and stars are indicative of the adjusted p value result of a one-way ANOVA with Tukey's multiple corrections to account for multiple comparisons. key: $p \leq 0.05$ = *, $p \leq 0.01$ = **, $p \leq 0.001$ = ***, $p \leq 0.0001$ = ****, and non-significant (n.s.) comparisons are not shown.

invasion within A- and AKP-tumors, Figure 4.33b. Because pAPC efflux correlates with less invasion, the tdLNs should be evaluated for increased pAPC presence and the identity of those cells (dendritic cells or macrophages). Furthermore, when the tumor was examined for classical memory markers like CD62L and CD44, AK tumors showed an enrichment in $CD4^+$ $CD62L^+CD44^+$ effector T cells at 18-weeks post tamoxifen, indicating that perhaps T cells had been educated and licensed in the tdLN between the 12-and 18-weeks timepoints, Figure 4.46. AKP-tumors however, are observed at 6-weeks post-tamoxifen all the way through 24-weeks post-tamoxifen as having very few myeloid cells without much fluctuation, Figure 4.45.

Interestingly, with this longitudinal data, we can observe when T cell infiltration "peaks" within each tumor. For example, A- and AKP-tumors show a peak of TCRβ^+ T cells at 12-weeks post-tamoxifen while AK-tumors' T cells seem to peak at or before the 6-week timepoint, Figure 4.45. In the next section, we will address whether this expansion correlates with a expansion of non-unique TCRs or rather a general expansion of non-specific T cells in AKP tumors.

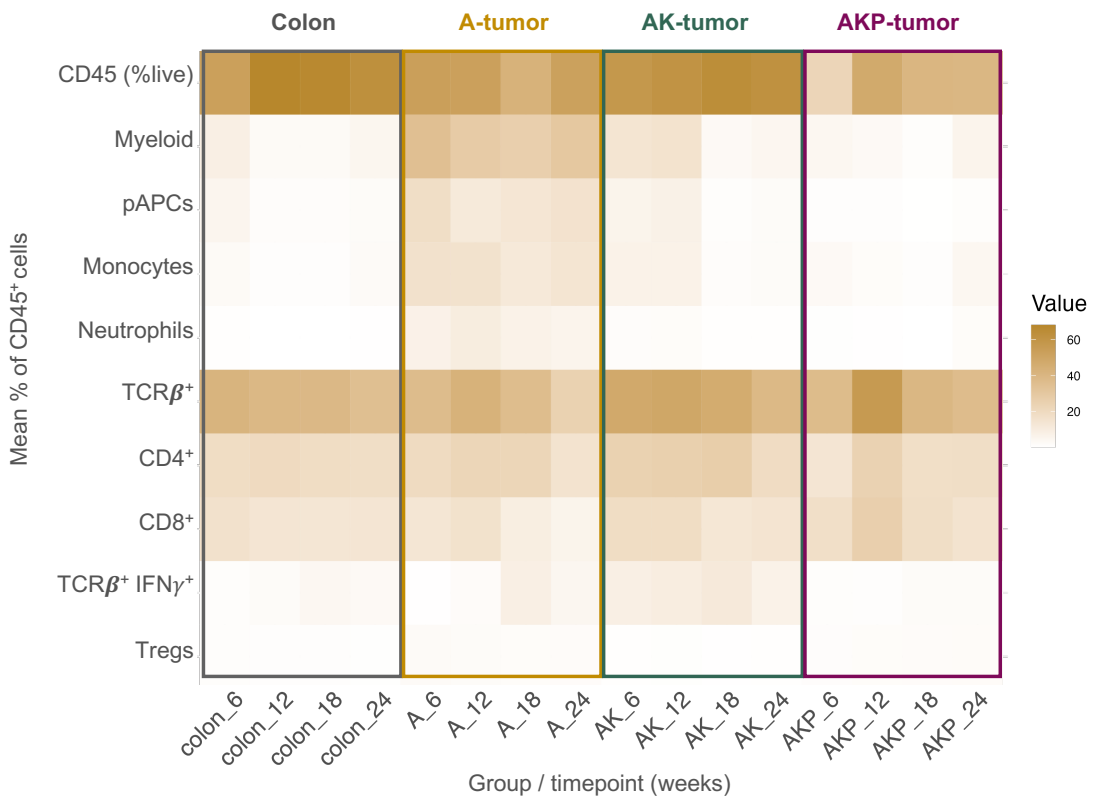

Figure 4.45 Overview of colon, A-, AK- and AKP-tumor microenvironments over time. Heatmap displaying the mean value for each immune subset measured for each group in the experiment. colon_6 is the colon at 6 weeks, A_12 is the A-tumor group at 12 weeks, etc. Data shown includes the following number of mice in each respective group: colon (n=4, 4, 2 and 6), A-mice (n=5, 8, 4 and 6), AK-mice (n=5, 3, 5 and 9), and AKP-mice (n=6, 7, 3, and 6) for timepoints 6-, 12-, 18- and 24-weeks, respectively. Data is from two independent experiments

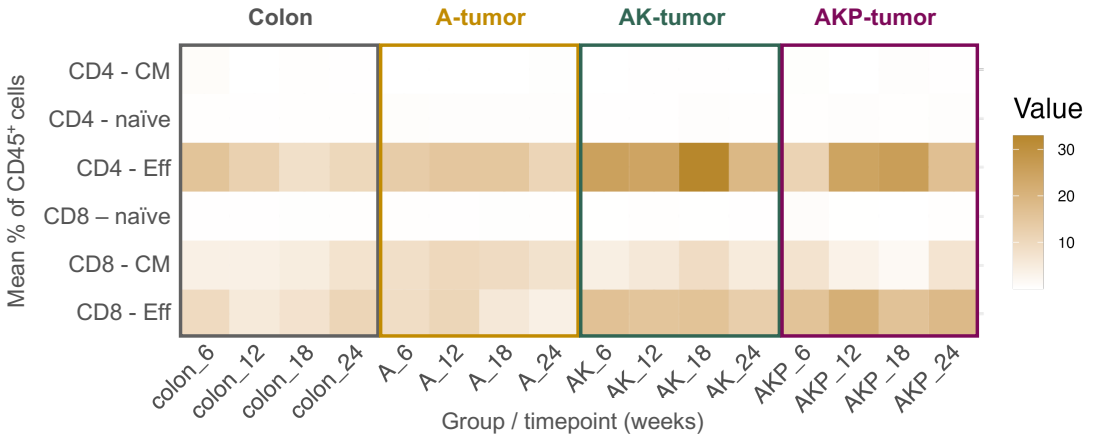

Figure 4.46 Overview of colon, A-, AK- and AKP-tumor-infiltrating naive, central memory and effector T cells. Heatmap displaying the mean value for each immune subset measured for each group in the experiment. colon_6 is the colon at 6 weeks, A_12 is the A-tumor group at 12 weeks, etc. Naive T cells = $CD62L^{+}CD44^{+}$, CM = central memory T cells = $CD62L^{+}CD44^{+}$, and Eff = effector T cells = $CD62L^{-}CD44^{+}$. Data shown includes the following number of mice in each respective group: colon (n=4, 4, 2 and 6), A-mice (n=5, 8, 4 and 6), AK-mice (n=5, 3, 5 and 9), and AKP-mice (n=6, 7, 3, and 6) for timepoints 6-, 12-, 18- and 24-weeks, respectively. Data is from two independent experiments.

4.2.3 Longitudinal single-cell RNA and TCR sequencing in AKP-tumor mice shows clonal expansion of CD8 and CD4 T cells at 6- and 12-weeks post-tamoxifen

As part of our second aim within this longitudinal study which was to define the changes within the TME of A-, AK- and AKP-tumors, we conducted single-cell RNA and TCR sequencing on three AKP-tumor samples from each timepoint in order to identify potential mechanisms that could be driving the immune cell repertoire changes in the TME. The paired single-cell TCR sequencing allows us to identify which TCR each T cell expresses and thus whether any TCRs are preferentially expanded and what types of T cells bear the expanded TCRS. Due to the large number of samples in the experiment, we utilised hashing antibodies (αMHCI and αCD45 antibodies tagged with a DNA barcode) to multiplex the sequencing libraries.

After dead cell, doublet and empty cell filtering, 26,295 cell remained in the experiment for analyis. Unsupervised clustering isolated 10 clusters in the data, Figure 4.47a. Among these clusters, we were able to identify several large clusters. plasmacytoid dendritic cells

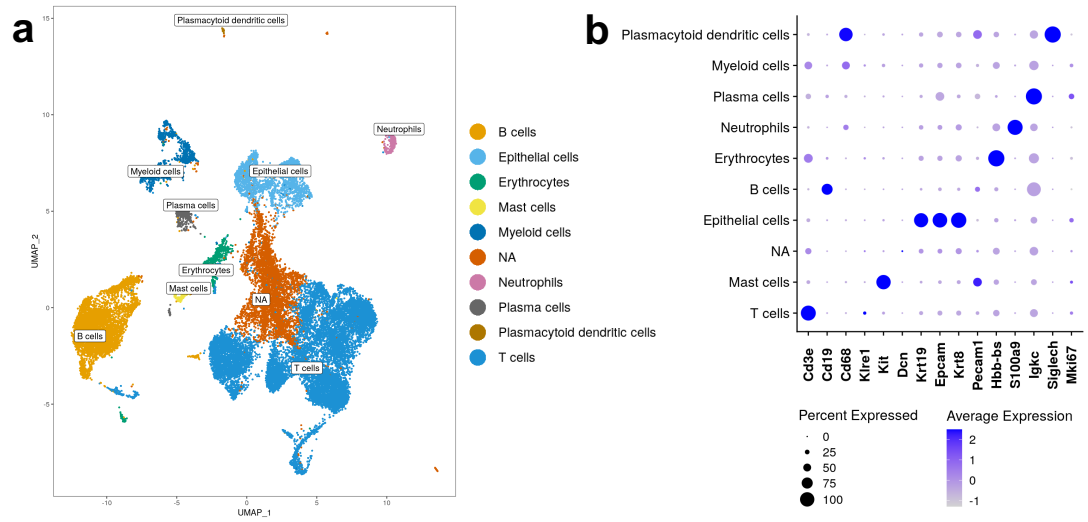

Figure 4.47 UMAP and annotation justification dot plot for AKP-tumors over time. **a.** UMAP dimensional reduction . **b.** dot plots displaying average and percent expression key transcripts used for annotation in each cluster.

(pDCs) were identified by their *Siglech* expression and myeloid cells were annotated based on their *Cd68* expression (but this cluster has a relatively low-depth read, meaning no markers were very highly expressed), Figure 4.47b. Erythrocytes were clearly identifiable by their expression of hemaglobin transcripts like *Hbb-bs*. B cells were distinguishable from plasma cells by their strong *Cd19* expression, while plasma cells universally expressed *Igkc* transcripts, Figure 4.47b. Neutrophils expressed *S100a9* at high levels. Mast cells were distinguished by their *Kit* expression and T cells by their *Cd3* expression, Figure 4.47b. Finally, one quite large cluster was annotated as N/A due to its lack of transcripts that indicate clearly the identity of this population. Quality control had already removed ambient RNA and doublets, and the identity and whether this cluster should remain in the study are still underway.

With extreme interest, we assessed the differential abundance of each main cell type within the TME of the AKP-tumors over time. First, for the healthy colon, it is important to note, that only one sample was sequenced, so the healthy colon cell counts can be compared amongst themselves but not to the tumor samples, Figure 4.48a. Among AKP-tumors, several striking points stand out when we observe the number of cells per cluster at each timepoint.

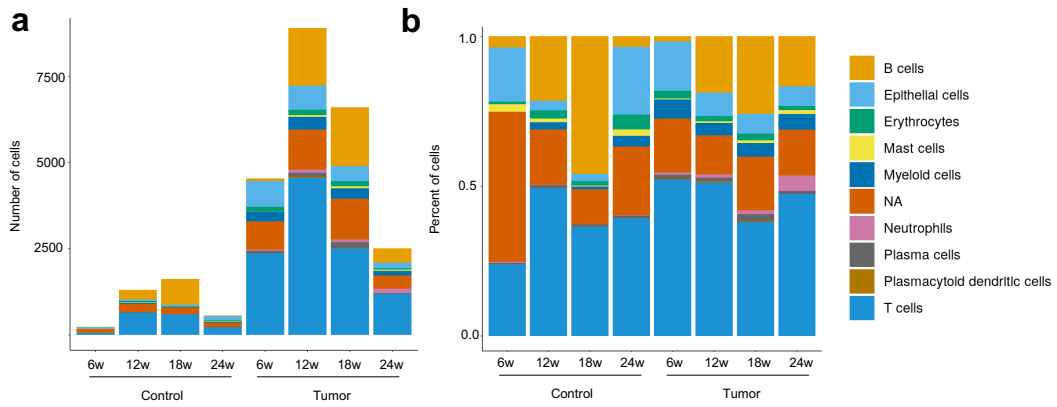

Figure 4.48 T lymphocytes are abundant 12 weeks post-tamoxifen and B lymphocytes accumulate over time in AKP-mice. scRNAseq data of low-dose tamoxifen healthy colon and AKP-tumors **a.** stacked bar plot showing number of cells captured per condition in each cluster, **b.** stacked bar plot showing proportion of cells captured per condition belonging to each cluster.

First, the absolute number of T cells peaks 12-weeks post-tamoxifen induction, confirming our observations by flow cytometry, Figure 4.48a. Second, B cells clearly accumulated in the tumors at the 12- and 18-week post-tamoxifen time point, and were proportionally more present at 24-weeks, Figure 4.48a and b. The myeloid cell population remains small throughout the experiment, confirming our flowcytometry data, Figure 4.48b. Erythrocytes, mast cells, plasma cells, and pDCS are small and not dynamic populations in the experiment, Figure 4.48b. Epithelial cells, of course, expanded within the tumor conditions compared to the healthy controls, Figure 4.48a, but became less abundant over time, Figure 4.48b.

The epithelial, T cell and myeloid clusters were sub-clustered and annotated in a similar manner to those in the "standard-dose" tamoxifen experiments. The TCR sequencing data was then joined together with the scRNAseq data using the common cell barcodes. After TCR mapping, we assessed the proportion of the TCR repertoire that was occupied by clonal populations. The TCR repertoire was composed of uniquely found clones per sample (red; unique, not enriched clones), clones found 2-3 times in that sample (orange; slightly expanded clones), clones found 4-10 times in that sample (green; lightly expanded clones), clones found 11-30 times in that sample (light blue; expanded clones), clones found 31-100 times in that sample (medium blue; more expanded clones), and clones found 101+ times

in that sample (dark blue; heavily expanded clones) clones, Figure 4.49a. Healthy control colons contained more unique clones, indicating a highly varied TCR-repertoire presumably poised for any type of invasion of the system, be it pathogen, virus or tumor, Figure 4.49a. Six-weeks post-tamoxifen induction, heavily expanded TCRs (dark blue) can already be identified within and AKP-tumor sample, indicating that the adaptive immune system has identified a threat and T cells have become educated and expanded, Figure 4.49a. Twelve-weeks post-tamoxifen, even more heavily expanded TCRs occupy the TCR repertoire space, Figure 4.49a. After 18 weeks, however, heavily expanded TCRs can no longer be observed in the TME of AKP tumors, and by 24 weeks the maximum clonotypes of a single TCR is 30, as opposed to more than 100 at 6- and 12-weeks, Figure 4.49a. We then inspected what type of T cells the expanded clones (an expanded clone was defined as being expressed by more than 5 T cells within the same sample) were, Figure 4.49b. The majority of expanded clones were $CD8^+$ cytotoxic T cells, followed by $CD4^+$ helper T cells and Th17 cells, Figure 4.49b. This suggests that the adaptive immune system of the mice initially identifies a threat, expands one or many TCR clonotypes on cytotoxic T cells to counteract the tumors, but, over time the TCR repertoire becomes varied again, Figure 4.49a. This could mean that the immune system changes strategy, producing more and varied TCR clonotypes to attack the tumor or–rather more likely–that the TCRs initially specific for the tumor have done their job and the tumor is now evading anti-tumor immunity either by up-regulating checkpoint molecules, by down-regulating antigen presentation, or that of tumor cells without neoantigens are negatively selected for by the cytotoxic T cells. Whether and which of these strategies is being used by the tumor population remains an interest of the laboratory, and will be explored by Elia Escoffier, a PhD student in the lab.

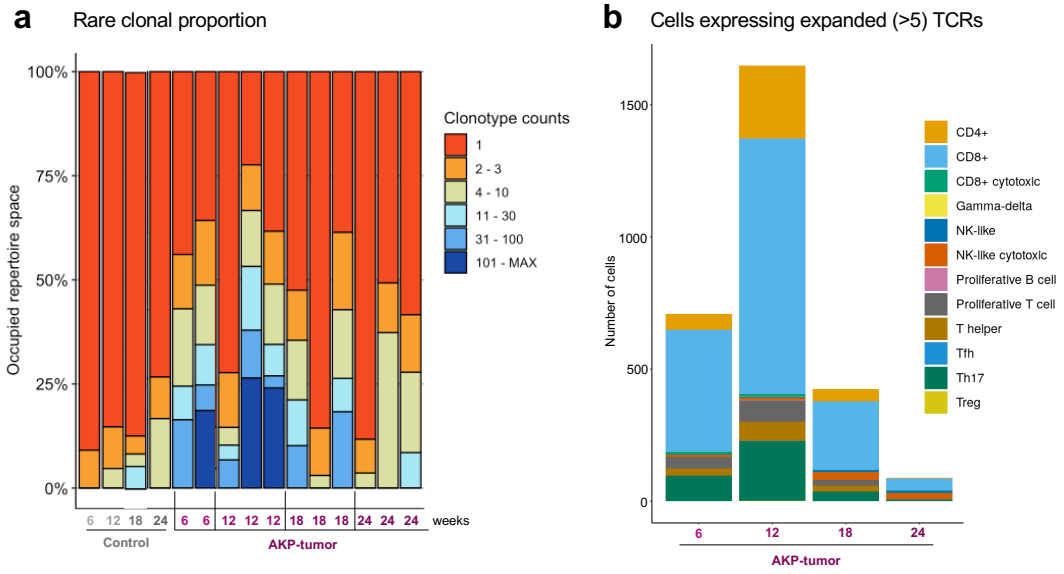

Figure 4.49 Clonal expansion of TCRs is apparent at 6- and 12-weeks post-taomxifen in AKP-tumors. **a.** stacked bar plot showing percent of occupied repertoire space by clones with counts clonotype counts as specified by color. **b.** stacked bar plot showing number of cells captured per condition that contained an expanded TCR ("expanded TCR" was defined here as being counted more than 5 times within the same sample).

4.3 Aim 3: Contribute to the development of a light-inducible colon-on-a-chip tumorigenesis model for colorectal cancer.

The discovery that 3D-culture of intestinal stem cells leads to the formation of organoids has accelerated tumor-cell based research[154]. Organoids can be used for high-throughput screening or to validate various hypotheses on a smaller scale[64,155,156]. Conventional organoid culture, however, cannot be maintained without disruption for more than about one week. To address this problem, Nikolaev *et al.* [157] developed 3D hydrogel scaffold that, when perfused with murine colonic epithelial cells, showed that the cells organise as they do in tissue: stem cells localise to the bottom of the crypt, and more differentiated cells transit toward the top of the crypt. They were further able to maintain the culture for very long time periods *in vitro* thanks to the ability to flush the lumen with fresh media and thus expel waste and dead cells.

Together with the Lutolf group, we initiated a project wherein the goal was to induce

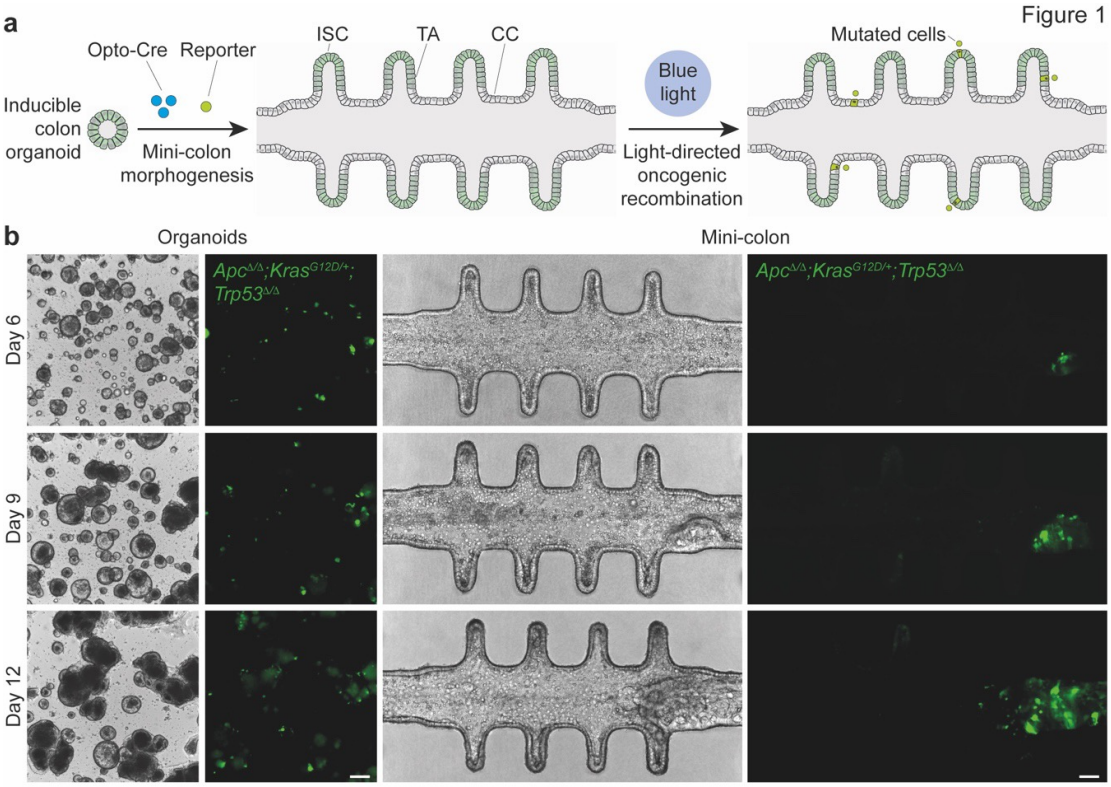

Figure 4.50 Light-mediated recombination of conditional alleles in colon organoids-on-a-chip from AKP-mice leads to spatiotemporally controlled *de novo* tumorigenesis *in vitro*. **a.** Schematic of the experimental workflow used to induce tumorigenesis in mini-colons-on-a-chip. **b.** Brightfield and fluorescence images of time-course tumorigenesis experiments in conventional organoid culture and in colonic chips. Fluorescence signal indicates oncogenic recombination. ISC, intestinal stem cell; TA, transit-amplifying cell; CC, coloncyte. This data was produced by L. Francisco-Lorenzo Martin and Tania Hubscher.

spatial-temporally controlled tumorigenesis within these chips, which could enable the monitoring of tumor evolution over time as well as the early events of tumor formation. We generated organoids from A-, AK- and AKP-mice without the *Cdx2*-CreERT2 transgene. They then engineered the organoids to express a light-inducible Cre which would allow us to shine a light on restricted regions of the colon chip to initiate the recombination of our conditional alleles, Figure 4.50a. Indeed, light-induced Cre was efficient in the colon chip as well as in organoid culture, as indicated by the GFP expression from a Cre-reporter vector, Figure 4.50b. Tumor-like formations were observable in the colonic chips following blue light exposure that grew over time and eventually blocked the outlet of the chip, Figure 4.50b. The question then arose as to whether these growths were indeed cancer.

We therefore recovered the recombined cells (GFP^+) cells from the chip for brief conventional culture of the organoids in order to expand them. The organoids were then transplanted sub-cutaneously into immunodeficient NSG mice, Figure 4.51a. We included tumor organoids derived from AKP-tumors as a positive control for tumor growth. The growth of the tumors was followed over 20 days, and we saw that both groups indeed grew rapidly, a common trait of cancer cells, Figure 4.51b. Following euthanasia, we again measured the tumor volume and found that there was no significant difference between the growth of AKP-tumor-derived s.c. tumors and our chip organoids 4.51d and e. Taken together, this project represents a novel contribution to the field of colorectal cancer research enabling the maintenance of CRC organoids long-term in a microfluidic chip.

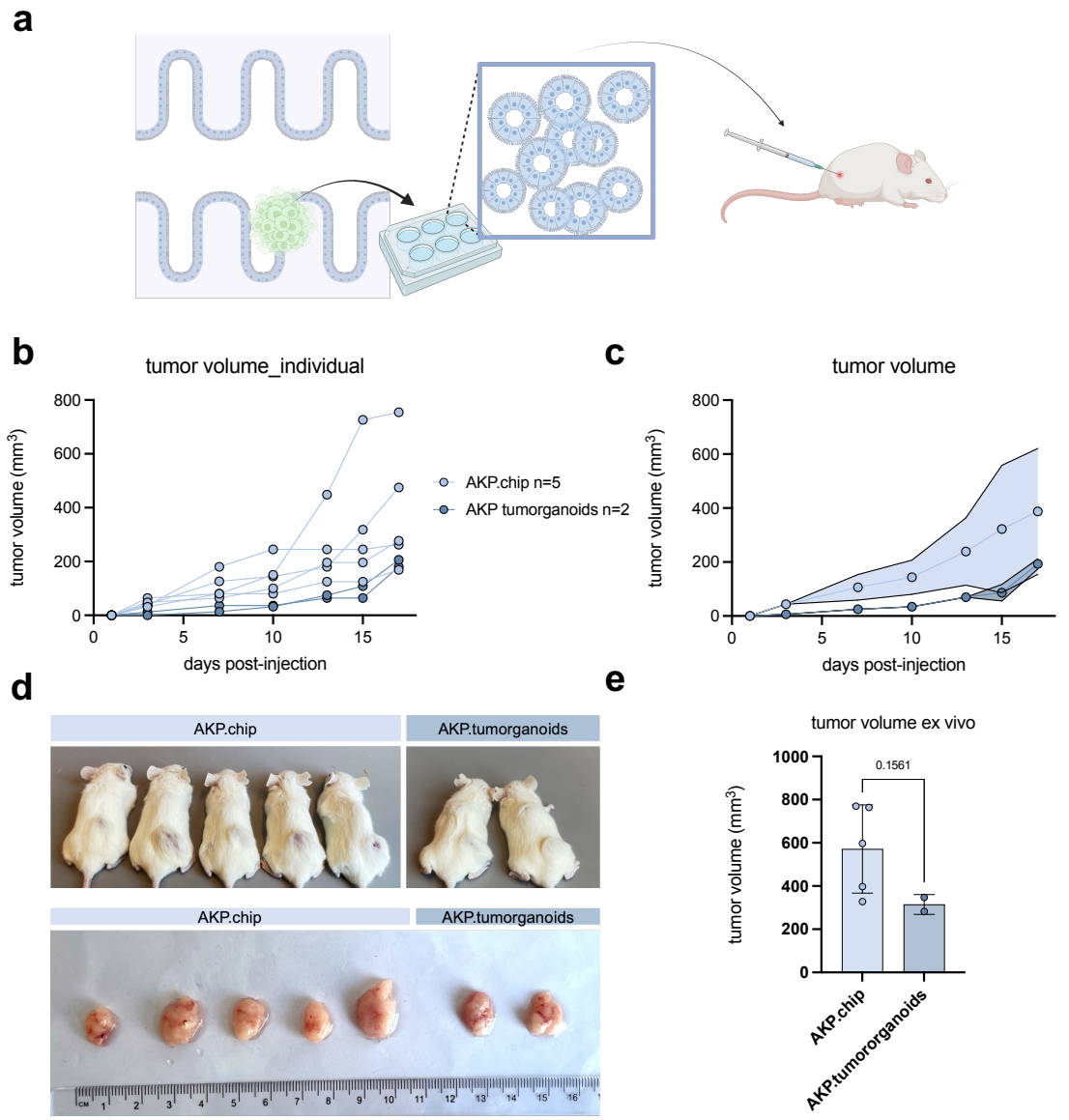

Figure 4.51 Organoids recombined by light-inducible Cre are cancer cells. **a.** Schematic of the experimental workflow used to determine whether cells recombined in the mini colon chip were indeed tumor cells. Recombined cells from the chip were cultured as conventional organoids and then transplanted sub-cutaneously into NSG mice. **b.** Tumor volume growth curves of AKP.chip organoids and AKP-tumor-derived organoids. **c.** Grouped tumor volume growth curves of AKP.chip organoids and AKP-tumor-derived organoids. **c.** (top) Image of sub-cutaneous AKP.chip and AKP.tumorganoid tumors in NSG mice, (bottom) sub-cutaneous AKP.chip and AKP.tumorganoid tumors after dissection. **e.** Tumor volume measured after dissection of AKP.chip and AKP.tumorganoid sub-cutaneous tumors. Student's T-Test. AKP.chip, organoids recombined in the colonic chip; AKP.tumorganoids, AKP organoids derived from tumor-bearing mice.

5 Conclusion and discussion

5.1 Aim 1: A-, AK- and AKP- mice have distinct tumor microenvironments that correlate with immunotherapy response

Colorectal cancer patients with advanced-stage disease at diagnosis have poor prognoses. Tumor T cell infiltration, however, is associated with favorable treatment outcomes. In a first step towards understanding the relationship between tumor immune infiltration and the oncogene composition of tumors, we characterised the tumor microenvironment of three colorectal cancer mouse models with different driver mutations using multiple modalities.

5.1.1 T cells are more prominent in Kras-mutant tumors

We found that the TME of A-, AK- and AKP-tumors were distinct from one another in terms of the composition of the infiltrating immune cells. A-tumors were characterised by high-level myeloid cell infiltration. Tumors bearing constitutive Kras contained significantly more T cells in the TME compared to tumors without this mutant protein. Explicitly, 50-60% of tumor infiltrating immune cells were T cells in AK- and AKP-tumors, while A-tumors contained only 20-30% T cells. There was, however, a prominent variation in the proportion of $CD45^+$ tumor-infiltrating immune cells, as measured by flow cytometry especially among AKP tumors.

There are two possible sources of this spread of observed values.

The first possibility is simply biological variation. Arbitrary biopsies of tumor were selected for digestion to single cells followed by flow cytometric analysis. When H&E sections are inspected, different regions of the tumor are indeed variably infiltrated with immune cells. The extreme flow cytometric values of very high and very low immune cell infiltration, however, are difficult to account for in this way given that the samples were a pool of biopsies from various tumor regions in the same mouse. A second potential source of the variation could be derived from stress imposed during tumor dissociation to single-cells. It could be that disproportionate numbers of tumor cells die in the process of enzyme and mechanical dissociation, potentially contributing to the observed variation in immune cell proportion by flow cytometry. The fact remains, however, that all tissue samples were subject to the same conditions and thus comparisons within the experiment are valid. These potential limitations confine the interpretation of the flow cytometry data to the relative composition of the tumor immune microenvironment, as presented herein. In the future, a more refined approach to the flow cytometric analysis of these tumors can be employed that involves sampling of a known weight of tumor, flow cytometric acquisition, and normalisation of number of cells to milligram of tumor. This method might reduce the observed variation in the data and allow for measurement of the number (rather than relative number) of immune cells within each tumor. Taken together with the IHC and scRNAseq data, however, we can remain confident in the observed phenotype of greater T cell presence within AK- and AKP-tumors (Kras-mutant tumors) compared to A-tumors.

By IHC we observed the same trend that was observed by flow cytometry: T cells were more abundant in AK- and AKP-tumors compared to A-tumors. Furthermore, the T cells were spatially excluded from A-tumors, while T cells in AK- and AKP-tumors were spatially intermingled with malignant cells. Finally, scRNAseq identified a greater proportion of the immune cell repertoire to be occupied by T cells in AK- and AKP-tumors when compared to A-tumors. By number, however, the difference between number of T cells infiltrating in the tumor is less pronounced, but the trend remains. Taken together, this data suggests that the

tumor-driver mutational composition may indeed influence the the recruitment or exclusion of TME elements such as immune cells.

Our findings with regard to the association of KRAS with T cell infiltration, however, stand in contrast to the findings of several studies. For example, Liu *et al.* [158] showed early this year that intratumoral $CD8^+$ T cells are significantly more dense in human colorectal tumors expressing wild-type KRAS. They also observed more numerous $CD8^+$ T cells in a mouse model of colorectal cancer bearing WT Kras compared to mutant-Kras[158]. The mouse model employed for this study was the *Villin*-CreERT2 mouse with conditional alleles for *Kras* and *Apc* wherein tumor formation was initiated with a 4-OH Tamoxifen enema. The discrepancy between our findings and those in Liu *et al.* [158] can therefore potentially be accounted for in two ways: the Cre expression was driven by a different promoter (Villin and Cdx2 are active in different cells in the mouse gut) and that the tumor was localised in the rectum rather than the proximal colon (the microbiota may vary significantly between different sections of the colon[159]). Furthermore, Luo *et al.* [160] defined a KRAS gene signature that was associated with low $CD4^+$ T cell subset infiltration, a phenomenon also identified in other studies[161,162]. On the other hand, Liu *et al.* [161] showed that while tumors expressing mutant KRAS had significantly fewer $CD4^+$ T cells, they also found fewer neutrophils, a phenotype we observed in our AK- and AKP-tumors. Further effects of the KRAS mutation have been shown to impose an immune suppressive TME by contributing to the recruitment or polarisation of pro-tumor macrophages or myeloid derived suppressor cells[128,163], in contrast to our findings.

Potential sources of the discrepancy between the results presented herein and conflicting studies referenced above are numerous, and mainly inherent to the use of engineered mouse models to model human disease. For example, in the compound mutation GEMMs used in the present study, the oncogenic alleles are induced simultaneously upon tamoxifen-mediated Cre recombinase activation, while in humans such somatic mutations accumulate over years. The abrupt, simultaneous activation of multiple oncogenes in the mouse models could induce numerous alterations within the cell that may dramatically differ from those that occur during the rather insidious and step-wise process of tumorigenesis in the human

colon. Explicitly, oncogene-induced senescence has been associated with RAS and RAF activating mutations[164], and some studies outline an interplay between RAS and P53[164,165] in the induction of senescence. In GEMMs, AK-epithelial cells might incur constitutive Wnt and Mapk activation simultaneously, increasing the likelihood of induction of senescence. The senescence-associated secretory phenotype (SASP) has been documented in a number of malignancies including CRC and involves the secretion of several soluble factors such as cytokines by the senescent cell[166,167]. Therefore, a potential source of the discrepancy between the results in this work and the work of others could be explained by the simultaneous induction of oncogenes which induce senescence and SASP which could profoundly impact the composition of the TME.

Another potential source of the divergence in findings from the current study and others is that the tumors of the GEMMs may be composed of a mosaic of single, double or triple mutant cells. Upon tamoxifen-mediated Cre-recombinase activation, the enzyme is liberated to enter the nucleus and excise DNA between two LoxP sequences. The possibility that the Cre targets one or two alleles instead of all conditional alleles cannot be excluded. That is to say that, in an AKP-mouse, for example, the tumor cells could be composed of a variety of cancer cells bearing one of 8 (2 possible states [on/off] of 3 conditional alleles, 2^3) configurations of tumor-driving mutations. In fact, our analysis of the relative frequency of recombination of targeted alleles using scRNAseq data showed a tendency for the recombination of both *Apc* and *Kras* alleles to be potentially less frequent as the mouse model gains conditional alleles. Unfortunately, however, because the depth of scRNAseq is quite low (75k reads/cell, approximately 4 reads per gene per cell), there are many cells without reads that allow for conclusive calling of the mutational status of the target alleles. Therefore, it remains to be shown what proportions of an AKP-tumor are actually composed of other combinations of the targeted alleles in addition to the targeted "AKP" composition. Nevertheless, due to the low frequency of recombination for each allele approximated herein, the possibility that compound mutant tumors may be an amalgam of cells bearing up to eight potential iterations of the oncogenic or WT targeted alleles remains a real limitation of the model.

In order to confirm the spatial distribution of each variant allele, one could, for example, perform FISH using RNA probes for the mutant and wildtype alleles on histological sections of the tumors[168]. It could be equally informative to collect single-cell WES data on the epithelial cells of A-, AK- and AKP-tumors. In this way, one would be able to determine the clonality of each genotype among tumor cells. Alternatively, the use of a different mouse model could provide a more homogenous tumor for this type of study. Orthotopic transplantation of tumor organoids into the submucosae of the cecum[67–69,169] offers the possibility to select for organoid cultures with specific mutations using culture conditions[84]. Selected organoids can be subsequently transplanted into an immune-competent setting for downstream experimentation. In the context of the current study, one could select for A- AK- and AKP-tumor organoids, graft them into the cecum and assess the immune compartment of the tumor to validate whether the findings presented here remain true when tumors are clonal as opposed to a patchwork of cells with variable driver mutations.

In the same vein, we found that our tumors bare variant alleles at a relatively low frequency between 15-30% of epithelial cells for *Apc* and *Kras* (and *much* less frequent for *Trp53*, Figures 4.2d, 4.3d and 4.4c). Human colorectal carcinomas, however, demonstrate that once a mutation is acquired, it likely confers a selective advantage and the oncogenic allele becomes clonal, Figure 4.6b. These findings highlight again the fact that the mouse models employed in this work contain tumors which are likely mosaics of the engineered alleles in the mouse. This raises the question as to what should be referred to as an "A-, AK- or AKP-tumor." In order to address this question, we must examine the human data to determine an appropriate variant allele frequency that could define a threshold for tumor mutation calling.

The TCGA samples multiple areas of the same tumor for the collection of material for analysis, but each biopsy is designanted to a single analysis modality, i.e., one sample for WES, one for whole genome sequencing (WGS), etc. We therefore searched the literature for data that studied mutations at the tissue level which would indicate whether or not mutations are indeed spatially clonal as indicated by the TCGA WES data. One study conducted

slide-DNA-seq on a tissue micro-array punch from a single human CRC sample[170], but exploring this data for tumor-driving mutations may not give adequate information on the variability of tumor-driving mutations across the entire tumor. On the other hand, one group based in London took four biopsies from "north", "south", "east" and "west pole" regions of multiple human adenocarcinomas and conducted RNA-seq, assay for transposase-accessible chromatin sequencing (ATAC-seq) and WGS on each sample[171]. That study identified that the majority of tumors bearing each tumor-driving mutation (*APC, KRAS* and *TP53*) contained the mutation in all four biopsied regions (by WGS), underscoring the fact that human CRC adenocarcinomas are largely clonal[171]. This would indicate that the threshold that should be applied in mouse models of colorectal cancer should be quite stringent, as in greater than about 80% mutant-bearing cells, when attempting to model carcinomas.

In a sister study, the same group based in London used BaseScope[168], a commercially available RNA *in situ* hybridisation detection technique for mutant and WT *KRAS* on histological sections of the CRC tumors largely found that *KRAS* point mutations are clonal[172]. One tumor in the cohort of adenocarcinomas, however, was heterogenous and displayed spatially distinct regions bearing mutant or WT *KRAS*[172]. This indicates that, though clonality of mutations is a general rule, there can be exceptions. Intriguingly, the group also studied CRC adenomas that contained foci of carcinoma ("Ca-in-ad") using the same methodology and found multiple samples in which *KRAS* mutations were present at a sub-clonal frequency of 3-95% of the total tumor[168]. This study also found that in two out of three tumors examined (for this particular parameter), *KRAS* mutant regions were found to contain significantly more $CD8^+$ T cells than WT *KRAS* regions. This finding represents one study that aligns with the results of our study, and thus could be indicative for the human context in which our findings are implicated. Namely, our research and Baker *et al.* [168] both show greater T cell presence in adenomatous tumors with sub-clonal KRAS mutations. The findings herein may therefore be informative in the early stages of oncogenic transformation in which tumors bear sub-clonal levels of oncogenic drivers. This raises the question of why the T cells may not be sufficient to combat tumor progression.

The actual function of tumor-infiltrating T cells in the tumor microenvironment of our mouse models remains largely unknown. In an attempt to understand what their role could be, we previously performed antibody-mediated (αCD4 and αCD8) T cell depletion in AK- and AKP-mice. Though the antibodies were efficient in the elimination of T cells in the peripheral blood, the antibodies were incapable of depleting the tumor-residing T cells[I]. We were therefore unable to determine whether the tumor-infiltrating T cells played a pro- or anti-tumor role. One alternative way to answer this question could be with the use of the mouse models expressing the diphtheria toxin receptors under the control of a T cell-specific promoter, therefore enabling their death upon administration of diphtheria toxin administrations[173–175]. Alternately, a T cell receptor knockout mouse could also be considered for this purpose, which results in mice without mature TCR$\alpha\beta$ T cells[176]. Both of these options would require crossing with our AKP-mice, which are prohibitively time-consuming.

Though the direct influence of KRAS on tumor immune cell infiltration is a rather new area of focus, the data within human CRC is mounting that indicates that greater T cell infiltration is more prominent in tumors bearing wild-type KRAS and not mutant KRAS. This is in contrast to what we have found in our mouse models, potentially largely due to the mouse models' tumors being composed of mutations at likely sub-clonal frequency (though this remains to be shown), leading to the formation of a tumor composed of a mosaic of tumor-driving mutations. Regardless of these facts, our GEMMs of CRC represent an opportunity to define how elevated Mapk signaling (ostensibly due to *Kras* mutations) drives T cell infiltration into these adenomas due to the clear significant increase in pERK[II] and T cells in AK- and AKP-tumors compared to A-tumors. Though our data is quite definitive – flow cytometry, scRNAseq and IHC all agree and significantly correlate with each other– one final experiment could truly define whether it is the Kras/Erk module that drives the observed flux of T cells into the TME: treatment of AK- and AKP-mice with trametinib, a MEK inhibitor that acts upstream

[I] In our experience in the lab, it is possible to deplete T cells in the colon tumors for up to one week after tamoxifen induction, the antibodies are not able to effectively deplete the T cells in the tumor after this time

[II] This is the appropriate measurement of Mapk signaling in fixed tissue, but may not represent all areas of Kras-activation due to the inherent oscillatory nature of Erk signaling[177–179]

of ERK[III]. As a final note, there are several immunotherapeutic trials that aim to combine immunotherapy with MAPK inhibition using trametinib, so we may be able to observe what the consequence of abrogated MAPK signaling is on immunotherapy response in the coming years[181].

5.1.2 αCTLA4 and αCD40 immunotherapies are mildly effective in MMRp tumors with elevated T cell infiltration

scRNAseq and IHC of A-, AK- and AKP-tumors showed that the dominant checkpoint molecule expressed on tumor-infiltrating T cells in our mouse model was CTLA4, and not PD1. Interestingly, two studies reported the up-regulation of checkpoint blockade transcripts (including PD1, PDL1, CD40, CD40L and CTLA4) within the TME of mutant KRAS tumors[162,182]. αPD1 monoclonal antibodies are used much more frequently in the clinic due to its efficacy and relative tolerability[36]. αCTLA4 monoclonal antibodies, however, are less frequently employed due to the more frequent occurrence of immune related adverse events in clinical trials[36]. Furthermore, checkpoint blockade therapies are typically indicated for patients with MMRd – a small portion of the total patient population[41].

Within our models, when we administered αCTLA4 or αCD40 (but not the combination of the two) therapy in A-, AK- and AKP-mice, we were able to observe a minor anti-tumor effect in tumors that we had previously observed to be infiltrated with T cells (ie AK- and AKP-tumors, but not A-tumors). Though the mouse models responded well to the therapy, this was not necessarily expected as the mouse models are not MMRd. The fact that A-tumors did not respond to αCTLA4 or αCD40 monotherapy and AK- and AKP-tumors did mimic the correlation observed in humans: greater T cell infiltration is associated with favorable treatment outcomes[7]. Whether the efficiency of the treatment was due to the presence of the T cells or the absence of myeloid-derived suppressor cells (for example) was not tested. We were also able to observe that, within tumors that responded to the therapy, there were fewer pAPCs in the TME. The tumor-draining lymph nodes need be assessed for signs of T

[III]This should also be performed with an EGFR inhibitor in combination with the MEK inhibitor[177,180]

cell education, like the loss of Cd62l or the gain of Cd44 expression on T cells, for example.

5.1.3 Anxa1 is associated with tumor T cell infiltration in CRC GEMMS and *ANXA1* is associated with immune infiltration in human colorectal cancer

By carefully identifying and isolating the tumor cell populations in the scRNAseq of A-, AK-, and AKP-mice, we were able to validate that the expected signaling pathways (namely KRAS and P53) were indeed perturbed as expected when we compared the mutant tumors. Furthermore, we were then able to perform DGE with these populations to produce a list of candidates that were differentially expressed in the cells that bore the mutant proteins. The top candidate in our data was Anxa1. We confirmed that Anxa1 was indeed differentially expressed by AK- and AKP-tumors compared to A-tumors on the protein level with IHC. We were further able to observe that Anxa1 was expressed by immune cells in all 3 models, but importantly Anxa1 was expressed highly on malignant cells in AK- and AKP-tumors but not expressed by A-tumor cells. The potential mechanistic connection of mutant Kras and the expression of Anxa1 is suspected to be through the activation of Erk by the Mapk pathway, leading to Fos-, Myc- or Stat3-mediated transcription of the Anxa1 gene, Figure 5.1, points 1-3. Importantly, STAT3 has been shown to be upregulated in mutant KRAS tumors compared to wildtype in a small study of human colorectal cancer[182]. Within our hypothesis, cytoplasmic Anxa1 can then be phosphorylated by protein kinase c[183], enabling its transit to the membrane where it can inhibit phospholipase A2's synthesis of arachadonic acid by sequestering its substrates[76,77], Figure 5.1, points 4 and 5.

In the literature, the link between Anxa1 and calcium signaling is inextricable. Though phosphorylation induces Anxa1 to locate to the membrane, its phospholipase A2 inhibitory function of binding membrane phospholipids is calcium-dependent[143,184,185]. We therefore propose that the Kras activation is additionally activating phospholipase c and its liberation DAG that induces calcium efflux from the endoplasmic reticulum, a well-known function of Ras proteins[186,187], Figure 5.1 point 6. The elevated intracellular calcium levels are likely to be

supporting the Anxa1's anti-phospholipase A2 activity. Finally, Anxa1 is known to be secreted by ABCA1, which could be the mechanism by which the excess Anxa1 in Kras-mutant cells is entering the tumor microenvironment to affect immune cells, Figure 5.1 point 7[183].

Finally, our approach to identifying potential drivers of T cell infiltration in AK- and AKP-tumors is biased toward cancer-cell intrinsic changes having an immediate effect on the surrounding cells. We searched specifically for known ligands that were specifically produced by tumor cells . In reality, non-secreted factors or protein currently not know to be active ligands could be causing the phenotype. Furthermore, the tumor cells could produce other elements in the tumor microenvironment that drive secondary cells to express an element that is truly responsible for the observed phenotype.

In the human context, we showed that an ANXA1 expression divided into high and low expression was able to identify a cluster of colorectal cancer patients with elevated immune cell infiltration in their tumors. In the context of other studies, ANXA1 has been observed to be differentially expressed in a subset of cancer patient epithelial cells associated with elevated MAPK signaling (iCMS3), and a subset of those patients appear to be associated with immune cell infiltration[188]. Interestingly, the data in this study implicate IL1B in the induction of ANXA1 expression. The subset of patients, however, was clearly shown in the study to be associated with reduced progression-free survival and overall survival[188]. This study confirms that ANXA1 is associated with greater MAPK activity in colorectal cancer, a finding that was also reported in Su *et al.* [189]. The study of the iCMS3 patient subset further confirms that ANXA1 is affiliated with increased immune cell infiltration in colorectal tumors[188]. What is surprising, however, is the worse overall survival in these patients. This could indicate that ANXA1 could also play a pro-tumor role in colorectal cancer in addition to promoting immune cell presence in the TME.

The role of ANXA1 expression on tumor progression has yet to be well-defined as conflicting reports have been released on the influence of ANXA1 presence or absence. As more studies accumulate it has been observed that in general ANXA1 expression is

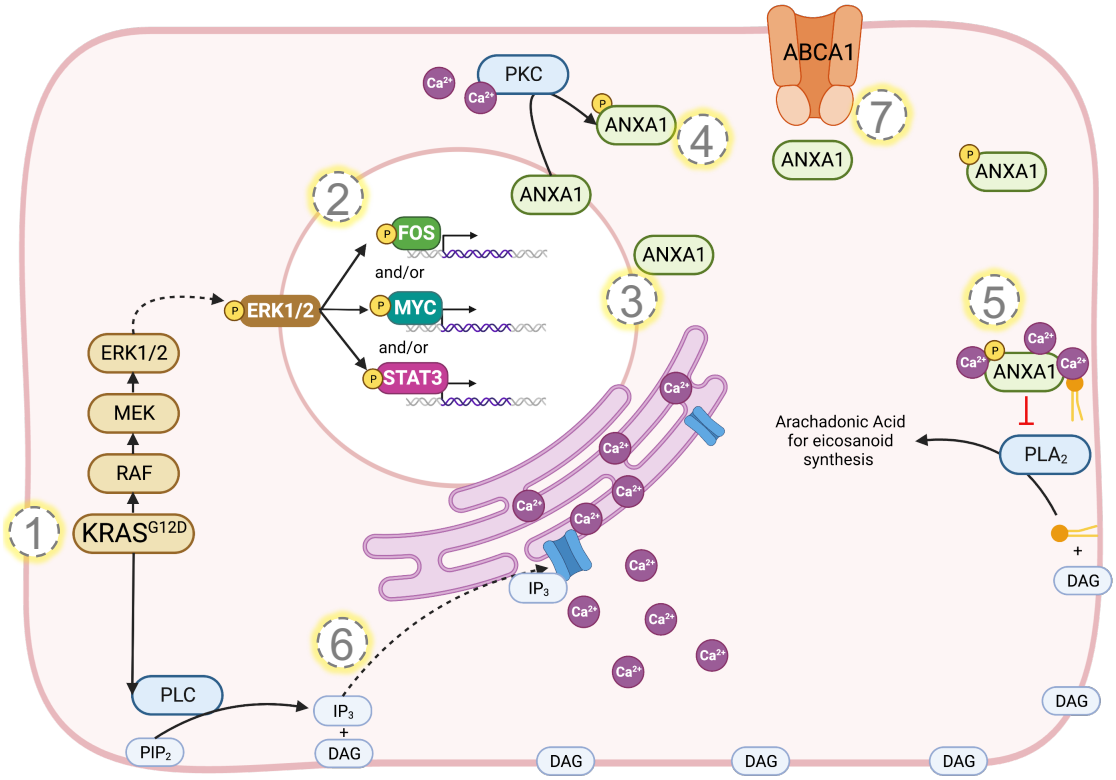

Figure 5.1 Hypothetical mechanism of Kras-mediated induction of Anxa1 expression and the function of Anxa1 in the cell. We hypothesize that oncogenic Kras could be inducing Anxa1 expression by the activation of Fos, Myc or Stat3 transcription factors downstream of Erk. Kras could also induce elevated intracellular calcium levels, which supports the inhibitory role of Anxa1 against phospholipase A2.

lost in head and neck cancers, while it tends to be augmented in gut cancer, lung caner, and breast cancers. The role of ANXA1 in cancer progression is emerging as tissue and stage-specific[190] and has been most thoroughly investigated in the context of breast cancer. Specifically, evidence that Anxa1 plays a roll in collaboration with Yes-associated protein 1 (Yap1) in DNA damage response was documented in Swa *et al.* [191] in mammary epithelial cells. This study, however, also showed increased propensity for migration and adhesion in Anxa1$^{+/-}$ compared to Anxa1$^{-/-}$ cells, which the authors postulate is indicative of greater propensity to oncogenic transformation. An elegant study determined a pro-proliferative role of ANXA1 in human breast cancer cell lines by assessing the effect of siRNA-mediated ANXA1 knock down and synthetic ANXA1 peptides on proliferation[192]. Finally, Anxa1 has been implicated in metastasis in a number of associative studies as it appears to increase migration and invasion capabilities of transformed breast cancer cells[193–196]. Conversely, some notable studies robustly show an anti-metastatic role for ANXA1, and thus make it difficult to assign a definitive general role for the protein in tumor growth, invasion, and proliferation[197–199].

As for the role of ANXA1 in disease progression of colorectal cancer, further research is needed to confirm existing studies and to define mechanisms. For example, a small study in benign gastrointestinal tissues indicate an anti-proliferative role of ANXA1 in these tissues[200]. On the other hand, several studies show that up-regulated ANXA1 expression in human gastrointestinal cancers is associated with greater invasion and metastasis[201–203], but these associations are greater in gastric cancer than they are in CRC. Early this year a study showed that augmented ANXA1 expression has a negative correlation with survival in human CRC[204]. Finally, ANXA1 expression is significantly higher in the CMS1 and CMS4 patient subsets compared to CMS2 and CMS3[135], which suggests that ANXA1 may negatively impact survival since these groups are associated with worse survival after relapse and overall survival, respectively[135,205]. The contrast between the implications of these studies highlights once again the likelihood that the role of ANXA1 may be tissue and stage-specific, but it seems that the majority of studies have found a pro-tumor progression role for ANXA1

in human gastrointestinal cancers[188,200–204].

In vivo and *in vitro* studies offer the opportunity to determine a mechanism of action for ANXA1's contribution to tumor progression or regression in various malignancies. One notable study found that ANXA1 drove degradation of EPHA2, contributing to reduced tumor growth of human CRC cell lines *in vitro* and *in vivo*[206]. A similar (but perhaps less detailed) study found that an ANXA1 peptide inhibited growth of human CRC cell lines[207], suggesting again an anti-proliferative role of ANXA1 in CRC. Genetic knock-down studies in human CRC cell lines showed an increase in stem-cell markers, also indicating an anti-tumor role for ANXA1 in CRC[208]. An additional study showed that tumors derived from AKP organoids with bolstered Anxa1 expression grew at the same rate as control, suggesting that Anxa1 does not stimulate tumor growth in this context[135]. The same study also showed that a genetic model with elevated Anxa1 expression moderately reduced tumor burden as measured by tumor weight and decreased stem cell numbers[135]. On the other hand, other studies of this style convincingly reported a pro-tumor role for ANXA1 by demonstrating its contribution to chemotherapy resistance and proliferation in colorectal cancer[204,209]. Thus, the role of ANXA1 in colorectal cancer progression and proliferation cannot yet be definitively defined as similar studies have reported divergent findings.

Though the definition of the role of ANXA1 in tumor growth remains disputed, a pattern may emerge when we consider which models are used to in the studies. In human disease, for example, ANXA1 is associated with worse outcomes[188,204] while studies in human cell lines of CRC define an anti-tumor role for the protein[206–208]. Murine organoid xenografts showed that its role is rather neutral, and finally, a genetic mouse model shows an anti-tumor role[135]. Thus, we can observe that human cell lines *in vitro* and *in vivo* (xenografts into immune-compromised mice) point to an anti-tumor role for ANXA1. Studies employing murine models including tumor organoids and immune-competent GEMMs echo the rather anti-tumor role of ANXA1. Therefore, there is a stark contrast between the implications of human survival data, human cell line experiments and murine models, which may indicate that existing *in vivo* and *in vitro* models of CRC are insufficient to study the role of ANXA1 on tumor progression.

The dichotomy of implications for ANXA1 defined by these various methodologies might be explained by the highly complex and context-specific niche of the tumor, which includes (but is not limited to) the vasculature, microbiome, immune cell infiltrates, soluble factors, extra-cellular matrix, and systemic context. Ultimately, however, because the human data implicate a negative correlation between ANXA1 expression and survival, it is more likely that ANXA1 plays a pro-tumor role in the disease, but this needs to be explicitly investigated.

Mechanisms of ANXA1 expression regulation have been defined in the physiological context of some cell types and in the context of colorectal cancer. The contrast between these studies highlights once again the likelihood that the role of ANXA1 may be tissue and stage-specific[70]. In humans, the most potent glucocorticoid is cortisol, which is released from the adrenal glands in a diurnal manner in accordance with the circadian rhythm[210–212]. Cortisol contributes the metabolic, cardiovascular, immunologic and homeostatic functions in the the human body[210,212]. Once inside the cell, glucocorticoids bind the glucocorticoid receptor (GR) (and displace molecular chaperones such as HSP90), which induces transcription of several genes including *ANXA1* by trans-activation. Target genes and the consequences of the pathways in which they act, of course, vary between cell types. Synthetic sources of glucocorticoids such as dexamethasone induce the expression of *ANXA1* as well, but the effects differ somewhat from the effects of endogenous cortisol, indicating multiple potential targets of GR trans-activation.

In colorectal cancer, it has been reported that the transcription factor PROX1 may suppress the expression of ANXA1, shown first by mutually exclusive immunohistochemical stainings for ANXA1 and PROX1 in both human and murine colorectal cancer tumors and corroborated by functional knockdown experiments[208]. Interestingly, the same study showed that *ANXA1* knockdown with shRNA in a PROX1-low cell line conferred greater tumor growth *in vivo*[208]. A similar study confirmed that when *Prox1* was deleted in the tumor, *Anxa1* expression was augmented, but organoids engineered to over-express ANXA1 in the same study did not grow faster nor larger than control[135]. Taken together, these two studies suggest that the expression of ANXA1 may be negatively regulated by PROX1 in colorectal cancer.

Given the highly complex nature of gene expression regulation, however, further studies that investigate the regulation of ANXA1 expression in colorectal cancer on the epigenetic, transcriptional and non-genetic levels could inform whether the expression of ANXA1 is induced downstream of constitutive KRAS, as suggested in this work.

In summary, more research is required to define the role that Annexin A1 plays in colorectal cancer disease progression, as current studies are conflicting. Next, the role that ANXA1 plays in inflammation in colorectal cancer has yet to be investigated. Furthermore, how ANXA1 is regulated in colorectal cancer has been partially defined (there is convincing evidence that PROX1 inhibits ANXA1 expression[135,208]), but how ANXA1 expression is induced remains to be show. There is, however, accumulating evidence–including the data presented herein–that ANXA1 expression is differentially up-regulated in colorectal cancer with elevated MAPK signaling[188,189,213]. This indicates that ANXA1 expression may be induced by MAPK signalling, and thus, potentially by constitutive KRAS in CRC, but this remains to be empirically shown in follow-up experiments.

5.2 Aim 2: Assess the temporal impact on the TME of accumulating tumor-driver mutations in CRC mouse models

A major limitation of mouse models of colorectal cancer is that metastatic disease is very difficult to model in an immune-competent setting. We hypothesized that a low-dose of tamoxifen would allow A-, AK- and AKP-mice to develop discreet tumors, allow them to live longer and thus allow the tumor to progress beyond the adenoma stage.

5.2.1 Low-dose tamoxifen in CRC GEMMs increases the penetrance of invasive disease and produces rare metastases in an immune-competent setting

We showed that indeed administration of a low-dose of tamoxifen in A-, AK- and AKP-mice allows the development of more invasive tumors, and even metastases in rare cases. The penetrance of the model, however, is low – comparable to previously established models of immune competent colorectal cancer[64,66,214]. Notably, Jackstadt *et al.* [215] showed that induced mouse models with *Villin-Cre* and conditional alleles $Kras^{LSL\text{-}G12D/+}$, $Trp53^{lox/lox}$, and $Rosa26^{LSL\text{-}N1icd/+}$ (KPN) reliably formed metastases with 100% penetrance overall with a similar low-dose long latency model. This phenomenon was largely shown to be due to the increased expression of Tgfb2 driven by the Notch transcription complex, which recruited neutrophils to the TME and thus contributed to tumor progression[215]. Furthermore, the latency of metastatic disease in our model is between 18 and 24 weeks, an experimental timeline that is very long, costly and difficult to manage. Other approaches, especially those involving orthotopic transplantation of colorectal cancer organoids into the cecum have similar metastatic penetrance (in immune-proficient mice) with shorter experimental timelines (6 to 12 weeks)[67–69].

5.2.2 A-tumors maintain higher levels of myeloid cells in the TME overtime compared to AK- and AKP-tumors, T cells are most abundant at early timepoints across all tumors, and TCR clontypes are specifically expanded at early timepoints

In our longitudinal study of the the TME of A-, AK- and AKP-mice over time, our main findings were that A-mice maintained an elevated level of myeloid cells in their TME throughout time when compared to AK- and AKP-mice. This could be indicative of an immune-suppressive TME in A-tumors[216–218]. In fact, unexpectedly, we were able to observe invasion into the submucosa in A-tumors. This is surprising considering multiple observations made from the

clinic wherein truncated APC is insufficient for the manifestation of clinical disease[8,14]. Due to the time allowed for tumor development in this model, this could be due to other somatic mutations acquired over time in the rapidly dividing cells. It would be informative to perform whole exome sequencing on these tumors and their invasive sites. We can speculate that the abundant myeloid cells in these tumors are promoting an immune-suppressive TME (as we showed previously[61]) and allowing malignant cells to invade.

We were further able to observe that T cell infiltration is largely an early event in A-, AK- and AKP-tumors. This finding shows what has long been suspected: T cells are excluded from the tumor microenvironment of colorectal cancer tumors over time. Furthermore, the trend of decreasing T cells over time is universal in all three tumor models. Because the success of immunotherapies are largely dependent on the physical presence of T cells in the TME[7], this finding implies that, should a T cell dependent therapy such as αPD1 be implicated for treatment, it is critical that the therapy is initiated sooner rather than later.

We conducted this longitudinal experiment to address a gap in the literature. To date, there are no other published studies (in mice or men) that follow the evolution of the TME of colorectal cancer over time. This study also offers the opportunity to compare the effects of the oncogenic mutations on the tumor microenvironment over time. Further repetitions of the experiment, however, could help to solidify what these changes could be. Furthermore, we have produced a scRNAseq data set of the AKP tumor microenvironment over time, enabling the study of the transcriptomic changes undergone by the immune and epithelial cells over time. This could lead to the generation of several hypotheses that could inform which therapies are implicated or useful at early and later stages in tumor progression.

5.3 Aim 3: Contribute to the development of a light-inducible colon-on-a-chip tumorigenesis model for colorectal cancer

This project was not the main aim of the thesis, but rather a collaboration for which we provided our GEMMs of CRC expertise and technical abilities. We generated six colon

organoid lines for this project, including A-, AK-, AKP-colon organoids as well as A-, AK- and AKP-tumor organoids that could serve as controls. Our collaborators then successfully introduced a light-inducible Cre-ERT2 vector into these organoids. The organoids, when seeded in a colonic chip (engineered to mimic the architecture and composition of the colonic lamina propria) populated the chip as if it were the colon. Blue light shined through a mask then enabled spatio-temporally controlled activation of the Cre-recombinase to initiate tumorigenesis.

We were subsequently able to validate that the recombinant cells derived from the light-mediated chip recombination were indeed bona fide tumor cells, as they demonstrated rapid growth when transplanted sub-cutaneously in immunodeficient mice. We next plan to assess the tumors by IHC for classical signs of colorectal cancer such as epithelial cells organised into crypt-like structures but lacking differentiated cell types such as goblet cells. This project is currently under revision following submission to *Nature*, and we anticipate that findings from this study will allow us to better understand the early events in oncogenic transformation.

5.4 Conclusion and future perspectives

In this work, we have conducted studies on the tumor microenvironment of colorectal cancer mouse models. In the first part, we show that the composition of the TME is strongly influenced by the oncogenic driver mutations of the tumors. In particular, Kras is associated with greater T cell infiltration. We then showed that Anxa1 could be induced by active Kras, which has been observed previously in human CRC[188,189]. Whether this is true and which transcription factor is induced remains to be shown. We suggest that Anxa1 could be driving the infiltration of T cells in Kras mutant tumors by inducing apoptosis in neutrophils or by direct interaction with T cells, but this is still under investigation. We hope to be able to combine a therapy that recruits T cells into the TME of CRC tumors with immunotherapies to improve the efficacy of these treatments. We showed that CRC GEMMs AK- and AKP-mice

responded modestly to immmunotherapies while A-mice did not. We therefore plan to use A-mice to determine whether T cell recruiting therapies could indeed improve the response to immunotherapy.

We further addressed a gap in the literature by creating a longitudinal AKP-tumor microenvironment scRNAseq dataset that monitors the transcriptomic changes of the TME over time. This resource can be used to generate hypotheses as to how T cells become exhausted over time or how the tumor adapts to the environment over time, for example.

Finally, we contributed to the development of an *ex vivo* model of light-inducible cancer initiation that enables the study of the early changes in the epithelial cells afforded by oncogenic transformation. This modality can be adapted to include components of the TME such as T cells and fibroblasts. This could enable controlled study of the interaction of malignant cells with components of the tumor microenvironment.

Bibliography

1. Siegel, R. L., Wagle, N. S., Cercek, A., Smith, R. A. & Jemal, A. Colorectal cancer statistics, 2023. *CA: A Cancer Journal for Clinicians* **73.** _eprint: https://onlinelibrary.wiley.com/doi/pdf/10.3322 233–254. ISSN: 1542-4863. https://onlinelibrary.wiley.com/doi/abs/10.3322/caac.21772 (2023) (2023).

2. Cercek, A. *et al.* PD-1 Blockade in Mismatch Repair–Deficient, Locally Advanced Rectal Cancer. *New England Journal of Medicine* **386.** Publisher: Massachusetts Medical Society _eprint: https://doi.org/10.1056/NEJMoa2201445, 2363–2376. ISSN: 0028-4793. https://doi.org/10.1056/NEJMoa2201445 (2023) (June 23, 2022).

3. Betof Warner, A. *et al.* Long-Term Outcomes and Responses to Retreatment in Patients With Melanoma Treated With PD-1 Blockade. *Journal of Clinical Oncology* **38.** Publisher: Wolters Kluwer, 1655–1663. ISSN: 0732-183X. https://ascopubs.org/doi/10.1200/JCO.19.01464 (2023) (May 20, 2020).

4. Brahmer, J. R. *et al.* Safety and Activity of Anti–PD-L1 Antibody in Patients with Advanced Cancer. *New England Journal of Medicine* **366.** Publisher: Massachusetts Medical Society _eprint: https://doi.org/10.1056/NEJMoa1200694, 2455–2465. ISSN: 0028-4793. https://doi.org/10.1056/NEJMoa1200694 (2023) (June 28, 2012).

5. Lesokhin, A. M., Callahan, M. K., Postow, M. A. & Wolchok, J. D. On being less tolerant: Enhanced cancer immunosurveillance enabled by targeting checkpoints and agonists of T cell activation. *Science Translational Medicine* **7.** Publisher: American Association

for the Advancement of Science, 280sr1–280sr1. https://www.science.org/doi/10.1126/scitranslmed.3010274 (2023) (Mar. 25, 2015).

6. Pagès, F. *et al.* International validation of the consensus Immunoscore for the classification of colon cancer: a prognostic and accuracy study. *The Lancet* **391,** 2128–2139. ISSN: 0140-6736. https://www.sciencedirect.com/science/article/pii/S014067361830789X (2023) (May 26, 2018).

7. Schenkel, J. M. & Pauken, K. E. Localization, tissue biology and T cell state — implications for cancer immunotherapy. *Nature Reviews Immunology.* Publisher: Nature Publishing Group, 1–17. ISSN: 1474-1741. https://www.nature.com/articles/s41577-023-00884-8 (2023) (May 30, 2023).

8. Fearon, E. R. & Vogelstein, B. A genetic model for colorectal tumorigenesis. *Cell* **61,** 759–767. ISSN: 0092-8674. https://www.sciencedirect.com/science/article/pii/009286749090186I (2023) (June 1, 1990).

9. Van Der Flier, L. G. & Clevers, H. Stem Cells, Self-Renewal, and Differentiation in the Intestinal Epithelium. *Annual Review of Physiology* **71,** 241–260. ISSN: 0066-4278, 1545-1585. https://www.annualreviews.org/doi/10.1146/annurev.physiol.010908.163145 (2023) (Mar. 1, 2009).

10. *Colon (Large Intestine): Function, Anatomy & Definition* Cleveland Clinic. https://my.clevelandclinic.org/health/body/22134-colon-large-intestine (2023).

11. Bray, F. *et al.* Global cancer statistics 2018: GLOBOCAN estimates of incidence and mortality worldwide for 36 cancers in 185 countries. *CA: A Cancer Journal for Clinicians* **68.** _eprint: https://onlinelibrary.wiley.com/doi/pdf/10.3322/caac.21492, 394–424. ISSN: 1542-4863. https://onlinelibrary.wiley.com/doi/abs/10.3322/caac.21492 (2023) (2018).

12. Giannakis, M. & Ng, K. A common cancer at an uncommon age. *Science* **379.** Publisher: American Association for the Advancement of Science, 1088–1090. https://www.science.org/doi/10.1126/science.ade7114 (2023) (Mar. 17, 2023).

13. Kinzler, K. W. & Vogelstein, B. Lessons from Hereditary Colorectal Cancer. *Cell* **87,** 159–170. ISSN: 0092-8674. https://www.sciencedirect.com/science/article/pii/S0092867400813331 (2023) (Oct. 18, 1996).

14. Vogelstein, B. *et al.* Cancer Genome Landscapes. *Science* **339.** Publisher: American Association for the Advancement of Science, 1546–1558. https://www.science.org/doi/10.1126/science.1235122 (2023) (Mar. 29, 2013).

15. Nusse, R. *et al.* A new nomenclature for int-1 and related genes: The Wnt gene family. *Cell* **64,** 231. ISSN: 0092-8674. https://www.sciencedirect.com/science/article/pii/009286749190633A (2023) (Jan. 25, 1991).

16. Liu, J. *et al.* Wnt/γ-catenin signalling: function, biological mechanisms, and therapeutic opportunities. *Signal Transduction and Targeted Therapy* **7.** Number: 1 Publisher: Nature Publishing Group, 1–23. ISSN: 2059-3635. https://www.nature.com/articles/s41392-021-00762-6 (2023) (Jan. 3, 2022).

17. Clevers, H. Wnt/γ-Catenin Signaling in Development and Disease. *Cell* **127,** 469–480. ISSN: 0092-8674. https://www.sciencedirect.com/science/article/pii/S0092867406013444 (2023) (Nov. 3, 2006).

18. Radtke, F. & Clevers, H. Self-Renewal and Cancer of the Gut: Two Sides of a Coin. *Science* **307.** Publisher: American Association for the Advancement of Science, 1904–1909. https://www.science.org/doi/10.1126/science.1104815 (2023) (Mar. 25, 2005).

19. Cargnello, M. & Roux, P. P. Activation and Function of the MAPKs and Their Substrates, the MAPK-Activated Protein Kinases. *Microbiology and Molecular Biology Reviews : MMBR* **75,** 50–83. ISSN: 1092-2172. https://www.ncbi.nlm.nih.gov/pmc/articles/PMC3063353/ (2023) (Mar. 2011).

20. Heuberger, J. *et al.* Shp2/MAPK signaling controls goblet/paneth cell fate decisions in the intestine. *Proceedings of the National Academy of Sciences* **111.** Publisher: Proceedings of the National Academy of Sciences, 3472–3477. https://www.pnas.org/doi/10.1073/pnas.1309342111 (2023) (Mar. 4, 2014).

21. Huang, L., Guo, Z., Wang, F. & Fu, L. KRAS mutation: from undruggable to druggable in cancer. *Signal Transduction and Targeted Therapy* **6.** Number: 1 Publisher: Nature Publishing Group, 1–20. ISSN: 2059-3635. https://www.nature.com/articles/s41392-021-00780-4 (2022) (Nov. 15, 2021).

22. Levine, A. J. p53, the Cellular Gatekeeper for Growth and Division. *Cell* **88,** 323–331. ISSN: 0092-8674. https://www.sciencedirect.com/science/article/pii/S0092867400818711 (2023) (Feb. 7, 1997).

23. Chen, J. The Cell-Cycle Arrest and Apoptotic Functions of p53 in Tumor Initiation and Progression. *Cold Spring Harbor Perspectives in Medicine* **6,** a026104. ISSN: 2157-1422 (Mar. 1, 2016).

24. Vogelstein, B., Lane, D. & Levine, A. J. Surfing the p53 network. *Nature* **408.** Number: 6810 Publisher: Nature Publishing Group, 307–310. ISSN: 1476-4687. https://www.nature.com/articles/35042675 (2023) (Nov. 2000).

25. Pellegata, N. S., Antoniono, R. J., Redpath, J. L. & Stanbridge, E. J. DNA damage and p53-mediated cell cycle arrest: Areevaluation. *Proceedings of the National Academy of Sciences of the United States of America* **93,** 15209–15214. ISSN: 0027-8424. https://www.ncbi.nlm.nih.gov/pmc/articles/PMC26382/ (2023) (Dec. 24, 1996).

26. Abuetabh, Y. *et al.* DNA damage response revisited: the p53 family and its regulators provide endless cancer therapy opportunities. *Experimental & Molecular Medicine* **54.** Number: 10 Publisher: Nature Publishing Group, 1658–1669. ISSN: 2092-6413. https://www.nature.com/articles/s12276-022-00863-4 (2023) (Oct. 2022).

27. Rufini, A., Tucci, P., Celardo, I. & Melino, G. Senescence and aging: the critical roles of p53. *Oncogene* **32.** Number: 43 Publisher: Nature Publishing Group, 5129–5143. ISSN: 1476-5594. https://www.nature.com/articles/onc2012640 (2023) (Oct. 2013).

28. Bieging, K. T., Mello, S. S. & Attardi, L. D. Unravelling mechanisms of p53-mediated tumour suppression. *Nature Reviews Cancer* **14.** Number: 5 Publisher: Nature Publishing Group, 359–370. ISSN: 1474-1768. https://www.nature.com/articles/nrc3711 (2023) (May 2014).

29. Aubrey, B. J., Kelly, G. L., Janic, A., Herold, M. J. & Strasser, A. How does p53 induce apoptosis and how does this relate to p53-mediated tumour suppression? *Cell Death & Differentiation* **25.** Number: 1 Publisher: Nature Publishing Group, 104–113. ISSN: 1476-5403. https://www.nature.com/articles/cdd2017169 (2023) (Jan. 2018).

30. Longley, D. B., Harkin, D. P. & Johnston, P. G. 5-Fluorouracil: mechanisms of action and clinical strategies. *Nature Reviews Cancer* **3.** Number: 5 Publisher: Nature Publishing Group, 330–338. ISSN: 1474-1768. https://www.nature.com/articles/nrc1074 (2023) (May 2003).

31. Graham, J., Muhsin, M. & Kirkpatrick, P. Oxaliplatin. *Nature Reviews Drug Discovery* **3.** Number: 1 Publisher: Nature Publishing Group, 11–12. ISSN: 1474-1784. https://www.nature.com/articles/nrd1287 (2023) (Jan. 1, 2004).

32. *Colon Cancer Treatment - NCI* Archive Location: nciglobal,ncienterprise. https://www.cancer.gov/types/colorectal/patient/colon-treatment-pdq (2023).

33. Buchler, T. *et al.* Sequential Treatment with Bevacizumab and Aflibercept for Metastatic Colorectal Cancer in Real-World Clinical Practice. *Targeted Oncology* **15,** 193–201. ISSN: 1776-260X. https://doi.org/10.1007/s11523-020-00705-1 (2023) (Apr. 1, 2020).

34. Vogelstein, B. *et al.* Genetic alterations during colorectal-tumor development. *The New England Journal of Medicine* **319,** 525–532. ISSN: 0028-4793 (Sept. 1, 1988).

35. Misale, S., Di Nicolantonio, F., Sartore-Bianchi, A., Siena, S. & Bardelli, A. Resistance to Anti-EGFR Therapy in Colorectal Cancer: From Heterogeneity to Convergent Evolution. *Cancer Discovery* **4,** 1269–1280. ISSN: 2159-8274. https://doi.org/10.1158/2159-8290.CD-14-0462 (2023) (Nov. 1, 2014).

36. Morad, G., Helmink, B. A., Sharma, P. & Wargo, J. A. Hallmarks of response, resistance, and toxicity to immune checkpoint blockade. *Cell* **184,** 5309–5337. ISSN: 0092-8674. https://www.sciencedirect.com/science/article/pii/S0092867421011016 (2023) (Oct. 14, 2021).

37. Hodi, F. *et al.* Improved survival with ipilimumab in patients with metastatic melanoma. *New England Journal of Medicine* **363,** 711–723. ISSN: 0028-4793 (2010).

38. O'Day, S. J. *et al.* Efficacy and safety of ipilimumab monotherapy in patients with pretreated advanced melanoma: a multicenter single-arm phase II study. *Annals of Oncology* **21,** 1712–1717. ISSN: 0923-7534. https://www.sciencedirect.com/science/article/pii/S0923753419394104 (2023) (Aug. 1, 2010).

39. Peggs, K. S., Quezada, S. A., Korman, A. J. & Allison, J. P. Principles and use of anti-CTLA4 antibody in human cancer immunotherapy. *Current Opinion in Immunology. Lymphocyte development / Tumour immunology* **18,** 206–213. ISSN: 0952-7915. https://www.sciencedirect.com/science/article/pii/S0952791506000148 (2023) (Apr. 1, 2006).

40. Ribas, A. Tumor Immunotherapy Directed at PD-1. *New England Journal of Medicine* **366.** Publisher: Massachusetts Medical Society _eprint: https://doi.org/10.1056/NEJMe1205943, 2517–2519. ISSN: 0028-4793. https://doi.org/10.1056/NEJMe1205943 (2023) (June 28, 2012).

41. Vilar, E. & Gruber, S. B. Microsatellite instability in colorectal cancer—the stable evidence. *Nature Reviews Clinical Oncology* **7.** Number: 3 Publisher: Nature Publishing Group, 153–162. ISSN: 1759-4782. https://www.nature.com/articles/nrclinonc.2009.237 (2023) (Mar. 2010).

42. Vonderheide, R. H. The Immune Revolution: A Case for Priming, Not Checkpoint. *Cancer Cell* **33,** 563–569. ISSN: 1535-6108. https://www.sciencedirect.com/science/article/pii/S1535610818301120 (2023) (Apr. 9, 2018).

43. Vilar, E. & Gruber, S. B. Microsatellite Instability in Colorectal Cancer. *Nature Reviews Clinical Oncology* **7,** 153–162 (2012).

44. Overman, M. J. *et al.* Nivolumab in patients with metastatic DNA mismatch repair-deficient or microsatellite instability-high colorectal cancer (CheckMate 142): an open-label, multicentre, phase 2 study. *The Lancet Oncology* **18,** 1182–1191. ISSN: 1470-

2045. https://www.sciencedirect.com/science/article/pii/S1470204517304229 (2023) (Sept. 1, 2017).

45. Ribas, A. & Wolchok, J. D. Cancer immunotherapy using checkpoint blockade. *Science* **359.** Publisher: American Association for the Advancement of Science, 1350–1355. https://www.science.org/doi/10.1126/science.aar4060 (2023) (Mar. 23, 2018).

46. Germano, G. *et al.* Inactivation of DNA repair triggers neoantigen generation and impairs tumour growth. *Nature* **552.** Number: 7683 Publisher: Nature Publishing Group, 116–120. ISSN: 1476-4687. https://www.nature.com/articles/nature24673 (2023) (Dec. 2017).

47. Brightman, S. E. *et al.* Neoantigen-specific stem cell memory-like CD4+ T cells mediate CD8+ T cell-dependent immunotherapy of MHC class II-negative solid tumors. *Nature Immunology.* Publisher: Nature Publishing Group, 1–13. ISSN: 1529-2916. https://www.nature.com/articles/s41590-023-01543-9 (2023) (July 3, 2023).

48. Bullock, T. N. J. CD40 stimulation as a molecular adjuvant for cancer vaccines and other immunotherapies. *Cellular & Molecular Immunology* **19.** Number: 1 Publisher: Nature Publishing Group, 14–22. ISSN: 2042-0226. https://www.nature.com/articles/s41423-021-00734-4 (2023) (Jan. 2022).

49. Vonderheide, R. H. CD40 Agonist Antibodies in Cancer Immunotherapy. *Annual Review of Medicine* **71,** 47–58. ISSN: 1545-326X (Jan. 27, 2020).

50. Sum, E. *et al.* The tumor-targeted CD40 agonist CEA-CD40 promotes T cell priming via a dual mode of action by increasing antigen delivery to dendritic cells and enhancing their activation. *Journal for ImmunoTherapy of Cancer* **10.** Publisher: BMJ Specialist Journals Section: Clinical/translational cancer immunotherapy, e003264. ISSN: 2051-1426. https://jitc.bmj.com/content/10/3/e003264 (2023) (Mar. 1, 2022).

51. Tichet, M. *et al.* Bispecific PD1-IL2v and anti-PD-L1 break tumor immunity resistance by enhancing stem-like tumor-reactive CD8+ T cells and reprogramming macrophages. *Immunity* **56.** Publisher: Elsevier, 162–179.e6. ISSN: 1074-7613. https://www.cell.com/immunity/abstract/S1074-7613(22)00642-2 (2023) (Jan. 10, 2023).

52. Coveler, A. L. *et al.* Phase 1 dose-escalation study of SEA-CD40: a non-fucosylated CD40 agonist, in advanced solid tumors and lymphomas. *Journal for ImmunoTherapy of Cancer* **11.** Publisher: BMJ Specialist Journals Section: Clinical/translational cancer immunotherapy, e005584. ISSN: 2051-1426. https://jitc.bmj.com/content/11/6/e005584 (2023) (June 1, 2023).

53. Perez, C. R. & De Palma, M. Engineering dendritic cell vaccines to improve cancer immunotherapy. *Nature Communications* **10.** Number: 1 Publisher: Nature Publishing Group, 5408. ISSN: 2041-1723. https://www.nature.com/articles/s41467-019-13368-y (2023) (Nov. 27, 2019).

54. Hanahan, D. Hallmarks of Cancer: New Dimensions. *Cancer Discovery* **12,** 31–46. ISSN: 2159-8274. https://doi.org/10.1158/2159-8290.CD-21-1059 (2023) (Jan. 12, 2022).

55. De Visser, K. E. & Joyce, J. A. The evolving tumor microenvironment: From cancer initiation to metastatic outgrowth. *Cancer Cell* **41,** 374–403. ISSN: 1535-6108. https://www.sciencedirect.com/science/article/pii/S1535610823000442 (2023) (Mar. 13, 2023).

56. Garner, H. & de Visser, K. E. Immune crosstalk in cancer progression and metastatic spread: a complex conversation. *Nature Reviews Immunology* **20.** Number: 8 Publisher: Nature Publishing Group, 483–497. ISSN: 1474-1741. https://www.nature.com/articles/s41577-019-0271-z (2023) (Aug. 2020).

57. Kalluri, R. The biology and function of fibroblasts in cancer. *Nature Reviews Cancer* **16.** Number: 9 Publisher: Nature Publishing Group, 582–598. ISSN: 1474-1768. https://www.nature.com/articles/nrc.2016.73 (2023) (Sept. 2016).

58. Petrova, V., Annicchiarico-Petruzzelli, M., Melino, G. & Amelio, I. The hypoxic tumour microenvironment. *Oncogenesis* **7.** Number: 1 Publisher: Nature Publishing Group, 1–13. ISSN: 2157-9024. https://www.nature.com/articles/s41389-017-0011-9 (2023) (Jan. 24, 2018).

59. Carmeliet, P. VEGF as a key mediator of angiogenesis in cancer. *Oncology* **69 Suppl 3,** 4–10. ISSN: 0030-2414 (2005).

60. Joyce, J. A. & Fearon, D. T. T cell exclusion, immune privilege, and the tumor microenvironment. *Science* **348.** Publisher: American Association for the Advancement of Science, 74–80. https://www.science.org/doi/10.1126/science.aaa6204 (2023) (Apr. 3, 2015).

61. Germann, M. *et al.* Neutrophils suppress tumor-infiltrating T cells in colon cancer via matrix metalloproteinase-mediated activation of TGFγ. *EMBO molecular medicine* **12,** e10681. ISSN: 1757-4684 (Jan. 9, 2020).

62. Tauriello, D. V. F. *et al.* TGFγ drives immune evasion in genetically reconstituted colon cancer metastasis. *Nature* **554.** Number: 7693 Publisher: Nature Publishing Group, 538–543. ISSN: 1476-4687. https://www.nature.com/articles/nature25492 (2022) (Feb. 2018).

63. Fridman, W. H., Pagès, F., Sautès-Fridman, C. & Galon, J. The immune contexture in human tumours: impact on clinical outcome. *Nature Reviews Cancer* **12.** Number: 4 Publisher: Nature Publishing Group, 298–306. ISSN: 1474-1768. https://www.nature.com/articles/nrc3245 (2023) (Apr. 2012).

64. Lannagan, T. R., Jackstadt, R., Leedham, S. J. & Sansom, O. J. Advances in colon cancer research: in vitro and animal models. *Current Opinion in Genetics & Development. Cancer Genomics* **66,** 50–56. ISSN: 0959-437X. https://www.sciencedirect.com/science/article/pii/S0959437X20301672 (2023) (Feb. 1, 2021).

65. Kersten, K., de Visser, K. E., van Miltenburg, M. H. & Jonkers, J. Genetically engineered mouse models in oncology research and cancer medicine. *EMBO Molecular Medicine* **9.** Publisher: John Wiley & Sons, Ltd, 137–153. ISSN: 1757-4676. https://www.embopress.org/doi/full/10.15252/emmm.201606857 (2023) (Feb. 2017).

66. Jackstadt, R. & Sansom, O. J. Mouse models of intestinal cancer. *The Journal of Pathology* **238.** _eprint: https://onlinelibrary.wiley.com/doi/pdf/10.1002/path.4645, 141–

151. ISSN: 1096-9896. https://onlinelibrary.wiley.com/doi/abs/10.1002/path.4645 (2023) (2016).

67. Fumagalli, A. *et al.* A surgical orthotopic organoid transplantation approach in mice to visualize and study colorectal cancer progression. *Nature Protocols* **13,** 235–247. ISSN: 1754-2189, 1750-2799. https://www.nature.com/articles/nprot.2017.137 (2023) (Feb. 2018).

68. O'Rourke, K. P. *et al.* Transplantation of engineered organoids enables rapid generation of metastatic mouse models of colorectal cancer. *Nature Biotechnology* **35.** Number: 6 Publisher: Nature Publishing Group, 577–582. ISSN: 1546-1696. https://www.nature.com/articles/nbt.3837 (2023) (June 2017).

69. Roper, J. *et al.* In vivo genome editing and organoid transplantation models of colorectal cancer and metastasis. *Nature Biotechnology* **35.** Number: 6 Publisher: Nature Publishing Group, 569–576. ISSN: 1546-1696. https://www.nature.com/articles/nbt.3836 (2023) (June 2017).

70. Burns, C. M. The History of Cortisone Discovery and Development. *Rheumatic Disease Clinics of North America. Corticosteroids* **42,** 1–14. ISSN: 0889-857X. https://www.sciencedirect.com/science/article/pii/S0889857X15000654 (2023) (Feb. 1, 2016).

71. Lewis, G. P. & Piper, P. J. Inhibition of release of prostaglandins as an explanation of some of the actions of anti-inflammatory corticosteroids. *Nature* **254.** Number: 5498 Publisher: Nature Publishing Group, 308–311. ISSN: 1476-4687. https://www.nature.com/articles/254308a0 (2023) (Mar. 1975).

72. Blackwell, G. J. *et al.* Macrocortin: a polypeptide causing the anti-phospholipase effect of glucocorticoids. *Nature* **287.** Number: 5778 Publisher: Nature Publishing Group, 147–149. ISSN: 1476-4687. https://www.nature.com/articles/287147a0 (2023) (Sept. 1980).

73. Pepinsky, R. B. *et al.* Purification and partial sequence analysis of a 37-kDa protein that inhibits phospholipase A2 activity from rat peritoneal exudates. *Journal of Biological Chemistry* **261,** 4239–4246. ISSN: 0021-9258. https://www.sciencedirect.com/science/article/pii/S0021925817356533 (2023) (Mar. 25, 1986).

74. Wallner, B. P. *et al.* Cloning and expression of human lipocortin, a phospholipase A2 inhibitor with potential anti-inflammatory activity. *Nature* **320.** Number: 6057 Publisher: Nature Publishing Group, 77–81. ISSN: 1476-4687. https://www.nature.com/articles/320077a0 (2023) (Mar. 1986).

75. Hwa, J., Sessa, W. C. & Martin, K. in *Basic & Clinical Pharmacology* (eds Katzung, B. G. & Vanderah, T. W.) 15th ed. (McGraw-Hill, New York, NY, 2021). accessmedicine.mhmedical.com/content.aspx?aid=1176464143 (2023).

76. Gassama-Diagne, A., Fauvel, J. & Chap, H. Calcium-independent phospholipases from guinea pig digestive tract as probes to study the mechanism of lipocortin. *Journal of Biological Chemistry* **265,** 4309–4314. ISSN: 0021-9258. https://www.sciencedirect.com/science/article/pii/S002192581939564X (2023) (Mar. 15, 1990).

77. Raynal, P. & Pollard, H. B. Annexins: the problem of assessing the biological role for a gene family of multifunctional calcium- and phospholipid-binding proteins. *Biochimica et Biophysica Acta (BBA)* **1197,** 63–93. ISSN: 0304-4157. https://www.sciencedirect.com/science/article/pii/0304415794900191 (2022) (Apr. 5, 1994).

78. Giannakis, M. *et al.* Genomic Correlates of Immune-Cell Infiltrates in Colorectal Carcinoma. *Cell Reports* **15,** 857–865. ISSN: 2211-1247. https://www.sciencedirect.com/science/article/pii/S2211124716303643 (2023) (Apr. 26, 2016).

79. Shibata, H. *et al.* Rapid Colorectal Adenoma Formation Initiated by Conditional Targeting of the Apc Gene. *Science* **278.** Publisher: American Association for the Advancement of Science, 120–123. https://www.science.org/doi/10.1126/science.278.5335.120 (2023) (Oct. 3, 1997).

80. Feng, Y. *et al.* Sox9 Induction, Ectopic Paneth Cells, and Mitotic Spindle Axis Defects in Mouse Colon Adenomatous Epithelium Arising From Conditional Biallelic Apc Inactivation. *The American Journal of Pathology* **183,** 493–503. ISSN: 0002-9440. https://www.sciencedirect.com/science/article/pii/S0002944013003313 (2023) (Aug. 1, 2013).

81. Jackson, E. L. *et al.* Analysis of lung tumor initiation and progression using conditional expression of oncogenic K-ras. *Genes & Development* **15.** Company: Cold Spring Harbor Laboratory Press Distributor: Cold Spring Harbor Laboratory Press Institution: Cold Spring Harbor Laboratory Press Label: Cold Spring Harbor Laboratory Press Publisher: Cold Spring Harbor Lab, 3243–3248. ISSN: 0890-9369, 1549-5477. http://genesdev.cshlp.org/content/15/24/3243 (2023) (Dec. 15, 2001).

82. Jonkers, J. *et al.* Synergistic tumor suppressor activity of BRCA2 and p53 in a conditional mouse model for breast cancer. *Nature Genetics* **29.** Number: 4 Publisher: Nature Publishing Group, 418–425. ISSN: 1546-1718. https://www.nature.com/articles/ng747z (2023) (Dec. 2001).

83. Shultz, L. D. *et al.* Human Lymphoid and Myeloid Cell Development in NOD/LtSz-scid IL2Rnull Mice Engrafted with Mobilized Human Hemopoietic Stem Cells 12. *The Journal of Immunology* **174,** 6477–6489. ISSN: 0022-1767. https://doi.org/10.4049/jimmunol.174.10.6477 (2023) (May 15, 2005).

84. Drost, J. *et al.* Sequential cancer mutations in cultured human intestinal stem cells. *Nature* **521.** Number: 7550 Publisher: Nature Publishing Group, 43–47. ISSN: 1476-4687. https://www.nature.com/articles/nature14415 (2023) (May 2015).

85. Bankhead, P. *et al.* QuPath: Open source software for digital pathology image analysis. *Scientific Reports* **7.** Number: 1 Publisher: Nature Publishing Group, 16878. ISSN: 2045-2322. https://www.nature.com/articles/s41598-017-17204-5 (2023) (Dec. 4, 2017).

86. Bienz, M. γ-Catenin: A Pivot between Cell Adhesion and Wnt Signalling. *Current Biology* **15,** R64–R67. ISSN: 0960-9822. https://www.sciencedirect.com/science/article/pii/S0960982204010413 (2023) (Jan. 26, 2005).

87. Blaj, C. *et al.* Oncogenic Effects of High MAPK Activity in Colorectal Cancer Mark Progenitor Cells and Persist Irrespective of RAS Mutations. *Cancer Research* **77,** 1763–1774. ISSN: 0008-5472. https://doi.org/10.1158/0008-5472.CAN-16-2821 (2023) (Apr. 2, 2017).

88. Hanahan, D. & Weinberg, R. A. The Hallmarks of Cancer. *Cell* **100,** 57–70. ISSN: 0092-8674. https://www.sciencedirect.com/science/article/pii/S0092867400816839 (2023) (Jan. 7, 2000).

89. Hanahan, D. & Weinberg, R. A. Hallmarks of Cancer: The Next Generation. *Cell* **144,** 646–674. ISSN: 0092-8674. https://www.sciencedirect.com/science/article/pii/S0092867411001279 (2023) (Mar. 4, 2011).

90. Lindström, M. S., Bartek, J. & Maya-Mendoza, A. p53 at the crossroad of DNA replication and ribosome biogenesis stress pathways. *Cell Death & Differentiation* **29.** Number: 5 Publisher: Nature Publishing Group, 972–982. ISSN: 1476-5403. https://www.nature.com/articles/s41418-022-00999-w (2023) (May 2022).

91. Aran, D., Sirota, M. & Butte, A. J. Systematic pan-cancer analysis of tumour purity. *Nature Communications* **6.** Number: 1 Publisher: Nature Publishing Group, 8971. ISSN: 2041-1723. https://www.nature.com/articles/ncomms9971 (2023) (Dec. 4, 2015).

92. Tarabichi, M. *et al.* A practical guide to cancer subclonal reconstruction from DNA sequencing. *Nature Methods* **18.** Number: 2 Publisher: Nature Publishing Group, 144–155. ISSN: 1548-7105. https://www.nature.com/articles/s41592-020-01013-2 (2023) (Feb. 2021).

93. Togashi, Y., Shitara, K. & Nishikawa, H. Regulatory T cells in cancer immunosuppression — implications for anticancer therapy. *Nature Reviews Clinical Oncology* **16.** Number: 6 Publisher: Nature Publishing Group, 356–371. ISSN: 1759-4782. https://www.nature.com/articles/s41571-019-0175-7 (2023) (June 2019).

94. Szeponik, L. *et al.* Intratumoral regulatory T cells from colon cancer patients comprise several activated effector populations. *BMC Immunology* **22,** 58. ISSN: 1471-2172. https://doi.org/10.1186/s12865-021-00449-1 (2023) (Aug. 19, 2021).

95. Cullen, S. P., Brunet, M. & Martin, S. J. Granzymes in cancer and immunity. *Cell Death & Differentiation* **17.** Number: 4 Publisher: Nature Publishing Group, 616–623. ISSN: 1476-5403. https://www.nature.com/articles/cdd2009206 (2023) (Apr. 2010).

96. Chowdhury, D. & Lieberman, J. Death by a Thousand Cuts: Granzyme Pathways of Programmed Cell Death. *Annual Review of Immunology* **26.** _eprint: https://doi.org/10.1146/annurev.immunol.26.0 389–420. https://doi.org/10.1146/annurev.immunol.26.021607.090404 (2023) (2008).

97. Afonina, I. S., Cullen, S. P. & Martin, S. J. Cytotoxic and non-cytotoxic roles of the CTL/NK protease granzyme B. *Immunological Reviews* **235.** _eprint: https://onlinelibrary.wiley.com/doi/pdf/10.1 2896.2010.00908.x, 105–116. ISSN: 1600-065X. https://onlinelibrary.wiley.com/doi/abs/10.1111/j.0105-2896.2010.00908.x (2023) (2010).

98. Lieberman, J. The ABCs of granule-mediated cytotoxicity: new weapons in the arsenal. *Nature Reviews Immunology* **3.** Number: 5 Publisher: Nature Publishing Group, 361–370. ISSN: 1474-1741. https://www.nature.com/articles/nri1083 (2023) (May 2003).

99. Zhao, J., Chen, X., Herjan, T. & Li, X. The role of interleukin-17 in tumor development and progression. *Journal of Experimental Medicine* **217,** e20190297. ISSN: 0022-1007. https://doi.org/10.1084/jem.20190297 (2023) (Nov. 14, 2019).

100. Liu, C. *et al.* Blocking IL-17A enhances tumor response to anti-PD-1 immunotherapy in microsatellite stable colorectal cancer. *Journal for ImmunoTherapy of Cancer* **9.** Publisher: BMJ Specialist Journals Section: Basic tumor immunology, e001895. ISSN: 2051-1426. https://jitc.bmj.com/content/9/1/e001895 (2023) (Jan. 1, 2021).

101. Murugaiyan, G. & Saha, B. Protumor vs Antitumor Functions of IL-17. *The Journal of Immunology* **183,** 4169–4175. ISSN: 0022-1767. https://doi.org/10.4049/jimmunol.0901017 (2023) (Oct. 1, 2009).

102. Martínez-Sabadell, A., Arenas, E. J. & Arribas, J. IFN Signaling in Natural and Therapy-Induced Antitumor Responses. *Clinical Cancer Research* **28,** 1243–1249. ISSN: 1078-0432. https://doi.org/10.1158/1078-0432.CCR-21-3226 (2023) (Apr. 1, 2022).

103. Gocher, A. M., Workman, C. J. & Vignali, D. A. A. Interferon-: teammate or opponent in the tumour microenvironment? *Nature Reviews Immunology* **22.** Number: 3 Publisher: Nature Publishing Group, 158–172. ISSN: 1474-1741. https://www.nature.com/articles/s41577-021-00566-3 (2023) (Mar. 2022).

104. Jorgovanovic, D., Song, M., Wang, L. & Zhang, Y. Roles of IFN- in tumor progression and regression: a review. *Biomarker Research* **8,** 49. ISSN: 2050-7771. https://doi.org/10.1186/s40364-020-00228-x (2023) (Sept. 29, 2020).

105. Garnier, L. *et al.* IFN-–dependent tumor-antigen cross-presentation by lymphatic endothelial cells promotes their killing by T cells and inhibits metastasis. *Science Advances* **8.** Publisher: American Association for the Advancement of Science, eabl5162. https://www.science.org/doi/10.1126/sciadv.abl5162 (2023) (June 8, 2022).

106. Ivashkiv, L. B. IFN: signalling, epigenetics and roles in immunity, metabolism, disease and cancer immunotherapy. *Nature Reviews Immunology* **18.** Number: 9 Publisher: Nature Publishing Group, 545–558. ISSN: 1474-1741. https://www.nature.com/articles/s41577-018-0029-z (2023) (Sept. 2018).

107. Gao, Y. *et al.* IFN--mediated inhibition of lung cancer correlates with PD-L1 expression and is regulated by PI3K-AKT signaling. *International Journal of Cancer* **143.** _eprint: https://onlinelibrary.wiley.com/doi/pdf/10.1002/ijc.31357, 931–943. ISSN: 1097-0215. https://onlinelibrary.wiley.com/doi/abs/10.1002/ijc.31357 (2023) (2018).

108. Kelly, S. A., Gschmeissner, S., East, N. & Balkwill, F. R. Enhancement of Metastatic Potential by -Interferon. *Cancer Research* **51,** 4020–4027. ISSN: 0008-5472 (Aug. 1, 1991).

109. Lo, U.-G. *et al.* IFN-Induced IFIT5 Promotes Epithelial-to-Mesenchymal Transition in Prostate Cancer via miRNA Processing. *Cancer Research* **79,** 1098–1112. ISSN: 0008-5472. https://doi.org/10.1158/0008-5472.CAN-18-2207 (2023) (Mar. 15, 2019).

110. Beziaud, L. *et al.* IFNg-induced stem-like state of cancer cells as a driver of metastatic progression following immunotherapy. *Cell Stem Cell* **30,** 818–831.e6. ISSN: 1934-5909. https://www.sciencedirect.com/science/article/pii/S1934590923001777 (2023) (June 1, 2023).

111. Bhaumik, S. & Basu, R. Cellular and Molecular Dynamics of Th17 Differentiation and its Developmental Plasticity in the Intestinal Immune Response. *Frontiers in Immunology* **8.** ISSN: 1664-3224. https://www.frontiersin.org/articles/10.3389/fimmu.2017.00254 (2023) (2017).

112. De Simone, V., Pallone, F., Monteleone, G. & Stolfi, C. Role of TH17 cytokines in the control of colorectal cancer. *Oncoimmunology* **2,** e26617. ISSN: 2162-4011. https://www.ncbi.nlm.nih.gov/pmc/articles/PMC3902118/ (2023) (Dec. 1, 2013).

113. Andreatta, M. *et al.* Interpretation of T cell states from single-cell transcriptomics data using reference atlases. *Nature Communications* **12.** Number: 1 Publisher: Nature Publishing Group, 2965. ISSN: 2041-1723. https://www.nature.com/articles/s41467-021-23324-4 (2023) (May 20, 2021).

114. Zilionis, R. *et al.* Single-Cell Transcriptomics of Human and Mouse Lung Cancers Reveals Conserved Myeloid Populations across Individuals and Species. *Immunity* **50,** 1317–1334.e10. ISSN: 1074-7613. https://www.sciencedirect.com/science/article/pii/S1074761319301268 (2022) (May 21, 2019).

115. Zhang, L. *et al.* Single-Cell Analyses Inform Mechanisms of Myeloid-Targeted Therapies in Colon Cancer. *Cell* **181,** 442–459.e29. ISSN: 0092-8674. https://www.sciencedirect.com/science/article/pii/S009286742030341X (2023) (Apr. 16, 2020).

116. Cheng, S. *et al.* A pan-cancer single-cell transcriptional atlas of tumor infiltrating myeloid cells. *Cell* **184,** 792–809.e23. ISSN: 0092-8674. https://www.sciencedirect.com/science/article/pii/S0092867421000106 (2023) (Feb. 4, 2021).

117. Grieshaber-Bouyer, R. *et al.* The neutrotime transcriptional signature defines a single continuum of neutrophils across biological compartments. *Nature Communications*

12. Number: 1 Publisher: Nature Publishing Group, 2856. ISSN: 2041-1723. https://www.nature.com/articles/s41467-021-22973-9 (2023) (May 17, 2021).

118. Szklarczyk, D. *et al.* The STRING database in 2023: protein–protein association networks and functional enrichment analyses for any sequenced genome of interest. *Nucleic Acids Research* **51,** D638–D646. ISSN: 0305-1048. https://doi.org/10.1093/nar/gkac1000 (2023) (D1 Jan. 6, 2023).

119. Maier, B. *et al.* A conserved dendritic-cell regulatory program limits antitumour immunity. *Nature* **580.** Number: 7802 Publisher: Nature Publishing Group, 257–262. ISSN: 1476-4687. https://www.nature.com/articles/s41586-020-2134-y (2023) (Apr. 2020).

120. Swiecki, M. & Colonna, M. The multifaceted biology of plasmacytoid dendritic cells. *Nature Reviews Immunology* **15.** Number: 8 Publisher: Nature Publishing Group, 471–485. ISSN: 1474-1741. https://www.nature.com/articles/nri3865 (2023) (Aug. 2015).

121. Gafencu, A. V. *et al.* Inflammatory Signaling Pathways Regulating ApoE Gene Expression in Macrophages *. *Journal of Biological Chemistry* **282.** Publisher: Elsevier, 21776–21785. ISSN: 0021-9258, 1083-351X. https://www.jbc.org/article/S0021-9258(20)78130-5/abstract (2023) (July 27, 2007).

122. Bonacina, F. *et al.* Myeloid apolipoprotein E controls dendritic cell antigen presentation and T cell activation. *Nature Communications* **9.** Number: 1 Publisher: Nature Publishing Group, 3083. ISSN: 2041-1723. https://www.nature.com/articles/s41467-018-05322-1 (2023) (Aug. 6, 2018).

123. Domanska, D. *et al.* Single-cell transcriptomic analysis of human colonic macrophages reveals niche-specific subsets. *Journal of Experimental Medicine* **219,** e20211846. ISSN: 0022-1007. https://doi.org/10.1084/jem.20211846 (2023) (Feb. 9, 2022).

124. Chakarov, S. *et al.* Two distinct interstitial macrophage populations coexist across tissues in specific subtissular niches. *Science* **363.** Publisher: American Association for the Advancement of Science, eaau0964. https://www.science.org/doi/full/10.1126/science.aau0964 (2023) (Mar. 15, 2019).

125. Kieu, T. Q. *et al.* Kinetics of LYVE-1-positive M2-like macrophages in developing and repairing dental pulp in vivo and their pro-angiogenic activity in vitro. *Scientific Reports* **12.** Number: 1 Publisher: Nature Publishing Group, 5176. ISSN: 2045-2322. https://www.nature.com/articles/s41598-022-08987-3 (2023) (Mar. 25, 2022).

126. El Sayed, S. *et al.* CCR2 promotes monocyte recruitment and intestinal inflammation in mice lacking the interleukin-10 receptor. *Scientific Reports* **12.** Number: 1 Publisher: Nature Publishing Group, 452. ISSN: 2045-2322. https://www.nature.com/articles/s41598-021-04098-7 (2023) (Jan. 10, 2022).

127. Mao, Y., Shi, D., Li, G. & Jiang, P. Citrulline depletion by ASS1 is required for proinflammatory macrophage activation and immune responses. *Molecular Cell* **82,** 527–541.e7. ISSN: 1097-2765. https://www.sciencedirect.com/science/article/pii/S1097276521010686 (2023) (Feb. 3, 2022).

128. Liu, H. *et al.* Mutant KRAS triggers functional reprogramming of tumor-associated macrophages in colorectal cancer. *Signal Transduction and Targeted Therapy* **6.** Number: 1 Publisher: Nature Publishing Group, 1–13. ISSN: 2059-3635. https://www.nature.com/articles/s41392-021-00534-2 (2023) (Apr. 9, 2021).

129. Silva-Santos, B., Mensurado, S. & Coffelt, S. B. T cells: pleiotropic immune effectors with therapeutic potential in cancer. *Nature Reviews Cancer* **19.** Number: 7 Publisher: Nature Publishing Group, 392–404. ISSN: 1474-1768. https://www.nature.com/articles/s41568-019-0153-5 (2023) (July 2019).

130. Mensurado, S., Blanco-Domínguez, R. & Silva-Santos, B. The emerging roles of T cells in cancer immunotherapy. *Nature Reviews Clinical Oncology* **20.** Number: 3 Publisher: Nature Publishing Group, 178–191. ISSN: 1759-4782. https://www.nature.com/articles/s41571-022-00722-1 (2023) (Mar. 2023).

131. Nozaki, K. *et al.* Co-culture with intestinal epithelial organoids allows efficient expansion and motility analysis of intraepithelial lymphocytes. *Journal of Gastroenterology* **51,** 206–213. ISSN: 1435-5922. https://doi.org/10.1007/s00535-016-1170-8 (2023) (Mar. 1, 2016).

132. Mowat, A. M. & Agace, W. W. Regional specialization within the intestinal immune system. *Nature Reviews Immunology* **14.** Number: 10 Publisher: Nature Publishing Group, 667–685. ISSN: 1474-1741. https://www.nature.com/articles/nri3738 (2023) (Oct. 2014).

133. Blank, C. U. *et al.* Defining 'T cell exhaustion'. *Nature Reviews Immunology* **19.** Number: 11 Publisher: Nature Publishing Group, 665–674. ISSN: 1474-1741. https://www.nature.com/articles/s41577-019-0221-9 (2023) (Nov. 2019).

134. Noh, B.-J., Kwak, J. Y. & Eom, D.-W. Immune classification for the PD-L1 expression and tumour-infiltrating lymphocytes in colorectal adenocarcinoma. *BMC Cancer* **20,** 58. ISSN: 1471-2407. https://doi.org/10.1186/s12885-020-6553-9 (2023) (Jan. 28, 2020).

135. Ragusa, S. *et al.* Antiangiogenic immunotherapy suppresses desmoplastic and chemoresistant intestinal tumors in mice. *The Journal of Clinical Investigation* **130.** Publisher: American Society for Clinical Investigation, 1199–1216. ISSN: 0021-9738. https://www.jci.org/articles/view/129558 (2023) (Mar. 2, 2020).

136. Rakhmilevich, A. L. *et al.* Effective Combination of Innate and Adaptive Immunotherapeutic Approaches in a Mouse Melanoma Model. *Journal of Immunology (Baltimore, Md.: 1950)* **198,** 1575–1584. ISSN: 1550-6606 (Feb. 15, 2017).

137. Pavlova, N. N. & Thompson, C. B. The Emerging Hallmarks of Cancer Metabolism. *Cell Metabolism* **23,** 27–47. ISSN: 1550-4131. https://www.sciencedirect.com/science/article/pii/S155041311500621X (2023) (Jan. 12, 2016).

138. Squair, J. W. *et al.* Confronting false discoveries in single-cell differential expression. *Nature Communications* **12.** Number: 1 Publisher: Nature Publishing Group, 5692. ISSN: 2041-1723. https://www.nature.com/articles/s41467-021-25960-2 (2023) (Sept. 28, 2021).

139. Browaeys, R., Saelens, W. & Saeys, Y. NicheNet: modeling intercellular communication by linking ligands to target genes. *Nature Methods* **17.** Number: 2 Publisher: Nature

Publishing Group, 159–162. ISSN: 1548-7105. https://www.nature.com/articles/s41592-019-0667-5 (2023) (Feb. 2020).

140. Perretti, M. & D'Acquisto, F. Annexin A1 and glucocorticoids as effectors of the resolution of inflammation. *Nature Reviews Immunology* **9.** Number: 1 Publisher: Nature Publishing Group, 62–70. ISSN: 1474-1741. https://www.nature.com/articles/nri2470 (2022) (Jan. 2009).

141. He, R., Sang, H. & Ye, R. D. Serum amyloid A induces IL-8 secretion through a G protein–coupled receptor, FPRL1/LXA4R. *Blood* **101,** 1572–1581. ISSN: 0006-4971. https://doi.org/10.1182/blood-2002-05-1431 (2023) (Feb. 15, 2003).

142. Hayhoe, R. P. G. *et al.* Annexin 1 and its bioactive peptide inhibit neutrophil-endothelium interactions under flow: indication of distinct receptor involvement. *Blood* **107,** 2123–2130. ISSN: 0006-4971. https://doi.org/10.1182/blood-2005-08-3099 (2023) (Mar. 1, 2006).

143. Solito, E. *et al.* A novel calcium-dependent proapoptotic effect of annexin 1 on human neutrophils. *The FASEB Journal* **17.** _eprint: https://onlinelibrary.wiley.com/doi/pdf/10.1096/fj.02-0941fje, 1–27. ISSN: 1530-6860. https://onlinelibrary.wiley.com/doi/abs/10.1096/fj.02-0941fje (2023) (2003).

144. Vago, J. P. *et al.* Annexin A1 modulates natural and glucocorticoid-induced resolution of inflammation by enhancing neutrophil apoptosis. *Journal of Leukocyte Biology* **92,** 249–258. ISSN: 1938-3673 (Aug. 2012).

145. D'Acquisto, F., Piras, G. & Rattazzi, L. Pro-inflammatory and pathogenic properties of Annexin-A1: The whole is greater than the sum of its parts. *Biochemical Pharmacology* **85,** 1213–1218. ISSN: 0006-2952. https://www.sciencedirect.com/science/article/pii/S0006295213001159 (2023) (May 1, 2013).

146. D'Acquisto, F. *et al.* Annexin-1 modulates T-cell activation and differentiation. *Blood* **109,** 1095–1102. ISSN: 0006-4971. https://doi.org/10.1182/blood-2006-05-022798 (2023) (Sept. 28, 2006).

147. Ünal, E. B., Uhlitz, F. & Blüthgen, N. A compendium of ERK targets. *FEBS Letters* **591.** _eprint: https://onlinelibrary.wiley.com/doi/pdf/10.1002/1873-3468.12740, 2607–2615. ISSN: 1873-3468. https://onlinelibrary.wiley.com/doi/abs/10.1002/1873-3468.12740 (2023) (2017).

148. Hollenhorst, P. C. RAS/ERK pathway transcriptional regulation through ETS/AP-1 binding sites. *Small GTPases* **3,** 154–158. ISSN: 2154-1248. https://www.ncbi.nlm.nih.gov/pmc/articles/PMC3442800/ (2023) (July 1, 2012).

149. Chang, F. *et al.* Signal transduction mediated by the Ras/Raf/MEK/ERK pathway from cytokine receptors to transcription factors: potential targeting for therapeutic intervention. *Leukemia* **17.** Number: 7 Publisher: Nature Publishing Group, 1263–1293. ISSN: 1476-5551. https://www.nature.com/articles/2402945 (2023) (July 1, 2003).

150. ENCODE Project Consortium. The ENCODE (ENCyclopedia Of DNA Elements) Project. *Science (New York, N.Y.)* **306,** 636–640. ISSN: 1095-9203 (Oct. 22, 2004).

151. Becht, E. *et al.* Estimating the population abundance of tissue-infiltrating immune and stromal cell populations using gene expression. *Genome Biology* **17,** 218. ISSN: 1474-760X. https://doi.org/10.1186/s13059-016-1070-5 (2023) (Oct. 20, 2016).

152. Sobin, L. H., Gospodarowicz, M. K. & Wittekind, C. *TNM Classification of Malignant Tumours* Google-Books-ID: 72sC1Zk6OgQC. 209 pp. ISBN: 978-1-4443-5896-4 (John Wiley & Sons, Aug. 31, 2011).

153. Dow, L. E. *et al.* Apc Restoration Promotes Cellular Differentiation and Reestablishes Crypt Homeostasis in Colorectal Cancer. *Cell* **161,** 1539–1552. ISSN: 0092-8674. https://www.sciencedirect.com/science/article/pii/S0092867415006236 (2023) (June 18, 2015).

154. Sato, T. *et al.* Single Lgr5 stem cells build crypt-villus structures in vitro without a mesenchymal niche. *Nature* **459.** Number: 7244 Publisher: Nature Publishing Group, 262–265. ISSN: 1476-4687. https://www.nature.com/articles/nature07935 (2023) (May 2009).

155. Norkin, M. & Huelsken, J. TORNADO-seq: A Protocol for High-Throughput Targeted RNA-seq-Based Drug Screening in Organoids. *Methods in Molecular Biology (Clifton, N.J.)* **2650,** 65–75. ISSN: 1940-6029 (2023).

156. Álvarez-Varela, A. *et al.* Mex3a marks drug-tolerant persister colorectal cancer cells that mediate relapse after chemotherapy. *Nature Cancer* **3.** Number: 9 Publisher: Nature Publishing Group, 1052–1070. ISSN: 2662-1347. https://www.nature.com/articles/s43018-022-00402-0 (2022) (Sept. 2022).

157. Nikolaev, M. *et al.* Homeostatic mini-intestines through scaffold-guided organoid morphogenesis. *Nature* **585.** Number: 7826 Publisher: Nature Publishing Group, 574–578. ISSN: 1476-4687. https://www.nature.com/articles/s41586-020-2724-8 (2023) (Sept. 2020).

158. Liu, H. *et al.* Mutant KRAS Drives Immune Evasion by Sensitizing Cytotoxic T-Cells to Activation-Induced Cell Death in Colorectal Cancer. *Advanced Science (Weinheim, Baden-Wurttemberg, Germany)* **10,** e2203757. ISSN: 2198-3844 (Feb. 2023).

159. Arnoldini, M., Cremer, J. & Hwa, T. Bacterial growth, flow, and mixing shape human gut microbiota density and composition. *Gut Microbes* **9,** 559–566. ISSN: 1949-0976. https://www.ncbi.nlm.nih.gov/pmc/articles/PMC6287699/ (2023) (May 9, 2018).

160. Luo, K. *et al.* A KRAS-Associated Signature for Prognostic, Immune and Chemical Anti-Cancer Drug-Response Prediction in Colon Cancer. *Frontiers in Pharmacology* **13,** 899725. ISSN: 1663-9812. https://www.ncbi.nlm.nih.gov/pmc/articles/PMC9237412/ (2023) (June 14, 2022).

161. Liu, J. *et al.* Immune landscape and prognostic immune-related genes in KRAS-mutant colorectal cancer patients. *Journal of Translational Medicine* **19,** 27. ISSN: 1479-5876. https://doi.org/10.1186/s12967-020-02638-9 (2023) (Jan. 7, 2021).

162. Watterson, A. & Coelho, M. A. Cancer immune evasion through KRAS and PD-L1 and potential therapeutic interventions. *Cell Communication and Signaling* **21,** 45. ISSN: 1478-811X. https://doi.org/10.1186/s12964-023-01063-x (2023) (Mar. 2, 2023).

163. Liao, W. *et al.* KRAS-IRF2 Axis Drives Immune Suppression and Immune Therapy Resistance in Colorectal Cancer. *Cancer Cell* **35,** 559–572.e7. ISSN: 1535-6108. https://www.sciencedirect.com/science/article/pii/S1535610819301035 (2023) (Apr. 15, 2019).

164. Liu, X.-l., Ding, J. & Meng, L.-h. Oncogene-induced senescence: a double edged sword in cancer. *Acta Pharmacologica Sinica* **39.** Number: 10 Publisher: Nature Publishing Group, 1553–1558. ISSN: 1745-7254. https://www.nature.com/articles/aps2017198 (2023) (Oct. 2018).

165. Yaswen, P. & Campisi, J. Oncogene-Induced Senescence Pathways Weave an Intricate Tapestry. *Cell* **128.** Publisher: Elsevier, 233–234. ISSN: 0092-8674, 1097-4172. https://www.cell.com/cell/abstract/S0092-8674(07)00057-8 (2023) (Jan. 26, 2007).

166. Coppé, J.-P., Desprez, P.-Y., Krtolica, A. & Campisi, J. The Senescence-Associated Secretory Phenotype: The Dark Side of Tumor Suppression. *Annual review of pathology* **5,** 99–118. ISSN: 1553-4006. https://www.ncbi.nlm.nih.gov/pmc/articles/PMC4166495/ (2023) (2010).

167. Cuollo, L., Antonangeli, F., Santoni, A. & Soriani, A. The Senescence-Associated Secretory Phenotype (SASP) in the Challenging Future of Cancer Therapy and Age-Related Diseases. *Biology* **9,** 485. ISSN: 2079-7737. https://www.ncbi.nlm.nih.gov/pmc/articles/PMC7767554/ (2023) (Dec. 21, 2020).

168. Baker, A.-M. *et al.* Robust RNA-based in situ mutation detection delineates colorectal cancer subclonal evolution. *Nature Communications* **8.** Number: 1 Publisher: Nature Publishing Group, 1998. ISSN: 2041-1723. https://www.nature.com/articles/s41467-017-02295-5 (2023) (Dec. 8, 2017).

169. Céspedes, M. V. *et al.* Orthotopic Microinjection of Human Colon Cancer Cells in Nude Mice Induces Tumor Foci in All Clinically Relevant Metastatic Sites. *The American Journal of Pathology* **170,** 1077–1085. ISSN: 0002-9440. https://www.sciencedirect.com/science/article/pii/S0002944010609261 (2023) (Mar. 1, 2007).

170. Zhao, T. *et al.* Spatial genomics enables multi-modal study of clonal heterogeneity in tissues. *Nature* **601.** Number: 7891 Publisher: Nature Publishing Group, 85–91. ISSN: 1476-4687. https://www.nature.com/articles/s41586-021-04217-4 (2023) (Jan. 2022).

171. Heide, T. *et al.* The co-evolution of the genome and epigenome in colorectal cancer. *Nature* **611.** Number: 7937 Publisher: Nature Publishing Group, 733–743. ISSN: 1476-4687. https://www.nature.com/articles/s41586-022-05202-1 (2023) (Nov. 2022).

172. Househam, J. *et al.* Phenotypic plasticity and genetic control in colorectal cancer evolution. *Nature* **611.** Number: 7937 Publisher: Nature Publishing Group, 744–753. ISSN: 1476-4687. https://www.nature.com/articles/s41586-022-05311-x (2023) (Nov. 2022).

173. Buch, T. *et al.* A Cre-inducible diphtheria toxin receptor mediates cell lineage ablation after toxin administration. *Nature Methods* **2.** Number: 6 Publisher: Nature Publishing Group, 419–426. ISSN: 1548-7105. https://www.nature.com/articles/nmeth762 (2023) (June 2005).

174. Ruedl, C. & Jung, S. DTR-mediated conditional cell ablation—Progress and challenges. *European Journal of Immunology* **48.** _eprint: https://onlinelibrary.wiley.com/doi/pdf/10.1002/eji.201847527, 1114–1119. ISSN: 1521-4141. https://onlinelibrary.wiley.com/doi/abs/10.1002/eji.201847527 (2023) (2018).

175. Cebula, A. *et al.* Dormant pathogenic CD4+ T cells are prevalent in the peripheral repertoire of healthy mice. *Nature Communications* **10.** Number: 1 Publisher: Nature Publishing Group, 4882. ISSN: 2041-1723. https://www.nature.com/articles/s41467-019-12820-3 (2023) (Oct. 25, 2019).

176. Mombaerts, P. *et al.* Mutations in T-cell antigen receptor genes and γ block thymocyte development at different stages. *Nature* **360.** Number: 6401 Publisher: Nature Publishing Group, 225–231. ISSN: 1476-4687. https://www.nature.com/articles/360225a0 (2023) (Nov. 1992).

177. Albeck, J. G., Mills, G. B. & Brugge, J. S. Frequency-Modulated Pulses of ERK Activity Transmit Quantitative Proliferation Signals. *Molecular Cell* **49,** 249–261. ISSN: 1097-2765. https://www.sciencedirect.com/science/article/pii/S1097276512009331 (2023) (Jan. 24, 2013).

178. Corcoran, R. B. *et al.* EGFR-mediated re-activation of MAPK signaling contributes to insensitivity of BRAF mutant colorectal cancers to RAF inhibition with vemurafenib. *Cancer Discovery* **2,** 227–235. ISSN: 2159-8290 (Mar. 2012).

179. Sun, C. *et al.* Intrinsic Resistance to MEK Inhibition in KRAS Mutant Lung and Colon Cancer through Transcriptional Induction of ERBB3. *Cell Reports* **7,** 86–93. ISSN: 2211-1247. https://www.sciencedirect.com/science/article/pii/S2211124714001612 (2023) (Apr. 10, 2014).

180. Muta, Y. *et al.* Composite regulation of ERK activity dynamics underlying tumour-specific traits in the intestine. *Nature Communications* **9.** Number: 1 Publisher: Nature Publishing Group, 2174. ISSN: 2041-1723. https://www.nature.com/articles/s41467-018-04527-8 (2023) (June 5, 2018).

181. Hamarsheh, S., Groß, O., Brummer, T. & Zeiser, R. Immune modulatory effects of oncogenic KRAS in cancer. *Nature Communications* **11.** Number: 1 Publisher: Nature Publishing Group, 5439. ISSN: 2041-1723. https://www.nature.com/articles/s41467-020-19288-6 (2023) (Oct. 28, 2020).

182. Tanjak, P. *et al.* The KRAS-Mutant Consensus Molecular Subtype 3 Reveals an Immunosuppressive Tumor Microenvironment in Colorectal Cancer. *Cancers* **15,** 1098. ISSN: 2072-6694. https://www.ncbi.nlm.nih.gov/pmc/articles/PMC9953921/ (2023) (Feb. 8, 2023).

183. D'Acunto, C. W., Gbelcova, H., Festa, M. & Ruml, T. The complex understanding of Annexin A1 phosphorylation. *Cellular Signalling* **26,** 173–178. ISSN: 0898-6568. https://www.sciencedirect.com/science/article/pii/S089865681300301X (2022) (Jan. 1, 2014).

184. Rosengarth, A. & Luecke, H. A Calcium-driven Conformational Switch of the N-terminal and Core Domains of Annexin A1. *Journal of Molecular Biology* **326,** 1317–1325. ISSN: 0022-2836. https://www.sciencedirect.com/science/article/pii/S0022283603000275 (2022) (Mar. 7, 2003).

185. Lim, L. H. K. & Pervaiz, S. Annexin 1: the new face of an old molecule. *The FASEB Journal* **21.** _eprint: https://onlinelibrary.wiley.com/doi/pdf/10.1096/fj.06-7464rev, 968–975. ISSN: 1530-6860. https://onlinelibrary.wiley.com/doi/abs/10.1096/fj.06-7464rev (2022) (2007).

186. Kelley, G. G., Reks, S. E., Ondrako, J. M. & Smrcka, A. V. Phospholipase C: a novel Ras effector. *The EMBO Journal* **20,** 743–754. ISSN: 0261-4189. https://www.ncbi.nlm.nih.gov/pmc/articles/PMC145421/ (2023) (Feb. 15, 2001).

187. Bill, C. A. & Vines, C. M. PHOSPHOLIPASE C. *Advances in experimental medicine and biology* **1131,** 215–242. ISSN: 0065-2598. https://www.ncbi.nlm.nih.gov/pmc/articles/PMC7790445/ (2023) (2020).

188. Joanito, I. *et al.* Single-cell and bulk transcriptome sequencing identifies two epithelial tumor cell states and refines the consensus molecular classification of colorectal cancer. *Nature Genetics* **54.** Number: 7 Publisher: Nature Publishing Group, 963–975. ISSN: 1546-1718. https://www.nature.com/articles/s41588-022-01100-4 (2022) (July 2022).

189. Su, N. *et al.* Increased Expression of Annexin A1 Is Correlated with K-Ras Mutation in Colorectal Cancer. *The Tohoku Journal of Experimental Medicine* **222,** 243–250 (2010).

190. Foo, S. L., Yap, G., Cui, J. & Lim, L. H. Annexin-A1 – A Blessing or a Curse in Cancer? *Trends in Molecular Medicine* **25,** 315–327. ISSN: 14714914. https://linkinghub.elsevier.com/retrieve/pii/S1471491419300395 (2022) (Apr. 2019).

191. Swa, H. L. F., Blackstock, W. P., Lim, L. H. K. & Gunaratne, J. Quantitative Proteomics Profiling of Murine Mammary Gland Cells Unravels Impact of Annexin-1 on DNA Damage Response, Cell Adhesion, and Migration. *Molecular & Cellular Proteomics*

: MCP **11,** 381–393. ISSN: 1535-9476. https://www.ncbi.nlm.nih.gov/pmc/articles/PMC3412969/ (2023) (Aug. 2012).

192. Khau, T. *et al.* Annexin-1 signals mitogen-stimulated breast tumor cell proliferation by activation of the formyl peptide receptors (FPRs) 1 and 2. *The FASEB Journal* **25.** _eprint: https://onlinelibrary.wiley.com/doi/pdf/10.1096/fj.09-154096, 483–496. ISSN: 1530-6860. https://onlinelibrary.wiley.com/doi/abs/10.1096/fj.09-154096 (2023) (2011).

193. De Graauw, M. *et al.* Annexin A1 regulates TGF-γ signaling and promotes metastasis formation of basal-like breast cancer cells. *Proceedings of the National Academy of Sciences* **107.** Publisher: Proceedings of the National Academy of Sciences, 6340–6345. https://www.pnas.org/doi/full/10.1073/pnas.0913360107 (2022) (Apr. 6, 2010).

194. Boudhraa, Z. *et al.* Annexin A1 in primary tumors promotes melanoma dissemination. *Clinical & Experimental Metastasis* **31,** 749–760. ISSN: 1573-7276. https://doi.org/10.1007/s10585-014-9665-2 (2023) (Oct. 1, 2014).

195. Yang, Y. *et al.* Annexin 1 Released by Necrotic Human Glioblastoma Cells Stimulates Tumor Cell Growth through the Formyl Peptide Receptor 1. *The American Journal of Pathology* **179.** Publisher: Elsevier, 1504–1512. ISSN: 0002-9440, 1525-2191. https://ajp.amjpathol.org/article/S0002-9440(11)00559-1/fulltext (2023) (Sept. 1, 2011).

196. Belvedere, R. *et al.* Annexin A1 contributes to pancreatic cancer cell phenotype, behaviour and metastatic potential independently of Formyl Peptide Receptor pathway. *Scientific Reports* **6.** Number: 1 Publisher: Nature Publishing Group, 29660. ISSN: 2045-2322. https://www.nature.com/articles/srep29660 (2023) (July 14, 2016).

197. Maschler, S. *et al.* Annexin A1 attenuates EMT and metastatic potential in breast cancer. *EMBO Molecular Medicine* **2,** 401–414. ISSN: 1757-4676. https://www.ncbi.nlm.nih.gov/pmc/articles/PMC3377343/ (2023) (Oct. 2010).

198. Xiao, Y. *et al.* Annexin A1 can inhibit the in vitro invasive ability of nasopharyngeal carcinoma cells possibly through Annexin A1/S100A9/Vimentin interaction. *PLOS ONE* **12.** Publisher: Public Library of Science, e0174383. ISSN: 1932-6203. https://journals.plos.org/plosone/article?id=10.1371/journal.pone.0174383 (2023) (Mar. 29, 2017).

199. Liu, A. *et al.* Expression of the Annexin A1 gene is associated with suppression of growth, invasion and metastasis of nasopharyngeal carcinoma. *Molecular Medicine Reports* **10.** Publisher: Spandidos Publications, 3059–3067. ISSN: 1791-2997. https://www.spandidos-publications.com/10.3892/mmr.2014.2656 (2023) (Dec. 1, 2014).

200. Gao, Y., Chen, Y., Xu, D., Wang, J. & Yu, G. Differential expression of ANXA1 in benign human gastrointestinal tissues and cancers. *BMC Cancer* **14,** 520. ISSN: 1471-2407. https://doi.org/10.1186/1471-2407-14-520 (2023) (July 19, 2014).

201. He, Z.-Y., Wen, H., Shi, C.-B. & Wang, J. Up-regulation of hnRNP A1, Ezrin, tubulin γ-2C and Annexin A1 in sentinel lymph nodes of colorectal cancer. *World Journal of Gastroenterology : WJG* **16,** 4670–4676. ISSN: 1007-9327. https://www.ncbi.nlm.nih.gov/pmc/articles/PMC2951517/ (2023) (Oct. 7, 2010).

202. SATO, Y. *et al.* Up-regulated Annexin A1 expression in gastrointestinal cancer is associated with cancer invasion and lymph node metastasis. *Experimental and Therapeutic Medicine* **2,** 239–243. ISSN: 1792-0981. https://www.ncbi.nlm.nih.gov/pmc/articles/PMC3440640/ (2023) (2011).

203. Duncan, R., Carpenter, B., Main, L. C., Telfer, C. & Murray, G. I. Characterisation and protein expression profiling of annexins in colorectal cancer. *British Journal of Cancer* **98.** Number: 2 Publisher: Nature Publishing Group, 426–433. ISSN: 1532-1827. https://www.nature.com/articles/6604128 (2023) (Jan. 2008).

204. Wang, X. *et al.* Targeting Annexin A1 as a Druggable Player to Enhance the Anti-Tumor Role of Honokiol in Colon Cancer through Autophagic Pathway. *Pharmaceuticals* **16.** Number: 1 Publisher: Multidisciplinary Digital Publishing Institute, 70. ISSN: 1424-8247. https://www.mdpi.com/1424-8247/16/1/70 (2023) (Jan. 2023).

205. Guinney, J. *et al.* The consensus molecular subtypes of colorectal cancer. *Nature Medicine* **21.** Number: 11 Publisher: Nature Publishing Group, 1350–1356. ISSN: 1546-170X. https://www.nature.com/articles/nm.3967 (2023) (Nov. 2015).

206. Feng, J. *et al.* ANXA1-derived peptides suppress gastric and colon cancer cell growth by targeting EphA2 degradation Corrigendum in /10.3892/ijo.2020.5149. *International Journal of Oncology* **57.** Publisher: Spandidos Publications, 1203–1213. ISSN: 1019-6439. https://www.spandidos-publications.com/10.3892/ijo.2020.5119 (2023) (Nov. 1, 2020).

207. Zhang, Z., Huang, L., Zhao, W. & Rigas, B. Annexin 1 induced by anti-inflammatory drugs binds to NF-B inhibiting its activation: Anticancer effects in vitro and in vivo. *Cancer research* **70,** 2379–2388. ISSN: 0008-5472. https://www.ncbi.nlm.nih.gov/pmc/articles/PMC2953961/ (2023) (Mar. 15, 2010).

208. Wiener, Z. *et al.* Prox1 Promotes Expansion of the Colorectal Cancer Stem Cell Population to Fuel Tumor Growth and Ischemia Resistance. *Cell Reports* **8,** 1943–1956. ISSN: 2211-1247. https://www.sciencedirect.com/science/article/pii/S2211124714007104 (2023) (Sept. 25, 2014).

209. Onozawa, H. *et al.* Annexin A1 is involved in resistance to 5-FU in colon cancer cells. *Oncology Reports* **37.** Publisher: Spandidos Publications, 235–240. ISSN: 1021-335X. https://www.spandidos-publications.com/10.3892/or.2016.5234 (2023) (Jan. 1, 2017).

210. Gensler, L. S. Glucocorticoids. *The Neurohospitalist* **3,** 92–97. ISSN: 1941-8744. https://www.ncbi.nlm.nih.gov/pmc/articles/PMC3726115/ (2023) (Apr. 2013).

211. Price, D. A., Close, G. C. & Fielding, B. A. Age of appearance of circadian rhythm in salivary cortisol values in infancy. *Archives of Disease in Childhood* **58.** Publisher: BMJ Publishing Group Ltd Section: Research Article, 454–456. ISSN: 0003-9888, 1468-2044. https://adc.bmj.com/content/58/6/454 (2023) (June 1, 1983).

212. Mohd Azmi, N. A. S. *et al.* Cortisol on Circadian Rhythm and Its Effect on Cardiovascular System. *International Journal of Environmental Research and Public Health*

18, 676. ISSN: 1661-7827. https://www.ncbi.nlm.nih.gov/pmc/articles/PMC7830980/ (2023) (Jan. 2021).

213. Hagihara, T. *et al.* Hydrodynamic stress stimulates growth of cell clusters via the ANXA1/PI3K/AKT axis in colorectal cancer. *Scientific Reports* **9.** Number: 1 Publisher: Nature Publishing Group, 20027. ISSN: 2045-2322. https://www.nature.com/articles/s41598-019-56739-7 (2023) (Dec. 27, 2019).

214. Chanrion, M. *et al.* Concomitant Notch activation and p53 deletion trigger epithelial-to-mesenchymal transition and metastasis in mouse gut. *Nature Communications* **5.** Number: 1 Publisher: Nature Publishing Group, 5005. ISSN: 2041-1723. https://www.nature.com/articles/ncomms6005 (2023) (Oct. 8, 2014).

215. Jackstadt, R. *et al.* Epithelial NOTCH Signaling Rewires the Tumor Microenvironment of Colorectal Cancer to Drive Poor-Prognosis Subtypes and Metastasis. *Cancer Cell* **36,** 319–336.e7. ISSN: 1535-6108. https://www.sciencedirect.com/science/article/pii/S153561081930371X (2023) (Sept. 16, 2019).

216. Siemińska, I. *et al.* Mo-MDSCs are pivotal players in colorectal cancer and may be associated with tumor recurrence after surgery. *Translational Oncology* **17,** 101346. ISSN: 1936-5233. https://www.sciencedirect.com/science/article/pii/S1936523322000080 (2023) (Mar. 1, 2022).

217. Kumar, V., Patel, S., Tcyganov, E. & Gabrilovich, D. I. The Nature of Myeloid-Derived Suppressor Cells in the Tumor Microenvironment. *Trends in Immunology* **37,** 208–220. ISSN: 1471-4906. https://www.sciencedirect.com/science/article/pii/S1471490616000053 (2023) (Mar. 1, 2016).

218. Gabrilovich, D. I., Ostrand-Rosenberg, S. & Bronte, V. Coordinated regulation of myeloid cells by tumours. *Nature Reviews Immunology* **12.** Number: 4 Publisher: Nature Publishing Group, 253–268. ISSN: 1474-1741. https://www.nature.com/articles/nri3175 (2023) (Apr. 2012).

List of acronyms

5FU 5-fluorouracil. 9

A-mice *Apc$^{lox/lox}$Cdx2-CreERT2$^{Tg/+}$* -mice. 39

ABCA1 ATP-binding cassette A1. 17, 132

AK-mice *Apc$^{lox/lox}$ LSL-Kras$^{G12D/+}$ Cdx2-CreERT2$^{Tg/+}$*-mice. 39

AKP-mice *Apc$^{lox/lox}$ LSL-Kras$^{G12D/+}$ Trp53$^{lox/lox}$ Cdx2-CreERT2$^{Tg/+}$*-mice. 39

ANOVA analysis of variance. 41, 47, 54, 56

ANXA1 Annexin A1. 15

APC adenomatous polyposis coli. 3, 4, 6, 10, 44

ATAC-seq assay for transposase-accessible chromatin sequencing. 128

CAR chimeric antigen receptor. 12

CCF cancer cell fraction. 48

CI confidence interval. 90

COAD colon adenocarcinoma. 48, 88

CRC colorectal cancer. 3–5, 14, 70, 72, 90, 129

CTLA4 cytotoxic T lymphocyte antigen 4. 10

DAG diacylglycerol. 16, 131

DGE differential gene expression. 83–85, 131

EDTA ethylenediaminetetraacetic acid. 26

EGF epidermal growth factor. 6

EGFR epidermal growth factor receptor. 6, 45, 130

ERK extracellular-related protein kinase. 6

FMIC fluorescence minus intracellular staining. 53, 58

FPR2 formyl peptide receptor 2. 16

GCR glucocorticoid receptor. 87

GDP guanosine diphosphate. 6

GEMM genetically engineered mouse models. 14, 19, 46, 48, 62, 125, 126, 129, 135, 139

GPCR G protein coupled receptor. 16, 87

GSEA gene set enrichment analysis. 83

GTP guanosine triphosphate. 6

GZMb granzyme b. 53, 77

HIF hypoxia-inducible factors. 13

IC intracellular. 53, 58

IEL intra-epithelial lymphocyte. 68, 69

IHC immunohistochemistry. 43, 46, 60, 62, 63, 75, 94, 130, 131, 140

Il17a interleukin 17a. 53, 54

ILC2 type 2 innate lymphoid cell. 68

KRAS kirsten rat sarcoma. 4–6

LP lamina propria. 2

LUAD lung adenocarcinoma. 3

mAb monoclonal antibody. 9

MAPK mitogen-activated kinase. 5, 6

MEK mitogen activated protein kinase. 6

MHC major histocompatibility complex. 10, 11

MLN mesenteric lymph node. 94, 96, 98

MM muscularis mucosae. 94, 97

MMP9 matrix metalopeptidase 9. 13

MMRd mismatch repair deficient. 11, 130

MMRp mismatch repair proficient. 72, 73

MP muscularis propria. 94, 97, 98

MSI microsatellite instable. 11

MSS microsatellite stable. 12

NBCS newborn calf serum. 26

NES normalised enrichment score. 83

NK natural killer cells. 68

OCT optimal cutting temperature. 24

OR odds ratio. 90

pAPC professional antigen presenting cell. 11, 12, 66, 75, 100, 103, 107, 109, 130

PBND PCR buffer with non-ionic detergents. 22

PBS phosphate-buffered saline. 23

PCA principle component analysis. 64

PCC pearson correlation coefficient. 85

PCR polymerase chain reaction. 22, 40

PD1 programmed cell death protein 1. 10

pDC plasmacytoid dendritic cells. 66

pDCs plasmacytoid dendritic cells. 115

PDL1 programmed cell death ligand 1. 10

PLA2 phospholipase A2. 16

PMA phorbol myristate acetate. 30

RAF rapidly accelerated fibrosarcoma. 6

SASP senescence-associated secretory phenotype. 126

scRNAseq single-cell RNA sequencing. 40, 62, 63, 65, 130

SM submucosae. 94

SM++ staining media supplemented with EDTA and NBCS. 26

TCF T cell factor. 4, 5

TCGA the cancer genome atlas. 48, 88, 127

TCR T cell receptor. 10

tdLN tumor-draining lymph node. 94, 97

Th1 type 1 helper T cells. 54

Th17 T helper 17 cell. 68

TIL tumor-infiltrating lymphocyte. 67, 69, 70

TILs tumor-infiltrating lymphocytes. 53

Tis tumor in situ. 94

TLS tertiary lymphoid structure. 69, 75

TME tumor microenvironment. 12–14, 49, 53, 54, 60, 62–64, 69, 73, 75, 87, 90, 97, 116, 123, 125, 138

TP53 tumor protein p53. 4

Tregs regulatory T cells. 53

UMAP uniform manifold approximation and projection. 62, 65

VAF variant allele frequency. 48

VEGF vascular endothelial growth factor. 9

WES whole exome sequencing. 48, 127

WGS whole genome sequencing. 127, 128

WT wildtype. 40

Amber D Bowler, PhD candidate

LinkedIn |•| ORCID

LANGUAGES English – Native speaker
French – B1 (FIDE certified)

EXPERIENCE

2018-Present	Molecular Biology in Cancer (EDMS) PhD Student, Radtke Lab, ISREC, SV (Life Sciences), École Polytechnique Fédérale de Lausanne
2017-2018	Intern, Hantschel Lab, ISREC, SV, École Polytechnique Fédérale de Lausanne
2014-2017	Undergraduate Researcher, Deininger/O'Hare Lab, Huntsman Cancer Institute

EDUCATION

2018-Present	Doctorate of Philosophy – Molecular Biology École Polytechnique Fédérale de Lausanne (EPFL)
2013-2017	Honors Bachelor of Science - Chemistry, Biological Emphasis Honors College, University of Utah

PUBLICATIONS

2023	(In revision) L.F. Lorenzo-Matin*, T. Hübscher*, N. Broguiere, **A.D. Bowler**, J. Langer, L. Tillard, M. Nikolaev, F. Radtke and M.P. Lutolf. Spatiotemporally resolved ex vivo colorectal cancer development in engineered mini-colons. In revision with *Nature*.
2023	(In revision) A. Bodac, A. Mayet, J. Pascual, **A.D. Bowler**, V. Roh, N. Fournier, L. Craciun, P. Demetter, F. Radtke, and E. Meylan. Bcl-xL targeting eliminates ageing tumor-promoting neutrophils and inhibits lung tumor growth. In revision with *EMBO Molecular Medicine*.
2023	(Submission) A.C. André, M.V. Barroso, J. Skerniskyte, M.Siegwald, L. Debande, V. Paul, N. Broussaudier, T. Thahouly, C. Ridley, I. Svahn, **A.D. Bowler**, S. Rigaud, J-Y. Tinevez, R.R. Vivès, P.J. Sansonetti, F. Radtke, D.J. Thornton, and B.S. Marteyn. Neutrophils release glycosaminoglycans to form proteoglycofili and NETs. Submission underway.
2022	A.M. Eiring, J.S. Khorashad, A. Agarwal, C.C. Mason, R. Bell, A. Senina, A.D. Pomicter, F.Yu, H.M. Redwine, **A.D. Bowler,** P.M. Clair, S.K. Tantravahi, S.K. McWeeney, B.J. Druker, D.L. Stirewalt, V. Oehler, T. O'Hare, M.W. Deininger. MS4A3 Promotes Differentiation in Chronic Myeloid Leukemia by Enhancing Common β Chain Cytokine Receptor Endocytosis. *Blood.* DOI: 10.1182/blood.2021011802. Epub 2022 Feb 3.
2020	M.Germann, N. Fournier, M. Sauvain, C. Sempoux, **A.D. Bowler**, P. Wirapati, L. E. Kandalaft, M. Delorenzi, S. Tejpar, G. Coukos, F. Radtke. Neutrophils suppress tumor-infiltrating T cells in colon cancer via matrix metalloproteinase-mediated activation of TGFβ. *EMBO Mol Med.* 2020 Jan 9; 12: e10681. DOI: 10.15252/emmmm.201910681. Epub 2019 Dec 2.
2019	C.A. Eide, M.S. Zabriskie, S.L.S. Stevens, O. Antelope, N.A. Vellore, H. Than, A.R. Schultz, P. Clair, **A.D. Bowler**, A. D. Pomicter, D. Yan, A.V. Senina, W. Qiang, T.W. Kelley, P. Szankasi, M.C. Heinrich, J.W. Tyner, D. Rea, J-M. Cayuela, D-W. Kim, C.E. Tognon, T. O'Hare, B.J. Druker, M.W. Deininger. Combining the Allosteric Inhibitor Asciminib with Ponatinib Suppresses Emergence of and Restores Efficacy against Hightly

Resistant BCR-ABL1 Mutants. *Cancer Cell.* 2019 Oct 14;36(4):431-443.e5. DOI: 10.1016/j.ccell.2019.08.004. Epub 2019 Sep 19.

2015 A.M. Eiring, J.S. Khorashad, D.J. Anderson, F. Yu, H.M. Redwine, C.C. Mason, K.R. Reynolds, P.M. Clair, K.C. Gantz, T.Y. Zhang, A.D. Pomicter, I.L. Kraft, **A.D. Bowler**, K. Johnson, M.M. Partlin, T. O'Hare, M.W. Deininger. β-Catenin is required for intrinsic but not extrinsic BCR-ABL1 kinase-independent resistance to tyrosine kinase inhibitors in chronic myeloid leukemia. *Leukemia.* 2015 Dec;29(12):2328-37. DOI: 10.1038/leu.2015.196. Epub 2015 Jul 23.

2015 J.S. Khorashad, A.M. Eiring, C.C. Mason, K.C. Gantz, **A.D. Bowler,** H.M. Redwine, F. Yu, I.L. Kraft, A.D. Pomicter, K.R. Reynolds, A.J. Iovino, M.S. Zabriskie, W.L. Heaton, T. O'Hare, M.W. Deininger. shRNA library screening identifies nucleocytoplasmic transport as a mediator of BCR-ABL1 kinase-independent resistance. *Blood*. 2015 Mar 12;125(11):1772-81. DOI: 10.1182/blood-2014-08-588855. Epub 2015 Jan 8.

TECHNICAL EXPERIENCE

Software and programming: R, GraphPad Prism, FlowJo, QuPath, IGV, Zotero, LaTex.

Molecular and cellular biology: Murine organoid culture, creation and maintenance, drug screening, viability assays, RNA and DNA preparation, qRT-PCR, SDS-PAGE, PCR, multicolor conventional flow cytometry, spectral flow cytometry, immunohistochemistry, ELISA, scRNAseq, TCRseq, adherent and suspension cell culture, protein isolation and purification, FRET, molecular cloning,

Mouse: mouse handling, subcutaneous injection, intravenous injection, intraperitoneal injection, oral gavage, suturing, *in vivo* imaging, dissection and license writing and design.

Transferrable skills: Strong oral presentation and writing abilities, experimental design, literature review, data interpretation, project management.

LEADERSHIP

2020-2022 EDMS Student Representative
2020-2022 ADSV (Association des doctorants en science de la vie) President

TEACHING

2022 Supervised Master's thesis research and writing of Elia Escoffier.
2021 Supervised Bachelor project of Helena Binkova.
2018-2021 Teaching assistance for practical laboratory course for molecular biology (BIO-203 and BIO-204)

HOBBIES

Skiing, hiking, knitting, puzzles, board games, cycling.